NASA Contractor Report 3318

Satellite Power Systems (SPS) Concept Definition Study

Volume II, Part 1 - System Engineering

G. M. Hanley

NASA

NASA Contractor Report 3318

Satellite Power Systems (SPS) Concept Definition Study

Volume II, Part 1 - System Engineering

G. M. Hanley
Rockwell International
Downey, California

NASA

National Aeronautics
and Space Administration

Scientific and Technical
Information Branch

1980

FOREWORD

Volume II, System Engineering, is presented in two parts. Part 1 encompasses SPS system engineering aspects. Part 2 consists of a volume on SPS cost and programmatics; an appendix is included in Part 2 to cover the SPS WBS and cost estimates. Volume II of the SPS Concept Definition Study final report is submitted by Rockwell International through the Satellite Systems Division. All work was completed in response to NASA/MSFC Contract NAS8-32475, Exhibit C, dated March 28, 1978.

The SPS final report will provide the NASA with additional information on the selection of a viable SPS concept, and will furnish a basis for subsequent technology advancement and verification activities. Other volumes of the final report are listed as follows:

Volume	Title
I	Executive Summary
III	Experimentation/Verification Element Definition
IV	Transportation Analyses
V	Special-Emphasis Studies
VI	In-Depth Element Investigations
VII	Systems/Subsystems Requirements Data Book

The SPS Program Manager, G. M. Hanley, may be contacted on any of the technical or management aspects of this report. He can be reached at 213/594-3911, Seal Beach, California.

CONTENTS

ILLUSTRATIONS

Figure

Page

TABLES

1.0 SPS CONCEPTS

1.0 SPS CONCEPTS

This volume presents results of studies designed to evaluate the SPS satellite photovoltaic design concept on the basis of new data, to show improvement in the design concept, and to resolve or reduce key areas of uncertainty in the reference concept. These evaluations are an integral part of the narrowing down process for point design definition.

Included in this section are descriptions of the various candidate concepts considered and conclusions and recommendations for a preferred concept. An initial concept resulting from Exhibit A/B of the previous study (SD 78-AP-0023) is utilized as the starting point. This concept is evaluated for solid state dc-RF conversion (to replace klystrons) and configuration trades were performed to update concentration ratio and structural material selections. Based on these initial study results and NASA/DOE configuration decisions (October 1978) a new Rockwell reference concept was developed. Configuration options were evaluated and compared against this reference concept and against the NASA/DOE baseline. Recommendations were then made to define an updated and preferred concept.

1.1 INITIAL CONCEPTS

This study was initiated using a preliminary baseline concept designated by NASA/MSFC at the conclusion of Exhibits A/B of the SPS contract. The initial concept is shown in Figure 1.1-1 and has the following major characteristics:
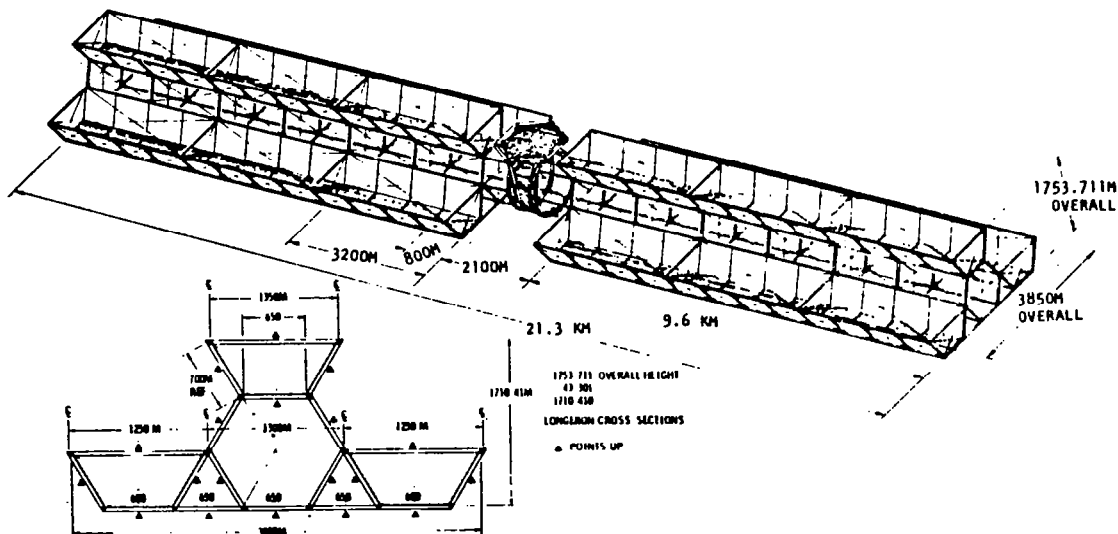
Figure 1.1-1. Preliminary Baseline Satellite Concept

- GaAlAs solar cells with reflectors having a geometric concentration ratio of 2:1

- 2 tier cross section

- Aluminum structure

- 5 GW power output at ground utility busbar

- Single, centrally-located microwave antenna with klystron dc-RF converters

Starting from this baseline a number of major system trade studies were conducted. These included: a solid state (transistor) replacement for the klystrons; flat plate concentrators giving a concentration ratio (CR) up to 2.7; and composites versus aluminum structure. All subsystem areas were investigated and, where appropriate, trade studies or analyses conducted to update and further define the satellite concept.

1.1.1 SOLID STATE REPLACEMENT OF KLYSTRONS

The baseline satellite concept utilizes high voltage (HV) klystron dc-RF converters to convert the dc power generated to the 2.45 GHz microwave state. The power for the RF converters is transferred at 40 kV dc (nominal) across the antenna slip rings, converted to five selected HV dc voltages and utilized by the klystrons. Solid state dc-RF converters require an input voltage of probably less than 100 V (present design indicates an input voltage of approximately 40 V dc). If the appropriate voltage (40 V dc) is generated the current carrying capability of the rings would need to be probibitively large (one half of approximately 10 GW @ 40 V $\approx$ 125$\times$10^6 amps dc). If relatively high voltage is generated (20-40 kV dc) and transferred across the rings, the subsequent dc-dc conversion results in large increases in antenna mass or significantly advanced technology is required for dc converters.

The concept initially studied for application of solid state technology assumed that 50 kW solid state power modules would replace the 50 kW klystrons in an antenna configuration basically the same as that used for the klystrons. In order to provide adequate efficiency, the temperature of the solid state devices must be maintained at $\leq$150°C. It is necessary to radiate thermal energy from both sides of the antenna if reasonable antenna sizes are to be maintained. Alternative approaches with two-sided radiation include: (1) a reduction of RF power in the center of the antenna, (2) redistribution of the center power modules to increase their spacing and the use of wave guides to direct RF energy to the appropriate microwave radiators, and (3) increase in antenna diameter to increase thermal and microwave rqdiation area, while simultaneously reducing power output from the satellite.

The low voltage required by the solid state modules resulted in a large dc/dc power conditioning penalty. At 50 kW ratings the converter specific weight estimate is 1.0 kg/kW. To reduce the dc-dc converter weight penalty it is necessary to project significant improvements in specific weight. One

approach to lighter weights is to take advantage of larger converter ratings illustrated by the concept shown in Figure 1.1-2. Transformer weight varies to the 0.75 power of the rating if all parameters such as current density, flux density, etc., are kept constant.[1] Using a weight model with the magnetics (transformers) as 23.7% of the dc converter weight and the remaining elements scaled it is possible to project lightweight dc converters at large power ratings. The concept indicated in Figure 1.1-2 clusters the power modules to utilize central dc converters providing from 14.4 megawatts to 120 megawatts each. At these ratings, lower specific weights are anticipated for the converters and a direct comparison with the klystron antenna can be made. Another potential solution to the large masses due to step-down from high to low voltage is to use superconductivity technology to reduce conductor weights.
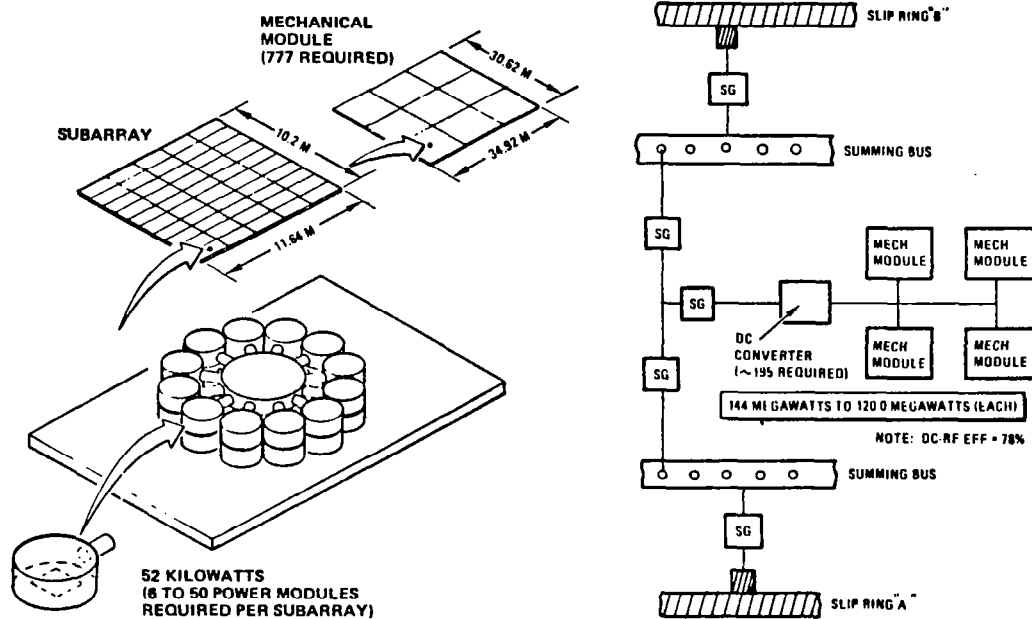
Figure 1.1-2. *Solid State Antenna Power Distribution Concept*

Three solar array mounted candidate solid state configuration concepts are identified in Figure 1.1-3. The solid state power modules are located on the solar array with power provided directly from the array at the required voltage. All three concepts restructure the solar blanket configuration to develop the low voltages required by the solid state devices and locate the dc-RF converters immediately adjacent to the solar blankets to reduce I^2R losses.

---

[1]Westinghouse Electric Corporation, Report LY20686, prepared for Rockwell International, Satellite Power Systems Study, December 1977
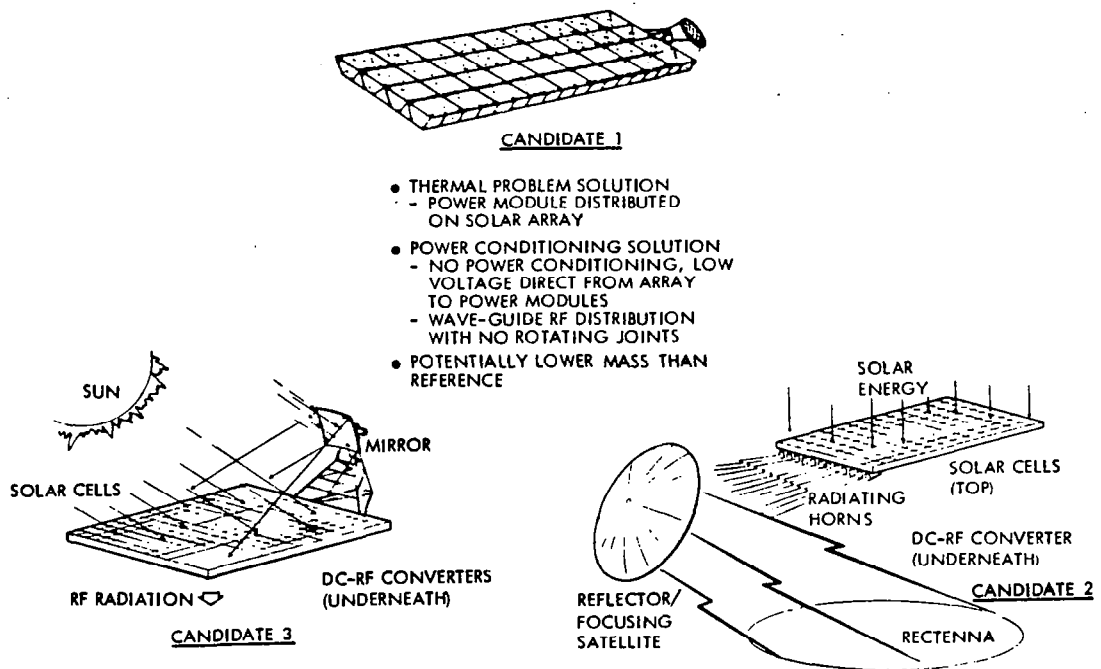
Figure 1.1-3. Solar Array Mounted Solid State
Power Modules

In the first candidate satellite the construction form is the same as the point design, however, the summed RF energy must now be transferred over a wave guide rotating joint with a capacity of over 4 GW @ 2.45 GHz. The second candidate completely restructures the satellite and requires that the plane of the solar blanket be sun stabilized. The collected RF energy is transmitted to a free-flying stationkeeping satellite and retransmitted to the receiving rectenna. In order to control the RF beam it will be necessary to provide extremely precise stationkeeping and pointing/focusing control. The third candidate is similar to the second except that the satellite is stabilized to the rectenna boresite and the variable sun angle is compensated for by using an attached (or if desirable a free flying) reflecting mirror. The pointing accuracies required for this concept would be significantly less than for the second concept. The alternative concepts may eliminate power distribution and thermal effects but each still present significant design problems although these are now in different areas, e.g., new technology problems related to high power wave guides.

1.1.2 FLAT PLATE CONCENTRATOR WITH CONCENTRATION RATIO UP TO 2.7

A summary of the design concepts that had been given final consideration in the selection of a baseline design concept is shown in Figure 1.1-4. The concentration ratios, reflector shape and angle, and area requirements are indicated. The selected design for the baseline concept is the 60° Vee-trough configuration. It is felt that an advantage might be realized by a higher

1-4
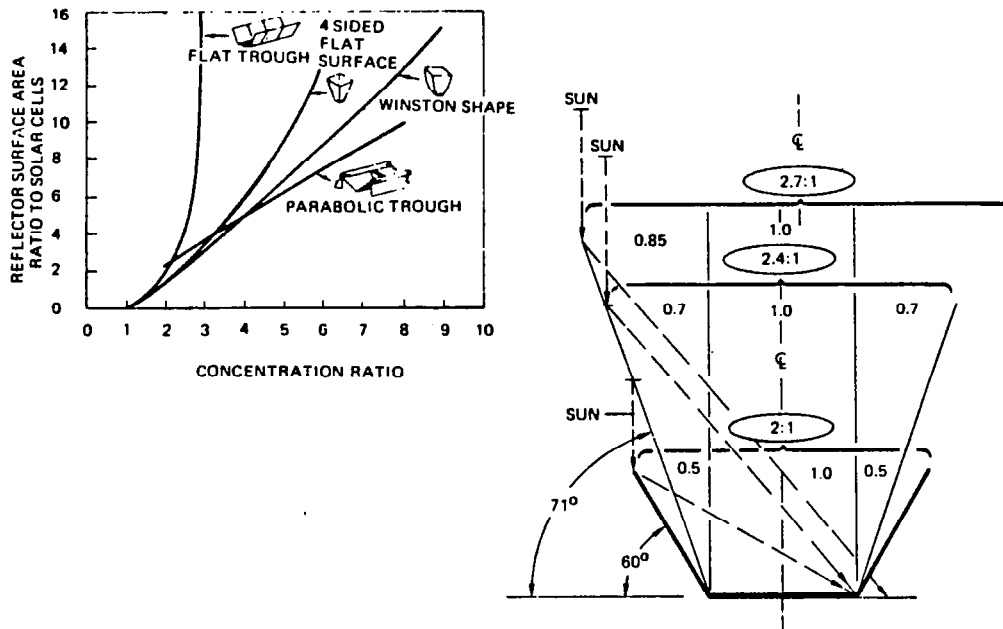
Figure 1.1-4. Reflector Shape

slant angle. The geometry and ray traces for the Vee-trough design for a 60°
and 71° reflector slant angle are shown. As illustrated, for a CR=2 the slant
angle is 60°, and for a CR=2.4 the slant angle is 71°. The SPS structural
cross sections were modeled to compare 60°, 65°, and 71° reflector angle (three
troughs) reflectors. Performance and mass comparison was made. Mass items
affected included mass structure, solar cells, reflectors and conductors. The
results of this comparison is shown in Table 1.1-1. The net mass variation is
minor. Bracketed mass numbers are referenced values. Subsystem cost comparison
as a function of reflector angle is shown in Table 1.1-2. As the reflector
angles increase the possible savings of the cost/mass are insufficient to over-
come the penalty from added structural complexity. The recommendation resulting
from this comparison is that the present baseline, utilizing CR=2 and 60° slant
angle, should be retained.

1.1.3   COMPOSITES VERSUS ALUMINUM STRUCTURE

        Using the substructure features of NASTRAN, the baseline design configura-
tion (Figure 1.1-1 shown previously) was modeled. Using the CRT printouts,
Figure 1.1-5 depict the buildup of the SPS structure through the combination
of the substructures. The right-hand wing is a combination of three translated
substructure number 1 units. Similarly, the left-hand wing is a combination of
three substructure number 4 units. The center structure is a combination of
the center section, substructure number 2, and the antenna and rotating ring,
substructure number 3. Finally, the center section, the left-hand wing, and
right-hand wing are combined to form the SPS structural model. Both composite
and aluminum structure were analyzed. Thermal constraints included equilibrium
operating temperatures, a construction temperature of 0°C and a temperature

Table 1.1-1. *Comparison of Reflector Angles*

PERFORMANCE PAR. AND MASS ELEMENT	REFLECTOR ANGLE		
	60°	65°	71°
TEMPERATURE °C	113	119	125
η (T)	.1816	.179	.176
SOLAR INPUT (W/M²)•	1319.5 ──────────────►		
CR$_{GEOM.}$	2.0	2.286	2.576
CR$_{EFF}$ (EOL)	1.83	2.067	2.308
ENERGY ONTO CELL (W/M²)	2414.7	2727.4	3045.4
ENERGY CONVERTED (W/M²)	438.5	488.2	536.0
ARRAY DESIGN FACTOR (.89)	390.27	434.5	477.0
SEASONAL VARIATION (.91)	355.1	395.4	434.1
ENVIR. DEGRAD (.96)	340.9	379.6	416.7
SOLAR CELL AREA (10⁶M²)	30.06	27.0	24.6
REFL. RATIO TO CELLS	2.0	3.04	4.84
REFL. SURFACE (10⁶M²)	60.12	82.13	119.09
DELTA MASS (10⁶ KG)			
STRUCT. & MECH.	(3.777)	+0.001	+0.222
SOLAR BLANKET	(7.586)	-0.771	-1.376
REFLECTOR	(1.088)	+0.398	+1.067
POWER DISTR.	(1.166)	+0.054	+0.062
SUBTOTAL Δ'S	(13.617)	-0.318	-0.025

NOTE: •SUMMER SOLSTICE

Table 1.1-2. *Subsystem Cost Comparison as a Function of Reflector Angle*

COST IN MILLIONS OF DOLLARS (TFU)

SUBSYSTEM ELEMENTS	REFLECTOR ANGLE			COST FACTOR
	60°	65°	71°	
STRUCTURES	390.554	+ .081	+ 17.9	$80.66'KG
SOLAR BLANKET	1978.481	-197.823	-352.989	$64.65/M²
REFLECTORS	150.79	+ 52.24	+138.4	$ 2.52/M²
WIRING	3.64	+ .08	+ .09	$ 1.52'KG
TRANSPORTATION	678.525	- 15.525	- 1.2	$37.5/KG
SUBTOTAL COST	3201.99	-160.947	-197.80	

NOTE: AVG COST REDUCTION FACTOR ~ .8611 TFU

✓ STAY WITH 60° REFL. ANGLE
  ● COST/MASS SAVINGS INSUFFICIENT
     TO OVERCOME ADDED COMPLEXITY

during the solar eclipse (by the earth) of -150°C. The results indicated maximum
deflections of the aluminum array structure of 100 meters compared to only 1
meter for the composite structure. Rotating joint deflections of 0.88 meters
were obtained compared with negligible composite deflections. Despite these
large deflections, it was concluded that an aluminum structure could be built
to SPS requirements. However, the results indicated that a structure material
thickness of up to 30 mils is necessary compared to 10 mils previously assumed.
This is due to the large stress magnitudes and low crippling allowables for
aluminum. Depending upon design methodology and degree of ingenuity, there
will be an increase in structural weight, as a result, of up to 10×10⁶ kg for
aluminum compared to 1.2×10⁶ kg for composite structure.
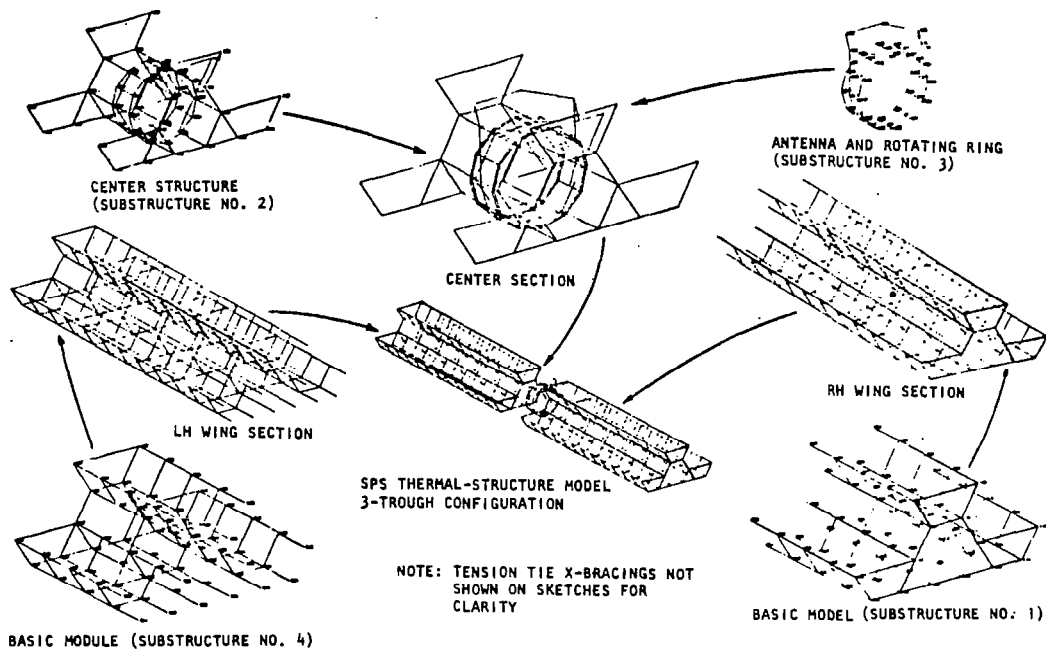
Figure 1.1-5. *SPS Computer Program Structural Model*

1.1.4 SATELLITE SYSTEM UPDATE

An update of the baseline SPS concept was documented as it had been defined through July 1978.[1] The mass of the updated SPS concept versus Exhibit A/B are shown in Table 1.1-3, and had resulted in an 8.3% increase in dry weight. The following tabulation identifies the reasons for these mass changes:

Collector Area

- Primary structure – Eighteen additional 50-m tribeams across top of reflector bays

- Attitude Control – Updated to reflect final Exhibit A/B

- Power Conditioning Equipment – Addition of 40,000 low-voltage converters plus increase in switchgears due to drop in system efficiencies

- Power Distribution – Increase in conductors and slip ring support

- Thermal Control – Radiator system added (320,000 m^2) for high voltage converters

---

[1]*Satellite Power Systems (SPS) Concept Definition Study, SPS Point Design Definition Update*, NAS8-32475, DPD 558, July 30, 1978

1-7

Table 1.1-3. Preliminary Baseline Concept
(2-Tier Cross Section)

SUBSYSTEM	END OF EXHIBIT A/B	UPDATED JUNE 21-22, 1978	Δ
COLLECTOR ARRAY	(13.919)	(14.169)	(+ 0.250)
STRUCTURE & MECHANISM	3.777	3.825	+ 0.048
ATTITUDE CONTROL	0.095	0.116	+ 0.021
POWER SOURCE	8.831	8.831	–
PDC	1.166	1.347	+ 0.181
IMS	0.050	0.050	–
ANTENNA SECTION	(14.204)	(16.297)	(+ 2.093)
STRUCTURE & MECHANISM	1.685	1.682	– 0.003
THERMAL CONTROL	1.408	2.457	+ 1.049
MICROWAVE POWER	7.012	7.012	
PDC	3.469	4.516	+ 1.047
IMS	0.630	0.630	
TOTAL SPS	28.123	30.466	+ 2.343
GROWTH (30%)	8.437	9.140	+ 0.703
TOTAL SPS (WITHGROWTH)	36.560	39.606	+ 3.046

- Power Conditioning Equipment – Addition of 144,000 low voltage
  converters and 136,000 regulators plus increase in switchgear
  due to lower system efficiency

- Power Distribution – Increase in conductors due to power system
  efficiency

1.1.5 REFERENCE CONCEPT

A new Rockwell reference satellite concept was developed based on the NASA/
DOE defined reference SPS system.[1] The satellite portion of the NASA/DOE system
is shown in Figure 1.1-6. Both the silicon and GaAs photovoltaic concepts are
coplanar, and have a single microwave antenna located at the end of the satel-
lite to provide 5 GW of power at the utility interface. The major overall dif-
ference between the two satellites is the use of flat concentrators on the GaAs
concept (CR=2), whereas, the silicon concept does not use concentrators (CR=1).
The mass properties for the NASA/DOE reference satellite is given in Table 1.1-4.
The total mass, 34.1×10^6 kg for GaAs and 51.0×10^6 kg for the silicon concept,
and includes a 25% growth factor. The mass is nearly evenly distributed between
the solar array and antenna for the GaAs concept; whereas, the solar array is
nearly twice the mass of the antenna for the silicon concept.

---

[1]*Concept Development and Evaluation Program,* Reference System Report,
U.S. Department of Energy and the National Aeronautics and Space
Administration, October 1978
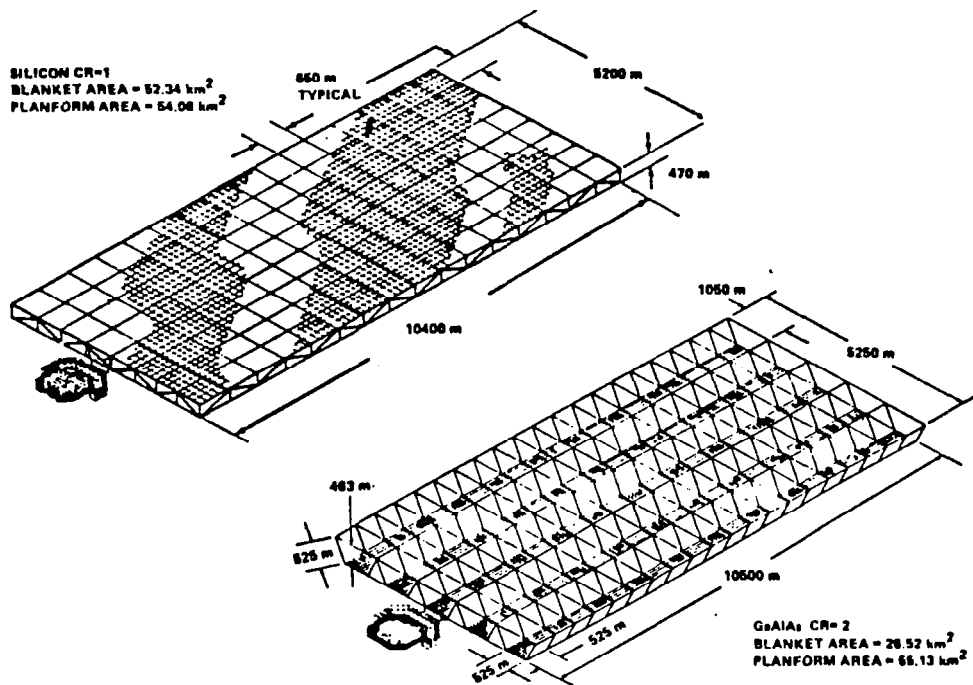
Figure 1.1-6. NASA/DOE Reference Satellite Concepts

Table 1.1-4. NASA/DOE Reference Satellite Mass Properties
(Millions of Kilograms)

SUBSYSTEM	GaALAs CR = 2 OPTION		SILICON CR = 1 OPTION	
SOLAR ARRAY		13.798		27.258
PRIMARY STRUCTURE	4.172		3.388	
SECONDARY STRUCTURE	0.581		0.436	
SOLAR BLANKETS	6.696		22.051	
CONCENTRATORS	0.955		—	
POWER DISTRIBUTION & CONDITIONING	1.144		1.134	
INFORMATION MANAGEMENT & CONTROL	0.050		0.050	
ANTENNA		13.382		13.382
PRIMARY STRUCTURE	0.250		0.250	
SECONDARY STRUCTURE	0.786		0.786	
TRANSMITTER SUBARRAYS	7.178		7.178	
POWER DISTRIBUTION & CONDITIONING	2.189		2.189	
THERMAL CONTROL	2.222		2.222	
INFORMATION MANAGEMENT & CONTROL	0.630		0.630	
ATTITUDE CONTROL	0.128		0.128	
ARRAY/ANTENNA INTERFACES*		0.147		0.147
PRIMARY STRUCTURE	0.094		0.094	
SECONDARY STRUCTURE	0.003		0.003	
MECHANISMS	0.033		0.033	
POWER DISTRIBUTION	0.017		0.017	
SUBTOTAL		27.327		40.787
CONTINGENCY (25%)		6.832		10.197
TOTAL		34.159		50.984

* ROTARY JOINT, SLIP RINGS, ANTENNA YOKE

The Rockwell reference satellite concept for GaAs solar cells CR=2 is shown in Figure 1.1-7. The design characteristics of this concept include: (1) 5 GW power to the utility interface; (2) Geosynchronous construction location; (3) single microwave antenna end-mounted; (4) GaAs solar cells with a concentration ratio of 2; (5) Y-POP attitude control and stationkeeping; (6) 45.5 kV dc power distribution; (7) composites as the structural material; and (8) klystron dc-RF conversion.
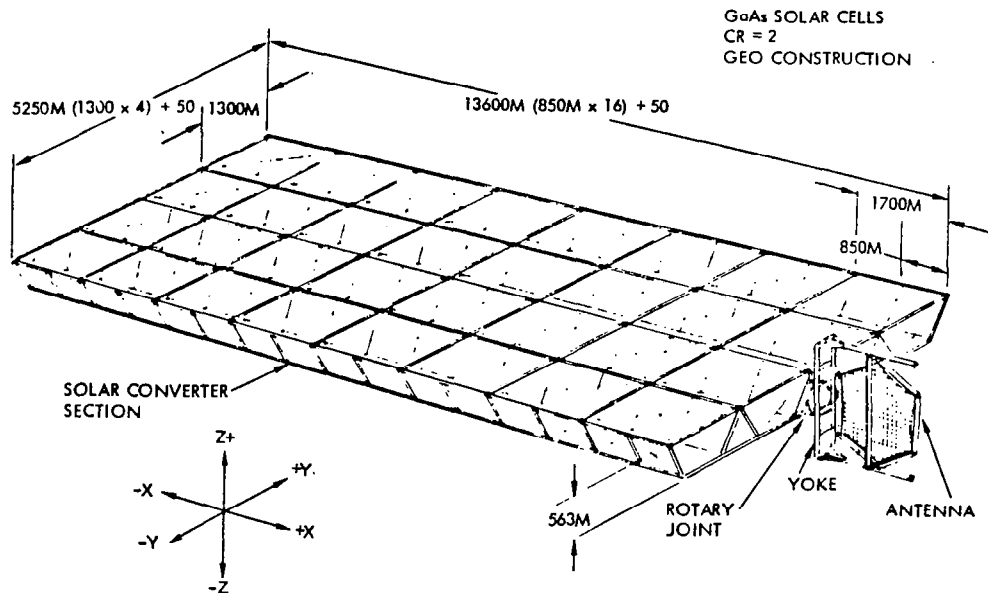
Figure 1.1-7. Rockwell Reference Satellite Concept

The mass properties for the Rockwell reference concept satellite is given in Table 1.1-5. The total mass of 36.8×10^6 kg, includes a 25% growth factor. The dominate mass in the collector array is the solar cells. Structural mass is only 10% of the total mass. Antenna mass is mainly comprised of the RF radiators, klystrons and power distribution.

1.1.6 CONCEPT VARIATIONS

Variations of the Rockwell reference concept that were studied to provide data for selection of the best design concept included: concentration ratio (CR=1 and CR=2); number of troughs (3, 4, 5, and 6); antenna location (central and end); and solar cell material (GaAs and silicon).

The study results indicate that the silicon concept is much heavier than the GaAs concept. The silicon concept is optimized without concentrators; whereas, the GaAs concept is near-optimum at CR=2. As the number of troughs vary from 3 to 6, the length-to-width of the planform decreases. The higher number of troughs generally have lower wiring mass but construction is more complex. The centrally-located antenna concepts have the lowest mass but are

1-10

*Table 1.1-5. Rockwell GaAs CR=2 Reference Satellite
Mass Statement*

SUBSYSTEM	WEIGHT (MILLION KG)
COLLECTOR ARRAY	
STRUCTURE & MECHANISMS	1.811
POWER SOURCE	8.440
POWER DISTRIBUTION & CONTROL	2.889
ATTITUDE CONTROL	0.116
INFORMATION MANAGEMENT & CONTROL	0.050
TOTAL ARRAY (DRY)	(13.306)
ANTENNA SECTION	
STRUCTURE & MECHANISMS	1.486
THERMAL CONTROL	2.457
MICROWAVE POWER	7.012
POWER DISTRIBUTION & CONTROL	4.516
INFORMATION MANAGEMENT & CONTROL	0.630
TOTAL ANTENNA SECTION (DRY)	(16.101)
TOTAL SPS DRY WEIGHT	29.407
GROWTH (25%)	7.352
TOTAL SPS DRY WEIGHT WITH GROWTH	36.759
PROPELLANT PER YEAR	0.085

somewhat more complex to construct. For both centrally-located and end-located
antenna concepts, three troughs appear to be the best compromise for mass and
constructability.

Mass property comparisons for an end mounted and center mounted antenna
coplanar concept is shown for GaAs CR=2 in Table 1.1-6. The collector array
for the center mounted antenna concept results in 1.636×10^6 kg less mass due
primarily to the difference in power distribution mass (1.503×10^6 kg versus
2.889×10^6 kg). The antenna section for both concepts are taken to be the same.
Total SPS dry mass with 25% growth shows a savings of 2.045×10^6 kg for the
center mounted antenna concept (34.714×10^6 kg versus 36.759×10^6 kg).

A number of antenna concepts were studied. The major variations in antenna
design are shown in Figure 1.1-8. The Rockwell baseline (2 Tier center mounted,
tension web configuration) was modified to include a space frame antenna struc-
ture, both end mounted and center mounted, and a tension web structure, end
mounted. Results of the trade study indicates that the central mounted antenna
is preferred because of its reduced satellite mass. Variations for the klystron
installation were also studied. Previous studies had considered cooling the
klystron collector from both the front and rear sides of the antenna. The base-
line, however, established during Exhibit A/B, is based on the "poke through"
concept shown in Figure 1.1-9 which provided heat rejection on the front only
and protected slip rings from excessive temperature. This reduced the propaga-
tion efficiency of the antenna. The Rockwell alternative klystron installation
concept shown in Figure 1.1-9 provides more flexibility in that it allows heat
rejection from the space facing surface in addition to the Earth side. During
this study (Exhibit C), it was determined that it is thermally acceptable to
radiate from the rear of the antenna, even with a centrally located antenna,
provided that the slip rings are not located directly under the antenna. When
comparing the two antenna structures, the thermal analysis concluded that the

SUBSYSTEM	CO-PLANAR (3 TROUGH)	
	END MOUNTED ANTENNA	CENTER MOUNTED ANTENNA
COLLECTOR ARRAY		
STRUCTURE AND MECHANISMS	(1.811)	(1.561)
PRIMARY STRUCTURE	.997	1.012
SECONDARY STRUCTURE	.581	.316
MECHANISM	.233	.233
ATTITUDE CONTROL	(0.116)	(0.116)
POWER SOURCE	(8.440)	(8.440)
SOLAR PANELS	7.258	7.258
SOLAR REFLECTORS	1.182	1.182
POWER DISTRIBUTION AND CONTROL	(2.889)	(1.503)
POWER CONDITIONING EQUIPMENT	(.262)	(.262)
POWER DISTRIBUTION	(2.627)	(1.241)
CONDUCTORS AND INSULATION	(2.408)	1.022
SLIP RINGS	.219	.219
INFORMATION MANAGEMENT & CONTROL	(0.050)	(0.050)
DATA PROCESSING	0.021	0.021
INSTRUMENTATION	0.029	0.029
TOTAL ARRAY, DRY	13.306	11.670
ANTENNA SECTION		
STRUCTURE & MECHANISM	(1.486)	(1.486)
PRIMARY STRUCTURE	.183	.183
SECONDARY STRUCTURE	.972	.972
ANTENNA	.14	.14
MECHANISM	.191	.191
THERMAL CONTROL	(2.457)	(2.457)
KLYSTRON COOLING	.851	.851
INSULATION	.557	.557
RADIATOR	1.049	1.049
MICROWAVE POWER	(7.012)	(7.012)
KLYSTRONS	4.250	4.250
ATT. SEN. ELECTRONICS & PHASE CONTROL	.142	.142
WAVEGUIDES	2.620	2.620
POWER DISTRIBUTION & CONTROL	(4.516)	(4.516)
POWER CONDITIONING EQUIPMENT	2.466	2.466
POWER DISTRIBUTION	(2.050)	(2.050)
CONDUCTOR & INSULATION	(1.904)	(1.904)
SLIP RING BRUSHES	(.139)	(.139)
INFORMATION MANAGEMENT & CONTROL	(.630)	(.630)
DATA PROCESSING	.380	.380
INSTRUMENTATION	.250	.250
TOTAL ANTENNA SECTION	16.101	16.101
TOTAL SPS DRY	29,407	27.771
GROWTH 25%	7.352	6.943
TOTAL SPS DRY WITH GROWTH	36.759	34.714

space frame antenna primary structure would encounter severe heating from the klystron collector (radiation from the rear of the antenna). High temperature composites would be necessary to provide the needed structural strength. This is not a problem with the tension web concept. Each of the concepts shown could be adapted to either the tension web or space frame antenna design.

ROCKWELL BASELINE

TENSION WEB

REFERENCE CONFIGURATION -
TENSION WEB

BASELINE CONFIGURATION -
SLIP RINGS NOT DIRECTLY
OVER ANTENNA

SAPCE FRAME

REFERENCE CONFIGURATION -
SPACE FRAME

BASELINE CONFIGURATION -
SPACE FRAME
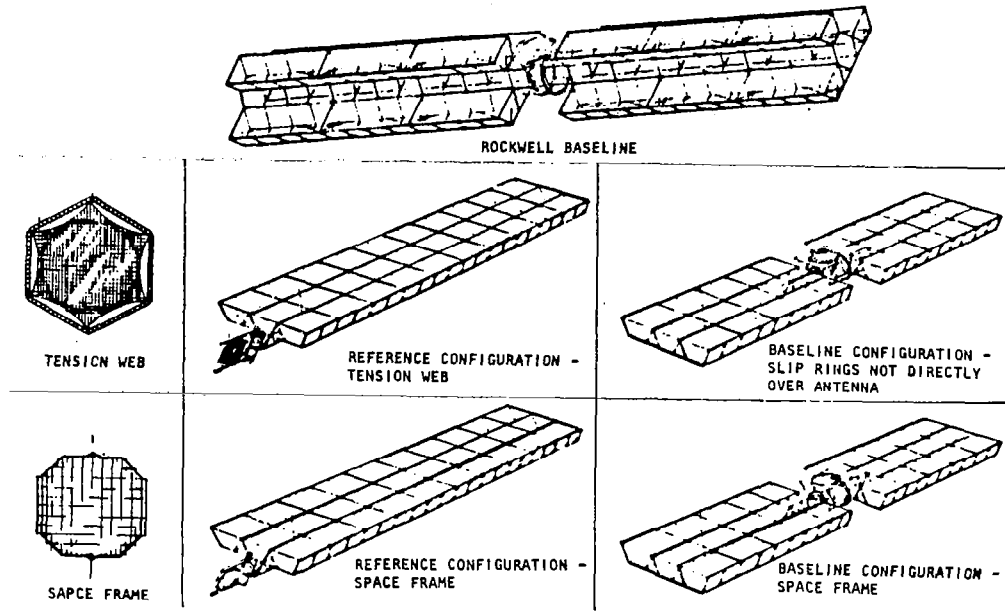
Figure 1.1-8. Antenna Design Concepts

SUBARRAY

KLYSTRON TUBE

ROCKWELL BASELINE "POKE THROUGH"
MECH MODULE PROVIDES EARTH-SIDE
HEAT REJECTION

ROCKWELL ALTERNATE MECH MODULE
PROVIDES EARTH SIDE & STRUCTURE SIDE
HEAT REJECTION

(PENTAHEDRON
SECONDARY STRUCTURE)

(PRIMARY STRUCTURE NOT SHOWN)

BOEING SUBARRAY INSTALLATION
PROVIDES STRUCTURE-SIDE HEAT REJECTION
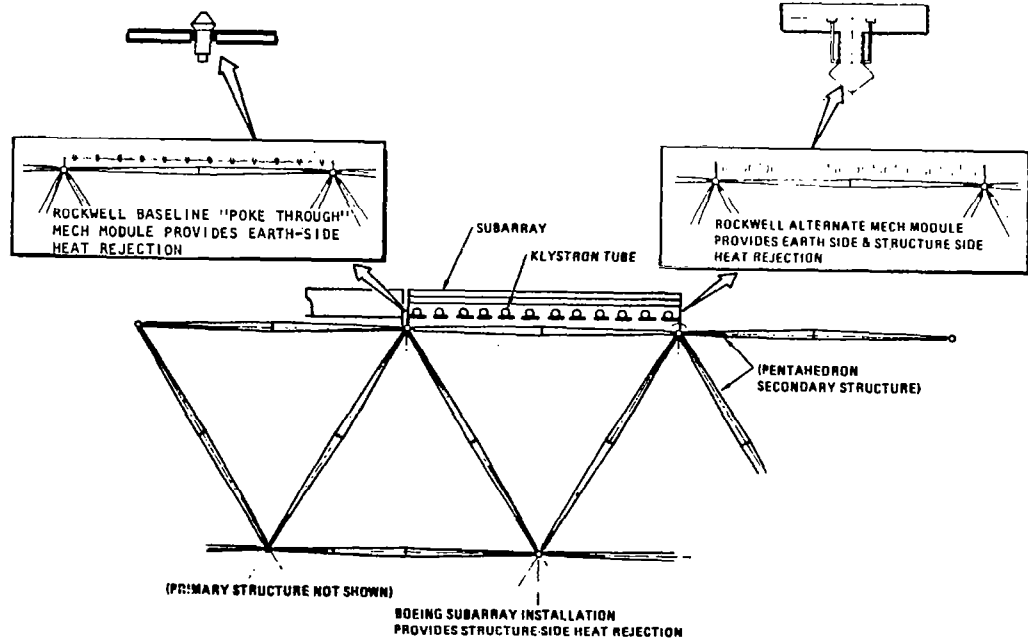
*Figure 1.1-9. RF Heat Rejection Options with
Space Frame Antenna*

1-13

Studies of attitude control and stationkeeping indicated that little difference in total thrust and propellant requirement exists among the various concepts. This is due to the dominance of the east-west stationkeeping requirements caused by solar pressure. East-west stationkeeping is required to assure non-interference of an SPS with another SPS or another satellite. If east-west stationkeeping thrust is constantly applied, all other attitude control and stationkeeping requirements can be satisfied by combined ion-thruster applications. Additionally, some relief can be obtained from efficiency losses due to solar seasonal variations by inclining the satellite up to 9° toward the sun. This is another "free" benefit obtained concurrent with east-west stationkeeping.

Eight different satellite configuration options that were studied are shown in Figure 1.1-10. These configurations were evaluated to obtain a better understanding of the impacts of solar cell selection (GaAs versus Si), antenna mounting location (end versus center), number of troughs (range from 3 to 10), concentration ratio (CR=2 versus nonconcentrated) and radiation degradation assumption (annealable versus non-annealable). For these studies, solar cell and power distribution efficiencies were held constant, as was the antenna mass.
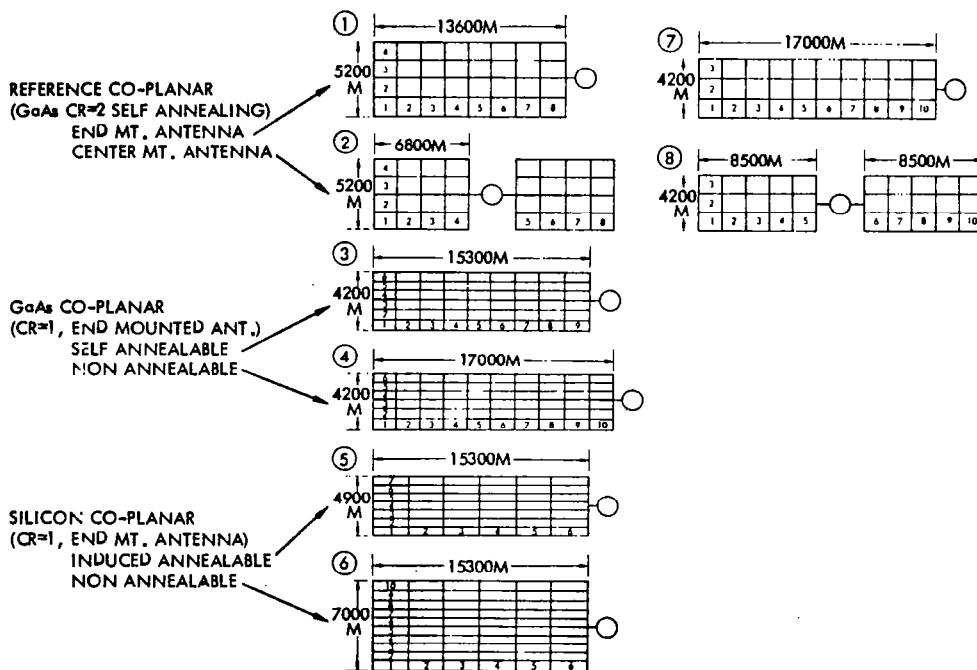
Figure 1.1-10. Satellite Configuration Options

The summary data for each of the eight configurations is given in Table 1.1-7. The first Quarter baseline (2 Tier configuration) data provides a reference. Options 1 and 2 are GaAs CR=2 for an end mounted and a center mounted antenna. Options 6 and 7 differ from 1 and 2 in that a narrower width is evaluated (i.e., 3 trough wide versus 4). Options 3 and 4 are for GaAs CR=1 evaluating annealable and nonannealable assumptions. Similarly, options 5 and 6 are for Si CR=1. The data shows a negligible difference between 4 trough

Table 1.1-7. Satellite Configuration Option Comparison Data
~ 5 GW Utility Interface

CONFIGURATION	1	2	3	4	5	6	7	8	FIRST Q BASELINE
CELL MATERIAL	GaAs	←	←	←	Si	←	GaAs	←	←
CONC RATIO	2	←	←	←	←	←	2	←	←
ANT MOUNT	END	CENTER	END	←	←	←	↑	CENTER	↑
RADIATION DEGRAD FACTOR	.96	←	↑	.84	.96	.70	.96	↑	↑
CELL OUTPUT (W/M²)	362.7	←	218.2	190.9	182.9	133.4	362.7	↑	336.6
SOLAR CELL AREA (10⁶ M²)	28.4	←	47.2	53.95	56.3	77.2	28.4	↑	30.6
REFLECTOR AREA (10⁶ M²)	57.6	←	←	←	←	←	57.6	↑	61.2 (650)
BAY DIMENSIONS (M)	700 X 1700	←	←	←	700 X 2550	←	750 X 1700	←	600 X 1600
NUMBER SOLAR CELL BAYS	4 X 8 = 32	←	6 X 9 = 54	6 X 10 = 60	7 X 6 = 42	10 X 6 = 60	3 X 10 = 30	←	3 X 12 = 36 (1350)
REFL BAY DIMENSION (M)	1300 X 1700	←	←	←	←	←	1400 X 1700	←	1250 X 1600
PLAN FORM (M)	5200 X 13600	←	4200 X 15300	4200 X 17000	4900 X 15300	7000 X 15300	4200 X 17000	←	3850 X 19200
PLAN FORM AREA (10⁶ M²)	70.72	←	64.3	71.4	74.97	107.1	71.4	←	73.92
NO. SWITCHGEAR (ON ARRAY)	1120	←	1890	2100	2436	3480	1140	←	1260
COLLECTOR ARRAY (10⁶ KG)									
STRUCTURE & MECH	2.156	←	2.043	2.168	2.230	2.791	2.156	←	3.825
SOLAR PANELS	7.258	←	11.897	13.595	23.988	34.506	7.258	←	7.722
SOLAR REFLECTORS	1.182	←	2.879	2.545	3.058	—	1.182	←	1.108
POWER DISTRIBUTION	2.719	1.55	.350	.389	.408	3.87	3.03	1.272	1.081
ATT CONTROL/IMS/ROT JT	.385	←	↑	↑	—	.583	.385	↑	.385
	(13.699)	(12.53)	(17.259)	(18.697)	(29.684)	(41.750)	(14.011)	(12.253)	(14.127)
ANTENNA SECTION	16.297	←	←	←	←	←	←	←	↑
SUBTOTAL	29.996	28.827	33.556	34.994	45.981	58.047	30.308	28.55	30.424
25% GROWTH	7.499	7.206	8.389	8.749	11.495	14.512	7.577	7.137	7.606
TOTAL	37.495	36.033	41.945	43.743	57.476	72.559	37.885	35.687	38.029

width and 3 trough width in terms of mass (<400,000 kg). However, there is a significant mass savings for a center mounted antenna configuration (~2.0×10^6 kg). A small difference in mass is shown between annealable and nonannealable GaAs CR=1 configurations. Major mass differences are shown for the silicon versus gallium arsenide and for annealable versus nonannealable silicon configurations.

1.2 PREFERRED CONCEPTS

1.2.1 RECOMMENDED CONCEPT ALTERNATIVES

As a result of the trade studies conducted on the various reference concept alternatives, the concept illustrated in Figure 1.2-1 was recommended for point design study. This coplanar concept has a single microwave antenna located in the center of the solar array. The solar array has 3 troughs containing GaAs solar cells with flat reflectors that give a CR=2. Construction and operation of this satellite are at geosynchronous orbit.
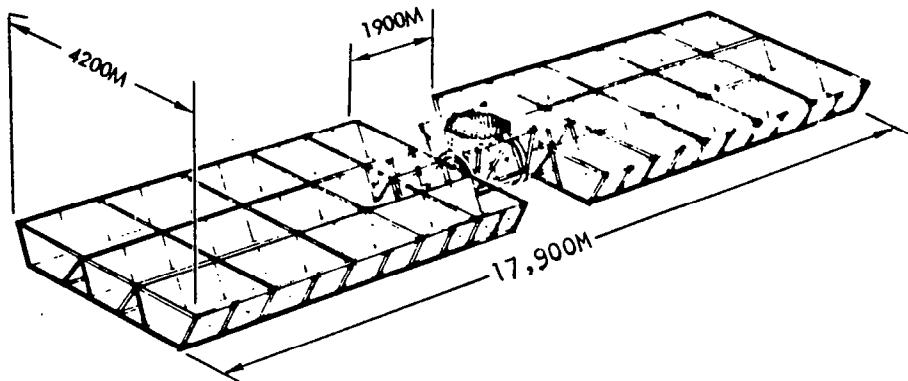
Figure 1.2-1. Recommended Satellite Concept for Point Design Study

A number of alternatives to the current DOE/NASA baseline were studied at Rockwell. Based on the results of these studies to date, the changes to the DOE/NASA baseline that are recommended are shown in Figure 1.2-2.

Results of a study of the efficiency chain indicates that the satellite has 4.61 GW output at the utility interface rather than the specified 5 GW. The Rockwell antenna layout was based on each klystron operating at 52 kW output power. Using efficiencies estimated (e.g., Exhibit A/B, 3rd Quarter), the system was sized to deliver 5.0 GW at the utility interface. Introducing updated estimates of device/element efficiencies in this design results in less power output at the utility interface. It was necessary to modify the klystron and increase its output to 56.5 kW/klystron. This new value results in slightly higher power densities at both the transmitter and the ionosphere as shown in Table 1.2-1. A redistribution of klystrons at the center of the antenna would be required to reduce these levels; however, this results in a power beam distribution function less than the optimum Gaussian.

Figure 1.2-2. Recommended Changes to NASA/DOE Reference System
- Overall GaAs Satellite Concept
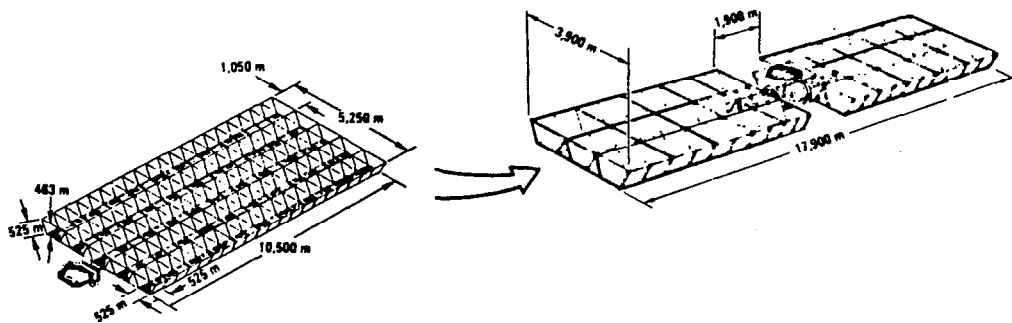
	CURRENT CONCEPT	REASON FOR CHANGE	RECOMMENDED CONCEPT
UTILITY POWER	5 GW	• EFFICIENCY CHAIN	4.61 GW
ANTENNA LOCATION	END	• LOWER MASS (2 X 10⁶ Kg) • STRUCTURE INTERFERENCE NOT A PROBLEM	CENTER
BAY GEOMETRY	5 X 20 BAYS	• EASIER CONSTRUCTION	3 X 10 BAYS
OVERALL DIMENSIONS	5.3 X 10.5 Km	• ARRAY PACKING FACTOR	3.9 X 16.0 Km
OVERALL EFFICIENCY	6.97%	• PARTIAL SUN TRACKING • SMALL CHANGES IN EFF CHAIN	6.72%
MASS	34 X 10⁶ Kg	• RESULT OF CHANGES	TBD

Table 1.2-1. Utility Interface Power

KLYSTRON POWER OUTPUT		EFFICIENCY CHAIN	UTILITY INTERFACE		POWER DENSITY AT TRANSMITTER	POWER DENSITY AT IONOSPHERE
(EACH)	(TOTAL 135,864)					
52 KW	7.07 GW	EXHIBIT A/B 3rd QUARTER	5.0 GW	(4.61 GW)	21 KW/M²	23 MW/CM²
54.3 KW	7.39 GW	EXHIBIT A/B 4th QUARTER	5.0 GW	(4.81 GW)	21.9 KW/M²	24 MW/CM²
56.5 KW	7.676 GW	EXHIBIT C 1st QUARTER	5.0 GW	(5.0 GW)	22.9 KW/M²	25 MW/CM²
( ) = USING EXHIBIT C 1st QUARTER EFFICIENCY CHAIN						

Studies of the overall concept indicate that 3 troughs are preferred
with a center-mounted antenna. Three troughs are preferred primarily because
of the increased size of the construction base as the number of troughs in-
creases. The center mounted antenna saves about 2 million kg of mass as com-
pared to the end-mounted antenna. The satellite system end to end efficiency
chain is continuously updated to reflect the latest values. The efficiency
values used in the Rockwell study were compared to the values used in the
NASA/DOE reference design for both GaAs and Silicon. These comparative effi-
ciencies are listed in Table 1.2-2. The major variations in efficiency values
are in the seasonal variation, margin, switchgear factor, antenna power dis-
tribution, rectenna energy collection, and ground interface. The array design
factor is significantly different for the Silicon design. The recommended
changes in satellite concept definition result in new planform dimensions,
solar blanket area, and mass statement.

1-17

Table 1.2-2. Efficiency Comparisons

EFFICIENCY FACTOR	NASA/DOE REFERENCE GaAs	ROCKWELL STUDY ALTERNATIVE	NASA/DOE REFERENCE Si	ROCKWELL STUDY ALTERNATIVE
SOLAR ARRAY				
SUMMER SOLSTICE	.9675	(.975)	.9675	(.975)
SEASONAL VARIATION	.91	.968	.91	.968
REFLECTOR REFL DEGRAD	.915	.915		
SOLAR CELL EFF AT AMO (28 C)	.20	.20	.173	.173
CELL TEMP DEGRAD (113°C)	.908	.908 .1335	.954	.954
ARRAY DESIGN FACTOR	.901	.89	.951	.89
UV & RADIATION DEGRAD	.96	.96	.9273	.9273
MARGIN	–	.975	–	.975
SWITCH GEAR FACTOR	–	.997	–	.997
ARRAY PWR DISTRIB	.9368	.939 .9381	.9368	.939
SLIP RINGS	.9995	.999	.9995	.999
ANTENNA/GROUND				
ANTENNA POWER DISTRIB	.963	.932	.963	.932
DC-RF CONV	.85	.85 .7608	.85	85
TRANSMIT ANT	.9653	.96	.9653	.96
ATMOSPHERIC LOSS	.98	.98	.98	.98
RECT ENERGY COLLECTION	.89	.862 .6991	.89	.862
RF-DC CONV	.88	.89	.88	.89
GROUND INTERFACE	.97	.936	.97	.936
OVERALL EFFICIENCY %	6.97	6.49*	7.058	6.176
MPTS EFFICIENCY (dc-RF-dc) %	(63.0)	(61.4)	(63.0)	(61.4)

*NOTE: $\dfrac{\text{TOTAL DELIVERED POWER}}{\text{TOTAL INTERCEPTED POWER}} = 5.6\%$

Three levels of configuration control can be applied to the point design concept: (1) basic controlling characteristics, (2) current overall system description, and (3) subsystem descriptions. The basic controlling parameters are relatively rigid and changed only at the highest program levels. The overall system characteristics are updated only occasionally; e.g., semi-annually. The subsystem descriptions form the basis for the overall system characteristics and changed as required by justifying studies.

1.2.2 BASIC CONTROLLING CHARACTERISTICS

A summary of the NASA/DOE reference satellite configuration characteristics are given in Table 1.2-3. This data was taken from the Reference System Report, United States Department of Energy and the National Aeronautical and Space Administration, October 1978. Matched against these reference characteristics are the major Rockwell study alternatives. Under the basic parameters, a laser transmission concept is being evaluated. Data is primarily being developed to aid in a determination of its potential environmental acceptability. All other basic parameters are similar to the reference NASA/DOE baseline.

1.2.3 CURRENT OVERALL SYSTEM DESCRIPTION

The current Rockwell point design is sized to deliver 4.61 Gigawatts to the utility interface. The utility interface was evaluated along with alternative satellite configurations, e.g., 3 trough planar array with a center mounted antenna. Planform, solar array blanket area, reflector area and weight characteristics shown were derived from sizing parameters such as overall (end to end) efficiency.

Table 1.2-3. NASA/DOE Reference Satellite Configuration
Characteristics

LEVEL	PARAMETER	REFERENCE CHARACTERISTICS	STUDY ALTERNATIVE
I BASIC	FREQUENCY POWER DENSITY CONSTRUCTION LOCATION OPERATIONAL ORBIT TRANSMISSION TECHNIQUE PHOTOVOLTAIC TECHNIQUE	2.45 GHz 23 MW/CM^2 (RECT. CENTER) 1 MW/CM^2 (RECT. EDGE) GEO GEO MICROWAVE GaAlAs SOLAR CELLS, CR=2 Si SOLAR CELLS, CR=1	 LASER
II SYSTEM	PWR @ UTILITIES INTERF. SOLAR ARRAY CONFIG. NUMBER OF TROUGHS ANTENNA MOUNT	5.0 GW PLANAR 5 (GaAs) END	4.61 GW 3 CENTER
	PLAN FORM	55.13 KM^2 (GaAs) 54.08 KM^2 (Si)	62.4 KM^2 65.5 KM^2
	SOLAR BLANKET AREA	26.52 KM^2 (GaAs) 52.34 KM^2 (Si)	27.0 KM^2 56.3 KM^2
	REFLECTOR AREA	53.04 KM^2 (GaAs)	54.0 KM^2
	OVERALL EFFICIENCY	6.97% (GaAs) 7.0% (Si)	6.47% 6.18%
	WEIGHT	34.16x10^6 KG (GaAs) 50.98x10^6 KG (Si)	33.02x10^6 KG 52.46x10^6 KG
	HLLV	2-STG, V-LAUNCH, SEQ. BURN, HORIZ. LAND, WINGED, REUSABLE, 425 MT TO LEO	PARALLEL BURN 227 MT TO LEO
	COTV	INDEPENDENT, REUSABLE, ELECTRIC ENGINE-POWERED	
	PLV	MODIFIED SPACE SHUTTLE ORBITER	
	POTV	2-STAGE, REUSABLE, CHEM. FUEL	
III SUBSYSTEM	POWER CONVER./DISTRIB. GaAs—BLANKET MATERIAL CELL THICKNESS CELL SUBSTRATE BOL CELL EFFICIENCY OPS TEMPERATURE BLANKET WEIGHT REFLECTOR MATERIAL BLANKET STOWAGE REFLECTOR STOWAGE PROJECTED COST	KAPTON (25 µM) 25 µM SYNTHETIC SAPPHIRE (INVERSE ORIENTATION) 20% (AMO, 28 C) 113 C (η = 18.15%) 0.252 KG/M^2 AL-KAPTON (12.5 µM) ROLL-UP ACCORDIAN-FOLD & ROLL-UP $71/M^2 (SOLAR BLANKET)	

LEVEL	PARAMETER	REFERENCE CHARACTERISTICS	STUDY ALTERNATIVE
III SUBSYSTEM (CONT.)	SI—CELL THICKNESS	50 µM	
	BOL CELL EFFICIENCY	17.3% (AMO, 28 C)	
	OPS TEMPERATURE·	36.5 C (η = 15.6%	
	ANNEALING ASSUMPTION	INDUCED (CO_2 LASER 500 C)	
	Si—PROJECTED COST	$35/$M^2$ (SOLAR BLANKET)	
	COVER	BOROSILICATE, 75 µM ELECTRICALLY BONDED (FRONT & BACK)	
	INTERCONNECTS	SILVER-PLATED COPPER (12.5 µM)	
	STOWAGE	ROLL-UP OR FOLDED	
	ARRAY OUTPUT VOLTAGE	40 TO 50 KV	
	CONDUCTORS	ALUMINUM	
	POWER TRANSFER (ROT. JOINT)	SLIP RINGS/BRUSHES	
	STRUCTURES		
	GEN. CONSTRUCTION MATERIAL	GRAPHITE COMPOSITES	
	ANTENNA CONFIGURATION	SPACE FRAME	TENSION WEB
	ANTENNA PRIMARY STRUCTURE	OPEN TRUSS, ·AUTOMATIC, FAB. IN SPACE (130 M DEEP)	
	ANTENNA SECONDARY STRUCTURE	DEPLOY. CUBIC TRUSS (9.93 M DEEP)	
	ROTARY JOINT	350 METERS DIAMETER	
	SLOTTED WAVEGUIDES	ALUMINUM	
	KLYSTRON INSTALLATION	BACKSIDE OF ANTENNA	
	ATT, CONTR, & STA, KEEPING		
	OPERATIONS	X-POP (LONG AXIS $\perp$ ORBIT PLANE)	
	ANTENNA POINTING	CMG's	
	RCS—THRUSTER TYPE	ARGON ION BOMBARDMENT	
	THRUSTER GIMBAL	INDIVIDUALLY	
	NO. OF THRUSTERS	64 (16 PER CORNER)	
	GRID LIFETIME	5000 HOURS	
	MTBF	5 YEARS	
	AVERAGE POWER	34 MEGAWATTS	
	SPECIFIC IMPULSE	13,000 SEC	
	THRUST	13 N	
	PROPELLANT STORAGE	CRYOGENIC	
	MICROWAVE		
	MICROWAVE CONVERTER	KLYSTRON	SOLID STATE
	MICROWAVE BEAM	10 dB EDGE TAPER GAUSSIAN (88% RADIATING ENERGY WITHIN 5 KM RADIUS $\perp$ BORESIGHT)	
	BEAM WIDTH	1.2 ARC MINUTES	
	AMPLITUDE TOLERANCE	±1 dB ACROSS SUBARRAY	
	ANT./SUBARRAY MECH. ALIGNMENT	±3 ARC MINUTES (GRATING LOBE CONSTRAINED TO $\leq$0.01 MW/CM^2)	
	NO. OF SUBARRAYS	7220 (10×10 M)	6993 (10.2×11.64 M)
	NO. OF POWER TUBES	36 PER SUBARRAY AT CENTER	50
		4 PER SUBARRAY AT EDGE	6
		101,552 TOTAL	135,864 TOTAL
	POWER PER TUBE	70 KW	50 KW
	FIRST SIDE LOBE	0.08 MW/CM^2	
	GRATING LOBES	<0.01 MW/CM^2	
	ERROR BUDGET—TOTAL RMS Ø ERROR	10°	
	—MAX BEAM Ø ERROR AT EDGE OF TRANSMIT ARRAY	2°	
	POWER RADIATED (TRANSMIT ARRAY)	6.72 GW	6.79 GW
	THERMAL LIMITS (ANTENNA)	22 KW/M^2	21 KW/M^2
	MPTS EFFICIENCY	63%	61.4%
	RECTENNA PANELS	MULTIPLE ELEMENTS FEEDING SINGLE DIODES	(STRIPLINE)
		OPEN-FACED	OPAQUE

1.2.4 SUBSYSTEM DESCRIPTIONS

A review of the Rockwell study alternatives show no change from the DOE/NASA reference characteristics for the power conversion/distribution subsystems. In the structure subsystem area a major study alternative is the tension web antenna structure. The Rockwell SPS microwave antenna concept evaluated and compared to the space frame is a hexagonal rigid frame (compression frame) to which is attached an adjustable cable system. The impacts on the satellite from the use of a tension web are on: mass, assembly time, and material selection. The tension web provides a very stiff and flat surface by a cable system. This configuration is thermally "stiff" but may be relatively complex in that it must be adjustable and self-compensating for effects of thermal variations. Antenna dynamics are a major area of concern requiring more detailed analysis to fully understand their impacts. The mass difference between a tension web structure and the space frame for a 1 km diameter antenna is not significant, i.e., $.067 \times 10^6$ kg tension web compared to $.250 \times 10^6$ kg space frame. The remainder of structural characteristics are the same as for the DOE/NASA reference concept. Attitude control and stationkeeping characteristics are also the same. In the microwave subsystem, two overall approaches were studied for the solid state microwave transmission concepts: antenna-mounted and solar array-mounted. The antenna mounted concepts include two means of solving the power conditioning problem: (1) series/parallel connection of the power amplifiers to obtain up to 2000 volts and (2) use of a two-stage, high power dc/dc converter approach. The parallel/series approach suffers a severely reduced efficiency because of phase matching.

Two approaches have been identified for the solar-array-mounted concepts: (1) use of high-power waveguides to collect and distribute microwave energy from array-mounted solid-state conversion devices to a reflecting antenna, and (2) a sandwich approach which has the solar cells on one side and antenna on the other side. Since the sandwich concept must be earth oriented to direct the microwave beam, it is necessary to use reflectors to direct solar energy onto the solar cells. Studies of the wave guide approach have indicated very difficult technology problems related to RF mode control. Initial studies of the reflector concept have shown that this approach is economically competitive with the reference concept although the utility power level is only 0.78 GW compared to the 5 GW reference concept.

The Rockwell alternative antenna design utilizes a nominal 50 kW klystron tube; therefore, the number of power tubes, number of subarrays and tube distribution differ from the reference concept.

Five rectenna concepts were considered: (1) dense array (billboard); (2) YAGI array; (3) short backfire array; (4) trough, and (5) square parabolas. These rectenna concept descriptions are shown in Figure 1.2-3. The trough and square parabolas concepts are severely penalized due to low aperture efficiencies. It was concluded that the dense array (billboard) stripline rectenna concept be retained for purposes of rectenna constructability analysis.

CONCEPT	NUMBER OF ELEMENTS (9 X 16 M AREA)	DESCRIPTION	COMMENTS
DENSE ARRAY (BILLBOARD)	36044	DIPOLES, λ/2 SPACING SQUARE CLUSTERS OF 49 ELEMENTS	STRIPLINE INTERCONNECT 0.5% MATCHING LOSS EDGE EFFECTS } NEEDS STUDY I^2H LOSS 0.5% TO 5.5 KM
YAGI ARRAY	9011	λ SPACING, RECTANGULAR CLUSTERS OF 12 ELEMENTS	MUTUAL COUPLING EFFECT NEEDS STUDY
SHORT BACKFIRE ARRAY	2254	2λ SPACING, SQUARE CLUSTERS OF 4 ELEMENTS	BEAMWIDTH SLIGHTLY TOO NARROW NEEDS STUDY
TROUGH	2205	18 PARABOLIC TROUGHS YAGI FEEDS SPACED λ	APERTURE EFFICIENCY <80%
SQUARE PARABOLAS	540	540 PARABOLAS YAGI FED	APERTURE EFFICIENCY < 70%

Figure 1.2-3. Alternative Rectenna Concepts

1.2.5 ROCKWELL POINT DESIGN MASS STATEMENT

The mass statement for the Rockwell recommended satellite concept (center mounted antenna) is given in Table 1.2-4. The end mounted antenna concept mass is provided along with earlier mass generated at the 2nd Quarter period of Exhibit C study. The major mass reduction is caused by resizing for a 4.61 GW utility interface. This reduces the requirement for the solar array output from 10.3 GW to 9.51 GW. The power source mass reduction is a direct result of lower array output power. The power distribution mass is the result of a complete new analysis of conductor and conditioning equipment requirements.

Antenna structure and mechanism mass is the result of calculating mass from a layout drawing of the gimbal structure and resizing of the actual antenna itself. The thermal control radiators on the antenna were incorporated into the dc converter power conditioning mass. These mass estimates were reduced by incorporating a design change to provide the 40 kV klystron power directly from the solar array, thereby, reducing power conditioning requirements. The other klystron voltages will be provided by dc converters. The power distribution mass estimate was the result of a complete new analysis of the system.

Table 1.2-4. Solar Photovoltaic Power Conversion Mass Statement – ~10^6 kg

	CO-PLANAR (3 TROUGH)		
	END-MOUNTED ANTENNA		CENTER-MOUNTED ANTENNA
SUBSYSTEM	2ND QUARTER 9/19-21/78	3RD QUARTER 9/6-7/78	4TH QUARTER 3/15/79
COLLECTOR ARRAY			
STRUCTURE AND MECHANISMS	(1.881)	(1.260)	(1.122)
PRIMARY STRUCTURE	.997	.702	.702
SECONDARY STRUCTURE	.581	.358	.187
MECHANISM	.233	.200	.233
ATTITUDE CONTROL	(0.116)	(0.116)	(0.116)
POWER SOURCE	(8.440)	(7.855)	(7.855)
SOLAR PANELS	7.258	6.818	6.818
SOLAR REFLECTORS	1.182	1.037	1.037
POWER DISTRIBUTION AND CONTROL	(2.889)	(2.603)	(0.882)
POWER CONDITIONING EQUIPMENT	0.262	0.193	.193
POWER DISTRIBUTION	2.627	2.410	.689
CONDUCTORS AND INSULATION	((2.408))	((2.367))	((0.646))
SLIP RINGS	((0.219))	((0.043))	((0.043))
INFORMATION MANAGEMENT & CONTROL	(0.050)	(0.050)	(0.050)
DATA PROCESSING	.021	.021	.021
INSTRUMENTATION	.029	.029	.029
TOTAL ARRAY, DRY	13.306	11.884	10.025
ANTENNA SECTION			
STRUCTURE AND MECHANISM	(1.486)	(0.977)	(0.977)
PRIMARY STRUCTURE	.183	.120	.120
SECONDARY STRUCTURE	.972	.599	.599
ANTENNA	.14	.067	.067
MECHANISM	.191	.191	.191
THERMAL CONTROL	(2.457)	(1.408)	(1.408)
KLYSTRON COOLING	.851	.851	.851
INSULATION	.557	.557	.557
RADIATOR	1.049	-	-
MICROWAVE POWER	(7.012)	(7.012)	(7.012)
KLYSTRONS	4.250	4.250	4.250
ATT. SEN. ELECTRONICS & PHASE CONTROL	.142	.142	.142
WAVE GUIDES	2.620	2.620	2.620
POWER DISTRIBUTION AND CONTROL	(4.516)	(4.505)	(4.505)
POWER CONDITIONING EQUIPMENT	2.466	1.901	1.901
POWER DISTRIBUTION	2.050	2.604	2.604
CONDUCTOR AND INSULATION	((1.904))	((2.587))	((2.587))
SLIP RING BRUSHES	((0.139))	((0.017))	((0.017))
INFORMATION MANAGEMENT & CONTROL	(0.630)	(0.630)	(0.630)
DATA PROCESSING	.380	.380	.380
INSTRUMENTATION	.250	.250	.250
TOTAL ANTENNA SECTION	26.101	14.532	14.532
TOTAL SPS DRY	29.407	26.416	24.557
GROWTH 25%	7.352	6.604	6.137
TOTAL SPS DRY WITH GROWTH	36.759	33.02	30.694

1-23

2.0 TRADE SUMMARY

2.0 TRADE SUMMARY

A review of the initial satellite baseline design concept was made and from this review, areas were identified for further study. The early part of the Exhibit C study focused on issues which are shown in Table 2.0-1. The trade study objectives were to reduce satellite design uncertainty and cost, mass, and design complexity. Special emphasis was placed on reducing overall cost. Following this preliminary investigation the study dealt with alternative reference satellite concepts to resolve system issues which included coplanar center mounted antenna, end mounted antenna, three and four trough and solid state microwave concepts. This section presents a summary of results of the various trade studies and analysis conducted during the course of this study.

Table 2.0-1. System Study Areas

SUBSYSTEM/ELEMENT	ANALYSIS/TRADE	PRELIMINARY STUDY CONCLUSION
SOLAR ARRAY	• SOLAR CELL PERFORMANCE • B.O.L. POWER • SOLAR CELL COST • E.O.L. REFLECTIVITY • CONCENTRATION RATIO • EARLY VERIFICATION	• GaAs SINGLE CRYSTAL CELL STILL PREFERRED ◇ BEST FOR FUTURE MAY BE GaAs MULTIPLE BAND GAP POLYCRYSTALLINE • EXCESS SOLAR ARRAY POWER SHOULD BE UTILIZED ~297 MW (AVG), 490 MW (PEAK) • GROUND STORAGE LOOKS MARGINAL • E.O.L. REFLECTIVITY INCREASED FROM 0.72 TO 0.83 ~500 MW GAIN • STAY WITH 60° SLANT ANGLE • CR-2 OFFERS COST ADVANTAGE
POWER DISTRIBUTION	• EFFICIENCY CHAIN • LOW VOLTAGE REQMT • BLOCK DIAGRAMS & POWER CONTROL ANALYSIS	• η O.A. REDUCED FROM 6.06% TO 5.78% • VERY DIFFICULT TO PROVIDE 40 KV TO 40 VDC (SOLID STATE)~0.5-1 KG/KW • INITIAL INTERFACES; START OF INTEGRATED BLOCK DIAGRAM
STRUCTURES	• NASTRAN ANALYSIS	• INCREASED NUMBER OF BRACES FOR STABILITY • PRELIMINARY STRESS ANALYSIS DESIGN LOOKS O.K.
THERMAL	• POWER CONDITIONING COMPONENT ANALYSIS • SOLID STATE DEVICE ANALYSIS	• THERMAL CONTROL RADIATORS FOR VOLTAGE CONVERTERS ~ 10^6 KG MASS INCREASE • THERMAL CONTROL CONCEPT FOR TRANSISTOR POWER MODULES ~2X DEVICE WEIGHT
ANTENNA	• SOLID STATE DC/RF CONVERSION	• 50 KW SOLID STATE POWER MODULE CONCEPT • EFFICIENCY DC-RF 78-85% WAS 85%; POWER DISTRIB. 80-95% WAS 96%
RECTENNA	• STRIP LINE VS "BACKFIRE" COAXIAL • UTILITY INTERFACE AC VS DC • DC TO AC CONVERSION CONCENTRATED VS DISTRIBUTED	• STAY WITH STRIP LINE • AC FOR < 300 MILES; DC FOR > 800 MILES • CONTROLLED QUASI-SINEWAVE DEVELOPED FROM RECTENNA ARRAY SEGMENTS LOOKS ATTRACTIVE (DISTRIBUTED CONCEPT).

2.1 SOLAR ARRAY

The major study areas for the solar photovoltaic array included: (1) solar cell performance and cost; (2) impact of seasonal variations and possible use of beginning of life (BOL) excess power; (3) reflector slant angle; (4) reflector degradation allowance; and (5) array configuration options.

2.1.1 SOLAR CELLS PERFORMANCE AND COST

Recent work at RCA Laboratories[1] has shown some promise for amorphous silicon (A-Si). Thin film solar cells, ≤ 1 µm thick, have been fabricated using metal Schottsky barriers on discharge produced amorphous silicon. Power conversion efficiencies as high as 5.5% have been obtained. The theoretical limit for the A-Si solar cell has been estimated to be ~15%.

A comparison was made between single crystal GaAlAs, single crystal silicon, and amorphous silicon configurations shown in Figure 2.1-1 to assess their relative advantages/disadvantages. The current GaAlAs solar cell configuration (Exhibit A/B) was utilized at an assumed mass of 0.252 kg/m^2. The single crystal silicon solar cell stack configuration was taken from the NASA/JSC SPS study. An amorphous silicon configuration was modeled from an RCA paper.[1] An assumption was made that the A-Si cell stack weight is equivalent to 1 mil of glass with the same blanket configuration as utilized in the GaAlAs case. In all cases a concentration ratio of 1 was used. The impact of concentration ratio will be shown later.

BLANKET DESCRIPTION	MASS
20 µm Al$_2$O$_3$	7.96
INTERCONNECTS &	3.4
GRID CONTACTS	.03
.03-.05 µM GaAlAs ⎫	
1.5 µM P-TYPE GaAs ⎬ 5 µM	2.66
4-6 µM N-TYPE GaAs ⎭	
.5-1 µM OHMS CONTACTS	4.0
13 µM FEP	2.7
25 µM KAPTON	3.6
6-12 µM POLYMER THIN COATING	0.9
	25.25 MG/CM

GaAlAs → 0.252 kg/m^2

3 MIL SILICA
2 MIL SILICON
1/2 MIL INTERCONNECTS
2 MIL SILICA

SINGLE CRYSTAL SILICON → 0.426 kg/m^2

GLASS (~25µM)
PT
UNDOPED a-Si (1µM)
n + a-Si   o
CR (1000 Å)

AMORPHOUS SILICON → 0.143 kg/m^2 *

*ASSUMES GaAs BLANKET CONFIGURATION

Figure 2.1-1. Solar Cell Configurations

---

[1]Twelfth IEEE Photovoltaic Specialists Conference, page 893

The relative performance and cost models used for these three solar cell configurations are shown in Table 2.1-1. For this comparison, the A-Si efficiency is a parameter with values ranging from 10% to 14%. The effect on mass for each configuration is shown in Table 2.1-2. The greatest mass penalty $(18.659 \times 10^6$ kg) occurs with single crystal silicon due to its greater cross section. The mass penalty for A-Si varies from 13.81×10^6 kg to 4.585×10^6 kg, depending upon its efficiency. The GaAs design is used as the reference for comparison. The major mass impact is driven by the performance model and occurs from solar cell and structural considerations due to the different solar array area requirements. Table 2.1-3 was prepared by translating these mass penalties into costs. The cost model used for this conversion is shown at the bottom of the table. The GaAs configuration is again used as the reference with the other cell costs representing cost deltas to the bracketed numbers. For example, silicon shows a cost increase of $526.3 \overline{M}$ (subtotal) added to the $4.731 \overline{B}$) GaAs cost. The cost advantage impact that comes from using reflectors (CR=2) is shown in Table 2.1-4. The Rockwell baseline SPS satellite utilizes GaAs solar cells at a concentration ratio of 2. Table 2.1-4 shows (subtotals) silicon CR=1 delta cost of +$2126.73 \overline{M}$ and GaAs CR=1 delta cost of +$1572.88 \overline{M}$.

Table 2.1-1. Solar Cell Performance and Cost Models

PERFORMANCE MODEL

	SUMMER SOLSTICE		
PARAMETER	GaAs	SILICON	A-SILICON
ENERGY ONTO CELL	1319.5 W/m^2	1319.5 W/m^2	1319.5 W/m^2
CONVERSION EFFICIENCY	20%	17.33%	10% — 14%
PWR OUTPUT f(T)	(1.0) 263.6 W/m^2	(.954) 218.11	(.954) 125.9 — 176.2
ARRAY DESIGN FACTOR (.89)	234.8	194.1	112.1 — 156.8
SEASONAL VARIATION (.91)	213.7	176.6	101.9 — 142.7
ENVIR DEGRAD	(.96) 205.2	(.85) 150.1	(.85) 86.6 — 121.2

(   ) = PERFORMANCE DEGRADATION FACTOR
NOTE: AMORPHOUS SILICON THEORETICAL EFFICIENCY ~15%

COST MODEL

SOLAR CELL CONFIGURATION	CELL/BLANKET MAT'L $/m^2	CELL PROCESS $/m^2	BLANKET PROCESS $/m^2	TOTAL $/m^2
GaAs/Al$_2$O$_3$	36.815	17.00	17.00	70.815
SILICON	13.251	17.00	17.00	47.251
A-SILICON	3.096	17.00	17.00	37.096

*ADL REFERENCE (COMPARISON)

TOTAL $/m^2
67.0
53.0
—

MATERIAL COSTS: GALLIUM - $500/KG
As - 150/KG
SAPPHIRE - 325/KG
SILICON - 60/KG
OTHERS - 20/KG

*REFERENCE: "EVAL OF SOLAR CELLS & ARRAYS FOR POTENTIAL SOLAR POWER SATELLITE APPLICATIONS" ARTHUR D. LITTLE INC. NASA9-15294, MARCH 31, 1978

Table 2.1-2. Solar Cell Delta Mass Comparisons

| SOLAR CELL CONFIGURATION | ARRAY | | Δ STRUCTURE (10^6 kg) | Δ PDC (10^6 kg) | TOTAL Δ MASS (10^6 kg) |
	AREA (10^6m^2)	MASS (10^6 kg)			
GaAlAs/Al$_2$O$_3$	49.96	(12.59)	(5.28)	(1.845)	(19.215)
SILICON	68.27	+16.507	+1.64	+.512	+18.659
A-SILICON 10%	118.4	+4.34	+6.139	+3.33	+13.81
12%	98.65	+1.51	+4.367	+2.507	+8.38
14%	84.55	-0.5	+3.10	+1.985	+4.585

NOTES

( ) = REFERENCE MASS

STRUCTURAL MASS PENALTY = 0.087 kg/m^2 (SA)

PDC " " = $\left(\frac{A_1}{A}\right)^2$ MAIN FEEDERS

= $\left(\frac{A_1}{A}\right)$ REMAINDER

Table 2.1-3. Solar Cell Cost Summary

| COST PARAMETER | GaAs | SILICON | A-SILICON | | |
			10%	12%	14%
SOLAR CELL COST	(3.5379B)	-312.1M̄	+843M̄	+113M̄	-240.9M̄
TRANSPORTATION	(739.31 M̄)	+699.71M̄	+517.87M̄	+314.25M̄	+171.93M̄
STRUCTURE	(425.88 M̄)	+132.28M̄	+495.17M̄	+352.24M̄	+250.05M̄
PDC	(28.05 M̄)	+6.37M̄	41.75M̄	34.41M̄	33.17M̄
SUBTOTALS	(4.731 B̄)	+526.76M̄	+1897.79M̄	+813.9M̄	+214.25M̄
30% GROWTH	-	158.028M̄	569.34M̄	244.17M̄	64.28M̄
TOTAL	-	+684.79M̄	2467.13M̄	1058.07M̄	278.53M̄

COST MODEL (TFU)
TRANSPORTATION TO GEO = $37.5/kg
STRUCTURES   = $80.66/kg
CONDUCTORS   = 1.52/kg
SWITCH GEAR   = 65/kg

A key difference between amorphous silicon and crystalline is expected to be in the manufacturing process. The use of A-Si should result in much lower process costs. The effect of a lower cell process cost for A-Si is shown in Figure 2.1-2. A comparison is made between A-Si with an efficiency of 10 to 14% and fixed design costs for single crystal silicon CR=1, GaAs CR=1 and GaAs CR=2.

Table 2.1-4. Concentration Ratio Comparison ~ Delta Costs

	DELTA COST		
PARAMETER	GaAs CR=2	SILICON CR=1	GaAs CR=1
SOLAR CELL COST	(2320 $\bar{M}$)	961 $\bar{M}$	1274.6 $\bar{M}$
TRANSPORTATION	(507.75 $\bar{M}$)	935.4 $\bar{M}$	211.5 $\bar{M}$
STRUCTURE	(285.51 $\bar{M}$)	208.1 $\bar{M}$	75.58 $\bar{M}$
P DC	(16.91 $\bar{M}$)	19.5 $\bar{M}$	11.2 $\bar{M}$
SUBTOTAL	(3130.2 $\bar{M}$)	2126.73	1572.88 $\bar{M}$
GROWTH 30%	(939.1 $\bar{M}$)	638.01	471.86
TOTAL	(4069.3 $\bar{M}$)	2764.75 $\bar{M}$	1944.74 $\bar{M}$

( ) = REFERENCE COST
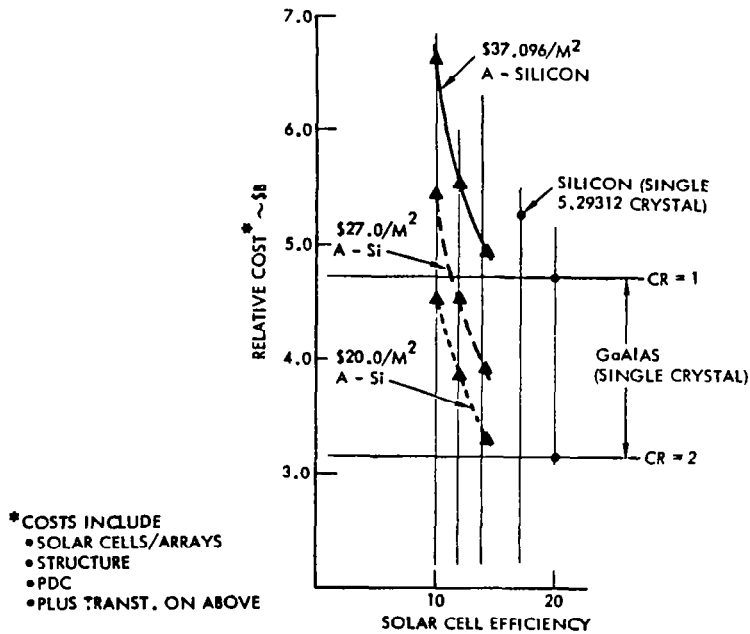
Figure 2.1-2. Solar Array Cost Comparisons

Amorphous silicon starts to look cost competitive at the higher efficiency, e.g., 14% for the lower costs (~$20/m^2). Single crystal silicon (even at high efficiency 17.3%) appears to be significantly higher in cost (Δ cost = $2.13 $\bar{B}$) compared to the GaAs CR=2 baseline.

2.1.2 SEASONAL VARIATIONS AND BEGINNING OF LIFE EXCESS POWER

Available solar array output power values are shown in Figure 2.1-3 for the different seasonal variations. A profile of the eclipse seasons is also shown. As indicated, there is approximately 10% additional power available (375 W/m^2 vs 341 W/m^2) from the solar array during spring and fall equinox periods as compared to summer solstice when taking into account change in solar input and the full 23.5° inclination angle (cosine) loss. A study was performed to assess potential worth of this excess power. Two possibilities for utilizing this energy exist: (1) size the satellite to deliver on a continuous basis all available power to the utility grid (this means that the grid must act as a variable demand), and (2) include a ground storage system and deliver the excess power from storage during the grid peak demand periods. This second alternative was evaluated.

	SPRING/FALL EQUINOX	SUMMER SOLSTICE	WINTER SOLSTICE
CR_G	2.0		
SOLAR INPUT	1360.8 W/m²	1319.5	1402.0
CR (EFF.) 1.83			
ENERGY ONTO CELL	2490.3 W/m²	2414.7	2565.7
TEMP. °C	125	113	119
CONV. EFF. I(T)	.176	.1818	.179
ENERGY CONVERTED	438.3 W/m²	438.5	459.3
ARRAY DESIGN FACTOR (.89)	390.087	390.265	408.78
SEASONAL VARIATION (.91)		355.14	371.99
ENVIR. DEGRAD. (.96)	374.48	340.94	357.11
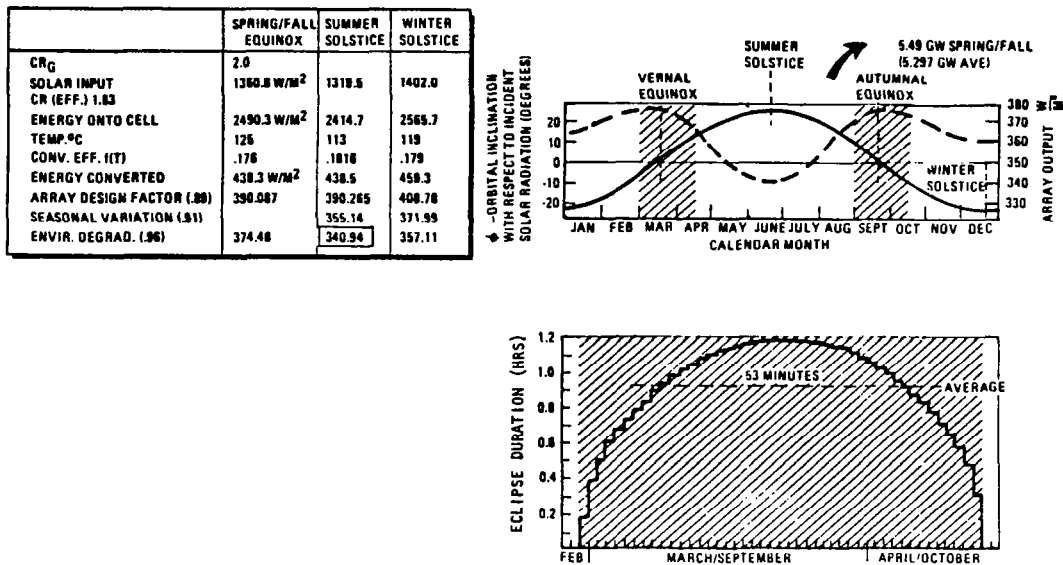
Figure 2.1-3. Seasonal Variations in Available Power

Based on values shown in Figure 2.1-3, it was determined that the initial baseline concept had the potential to provide to the utility interface 5.5 GW maximum or 5.297 GW average power (compared to a nominal 5.0 GW). Various energy storage devices were considered for the ground storage system. Energy storage capital cost estimates are shown in Figure 2.1-4 (taken from procedings of the 12th IECEC conference). A compressed air energy storage technique was used for cost trade offs. A representative daily load curve is illustrated to show the slight impact caused by delivering this excess power from storage during peak demand periods. The charge cycle consists of 24 hours at 297 megawatts average with peaks of 500 megawatts and a 10 hour discharge cycle of 490 megawatts average with peaks of 890 megawatts. To generate this excess power the satellite would need to be modified. Satellite penalties associated with this are itemized in Table 2.1-5. Klystron resizing represents the major change. The cost analysis indicates that it is potentially cost-effective to modify the satellite and utilize this excess energy. A lower cost per satellite

Figure 2.1-4. *Cost of Ground Storage*

Table 2.1-5. *Cost of Excess Power*

(~$47.3/kWe) can be achieved because the cost delta per added kilowatt is lower than the base satellite costs. The total program requirement of 600 GW could be met by 113.3 satellites, each with an average of 5.297 GW. A conclusion reached is that the SPS design criteria should specify provisions for utilization of excess solar array power.

2.1.3 REFLECTOR SLANT ANGLE

Three structural cross sections were compared to evaluate weight, cost, on-orbit assembly, and fabrication and design complexity for Vee-trough designs of 60°, 65° and 71° reflector slant angles. These cross sections are shown in Figure 2.1-5 with their configurational characteristics listed in Table 2.1-6. Performance and mass comparisons for these three configurations are given in Table 2.1-7. Weights and items affected by selection of slant angle include: array structure, solar cell area, reflector area, and conductors. The net weight variation is shown to be minor ($\leq$ 318,000 kg). Bracketed mass numbers are reference values. The cost comparisons of affected items for each configuration is shown in Table 2.1-8. As the reflector angles increase, there is an overall savings in cost due to the higher effective concentration ratio and solar cell cost savings. The net savings in mass and cost does not appear to be sufficient to overcome penalties associated with orbit assembly and fabrication and design complexity inherently greater for the larger cross sections.

The recommendation is that the present baseline, utilizing CR≈2 and 60° slant angle, be retained.

2.1.4 REFLECTOR DEGRADATION ALLOWANCE

The optical reflectance of aluminum as presented by Toulnkian[1] is shown in Figure 2.1-6. Reductions are shown in reflectance of evaporated films in the peak conversion wavelength region of GaAs which result in decreased reflection of desired solar radiation from the concentrators. It is expected that improvements will come from advanced technology developments by use of layered coatings or new aluminum mixtures. Radiation dose rates at geosynchronous orbit, 0° inclination, as functions of shield thickness are shown in Figure 2.1-7. In this 24-hour orbit, the natural Van Allen belt electrons are the primary radiation dose factor of concern. Solar flare particle and trapped fission electrons have secondary effects, except for a shield thickness ≥ 1 gm/cm^2. The 30 year SPS accumulative dosage is $<10^9$ rad. Test results reported by JPL (Wally Rowe) indicate that the threshold for mechanical reflectance degradation of kapton is 5×10^{10} rads.

An appropriate concentrator reflectivity value for SPS solar reflector design can be derived from measured data in the conversion band (spectral response) of GaAs. Data measured at Sandia[2] for an aluminized film indicate a beginning of life reflectivity of 0.87, and this value was applied to the SPS reflectors. Initial reflectivity values will not be affected by the film material. As part of the configuration update, lifetime deterioration estimates were recomputed. A math model of the meteoroid exposure levels was developed. The model indicates

---

[1]Thermo Physical Properties Handbook
[2]Reference, R. B. Pettit, NASA A77-4907A

Figure 2.1-5. SPS Structural Cross-Section—Three Trough

Table 2.1-6. Configuration Characteristics

STRUCTURAL CROSS SECTION	REFLECTOR SLANT ANGLE		
	60°	65°	71°
SATELLITE LENGTH (km)	20.9	19.35	19.11
CROSS SECTION BEAM LENGTHS (km)	11.1	11.92	13.3
CR_{GEOM}	2.0	2.286	2.576
SOLAR CELL AREA $10^6 m^2$	30.06	27.0	24.6
REFLECTOR SURFACE AREA $10^6 m^2$	60.12	82.13	119.09

Table 2.1-7. Comparison of Reflector Angles

PERFORMANCE PAR. AND MASS ELEMENT	REFLECTOR ANGLE		
	60^0	65^0	71^0
TEMPERATURE °C	113	119	125
η (T)	.1816	.179	.176
SOLAR INPUT (W/M^2)*	1319.5		
CR_{GEOM}	2.0	2.286	2.576
CR_{EFF} (EOL)	1.83	2.067	2.308
ENERGY ONTO CELL (W/M^2)	2414.7	2727.4	3045.4
ENERGY CONVERTED (W/M^2)	438.5	488.2	536.0
ARRAY DESIGN FACTOR (.89)	390.27	434.5	477.0
SEASONAL VARIATION (.91)	355.1	395.4	434.1
ENVIR. DEGRAD (.96)	340.9	379.6	416.7
SOLAR CELL AREA $(10^6 M^2)$	30.06	27.0	24.6
REFL. RATIO TO CELLS	2.0	3.04	4.84
REFL. SURFACE $(10^6 M^2)$	60.12	82.13	119.09
DELTA MASS $(10^6$ KG)			
STRUCT. & MECH.	(3.777)	+0.001	+0.222
SOLAR BLANKET	(7.586)	-0.771	-1.376
REFLECTOR	(1.088)	+0.398	+1.067
POWER DISTR.	(1.166)	+0.054	+0.062
SUBTOTAL Δ'S	(13.617)	-0.318	-0.025

NOTE: *SUMMER SOLSTICE

Table 2.1-8. Subsystem Cost Comparison as a Function of Reflector Angle

COST IN MILLIONS OF DOLLARS (TFU)

SUBSYSTEM ELEMENTS	REFLECTOR ANGLE			COST FACTOR
	60^0	65^0	71^0	
STRUCTURES	(390.554)	+ .081	+ 17.9	$80.66/KG
SOLAR BLANKET	(1978.481)	-197.823	-352.989	$64.65/M²
REFLECTORS	(150.79)	+ 52.24	+138.4	$ 2.52/M²
WIRING	(3.64)	+ .08	+ .09	$ 1.52/KG
TRANSPORTATION	(678.525)	- 15.525	- 1.2	$37.5/KG
SUBTOTAL COST	(3201.99)	-160.947	-197.80	

NOTE: AVG COST REDUCTION FACTOR ~ .8611 TFU

REFERENCE: THERMO PHYSICAL PROPERTIES HANDBOOK

Figure 2.1-6. Aluminum Spectral Reflectance Data

that a loss of about one-half of one percent can be expected. Because of the relatively low temperatures of the reflectors, thermal cycling degradation due to eclipse passage should be slight and is estimated to be one percent. Consideration of these factors indicates that an end-of-life reflectivity value of 0.827 can be expected, i.e., BOL reflectivity = 0.872 with 30 year degradation allowance factors of: meteoroid damage = .995, thermal cycling degradation = 0.99, and radiation degradation = 0.965.

2.1.5 SOLAR ARRAY CONFIGURATION OPTIONS

Introduction

Eight different configuration options were compared (Figure 1.1-10). The reference coplanar satellite configuration, (4×8 matrix shown previously in Figure 1.1-7), was used as the starting configuration. The resulting solar array/blanket cross section was shown in Figure 1.1-7. A basic module with dimensions of 600 m wide × 750 m length is utilized in the tradeoffs. Two of these modules are combined to provide the necessary 45.5 kV to the power distribution network.

6X10⁶

TRAPPED
FISSION
ELECTRONS

10⁶

NATURAL VAN ALLEN
BELT ELECTRONS

SOLAR
FLARE
PARTICLES

10⁵

DOSE RATE

$\left(\dfrac{RADS\ (Si)}{YEAR}\right)$

- ALUMINIUM .00072 G/CM²
- KAPTON .00181 G/CM²

- SPS 30 YR DOSAGE < 10⁹ RADS
- MECHANICALS REFLECTANCE
  DEGRADATION FOR KAPTON
  5 X 10¹⁰ RADS
  (JPL - SOLAR SAIL WORK
  WALLY ROWE)

10⁴

X-RAYS

10³

10⁻²   10⁻¹   1   10

SHIELD THICKNESS $\left(\dfrac{GM}{CM^2}\right)$
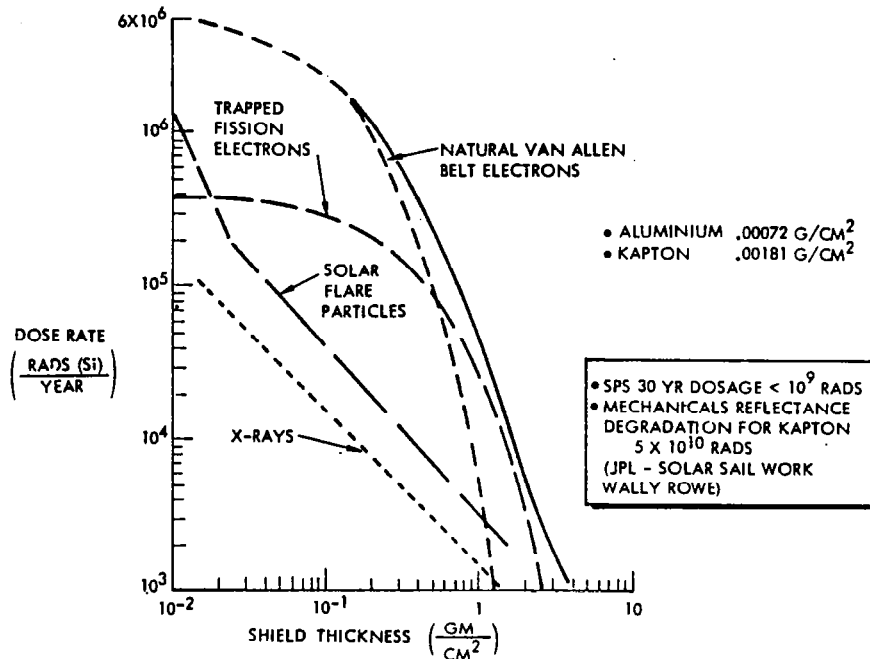
Figure 2.1-7. Radiation Dose Rates in 24 Hour
- Geosynchronous Orbit

The different configuration options compared were shown previously in Figure 1.1-10, i.e., (1) reference coplanar (4×8 matrix, GaAs, CR=2, self-annealing assumption, end mounted antenna; (2) reference coplanar (4×8 matrix), GaAs, CR=2, self-annealing assumption, center mounted antenna; (3) GaAs coplanar (6×9 matrix) CR=1, self-annealing assumption, end mounted antenna; (4) GaAs coplanar (6×10 matrix), CR=1, non-annealing assumption, end mounted antenna; (5) silicon coplanar (7×6 matrix), CR=1, induced annealing assumption, end mounted antenna; (6) silicon coplanar (10×6 matrix), CR=1, non-annealing assumption, end mounted antenna; (7) GaAs coplanar (3×10 matrix), CR=2, self-annealing assumption end mounted antenna; and (8) GaAs coplanar (3×10 matrix), CR=2, self-annealing assumption, center mounted antenna.

The following parameters were evaluated to show relative comparisons:

Efficiency. Based on the best experimental data obtained to date (Rockwell Science Center) a projected efficiency for GaAs of 22.1% can be made. The highest output for thin silicon cells that has been measured is 14.5%.[1] This was accomplished at Spectrolab by an integrated optimization of shallow junctions with optimized grid patterns, back surface fields, textured front surfaces, back surface reflectors, and higher resistivity. The SPS solar array designs are based on GaAs efficiency of 20% and silicon 17.3%. These operating efficiencies will require major technology advancements, particularly, considering the need for mass production at low solar cell cost.

---

[1]*Development of High Efficiency, Radiation Tolerant, Thin Silicon Solar Cells*, Spectrolab - JPL Contract 954600, Final Report, October 1977

2-12

The SPS solar array efficiency chain used in these trade offs is shown in Figure 2.1-8. Array orientation corrections have been made as a result of the satellite being tipped 9.02° during summer solstice, thereby, reducing the inclination angle to the sun from 23.5° to 14.48°. The comparative solar array specific power output for GaAs (CR=1, CR=2) and silicon (CR=1) are shown. These values were used to size the solar array for the comparisons. Summer solstice is taken as the sizing requirement since power output is a minimum during this period.

SUMMER SOLSTICE (WATTS/M^2)			
	GaAs (20%)		SILICON (17.33%)
	CR=2	CR=1	CR=1
SOLAR INPUT	1319.5 W/M^2		
OPERATING TEMP	113°C	28°C	36.5°C
ENERGY ONTO CELLS (T)	2414.7	1319.5	1319.5
	438.5	263.6	221.17
DESIGN FACTORS (.89)	390.27	234.8	196.85
SEASONAL FACTOR (.968)	377.78	227.28	190.55
DEGRAD FACTOR (.96)	362.67	218.19	182.93
DEGRAD FACTOR (.70)			(133.38)

• SOLAR CELL EFFICIENCY CHAIN

GaAs - CR = 2

ARRAY ORIENTATION — 96.8%

REFLECTOR
• REFLECTIVITY
• DEGRADATION
0.87 BOL   0.83 EOL

CR   BOL   EOL
η   1.9   1.83
          95%   91.5%

SWITCH GEARS (3) — 99.7%

ULTRAVIOLET & PARTICULATE DEGRADATION — 96%

ARRAY DESIGN FACTOR
• CELL EFFECTIVE AREA
• ASSY/MISMATCH — 94%

PACKING FACTOR
• CELLS
• BLANKETS — 95%

GaAlAs SOLAR CELL 113°C AVG EOC — 18.16%

Figure 2.1-8. Efficiency Chain Solar Cells

Radiation Degradation. The solar array electrical output is affected by the on-orbit environment which includes trapped particle radiation, solar flare proton radiation, ultraviolet radiation, and the temperature cycling associated with eclipse seasons. A composite 30 year GEO environment model is shown in Figure 2.1-9.

This model was developed in the Exhibit A/B study. A major contributor to the environmental model is solar flare protons. Estimated values were obtained by averaging the integral flux values for the five worst years of the 19th and 20th solar cycles and multiplying by 1.35 to allow for the six quiet years of the solar cycle. The values for a 11 year cycle are then multiplied by a factor of 3 to obtain a 30 year model. The natural trapped particle radiation environment was obtained from the "Solar Cell Radiation Handbook", TRW Report 21945-6001-RV-00. The values for damage equivalent 1 Mev electrons are taken from "A proposal for Global Positioning Satellite Electrical Power Subsystem", General Electric, Space Division Proposal No. N-30065, February 28, 1974.

The effects of 1 Mev electron radiation on solar cell power for 1-3 ohm cm N/P silicon solar cells of varying thickness is shown in Figure 2.1-10. These data are from "The Solar Cell Radiation Handbook", TRW Report 21945-6001-RV-00.

2-13
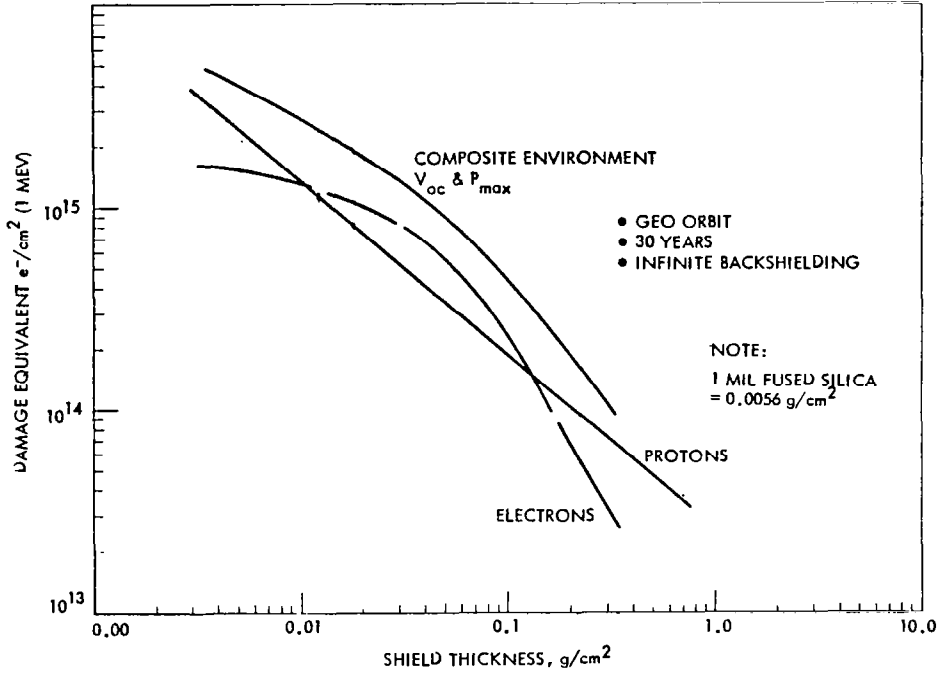
Figure 2.1-9. Solar Cell Damage Equivalent 1 Mev
Electron Fluence Versus Shield Density
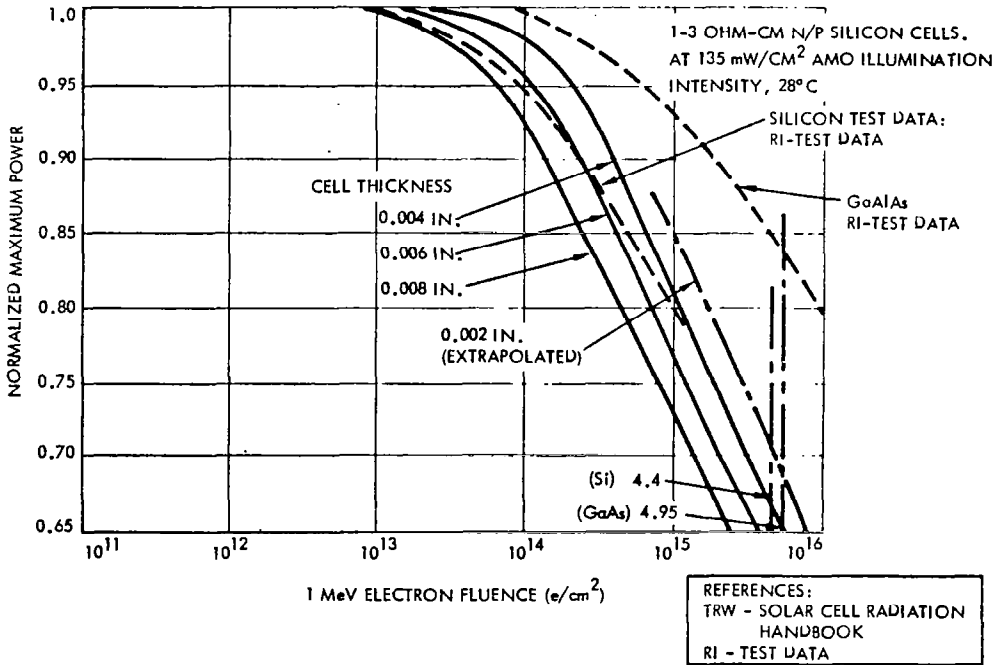
Figure 2.1-10. Normalized Maximum Power Versus
1-Mev Electron Fluence

The data shown are a composite of data from several sources and represents the mean behavior of N/P conventional solar cell production in the United States. Solar cells produced with significant changes in composition may not show the same radiation loss factors. The significance of the data shown is that thinner solar cells, percentage wise, show less radiation degradation than thicker solar cells. The data shown is obtained by dividing solar cell maximum power at each radiation fluence by the cell output (different for each cell thickness) before irradiation.

Gallium arsenide and silicon cell test data results from tests conducted by Rockwell are shown by the dash lines to provide a comparison.

Voltage. The open circuit voltage and maximum power voltage curves of the GaAs cells are shown in Figure 2.1-11. The curves are representative of experimental results obtained at the Rockwell Science Center and Hughes Research Laboratory in their GaAs solar cell development programs. The relationship for the maximum power output voltage is $V_{mp} = -0.0018$ (V/°C)T $+0.9$ V. At the solar array operating temperature of 125°C, the maximum power voltage of the cell is 0.69 V. A reference V_{mp} for silicon is 0.475 V. These values were to determine the overall blanket dimensions. A basic 750 meter length was selected for voltage considerations. The width of the blanket is dictated by structural considerations and the desire to stay with modular blanket widths of 25 meters. Configurations 7 and 8 require 650 meter wide solar blankets to stay within a 3 bay wide configuration. All other configurations are 600 meters widths. The silicon configuration requires 3 solar blankets in series to provide the necessary distribution voltage (compared to two blankets in series for GaAs).

Mass. The Si cell for advanced applications are projected to have a mass of from 0.53 to 0.338 kg/m^2. A mass of 0.427 kg/m^2 was used in the comparison. GaAs solar cells mass projections are from 0.304 to 0.228 kg/m^2. In this study, a mass of 0.252 kg/m^2 was used. These values are taken from the results of the Exhibit A/B study.

Configuration Option Comparisons

The summary comparison data on the eight configutation options was presented previously in Table 1.1-7. The preliminary trade results show that GaAs solar cells remain the preferred cell material (compared to silicon). This conclusion is based on GaAs having a higher efficiency (20% vs 17.3%); lower space radiation degradation (16% vs 30%); greater potential for self-annealing out of radiation damage (125°C threshold temperature vs >500°C); lower specific weight (0.252 kg/m^2 vs 0.427 kg/m^2); improved compatibility with concentrators; improved temperature coefficient; and smaller solar cell area requirement.

Silicon solar cells offer advantages in that silicon material is easily available; however, scale up is required to obtain the necessary quantity of semi-grade silicon (e.g., 11850 metric tons per 5 GW system). A more mature silicon technology exists. Gallium arsenide solar cell development will require a new industry to reclaim gallium from bauxite and to produce the required solar cell quantity of ~30×10^6 m^2 per 5 GW system.

Graph labels:
- OPEN CIRCUIT (V_{oc}) AND MAX POWER (V_{mp}) VOLTAGES (VOLTS)
- V_{oc}
- 1.09
- $V_{mp} = \dfrac{-.0018V}{°C} \times T + 0.9V$
- SCIENCE CENTERS
- V_{mp}
- HUGHES
- ($V_{mp} = .475$)
- ($V_{mp} = .28$)
- .46
- ≈ GaAs
- ≈ Si
- SOLAR CELL TEMPERATURE (°C)

Configuration diagrams:
- ←750M→ 487,500M² 650M GaAs CONFIG. ⑦ ⑧
- ←850M→ 750M 600M 700M 450,000M² 450,000M² →47.22 KV ←1700M→ GaAs CONFIGURATIONS ①, ②, ③, ④
- ←850M→ 750M 700M 600M 450,000M² 450,000M² 450,000M² →47.3 KV (42.0 KV) ←2550M→ Si CONFIGURATION ⑤, ⑥

CELL TYPE	OPS TEMP.	INITIAL CELL VOLTAGE	E.O.L. CELL VOLTAGE	VOLTAGE PER METER
GaAs	113°C	.69	.656	31.48
Si	36.5°C	.475	.438	21.02

Figure 2.1-11. Solar Panel Bay Dimensions
~ Voltage Consideration

The center mounted antenna configuration resulted in the lowest overall SPS mass. For the GaAs CR=2 center mounted configuration, power distribution mass savings ranged from 1.5×10^6 kg to 1.8×10^6 kg. Silicon CR=1 SPS mass penalties ranged from 21.8×10^6 kg to 36.9×10^6 kg depending upon annealing assumption. The GaAs CR=1 mass penalty ranged from 6.26×10^6 kg to 8.06×10^6 kg.

Mass differences between 4 trough and 3 trough width is negligible (<400,000 kg). However, the narrower 3 trough configuration is favored because of construction considerations.

The GaAs CR=2 configuration resulted in the lowest relative cost (Figure 2.1-2).

2.1.6 REFLECTIVITY PANEL TEST ANALYSIS

Literature data has shown that high film tensioning is required to obtain an adequate reflector surface which would make the concept impractical. This data was derived from small samples of reflecting material with a narrow beam of light. The small scale roughness has a great effect on the specular reflectivity. There is no data available for large scale panels.

Information is required to support the SPS solar array design using gallium-arsenide solar cells with concentration ratio greater than one. High film tensioning will have a direct impact on the structure and make the concept impractical.

2-16

A test program was initiated to determine the film stress requirements for aluminized plastic film reflectors. The major effort of this test program was accomplished by California State University - Fullerton under contract (M8M8GNS-892080E) to Satellite Systems Division of Rockwell International. Tests were performed on 18 inches square and 8 foot square panels. Sample backings were 1 mil mylar, 1/2 mil kapton and 1/2 mil teflon. All samples had 2000 angstroms of vapor deposited aluminum on the sun side. Test consisted of tensioning from 5 psi to 1000 psi (bi-lateral) and photographing a known grid pattern projected on to the imaging surface and measuring the deviation (at 0, 4, 24 and 48 hours) at each stress level.

Small samples required 400 to 1000 psi to obtain an imaging surface. The edge effect of the reinforcing tape had great effect on the tensioning required. Large samples of mylar took about 60 psi. Edge effects impacted the results. A follow-on test will be initiated to determine what impact tape splices have on the total reflectance of the panel.

Conclusion reached is that SPS design at tensioning requirements from 10-30 psi is acceptable when normalizing for edge effects (based on subjective normalization).

2.1.7   ELECTRIC ORBIT TRANSFER VEHICLE (EOTV) SOLAR ARRAY

A comparison between GaAs and Silicon solar cells was made for the EOTV requirements. The EOTV configurations are shown in Figure 2.1-12 along with a tabulation of solar array parameters and values. The silicon solar array mass is 725,904 kg compared to 263,511 kg for GaAs. This increased mass results from Si having a higher specific weight (.426 kg/m^2 vs .252 kg/m^2) and a requirement for larger solar cell area (1,704,252 m^2 vs 886,950 m^2). Note: The silicon configuration is non-concentrated while the GaAs has a concentration ratio of 2:1. The impact of reflector mass for the GaAs configurations are negligible. Note that the power output values for the array are taken at the beginning of life without degradation allowance for the space radiation environment.

The radiation environment for the EOTV was investigated and estimates made for the solar cell degradation. Trip times from LEO to GEO orbit of 90 days and 180 days were considered. The major contribution to solar cell degradation comes from trapped protons (Figure 2.1-13). Solar flares and trapped electrons were neglected. A nominal orbit inclination of 30 degrees was taken. About 8000 nmi trajectory data shows a lower inclination but the major damage would have already occurred, i.e., between 1000 and 7000 nmi. The analysis indicated that for one trip through the Van Allen belt, the radiation equivalent of 1 Mev electrons was approximately one order of magnitude greater than that received for the entire 30 year GEO operation, i.e., 5×10^{16} e/cm^2 compared to 5×10^{15} e/cm^2. Radiation degradations of 30-35% (Gallium Arsenide) and 50-55% (Silicon) are estimated for LEO to GEO using current SPS solar cell stack configurations and without annealing assumptions (Figure 2.1-14). The annealing characteristics of the solar cells is a critical consideration to an EOTV concept. This issue is identified for early resolution.
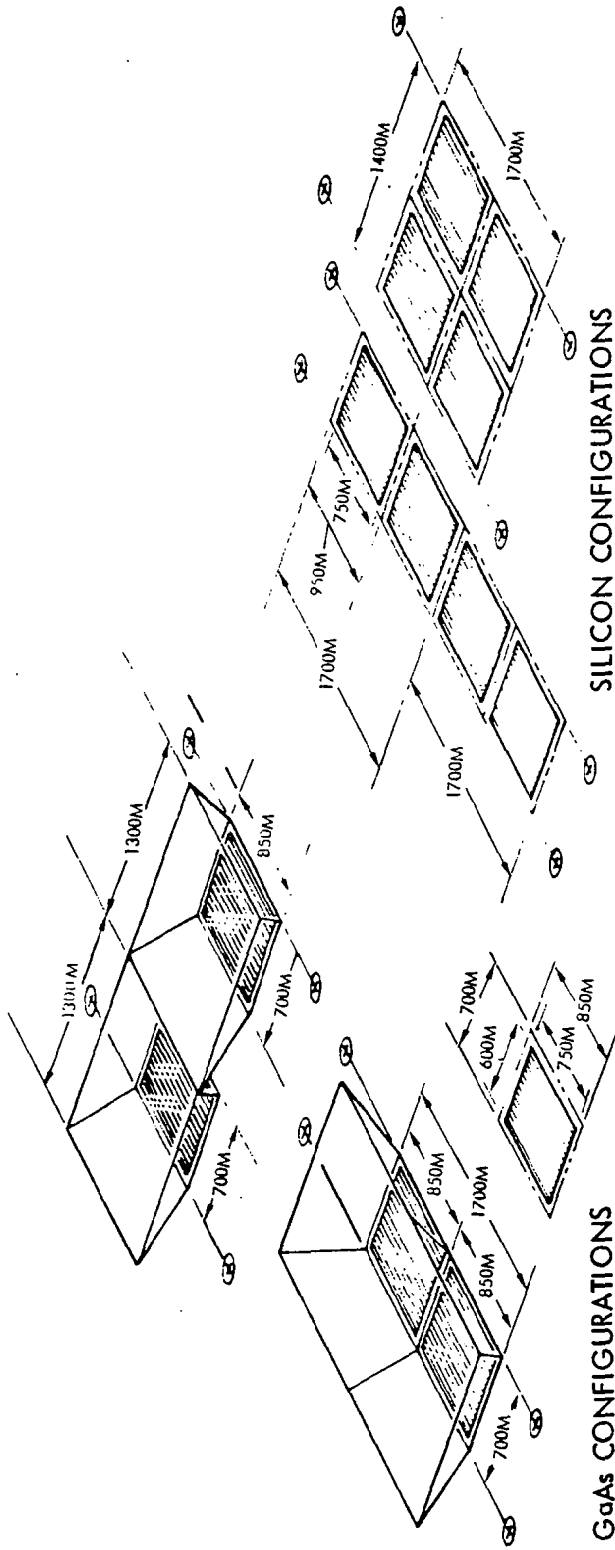
SILICON CONFIGURATIONS

GaAs CONFIGURATIONS

PARAMETER	GaAs	SILICON
SOLAR INPUT	1319.5 W/M^2	1319.5 W/M^2
ENERGY ONTO CELLS	2414.7 (CR = 1.83)	1319.5 (CR = 1)
η (T)	424.98 (17.6%)	221.17 (16.74%)
DESIGN FACTOR	278.24 (.89)	196.85 (.89)
POWER OUTPUT (ARRAY)[1]	335.48 MEGAWATTS	335.48 MEGAWATTS
AREA REQM'T	886,950 M^2	1,704,242 M^2
ARRAY AREA	900,000 M^2	1,800,000 M^2
ARRAY WEIGHT (KG)	223,511 (.252 KG/M^2)	725,904 (.426 KG/M^2)
REFLECTOR AREA	2,210,000 M^2	-
REFLECTOR WEIGHT	40,000 KG	-
SUBTOTAL	263,511 KG	725,904 KG

NOTE:
[1] NO SPACE DEGRADATION ALLOWANCES

Figure 2.1-12. EOTV Solar Array Comparison
(GaAs Versus Si Solar Cells)

TRAPPED PROTONS
ANNUAL.EQUIVALENT
30° INCL. CIRCULAR ORBIT
1.67E-02 GM/CM^2 SILICA

TRAPPED ELECTRON ANNUAL
EQUIV. <10^{14}

WORST CASE ANNUAL (1980-1982)
PREDICTED EQUIVALENT 1MEV
ELECTRON FLUENCE FOR SOLAR
FLARES

REFERENCE:
*Solar Cell Radiation
Handbook*—JPL PLUBLI-
CATION, 77-56

DAMAGE EQUIVALENT $^{-e}$/cm^2 (1 Mev)

10^{17}

10^{16}

10^{15}

ORBIT ALTITUDE, 10^3 nmi

2   4   6   8   10   12   14   16   18   20   22
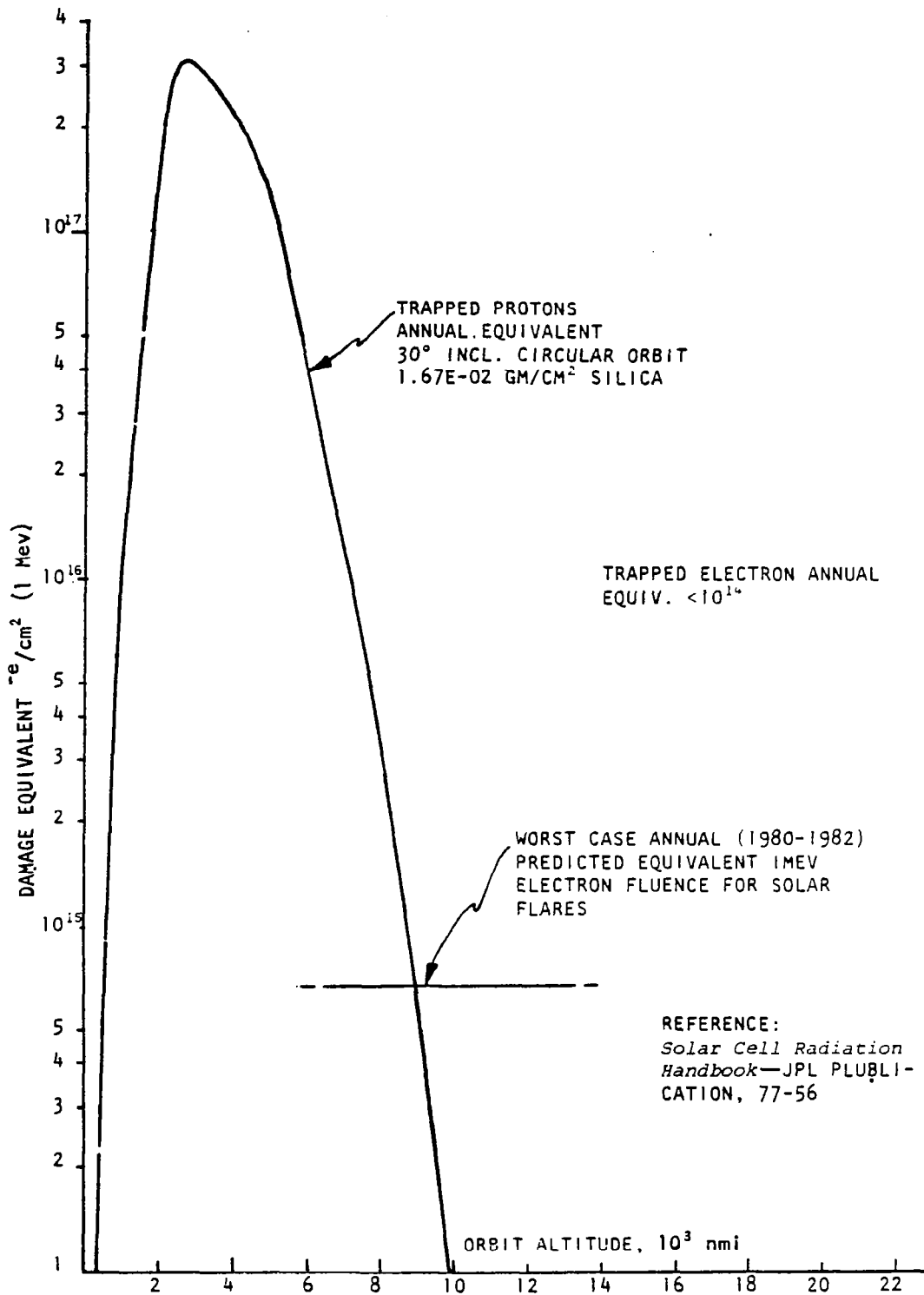
Figure 2.1-13. *Equivalent 1 Mev Electrons for Voc and P$_{MAX}$
(Infinite Back Shielding)*

2-19
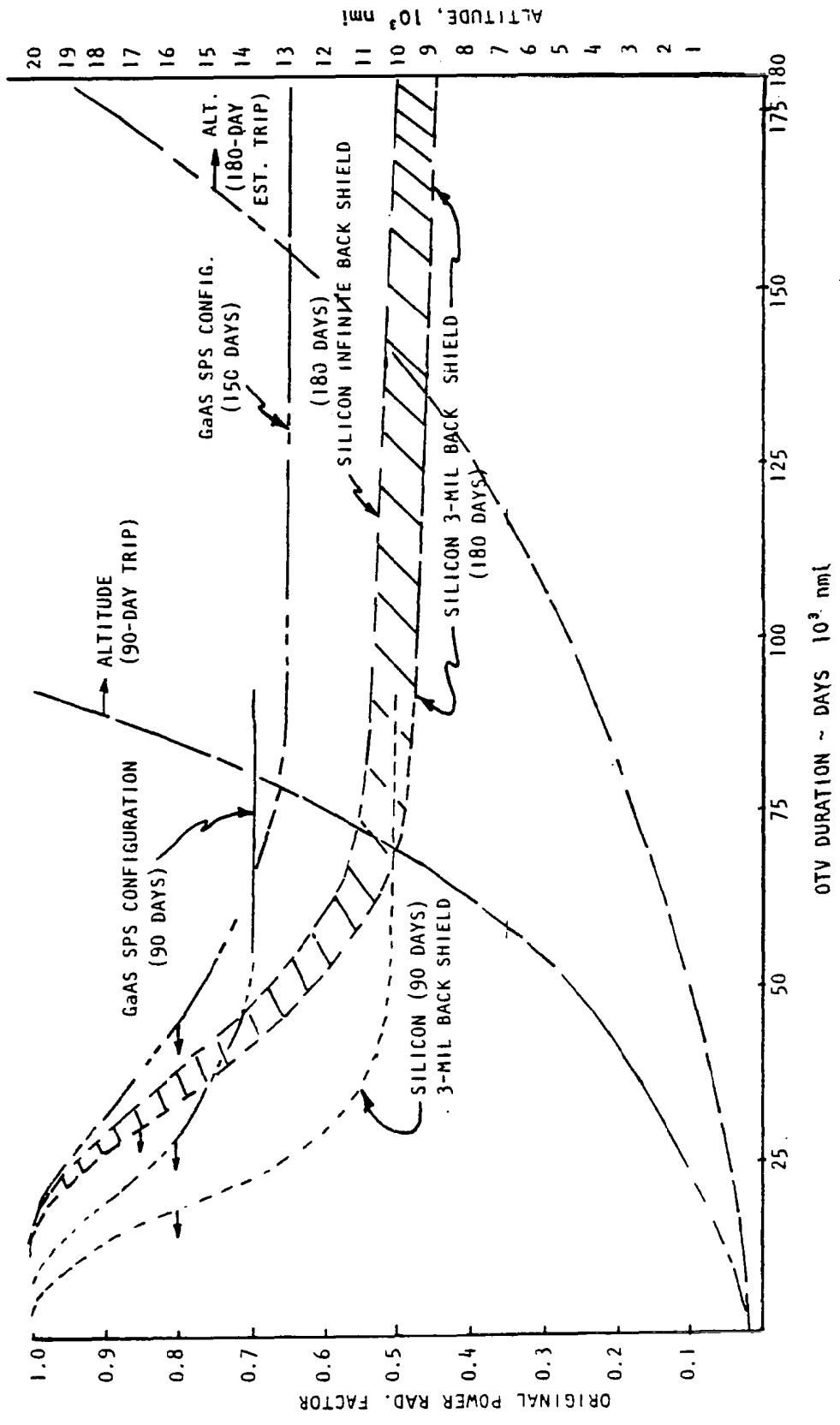
Figure 2.1-14. Solar Array Power Factor OTV Versus Days

2.2 POWER DISTRIBUTION

The power distribution and control subsystem (PDS) trade studies dealt with overall distribution efficiency comparisons, conductor weights, power distribution technology, solid state antenna power distribution, and electric orbit transfer vehicle (EOTV) power distribution. Ground receiving station power distribution is considered in Section 2.7.

2.2.1 EFFICIENCY CHAIN

The satellite system end to end efficiency chain is continuously being updated to reflect the latest design. The Rockwell alternative SPS concept is sized to deliver 4.61 GW at the utility interface. The solar array efficiency chain was shown previously in Figure 2.1-8. To provide 4.61 GW at the utility interface requires a solar array output of 9.52 GW. The efficiency chain for the remainder of the system, i.e., rotating antenna and ground reception, is shown in Figure 2.2-1. The transmission efficiency values of primary interest are: 6% line loss on the solar array, 2% on the antenna, and 2% at the ground receiving station. Additional efficiency values include: klystron dc-RF conversion efficiency of 85%; rectenna RF to dc conversion efficiency of 89%; and power conversion efficiency (dc-dc) of 96%. An end to end efficiency comparison was made between the Rockwell study alternative efficiency values for both GaAs and Silicon and the NASA/DOE reference concepts. The major items are listed and shown previously in Table 1.2-1. There are some obvious inconsistencies; however, generally the major differences result from either the degree of conservativeness employed or from design detail deltas. For example, the antenna power distribution (.963 vs .932) and ground interface differences (.97 vs .936). By examining details of the Rockwell efficiency chain dc-dc converters (or dc-ac converters) with an efficiency factor of 0.96 combined with switchgear and feeder losses produce an efficiency factor of 0.932 for antenna power distribution and 0.936 for the ground interface compared to 0.963 and 0.97 in the reference configuration. It is obvious that the differences reflect both design details (switchgear arrangements) and degree of conservatism (selection of dc-dc conversion efficiencies).
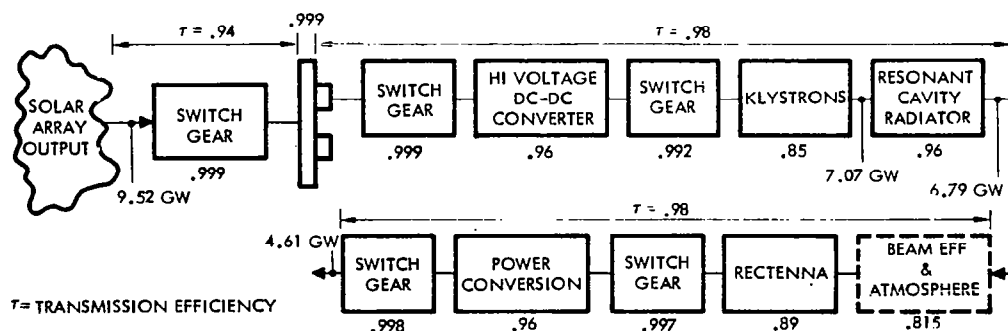
Figure 2.2-1. *Efficiency Chain - Rotating Antenna*
and Ground Reception

Overall system efficiency is taken to be the product of the end to end efficiency factors shown, with the exception that for the Rockwell alternative the summer solstice factor is not included in the overall efficiency. That is to say, effect of summer solstice are taken into account in sizing the solar array in that the solar input value used in the sizing is the summer solstice value, i.e., 1319.5 watts/m^2. An alternative (simplified) method that might be used for calculating overall efficiency is to take the ratio of total delivered power at the utility interface and total intercepted solar power. Using this ratio the Rockwell alternative GaAs configuration overall efficiency is 5.6%. This ratio does provide an indication of configuration plan area effectiveness in addition to end to end efficiency factors.

The difference in seasonal variations are the result of design approaches. Attitude control and stationkeeping concepts that were studied by Rockwell in Exhibit A/B employed a Y-POP reference orientation with collector cosine losses up to 9% resulting from ±23.5° seasonal inclination. Analysis, during the Exhibit C study, showed that a significant advantage can be realized if the spacecraft is pointed more directly toward the sun. A roll angle of 9.0° can be realized with no propellant penalty or loss of control authority. Essentially, this is achievable by simultaneously countering the large gravity gradient torques and the solar pressure forces through use of the thrusters at one end of the spacecraft. With this bank angle, the collector seasonal variation factor (cosine loss) is reduced from 0.91 to 0.968.

2.2.2 CONDUCTOR WEIGHT

A number of power distribution configurations have been reviewed. Of the configurations reviewed, two were selected for which power distribution masses were calculated. The evaluated are: (1) end mounted antenna and (2) center mounted antenna (Figure 2.2-2).

Analysis

The electrical power distribution subsystem is configuration dependent. Basic elements of the solar array power distribution subsystem are: secondary feeders, main feeders, summing bus, tie bar and insulation. Similarly basic elements of the antenna are risers, summing bus, main feeders and secondary feeders. An examination of the formulae for calculating the conductor weight shows that the weight is increased by the square of the length of the conductor. The formula for determining the conductor cross section is:

$$A = \frac{\gamma IL}{\Delta V}$$

The formula for weight is:

$$\omega = \rho AL$$

Where
A = cross section area
I = amperes flowing
γ = resistivity of wire
L = length of conductor

2-22
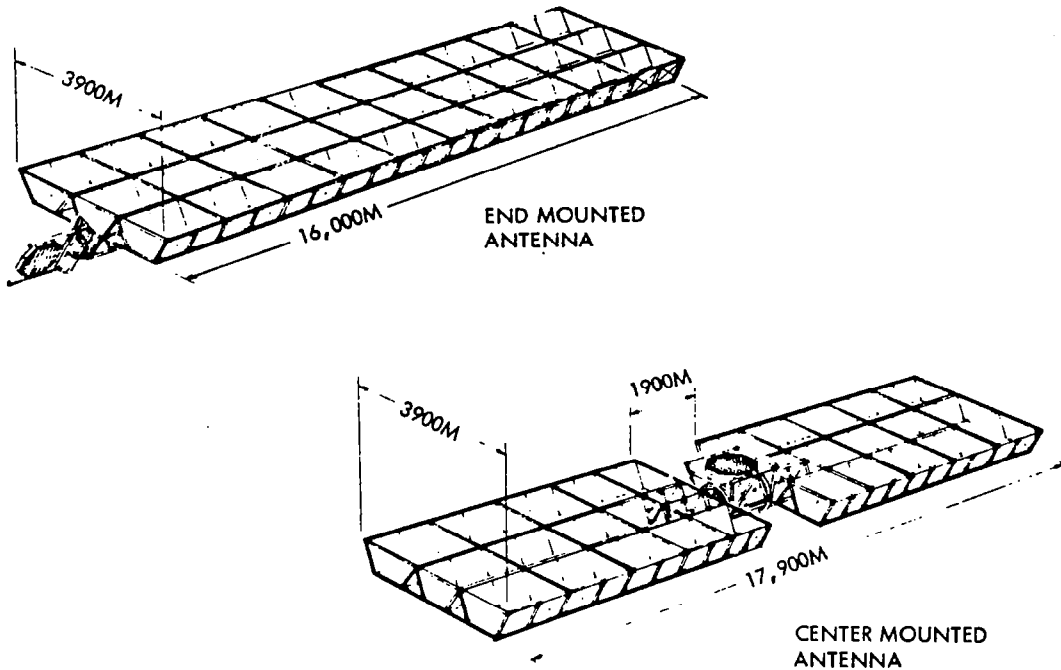
Figure 2.2-2. 3-Trough Coplanar Configurations

$$\Delta V = \text{voltage drop in conductor}$$
$$\omega = \text{conductor mass}$$
$$\rho = \text{density}$$

Therefore $\quad = \dfrac{\gamma IL}{\Delta V}(\rho L) = \dfrac{\rho \gamma IL^2}{\Delta V}$

It is seen that conductor mass varies as the square of its length. Examining the main elements of the power distribution subsystem it appears that the main feeders, tie bars and risers are impacted the most by a long, narrow configuration; while the summing bus favors a narrow configuration. The secondary feeders are not impacted to large extent by the aspect ratio of the configuration. The insulation weight is impacted by both the length of the conductor and its shape, i.e., flat or round. Round conductors require less insulation, being more compact. The round conductor also will have the lesser cooling surface for passive cooling, therefore, will become hotter, or require a greater cross section to operate at the same temperature.

Trades

Table 2.2-1 illustrates the weight differences of a long narrow (3×10 bay) versus a short-narrow (2-3×5 bay) configuration. Secondary support structure is directly effected by the amount of conductors (length) to be supported. The antenna configuration is the same for either candidate reviewed. It is seen that the summing busses, tie bars and secondary feeders are approximately the same. The desired trade-off is to design toward the array with a small aspect ratio.

2-23

Table 2.2-1. Comparison Principal Elements 3×10 Bay
versus 2-3×5 Bay Coplanar Configuration

CONDUCTORS	END-MOUNTED ANTENNA					CENTER-MOUNTED ANTENNA*				
	VOLTAGE DROP	CURRENT (AMPS)	LENGTH (M)	CROSS SECTION AREA,CM²	TOTAL WEIGHT KG×10⁶	VOLTAGE DROP	CURRENT (AMPS)	LENGTH (M)	CROSS SECTION AREA, CM²	TOTAL WEIGHT (KG)
SECONDARY FEEDERS	250	306	750	0.2596	0.076	250	306	750	0.2596	0.076
MAIN FEEDER 1	1550	7258	15,300	20.26	0.502	1550	7258	6800	8.916	0.196
2			13,700	18.14	0.403			5100	6.684	0.110
3			12,100	16.02	0.314			3400	4.446	0.449
4			10,500	13.91	0.237			1700	2.228	0.012
5			8,900	11.79	0.170		7258	50	0.066	0.001
6			7,300	9.67	0.114					
7			5,700	7.55	0.070					
8			4,100	5.43	0.036					
9			2,500	3.31	0.013					
10	1550	7258	900	1.19	0.002	1550				
SUMMING BUS	800	108,870	3,250	125.08	0.220	800	54,436	3400	51.96	0.226
TIE BUS	150	36,290	850	5.82	0.205	150	18,145	1000	34.21	0.222
INSULATION					0.036					0.015

*EACH OF TWO IDENTICAL SOLAR WINGS

2-24

2.2.3 POWER DISTRIBUTION TECHNOLOGY

An industry survey of power distribution technology was made to determine what the present and future development endeavors are within the industry to extend today's state of the art (SOA) for high voltage dc to dc converters and switchgear. The companies contacted are listed in Table 2.2-2. Problems and possible solutions were discussed with each company representative. Data on eight dc-dc converter systems were obtained and taken to be representative. The specific weight (kg/kW) for these eight systems are (Figure 2.2-3): (1) 37 watt, dc/dc converter, stripped down, unable to operate in a stand alone mode; (2) 250 watt, dc/dc converter, 20-80 volt dc input; (3) 1200 watt, dc/dc converter, 28 volt dc input; (4) 1500 watt, inverter operating at 20 kHz; (5) 2400 watt, dc/dc converter, 28 volt dc input; (6) 25 kW, extrapolation of TRW unit from (5); (7) 200 kW, dc/ac/dc power conditioner for dc motor drive, 600-900 volt dc input; and (8) 1.44 GW, dc high voltage transmission link, 800 kV, 1800 amps. A projection of technology gain was made based on these system data. The projections included gains from: (1) increase in operating frequency; (2) increase in efficiency; and (3) reduction in cooling system requirements. Equivalent size and mass reductions were calculated and a second, independent technology gain projected. The initial mass allocation of the system concepts are:

Magnetics	35%
Transformers	(25%)
Inductors	(10%)
Semiconductors and Mtg.	20%
Cooling system	30%
Mechanical	15%
Total	100%

Table 2.2-2. Companies Surveyed for Power Distribution Technology Assessment

DC-DC CONVERTERS	SWITCH GEAR
AIR RESEARCH - TORRANCE, CA	ITT-JENNINGS - SAN JOSE, CA
TRW - REDONDO BEACH, CA	TRW - REDONDO BEACH, CA
WESTINGHOUSE - LIMA, OHIO	CUTLER-HAMMER - LOS ANGELES, CA
GENERAL ELECTRIC - SCHENECTADY, NY	WESTINGHOUSE - LIMA, OHIO
AEROSPACE ELECTRONICS - BOHEMIA, NY	WESTINGHOUSE - PITTSBURGH, PA
POWER MARK DIV. OF TOPAZ ELECTRONICS - SAN DIEGO, CA	HUGHES-RESEARCH - MALIBU, CA
GOULD ELECTRONICS - EL MONTE, CA	AIR RESEARCH - TORRANCE, CA
ALLIS-CHALMERS - LOS ANGELES, CA	RCA - MORRISTOWN, N.J.
CHRISTIE ELECTRONICS - LOS ANGELES, CA	COMMONWEALTH EDISON - LOS ANGELES, CA
ABBOT ELECTRONICS - LOS ANGELES, CA	HARTMAN ENGINEERING - LOS ANGELES, CA
MAGNETIC CIRCUIT ELEMENTS - MONTERY, CA	

ID	SUPPLIER	SIZE (WATTS)	SPECIFIC WEIGHT (KG/KW)	COMMENT
①	AUTONETICS	37	1.216	STRIPPED DOWN
②	AUTONETICS	250	1.268	LOW VOLTAGE INPUT
③	TOPAZ ELECTRONICS	1200	18.815	
④	AEG TELEFUNKIN	1500	1.4	(INVERTER)
⑤	TRW	2400	9.438	
⑥	TRW	25,000	1.268	EXTRAPOLATED
⑦	AIRESEARCH	200,000	N/A	GRD RAPID TRANSIT
⑧	GE	1.44 GW	N/A	GRD DC LINK
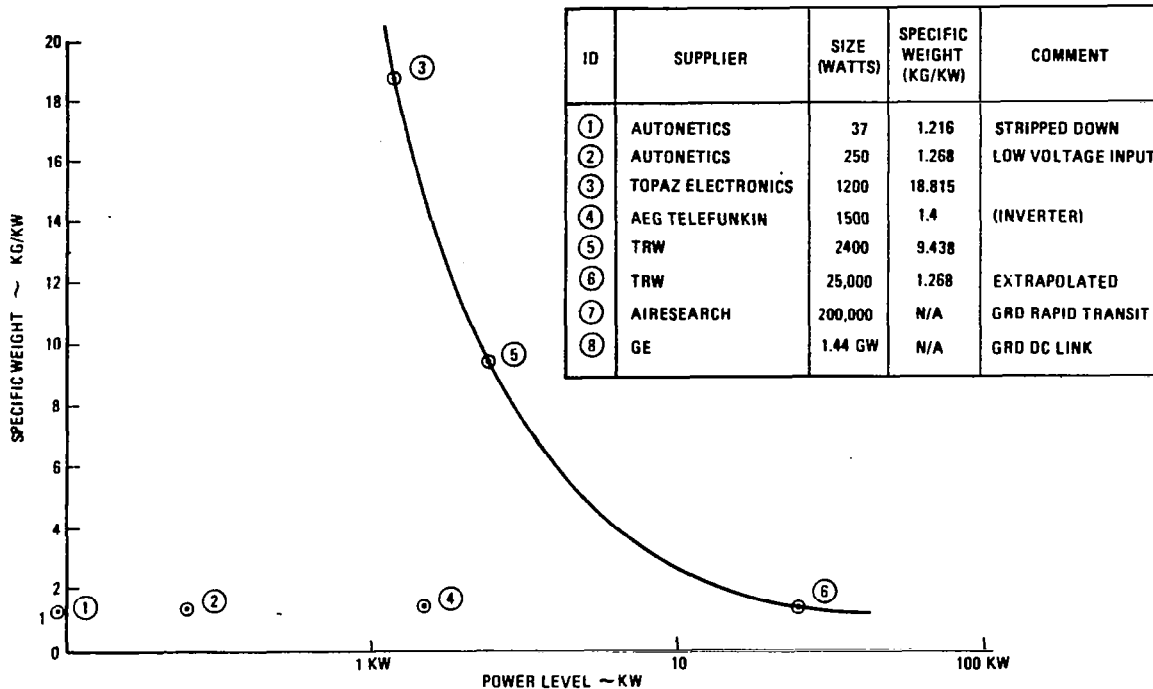
Figure 2.2-3. Current dc Converter Technology Status

In this way a technology goal for 1988 was established at 0.5 kg/kW and 97% converter efficiency. Based on todays state of art for a 250 kW dc converter at 96% efficiency we would expect to be able to achieve 0.96 kg/kW using available 200-400 V dc semiconductors, 25 kHz switching, and heat pipe cooling. By 1983 it is expected that higher frequency (500-100 kHz) can be achieved and by reconfiguration of the transformers, semiconductor higher voltage ratings, improved power gain, and complementary high efficiency drive techniques a specific weight of 0.7069 kg/kW can be achieved. By 1988, improved power semiconductors (transistors, SCR's, power FETS), increased transformer and inductor performance, and new core materials, new conductors and insulation techniques will result in further improvements to the 0.5 kg/kW goal.

Specific weight projection for dc converters as a function of size is shown in Figure 2.2-4. The base case, 432 mW, 400 Hz and 1000 volts (point 1), was provided by Westinghouse as part of the Exhibit A/B effort. The solid curve is plotted using data adjusted for 100 kHz frequency and using a scaling relationship[1] $(P_o/P)^{.75}$. The dashed curve was drawn taking existing dc converter masses and extrapolating to the 432 MW, 100 kHz base case. The Rockwell mass statement uses 0.197 kg/kW for the dc converter weight (point 2).

Technology Weight Impacts

A mass comparison was made using the projected specific weight (0.197 kg/kW) and estimated 1988 specific weight (0.5 kg/kW) to show dc converter technology

---
[1]Westinghouse Report LY20686, December 1977
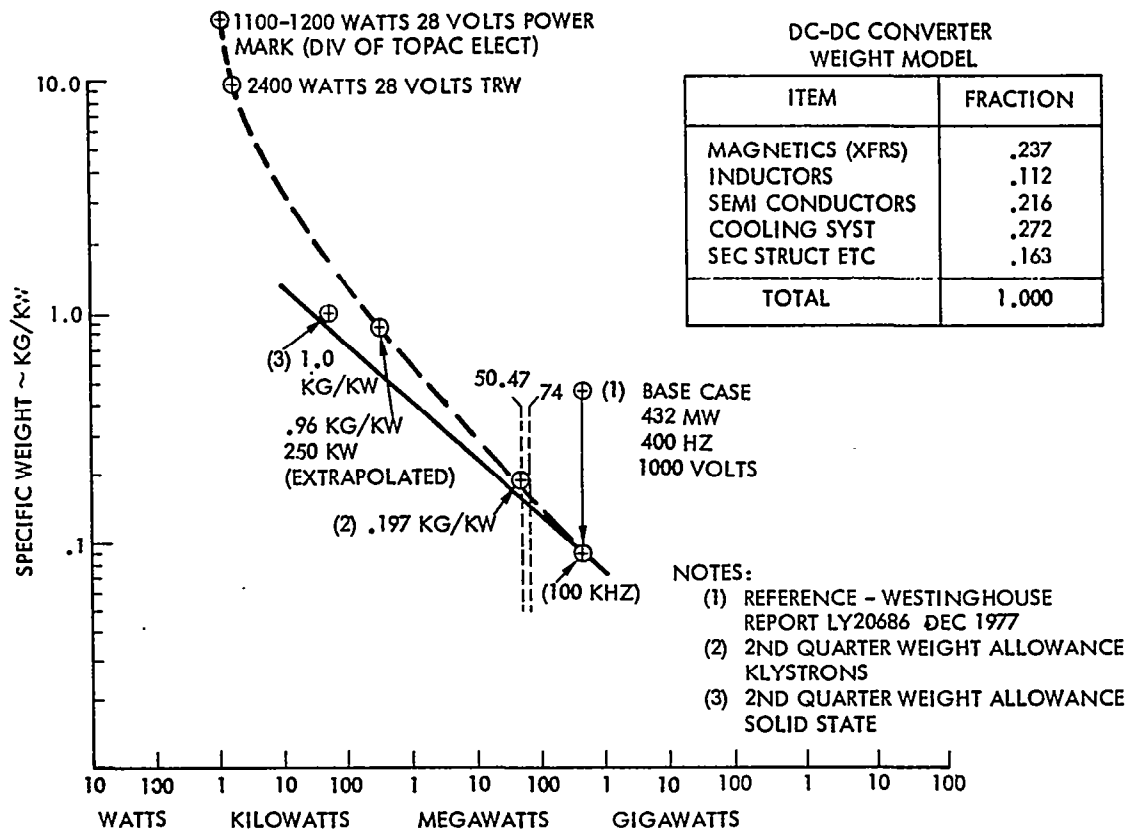
Figure 2.2-4. Dc-dc Converter Specific Weight Projections

mass impact. The requirements for voltage conversion and regulation are listed in Table 2.2-3 along with the calculated mass for the items affected, i.e., main conductors, voltage converters, slip rings and brushes. A number of configuration options are shown: (1) 40 kV direct – provide the 40 kV voltage requirement direct from the solar array; (2) 40 kV, 32 kV direct – provide both 40 kV and 32 kV direct from the solar array; and (3) all klystron volt direct – provide all klystron voltages direct from the array. Note: The initial Rockwell baseline resulting from Exhibit A/B study provided all klystron voltages from dc converters. An examination of Table 2.2-3 shows total mass ranging between 3.505×10^6 kg and 7.081×10^6 kg. The heavier specific weight would necessitate design changes moving towards dedicated solar array voltages to provide the klystron voltages directly from the array and elimination of dc converter requirements.

Switchgear

Satellite switchgear requirements are tabulated in Table 2.2-4 giving candidate sizes and number of each required in the satellite power distribution subsystem. The specific weight shown (0.00682 kg/kW) is a design goal; however, current studies indicate it is attainable. The kg/kW is the ratio of the mass of the switchgear to the product of the voltage and current handled by it.

2-27

Table 2.2-3.   *Technology Weight Impacts*
(dc-dc Converter)

WEIGHT IMPACT COMPARISONS (10^6 KG)

ITEM	REF WT	1988 WTS	CONFIGURATION OPTIONS		
			40 KV DIRECT	40 KV, 32 KV DIRECT	ALL KLYSTRON VOLT DIRECT
MAIN CONDUCTORS	1.902	1.902	1.902	1.928	3.345
HV CONVERT	1.74	4.413	3.229	2.422	-
LV CONVERT	.222	.468	.468	.468	.468
REGULATORS	.048	.238	.238	.238	.238
SLIP RINGS	.043	.043	.043	.086	.215
BRUSHES	.017	.017	.017	.084	.085
SUBTOTAL	3.929	7.081	5.897	5.176	4.351

REQMTS

VOLTAGE	POWER	QUANT	SP WT KG/KW *	SP WT KG/KW **
40 KV	74 MW	32	.1971	.5
32	50.47 MW	"	"	"
24	"	"	"	"
16	"	"	"	"
8	"	"	"	"
LV	.2 KW	8,547	1	3.4
	1.62 KW	135,864	1	2.1
REGULATORS ±1%	3.5 KW	135,864	.1	.5

*REFERENCE WEIGHTS - 2ND QUARTERLY
**EST. 1988 WEIGHTS

Table 2.2-4.   *Satellite Switchgear Requirements*

I.D.	VOLTAGE (kV)	CURRENT (A)	POWER (MW)	QUANTITY	WEIGHT (@ .00682 kg/kW)
ON ARRAY	22.85	290	6.61	360	16,229
	22.85	580	13.22	330	29,753
	45.7	580	26.44	360	64,915
	43.1	7258	312.8	30	64,000
	2.285	290	0.618	720	3,035
SUBTOTAL					177,932
ON ANTENNA	45	6,500	279	32	60,889
	45	6,407	264	32	57,528
	45	2,430	100	16	10,912
	45	6,077	250	16	27,280
	45	9,722	400	20	54,560
	45	12,150	500	30	102,300
	40	75	3	274	7,407
	40	50	2	1,278	19,576
	40	10	0.35	6,993	16,693
	8	0.0125	0.001	135,864	927
SUBTOTAL					358,072
TOTALS				146,355	536,004

Two major options were considered for switching high current and high voltage power: (1) forced commutation - solid state or mechanical breakers; and (2) cross field interruptors - mechanical breakers. Arc suppression across the metalic switch contacts of switchgear for dc voltages above 50 volts is the principle problem. Solid state devices, i.e., power transistors and SCR's used in various combinations, have no arcing problem; however, development programs to extend this technology to high dc voltages (40 kV range) do not appear encouraging. Electromechanical switches of various designs seem to be the most plausible approach. The cross field discharge tube technique appears to be the most viable approach to meet the SPS mass and efficiency design goals.

The Rockwell alternative SPS concept has as its baseline the cross field switchgear with a specific weight of 0.00682 kg/kW and an efficiency of 99.9%. The Rockwell industry survey reinforced our conviction that these goals can be met. Hughes Research Laboratory at Malibu, California concurred with these goals based on extensive work done on ground equipment. Westinghouse projected an order of magnitude improvement to the mass goal (Exhibit A/B subcontracted effort).

The cross field interruptors operate by using the arc voltage to drive a magnetic field tube. This creates an ionization (plasma path) for the current flow (parallel path). This field is then removed and the interrupted current is directed into resistor components. The power circuit schematic for this concept is shown in Figure 2.2-5. The figure illustrates each event as a function of interrupt time. The current is being commuted from the contacts of the electromechanical switch to the cross field interrupter tube and finally to the resistor to complete the current limiting sequence in about 1.3 milliseconds. About 2 kilowatts of power is required for the magnetic field after the fault is initiated.

TIME — MILLISECONDS

①   60 CYCLE SINEWAVE

②   THRESHOLD – PREDETERMINED VALUE

③   PROJECTED FAULT CURRENT CURVE

④   FAULT CURRENT APPROACHING THRESHOLD

* ⑤   ACTIVATE ELECTROMECHANICAL SWITCH AND MAGNET COIL

⑥   SWITCH OPENS – SF_6+N GAS BLAST ARC – POWER DISSIPATION INITIATES MAGNETIC COIL CIRCUIT. MAGNETIC FIELD IS BUILT UP. IONIZES AREA OF THE ELECTRODES GENERATING A PLASMA – ALLOWS CONDUCTION OF CURRENT THROUGH THE TUBE.

⑦   MAGNETIC FIELD IS REMOVED, IONIZATION CEASES, AND CURRENT INTERRUPTED

⑧   R-C CIRCUIT ABSORBS DISSIPATED POWER

* EXTERNAL POWER REQUIRED FOR MAGNETIC FIELD AND SWITCH INDUCTOR (>2.5 KW)

Figure 2.2-5.   Cross Field Discharge Tube Operation

This device has been developed for terrestrial use and applied to a number of high dc voltage applications as listed in Table 2.2-5. At the Calham Laboratory the cross field interrupter is to give high voltage protection to an

CUSTOMER	APPLICATION	VOLTAGE	CURRENT	POWER
CULHAM LABORATORY ABINGDON,U.K.	HIGH VOLTAGE SERIES PROTECTION OF A MEGAWATT NEUTRAL INJECTOR IN OPERATION 8 MONTHS	120 KV	40A	4.8 MW
ELECTRIC POWER RESEARCH INSTITUTE,PALO ALTO, CA	HIGH VOLTAGE D.C. CIRCUIT BREAKER DEVELOPED FOR POWER SYSTEM EQUIPMENT SUPPORTED BY THE NATIONS ELECTRIC UTILITIES. TESTED AT SYLMAR SUCCESSFULLY.	92 KV	620A	57.04 MW
AMERICAN ELECTRIC POWER SERVICE CORP N.Y., N.Y	INSTALLED MUSKINGUM RIVER, OHIO A.C. CURRENT LIMITING IN 9-78 (EXPERIMENTAL TESTING)	(A.C.) 138 KV RMS	4000A	552 MW
ELECTRIC POWER RESEARCH INSTITUTE,PALO ALTO, CA	BEING INSTALLED AT CELILO. NORTHERN TERMINAL PACIFIC HV-D.C. INTERTIE METALLIC RETURN TRANSFER BREAKER	80 KV	1000A	80 MW

injector system. The interrupter was stressed to 150 kV dc on a low level in-
terruption test and installed for testing a 120 kV/2-4 megawatt dc supply con-
nection to the injector test line. Both tests were successful. Electric Power
Research Institute (EPRI) successfully tested the crossed-field interruptor at
the Sylmar Substation as a circuit breaker on the Pacific high voltage dc inter-
tie. The crossed-field tube is being installed at the Northern Terminal Pacific
inter-tie as a transfer breaker in a metal return interrupter.

A major sensitivity of the switchgear design is its component efficiency.
The present system efficiency chain has fourteen switchgears required in the
chain shown in Figure 2.2-6. (Note: There are three additional switchgears on
the solar array for a total of 17.) A slight change in the switch efficiency
has a significant impact on end to end efficiencies. For example, if the switch-
gear efficiency reduces from 99.9% to 99.5% this has the following impact:
$\eta_{SG} = .999^{14} = .986$ (reference case) compared to $.995^{14} = .932$.

2.2.4 SOLID STATE ANTENNA POWER DISTRIBUTION

An alternate approach to a solid state antenna design was evaluated taking
advantage of advanced technology for lightweight dc converters as projected in
Figure 2.2-4. Individual power modules of 52 kilowatts each were clustered and
combined as shown in Figure 2.2-7 with central dc converters sized to provide
from 14.4 megawatts to 120 megawatts to each cluster. At these large sizes,
lower specific weights are projected for the converters. With this approach it
is possible to make a direct comparison with the klystron antenna design.

A two step converter design concept was assumed with the second section
providing the 100 V dc output. The front section was estimated to be equivalent
(i.e., no heavier) than that of the klystron dc converters and the output sec-
tion (low voltage section) estimated to increase overall converter mass by 38.6%,
i.e., inductors 10%, semiconductors 10%, cooling system 13.6% and mechanical 5%.
The new specific weight for the projected advanced dc converter was thereby taken
as .273 kg/kW. (Note: Compared to .197 kg/kW in the klystron case.)

Figure 2.2-6. System Efficiency Chain – Photovoltaic (CR-2)
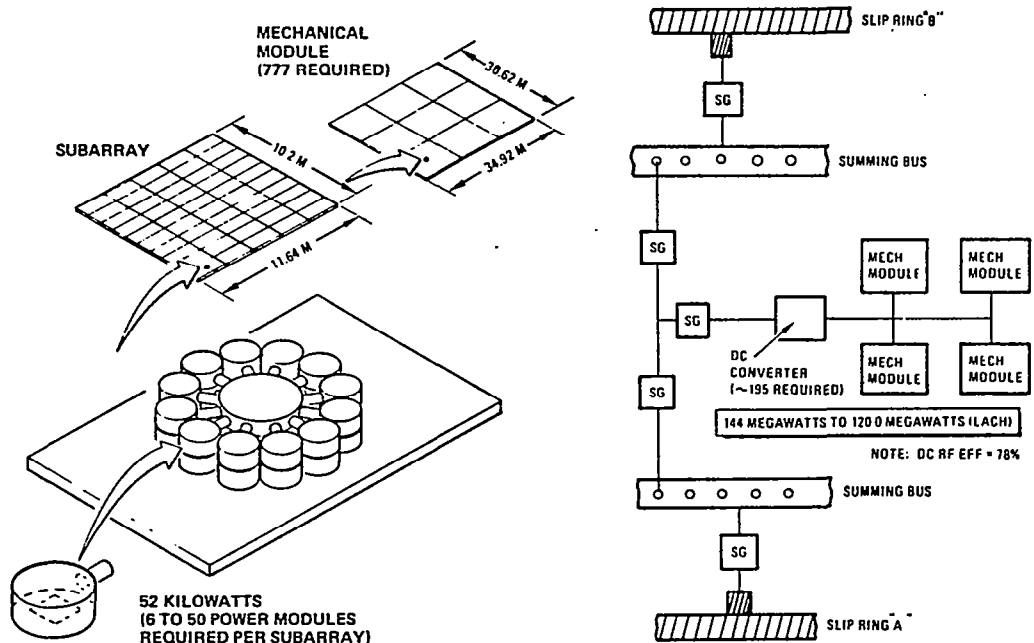
Figure 2.2-7. Solid State Antenna Power Distribution Concept

A comparison between the power distribution subsystem mass for solid state concept options and the klystron reference concept is given in Table 2.2-6. For the first option, (100 V dc, 2% secondary feeder, 82% dc-RF option) a major weight penalty is shown for antenna module cabling [1.66×10^6 kg versus $.131 \times 10^6$ kg (reference)] because of the low distribution voltage, i.e., 100 V dc. The second and third options illustrate approaches to reduce this penalty: (1) increase the allowable voltage drop from 2% to 7%; and (2) raise the distribution voltage from 100 V dc to 200 V dc. Raising the distribution voltage necessitates a series-parallel arrangement for the transistor devices. It was estimated that this would result in a drop in dc-RF efficiency from 82% to 78%. There are further trade offs between series-paralleling and large distribution voltage drop allowances. If, as a result of series-paralleling, dc-RF conversion efficiency drops below 78% then it would favor a larger voltage drop. The data shown in Table 2.2-6 indicates that solid state could be implemented at a power distribution mass penalty (compared to the reference klystron design) of probably less than 2×10^6 kg.

2.2.5 ELECTRIC ORBIT TRANSFER VEHICLE (EOTV) POWER DISTRIBUTION

The power distribution subsystem (PDS) mass comparisons for the different EOTV configurations that were studied are shown in Figure 2.2-8. A solar array voltage output of +2080 V dc was taken as the upper limit for power generation to stay within tolerable plasma power losses for low earth orbit operations. The 2080 V dc distribution results in the lowest mass concept and a power distribution subsystem mass of 288,440 kg. This configuration assumes a direct energy transfer of power from the solar arrays to the ion engines which are located at the four corners. This weight was calculated for a distribution

2-32

		CONCEPT OPTIONS (SOLID STATE)		
ITEM	KLYSTRON REFERENCE 85% dc-RF	100 VDC 2% SEC-FEEDERS 82% dc-RF	100 VDC 7% SEC. FEEDERS 82% dc-RF	200 VDC 2% SEC FEEDERS 78% dc-RF
MAIN FEEDERS	1.860			
SECONDARY FEEDERS	.076			
SUMMARY BUS	.219			
TIE BAR	.160			
INSULATION	.047	3.095	3.254	3.254
SWITCH GEAR	.178			
REG & CONVERTERS	.009			
ROTARY JOINT	.043			
AC THRUSTER CABL'G	.0053			
BATTERY	.006			
SUPPORT STRUCT	.254			
SUB NON ROTATING	2.986	3.095	3.254	3.254
CABLE FROM TOR TO AMT	1.25	1.295	1.362	1.362
SUMMARY BUS	.095	.098	.103	.103
ANTENNA CABLES	.832	.486	.511	.511
ANTENNA MODULE CABLE	.131	1.66	.475	.415
SWITCH GEAR	.358	.371	.390	.390
POT JOINT	.017	.0176	.0185	.0185
DC CONVERTERS	1.543	2.099	1.192	2.192
INSULATION	.189	.299	.315	.315
SUPPORT STRUCTURE	.450	.632	.536	.530
SUBTOTAL ROTATING	4.955	6.957	5.902	5.836
TOTAL PDS	7.941	10.052	9.156	9.09
SOLAR ARRAY/REFLECTOR	7.782	8.06	8.521	8.521
TOTALS	15.723	18.112	17.677	17.611

efficiency of 94% (i.e., 6% line loss). The power distribution subsystem cal-
culations ranged to 632,900 kg. A negative voltage system was then compared to
show impact of higher voltage. A negative 6300 volts was selected for this pur-
pose since this is the second voltage requirement of the EOTV thruster system.
This concept requires power conditioning at each thruster to provide the high
voltage dc (~1950 V) that is required by the engines. Note that the major power
requirement is high voltage dc (~95% of the total engine power). The silicon
solar array system was compared at the -6300 V dc since this represented the
lowest mass approach that was studied. The comparison showed a power distribu-
tion subsystem of 307,090 kg using silicon solar cells compared to 229,550 kg
(GaAs), i.e., a mass increase of ~33%. The +2080 volt direct energy transfer
concept is the recommended approach even though it is slightly higher in mass
since it minimizes the requirement for major power conditioning. The -6300 V
dc system is lower in mass but there is a major issue in that the system may be
susceptable to arcing problems in the low earth orbit plasma environment.

The solar array voltages must be kept as high as possible to reduce the
wiring mass penalties, yet, power loss by current leaking through the surround-
ing plasma must be at an acceptable level. There is no significant flight test

Figure 2.2-8. *EOTV Power Distribution and Control Weight Comparisons*

EOTV CONFIGURATION						
CELL MAT'L	GaAs →					SILICON
CR	2 →					1
TRANS. VOLTAGE	+2080V →				-6300V	-6300V
PANEL CONFIG.	SPLIT 2 PANELS	SPLIT 4 PANELS	SPLIT 4 PANELS	SPLIT 2 PANELS	SPLIT 4 PANELS	SPLIT 2 PANELS	SPLIT 4 PANELS
WEIGHTS (10^6 KG)							
INTERTIES	221,940	67,260	177,550	177,550	177,500	19,540	19,540
MAIN FEEDERS	144,520	119,230	57,810	57,810	57,810	22,850	83,740
SUMMING BUS	177,550	44,390	177,550	177,550	55,490	68,800	68,800
TIE BARS	24,660	24,660	24,660	24,660	24,660	8,140	8,140
SW GEARS	2,290	2,290	2,290	2,290	2,290	9,460	7,310
POWER CONDIT.	-	-	-	-	-	75,490	75,490
INSUL.	4,400	4,400	4,400	4,400	4,400	4,400	16,150
SEC. STRUCT.	57,540	26,220	44,200	44,430	3,220	20,870	27,920
TOTAL	632,900	288,440	486,180	488,690	354,420	229,550	307,090

2-34

data available on plasma-current leakage. Planned experiments aboard the SPHINX satellite (February 1974) were lost due to a launch failure.

Plasma loss estimates used in the study were taken from different sources. A summary is shown in Table 2.2-7. The positive arrays have a greater leakage power compared to negative arrays by a factor of 43:1 (square root of electron to proton mass). Experiments conducted at NASA Lewis Research Center have shown arcing problems with negative arrays for relatively low voltages ~500 Volts. However, the explanation is not clear and therefore because of their lighter mass the negative systems should not be ruled out. The power loss was found to be proportionally smaller for larger arrays; however, it is expected that this proportionality saturates in the order of several thousand square meters. The present data is not adequate to accurately predict plasma power loss. This is clearly an issue that needs to be resolved and may require large array tests in space.

Table 2.2-7. Plasma Loss Estimate for Solar Array

ALTITUDE (km)	KENNERUD 150 m^2 ARRAY (+2000 VOLTS)	GUIDICI (+5000 VOLTS) (28x10^6 m^2)	GUIDICI (+2000 VOLTS) (28x10^6 m^2)	KENNERUD 28x10^6 m^2 ARRAY (+2000 VOLTS)	CONSERVATIVE ESTIMATES(ROCKWELL) (+2000 VOLTS, 28x10^6 m^2)
200	67%	29.4%	11.8%	17%	17%
500	20%	14.4%	5.99%	5%	6%
1,000	5.7%	1.67%	0.695%	1.4%	1.4%
10,000	0.5%	0.0025%	0.001%	0.13%	0.13%
GEO	0.13%		·	0.03%	0.03%

The simplified block diagram of Figure 2.2-9 illustrates the EOTV power distribution interfaces for the GaAs solar photovoltaic concept. The distribution subsystem consists of inter-ties, main feeders, summing bus, tie bar, switchgears, and dc converters. The solar arrays feed the load buses utilizing a direct energy transfer approach. Provisions are included with the PDS to switch power from any bus to any thruster location. The basic voltages supplied are +2080 V dc and -6300 V dc. Individual power supplies are to be included as required at the thrusters to supply any other voltages.
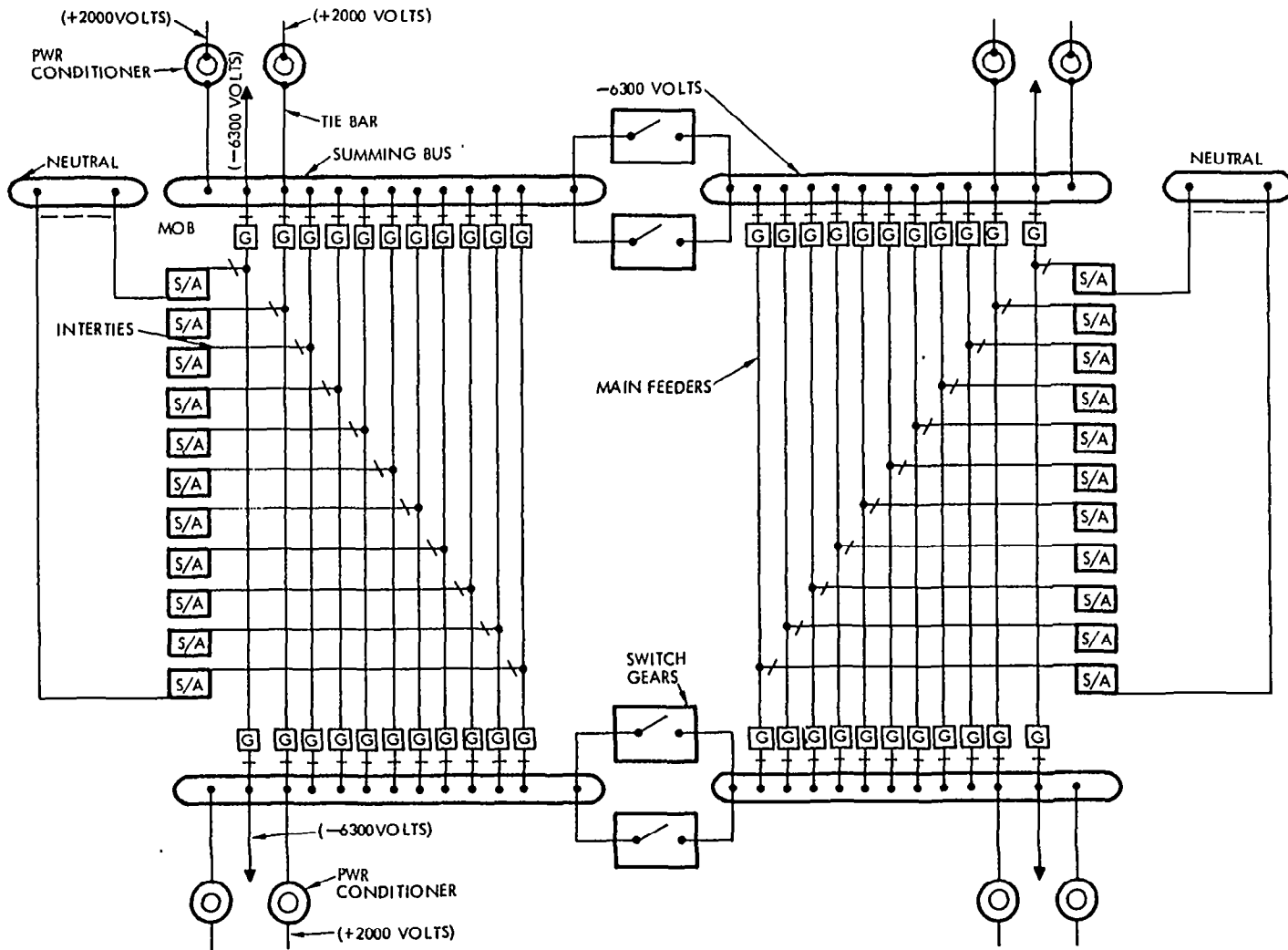
Figure 2.2-9. EOTV Power Distribution Simplified Block Diagram

2.3 STRUCTURES

There were two areas of investigation in the structures trade study:
Rockwell SPS microwave antenna concept involving use of a hexagonal rigid frame
(compression frame); and NASTRAN structural analysis of thermal effects to com-
pare aluminum with composite materials for structural members.

2.3.1 SPS MICROWAVE ANTENNA TENSION WEB – COMPRESSION FRAME CABLE CONCEPT

The Rockwell SPS satellite microwave antenna concept that was evaluated
and compared to the space frame involves the use of a hexagonal rigid frame
(compression frame) to which is attached an adjustable cable system. The cable
must support the slotted antenna panels within acceptable optical tolerances.
These antenna design requirements include:

1. Flat uniform surfaces to within 0.08 degree slope variation over
    the total diameter.

2. Flatness mismatch between mechanical modules (30.62 m by 34.92 m)
    may not exceed 1/10 wavelength.

3. Distance between mechanical modules to be 1/10 wavelength.

Antenna Concept Description

The antenna outer frame (Figure 2.3-1) is a hexagon-shaped platform and
rigid-frame structure with a cross section of a 50 m tribeam truss longeron.
The base of the tribeam truss is on the interior face of the hexagonal frame
which permits attachment of the slotted antenna panel cable support system.

The cable support system is a three layer cable array. The mid-plane
cable array (shown in Figure 2.3-2) is a set of crossed cables, forming 30.62 m
by 34.92 m rectangles, that are pretensioned and attached to a hexagonal shaped
perimeter cable which is pretensioned and attached to the corners of the exte-
rior located hexagonal-shaped, rigid frame structure. The mid-plane cable
array pretension is reacted by compression in the outer, rigid frame. The
size of cables and frame structure is defined by the amount of pretension
applied. A small ring loop is loosely wrapped around each mid-plane cable
crossing and permits in-plane relative cable motion but prevents normal to
plane relative cable motion. The mid-plane cable array overall flatness is
obtained by using three (every other one) of the six pretension attachments
to the outer hexagonal frame as plane reference points (3 points determine a
plane). The alternate three frame-attachment cables are aligned to the refer-
ence plane using laser optics. The panels of the phased-array antenna are
connected to the mid-plane cable system with temperature-expansion-compensation
fittings near cable crossings.

The accuracy of modern laser optical systems used as a metrology standard
are two orders of magnitude more precise than the wavefront in-plane phase re-
quirements of the SPS slotted antenna. Capstan actuator response rates can be
readily isolated from the two cycle per day distortional input and readily
provide true relative repositioning of all six cable support points.

ANTENNA REFERENCE PLANE ①.③.⑤

PRETENSION ATTACH CABLE
RIGID FRAME 50M TRIBEAM
PERIMETER CABLE
MID PLANE
CROSSED CABLES
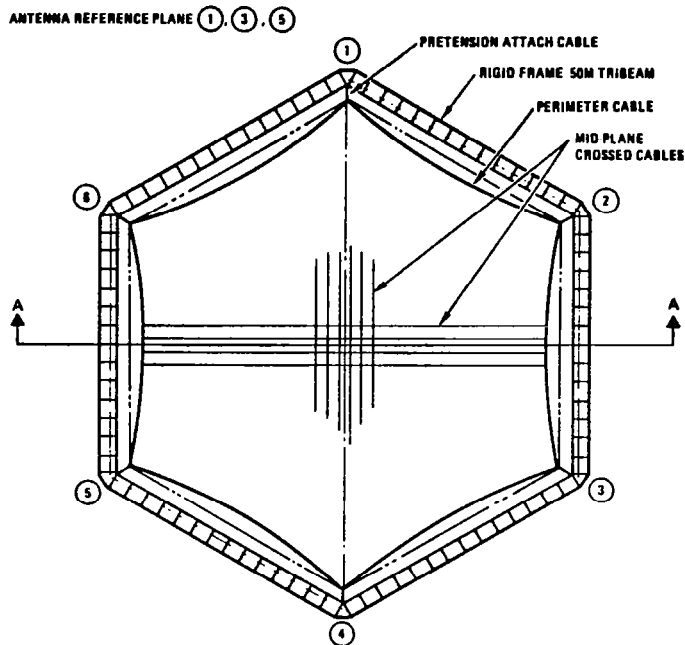
Figure 2.3-1.   Antenna Plane View Schematic

ADJUSTABLE TENSION ATTACH CABLES
SUSPENSION CABLES (FRONT)
ANTENNA PANEL
30.62-M BY 34.92-M
CABLE CAPSTAN
50M
CABLE CAPSTAN
MID-PLANE CROSSED CABLES
RIGID FRAME
(50-M TRI BEAM)
PERIMETER CABLES
SUPPORT CABLES
(ADJUSTABLE TENSION/POSITION)
SUSPENSION CABLES (REAR)
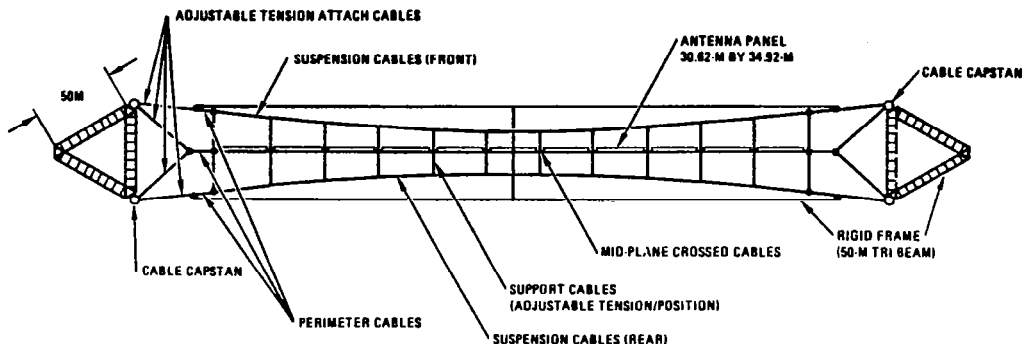
Figure 2.3-2.   Antenna Section A-A Schematic

The mid-plane cable array behaves similar to a thin, flat membrane, such
as a trampoline, to force fields applied normal to the plane of the array.
Small deflections from flatness produce large forces in the cables. This de-
flection/force sensitivity can be reduced several orders-of-magnitude by plac-
ing a cable system front and rear of the mid-plane array and attaching these
cable systems to the mid-plane array by support cables that are perpendicular
and attach to the antenna panels near crossed-cable intersections of the mid-
plane array (Figure 2.3-3). The cable systems each side of the mid-plane form
deep curves similar to suspension bridge cable systems. The entire cable
system is able to carry large mid-plane forces at low values of deflection.
The overall appearance of the three cable arrays is thick near the outer hexagon
frame and thin at the center of the antenna, similar to a negative meniscus lens
used in optical systems (Figure 2.3-4).

2-38
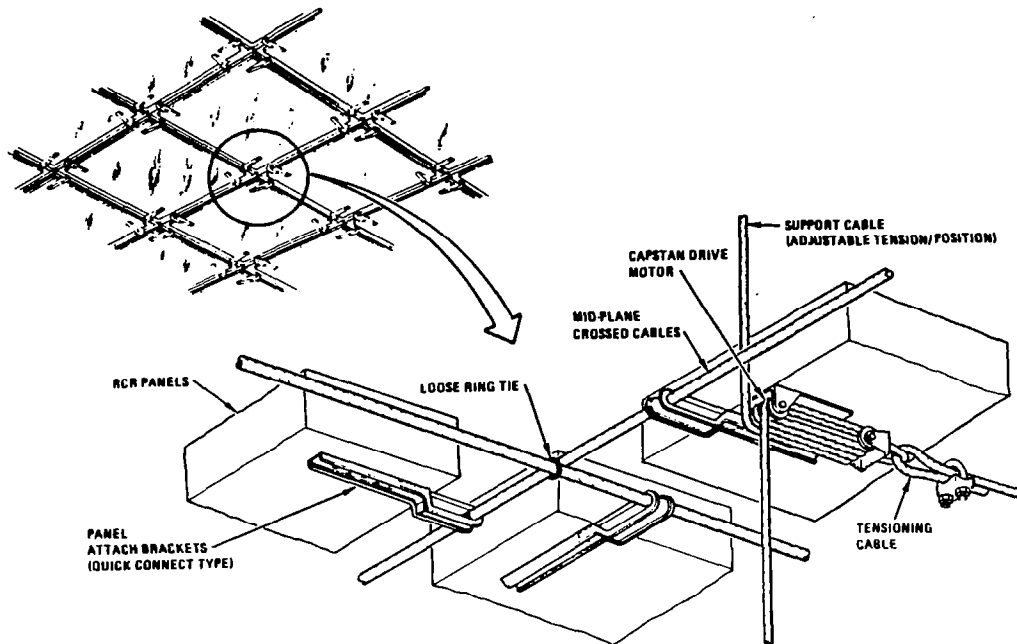
Figure 2.3-3. RCR Antenna Panel Installation
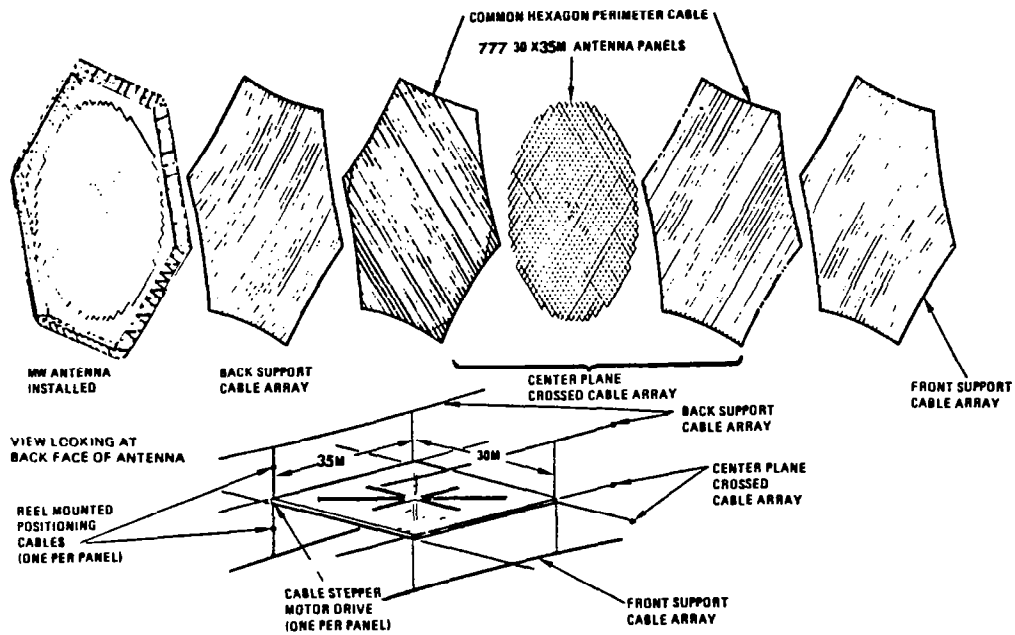
Figure 2.3-4. Three Membrane Negative Lens Concept

2-39

The perpendicular support cables perform the following functions:

* Provide a normal force load path interconnection among all three cable arrays;

* Provide adjustment of pretension forces in the perpendicular cable system;

* Provide precise position adjustment of local zones of the microwave multiple-panel, phased-array antenna surface.

Each corner of the antenna 30.62-m by 34.92-m microwave antenna panels is connected to the mid-plane cable array close to the cable crossings (Figure 2.3-3). At operating temperatures the panel is slightly smaller in planform than the space formed by the crossed cables of the mid-plane array. The panel-to-cable attach fittings are slotted to permit inplane thermal expansion of antenna panels and mid-plane cables but prevent normal to mid-plane relative motion between cables and panels. Since thermal expansion is compensated for between individual panels and adjacent support cables, panel-to-panel thermal expansion problems are avoided.

A capstan pulley assembly is mounted near or on only one of the four antenna-panel-to-mid-plane-cable attach fittings. The capstan assembly performs the following functions:

* Stores the perpendicular support cables prior to panel installation;

* Provides the pretensioning force to the support cable after panel installation;

* Provides mid-plane precise position adjustment of the antenna panel.

The support cable is connected to the antenna panel rather than the mid-plane cable crossing because of insufficient space between panels and cables due to the 1/10 wavelength panel-to-panel tolerance. The panel-to-cable attach fittings that have capstans are mounted as close as possible to the mid-plane cable crossing. The perpendicular cable for practical purposes is attached to the mid-plane cable intersection. Therefore, one support cable and capstan assembly per antenna panel is sufficient to provide normal-to-plane adjustment to each cable crossing of the mid-plane cable array. Perimeter antenna panels will require additional cable/capstan assemblies according to the number of exterior panel corners involved. The cable may be fabricated from metallic or non-metallic structural material.

Cables located in the antenna radiation field, including the perpendicular support cables, should not interfere or distort transmitted radiation patterns.

The cable support system is exposed to heat sources such as: solar, earth albedo, electrical conductor, and transmitter panel power amplifier waste heat. The resulting cable system temperature profile is non-uniform depending mainly on local conditions along each cable. A mid-plane cable will probably be reasonably cool near the hexagon, perimeter support cable and significantly

hotter near the antenna center. The slotted fittings that attach the 30.62-m
by 34.92-m antenna panels to the mid-plane, cross-cable system, the crossed-
cable ring ties and the cross-cables are anti-friction coated (non-volatile dry
lubricant or low friction plating) to permit the mid-plane cables to freely
expand and contract between hexagon perimeter support cables. Pretension in
the crossed cables should include thermal expansion effects. Since the mid-
plane cables are very long, they behave as springs to the pretension forces.
Random heating and cooling along the crossed-cables will cancel most of the
thermal expansion anomalies. However, pretension in all three hexagon-perimeter-
cables is maintained near constant values by the constant-tension properties of
the attachment to the corners of the rigid frame structure. The sag of the
hexagon-perimeter-cables will change at constant tension and tends to maintain
constant pretension in the entire cable system.

Laser optics maintain a check of the antenna radiation surface flatness
and support frame shape. The received earth-to-SPS master phase control signal
provides a standard for measuring SPS radiated beam wavefront quality. Tension
sensors, laser optics and master signal data may be used to control both mech-
anical and electrical systems, as required, to maintain proper earth pointing
and wavefront control of the transmitted power beam.

Impacts of Antenna Structure Concept on Satellite System

The major impacts on the satellite that result from the use of a tension
web (compression frame) antenna structure when compared to the reference space
frame are on: mass, assembly time, and material selection. The tension web
provides a lightweight, easily assembled configuration and permits the use of
low temperature composites. This configuration is a flat thermally "stiff"
surface but relatively complex since it relies on a cable system which must be
adjustable and/or self-compensating for effects of temperature variations. The
antenna dynamics are still a major concern with this concept and require more
detailed analysis to understand their impacts.

The antenna structure mass comparison is shown in Figure 2.3-5 for a 1 km
diameter microwave antenna. The tension web mass, 0.067×10^6 kg, represents a
lighter structure but when compared to the space frame, 0.250×10^6 kg, the
difference is not thought to be significant considering a total antenna mass
of ~14.5×10^6 kg.

A further resolution of the antenna configuration issue (tension web versus
space frame structural design) requires a more detailed structural dynamics
analysis (NASTRAN) which must be combined with subsystem evaluations for con-
figuration control, and microwave interactions.

2.3.2 NASTRAN STRUCTURAL ANALYSIS

The Rockwell 3-trough SPS design configuration (preliminary baseline con-
cept resulting from Exhibit A/B study) was modeled using the substructuring
features of NASTRAN; and the model was used to run three cases for investigat-
ing the thermal effects for two construction materials, aluminum and graphite.
The results of the study indicated: (1) that the deflections for aluminum
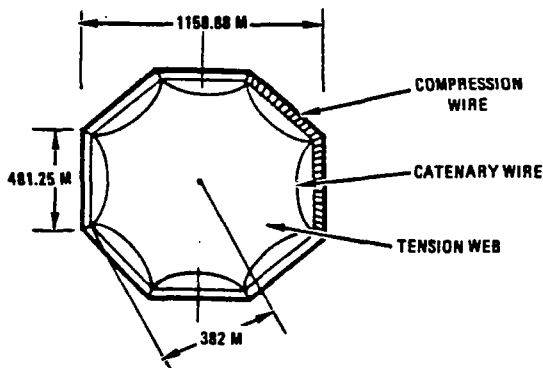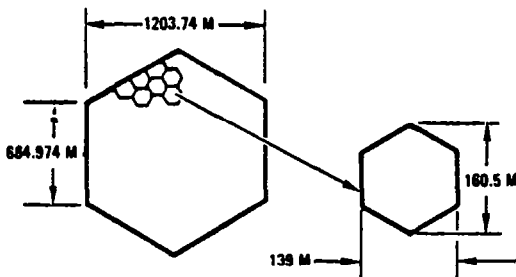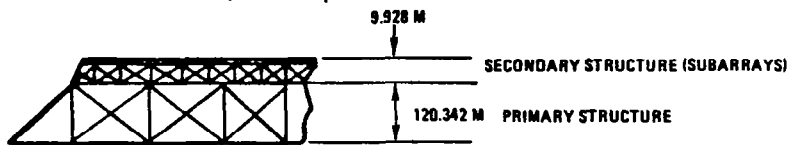
Figure 2.3-5. Antenna Structure Mass Comparison

material are several orders of magnitude larger than for graphite material;
(2) the stress magnitude for aluminum material runs three times (or more)
larger than for graphite material; (3) pretensioning of the X-bracing for the
aluminum (80 KSI) material is four times as high as for the graphite material
(20 KSI); and (4) additions and modifications to the NASTRAN program are requir-
ed to provide more efficient tool for stress/dynamic analysis of SPS structural
systems. The high stress values in the aluminum material exceeded the crippl-
ing allowables for the cap element and will result in a gauge size increase
(from the assumed 10 mil minimum gauge) leading to a larger structural weight
for the SPS structure.

Structural Model

    The Rockwell 3-trough design configuration, shown previously in Figure 1.1-1,
was used for the study of the thermal effects versus material selection for the
SPS structural system. The configuration was modeled using the substructuring
features of NASTRAN and used the 50-meter tribeam, stabilized by X-tension braces,
as the main beam element for the make-up of the substructures. The build-up of
the SPS structural system from the substructures is shown in Figure 2.3-6 and is
depicted through the use of CRT printouts. The right-hand wing is a combination
of three translated Substructure No. 1 units. Similarly, the left-hand wing is
a combination of three Substructure No. 4 units. The center structure is a
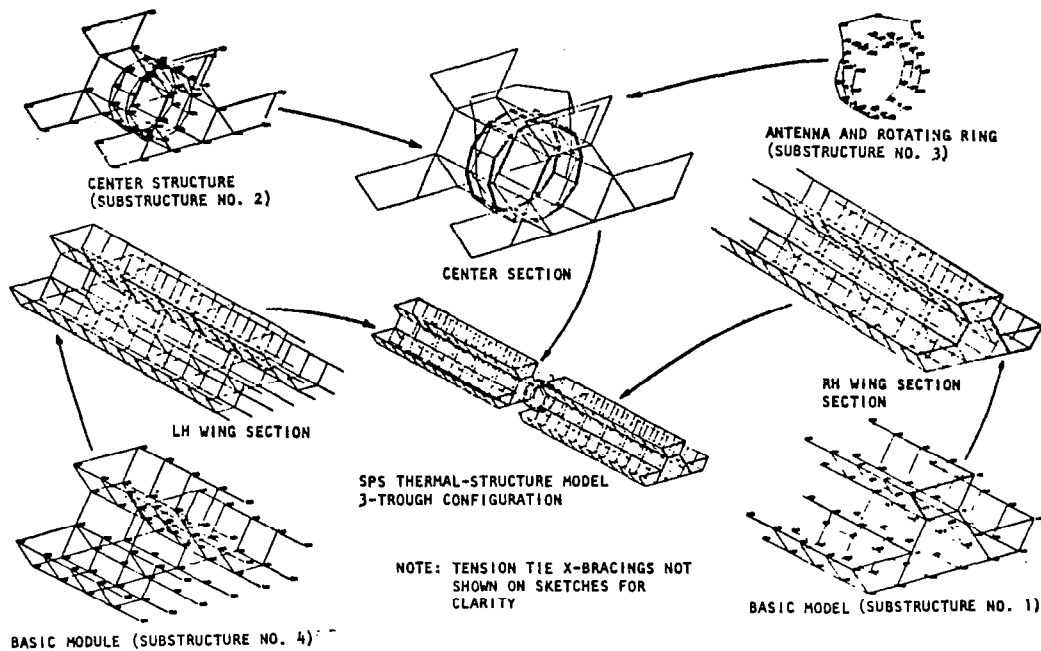
Figure 2.3-6. SPS Computer Program Structural Model

combination of the center section, Substructure No. 2, and the antenna and rotating ring, Substructure No. 3. Finally, the center section, the left-hand wing, and right-hand wing are combined to form the SPS structural model.

For the study, three cases were investigated considering two basic construction materials, metal (aluminum) and advanced composites (graphite/polysulfone). Case 1 assumes aluminum as the proposed construction material, with steel wire X-tension bracings and no prestressing of the X-bracings; Case 2 used graphite/ polysulfone as the beam material and graphite for the X-bracings, with initial prestress of 137 MPa (20 KSI); and Case 3 is the same as Case 1, except the X-braces have a prestress of 552 MPa (80 KSI). The pretension of the X-tension braces for Cases 2 and 3 was selected on the criteria that the braces were not to have compressive loads under the thermal and loading environment.

Structural Sectional and Material Properties

The basic structural element for the SPS structure is the 50-meter tribeam element, as shown in Figure 2.3-7, and is used throughout the structure with the exception of the antenna frame where a 30-meter tribeam element is used. The subelement makeup of the 30- and 50-meter beams are depicted in Figure 2.3-8. The sectional properties for the elements are listed in Table 2.3-1.

The material properties for the elements are a function of temperature. Table 2.3-2 lists the material properties at selected temperatures [room temperature, 177°C (composites) and 150°C (aluminum)]. The crippling stress of the cap element, not shown, is calculated to be 5800 psi at room temperature.

2-43

Figure 2.3-7. SPS Structural Cross-Sections

2-44

TRIBEAM GIRDER SECTION

50 M

TENSION TIE

50 M

2 M

2 M

BASIC BEAM ELEMENT

1.00 ℄

BEAD ON ℄

10.0 CM LIGHTENING HOLE 8.00 CM FROM ℄ (REF)

9.00 CM

BEAD ON ℄

2.00 CM

8.00 CM DIA.

6.00 CM

LIGHTENING HOLE 5 CM REF FROM ℄

3.50 CM

BASIC BEAM CAP
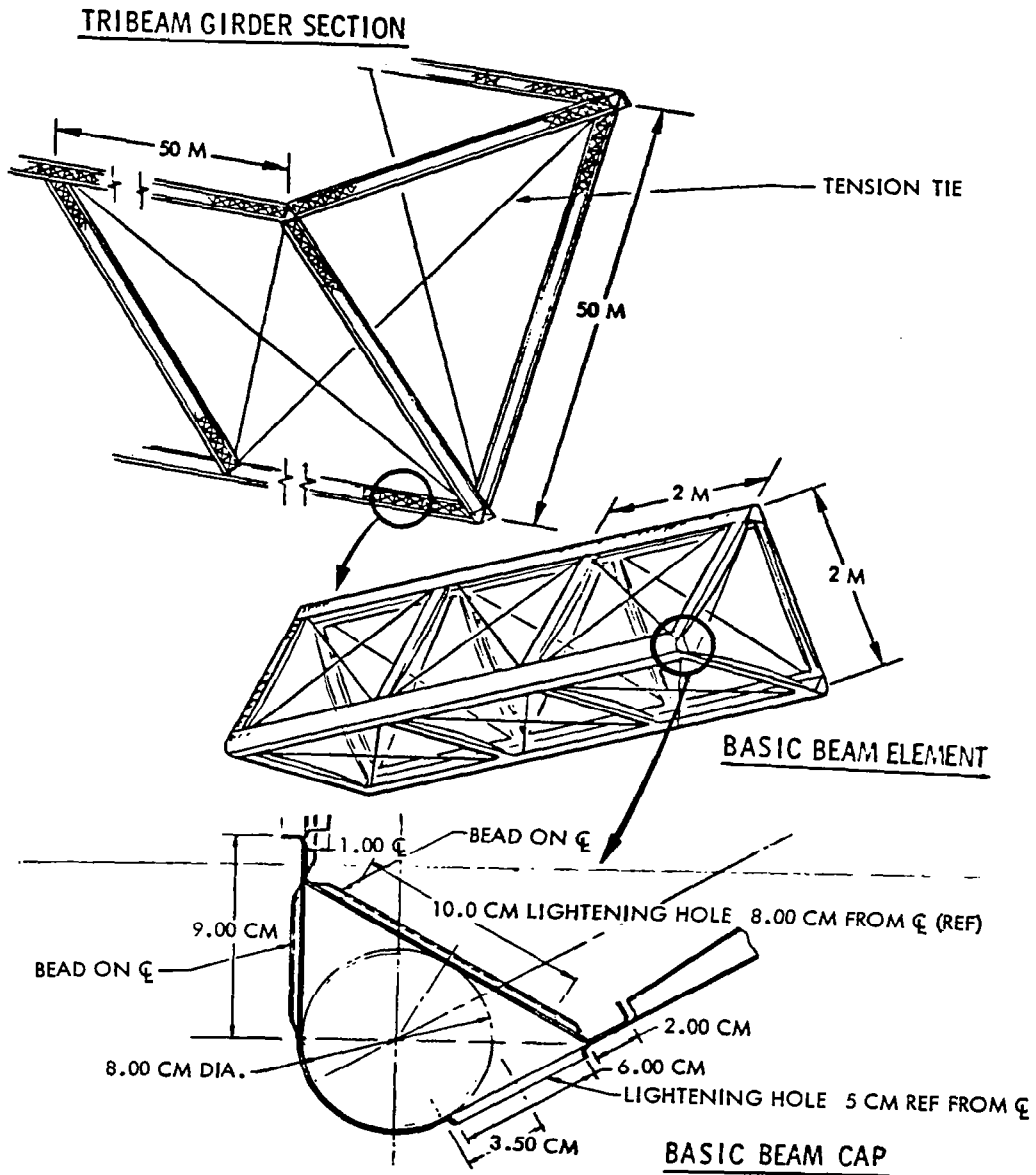
Figure 2.3-8. Tribeam Structure Composition

Table 2.3-1. Sectional Properties
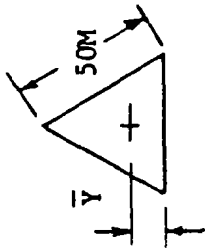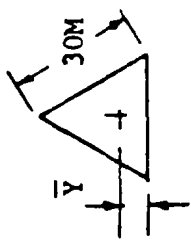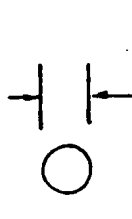
PROPERTY	TRIBEAM WING STRUCTURE	TRIBEAM ANTENNA FRAME STRUCTURE	TENSION TIE	EQUIVALENT BRUSH STRUCTURE (SPRING)
	50M	30M	1.59 x 10^{-3} M	
CROSS-SECTIONAL AREA	369.3×10^{-6} M^2	0.81×10^{-3} M^2	1.98×10^{-6} M^2	2.32×10^{-2} M^2
MOMENT OF INERTIA	0.154 M^4	0.126 M^4	‑	1.54 M^4
POLAR MOMENT	6.33×10^{-2} M^4	2.36×10^{-2} M^4	‑	0.60 M^4
CENTROID LOCATION ($\bar{Y}$)	14.43 M	8.82 M	‑	‑
AXIAL STIFFNESS ($K = EA/L$)	‑	‑	‑	5.97×10^5 N/M^2

Table 2.3-2. Material Properties

GRAPHITE COMPOSITE MATERIAL PROPERTIES

PROPERTY	ROOM TEMPERATURE	177°C (350°F)
ALLOWABLE STRENGTH		
F_x^{tu}	4.27×10^8 N/M (62 KSI)	3.59×10^8 N/M (52 KSI)
F_x^{cu}	3.93×10^8 N/M (57 KSI)	2.28×10^8 N/M (33 KSI)
F_y	1.58×10^8 N/M (23 KSI)	1.17×10^8 N/M (17 KSI)
MODULI OF ELASTICITY		
E_x	9.65×10^{10} N/M (14 MSI)	9.52×10^{10} N/M (13.8 MSI)
E_y	2.76×10^{10} N/M (4 MSI)	2.41×10^{10} N/M (3.5 MSI)
SHEAR MODULUS		
G_{XY}	2.41×10^{10} N/M (3.5 MSI)	2.34×10^{10} N/M (3.4 MSI)
POISSON'S RATIOS		
ν_{XY}	.72	.80
DENSITY	1350 KG/M³ (.057 LBS/IN³)	1350 KG/M³ (.056 LBS/IN³)
COEFFICIENT OF THERMAL EXPANSION M/M/°C	$.18 \times 10^{-6}$	$.18 \times 10^{-6}$
FIBER VOLUME ν_f	.60	.60

ALUMINUM (2014-T6) MATERIAL PROPERTIES

PROPERTY	ROOM TEMPERATURE	150°C (300°F)
ALLOWABLE STRENGTH		
F_{tu}	4.5×10^8 N/M (65 KSI)	2.41×10^8 N/M (35 KSI)
F_{ty}	3.93×10^8 N/M (57 KSI)	2.0×10^8 N/M (29 KSI)
F_{cy}	4.00×10^8 N/M (58 KSI)	1.72×10^8 N/M (25 KSI)
MODULUS OF ELASTICITY	7.24×10^{10} N/M (10.5 MSI)	6.83×10^{10} N/M² (9.9 MSI)
POISSON'S RATIO	0.33	0.33
DENSITY	2796 KG/M³ (.101 LBS/IN³)	2796 KG/M³ (.101 LBS/IN³)
COEFFICIENT OF THERMAL EXPANSION	22.3×10^{-6} M/M/°C (12.4×10^{-6} IN/IN/°F)	23.4×10^{-6} M/M/°C (13.0×10^{-6} IN/IN/°F)

TENSION TIE MATERIAL PROPERTIES

PROPERTY	GRAPHITE	SPRING WIRE 302 CRES
ULTIMATE TENSILE STRENGTH	16.5×10^8 N/M² (240 KSI)	17.6×10^8 N/M² (255 KSI)
MODULUS OF ELASTICITY	2.34×10^{11} N/M² (34 MSI)	1.95×10^{11} N/M² (28.2 MSI)
DENSITY	1600 KG/M³ (.065 LBS/IN³)	7920 KG/M³ (.286 LBS/IN³)
COEFFICIENT OF THERMAL EXPANSION	-0.4×10^{-6} M/M/°C (-0.22×10^{-6} IN/IN/°F)	14.4×10^{-6} M/M/°C (8.0×10^{-6} IN/IN/°F)

Thermal Profiles

The temperatures of the main structural elements for the composite and aluminum materials are given in Figure 2.3-9. The end of life temperatures were used and represent the most severe case. Figure 2.3-10 gives the temperature distribution used for the antenna and rotating ring·structure in the computer program analysis.

Graphite Structural Configuration Temperatures

Aluminum Structural Configuration Temperatures
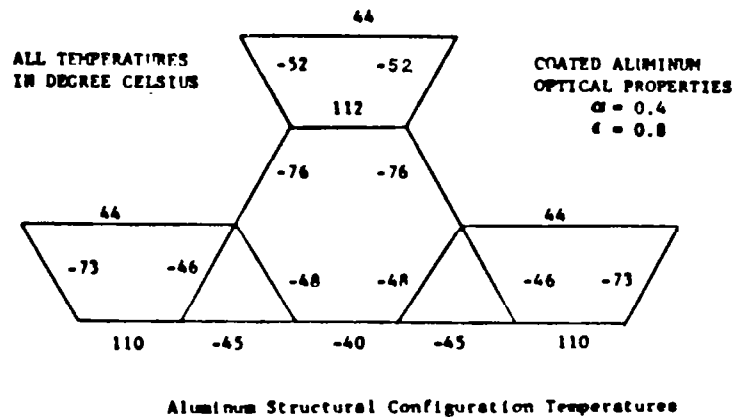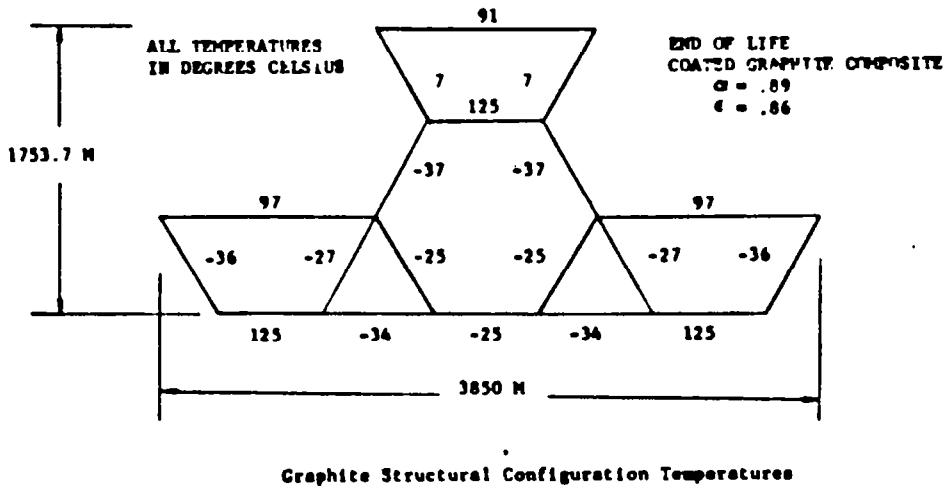
Figure 2.3-9. Basic Module Temperatures

Mechanical Loading

For this study the only mechanical loading considered to be acting on the structure is the reflector pretension loading as shown in Figure 2.3-11. The reflector pretension loading is assumed to be acting through the centroid of the tribeam element. The NASTRAN program beam element can not handle a concentrated or a distributive loading and therefore equivalent joint loads must be inputed to the program. A breakdown of the element point forces and the fixed-

TEMPERATURES SHOWN
ARE FOR ALUMINUM
CONSTRUCTION.
GRAPHITE CONSTRUCTION
APPROX. 3°C HIGHER.
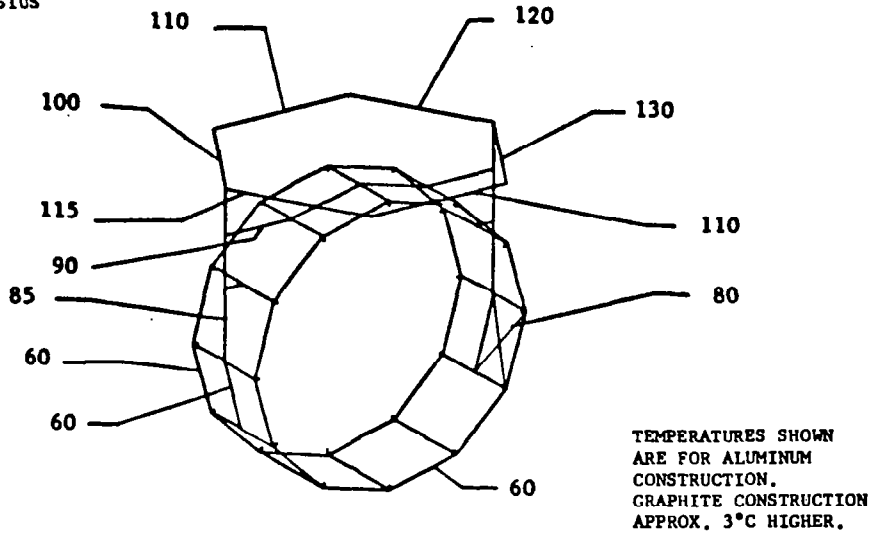
Figure 2.3-10. Antenna and Rotating Ring Temperatures

● REFLECTOR LOADING

REFLECTOR MATERIAL:

1/2 MIL ALUM. KAPTON
$t = 1.27 \times 10^{-5}$ M

REFLECTOR PRETENSION:

$\sigma = 0.517$ MPA (75 PSI)

EQUIVALENT LOADING:

$\omega = \sigma t = 6.567$ N/M (.0375 LB/IN)
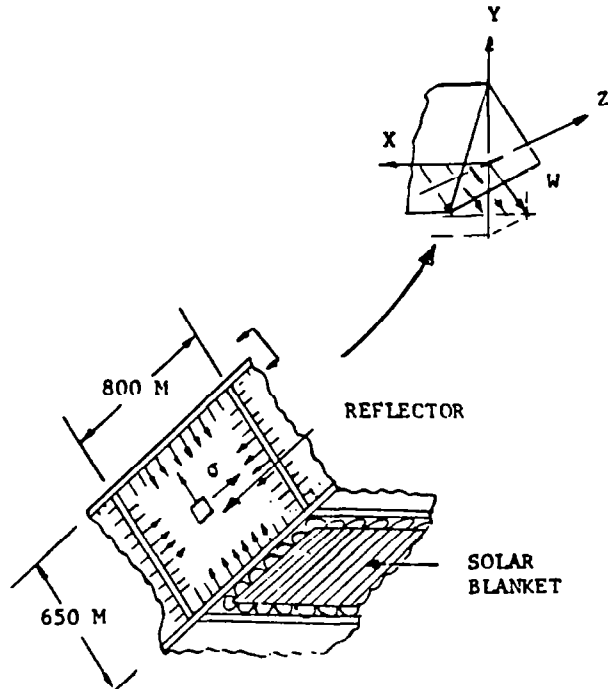
Figure 2.3-11. Mechanical Loading

end actions are shown in Figure 2.3-12. The values of the fixed-end actions must be added to the computer element loads for the true loads on the beam elements. The final member end reactions for a bar element used in the NASTRAN computer program is given by:

$$AMF = AM + FEA$$

where

AMF = matrix of the final member end actions

AM = matrix of the end action found by the computer program.

FEA = matrix of the fixed-end action for the bar element due to the reflector loading.

For the cases analyzed, the fixed-end actions are as follows:

$$\text{FEA}\binom{800M}{BEAM} = \begin{bmatrix} M_{1A} \\ M_{2A} \\ M_{1B} \\ M_{2B} \\ V_1 \\ V_1 \\ V_2 \\ V_2 \\ A \\ T \end{bmatrix} = \begin{bmatrix} -3.033 \times 10^5 \text{ N-M} \\ 1.751 \times 10^5 \text{ "} \\ -3.033 \times 10^5 \text{ "} \\ 1.751 \times 10^5 \text{ "} \\ -2278 \text{ N-} \\ 2278 \text{ "} \\ 1350 \text{ "} \\ -1350 \text{ "} \\ 0 \\ 0 \end{bmatrix} \qquad \text{FEA}\binom{650M}{BEAM} = \begin{bmatrix} 0 \\ 2.312 \times 10^5 \text{ N-M} \\ 0 \\ 2.312 \times 10^5 \text{ "} \\ 0 \\ 0 \\ 2137 \text{ N} \\ -2137 \text{ N} \\ 0 \\ 0 \end{bmatrix}$$

Deflection Results

   Figure 2.3-13 summarizes the end deflections of the SPS unit for the three analysis cases considered. The deflections for the aluminum cases are several orders of magnitude larger than those of the graphite case. The pretension, the force necessary to keep the X-braces from becoming compressive under the given thermal and mechanical loading environment, is as follows:

   Aluminum design; steel X-bracing   552 MPa (80 KSI)

   Graphite design; graphite X-bracing   137 MPa (20 KSI)
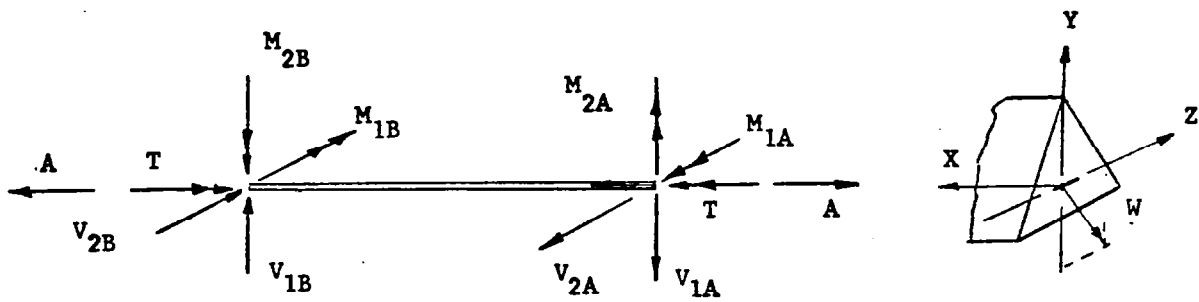
(a) BAR ELEMENT FORCES
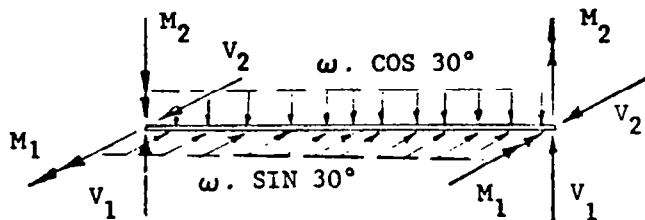
(b) FIXED-END ACTIONS

Figure 2.3-12. Nomenclature of Bar Element Forces
and Fixed End Actions

Figures 2.3-14, 2.3-15, and 2.3-16 show the displacements for selected points on the various substructures of the SPS unit for the graphite construction Case 2, and the aluminum construction Case 3. A comparison of the displacements will give the amount of distortion that the reflectors, solar blankets, and other equipment would have to undergo for the various materials. The CRT sketches cannot be compared directly due to the displacement scale factors used by the computer program. For more detailed study of the displacements, the computer printouts are available, but are not included in this report due to its voluminous nature.

Stress Results

The stress of selected members is presented in Figure 2.3-17, for the graphite and aluminum material construction under pretensioning. As shown in the table, the stresses are much higher for the aluminum case than for the graphite case. The maximum bending stresses for many of the members exceed the crippling allowables (5800 psi at RT) of the elemental beam caps.

NOTE:
ALL DIMENSIONS
IN METERS
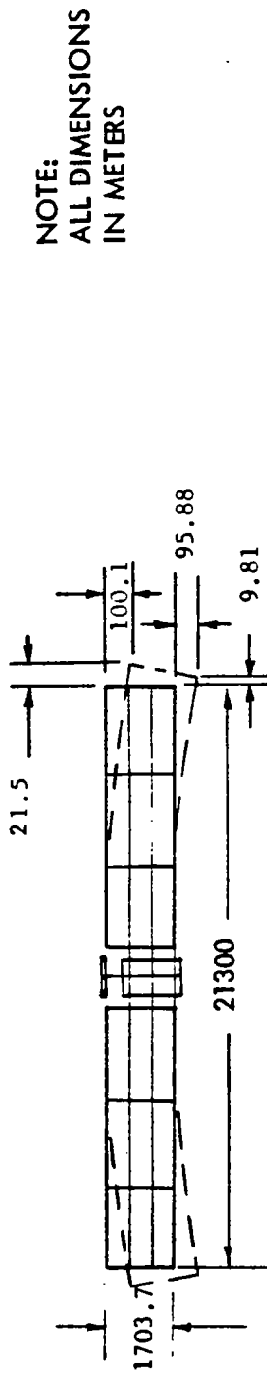
(a) CASE 1. ALUMINUM, NO PRETENSION IN X-BRACING
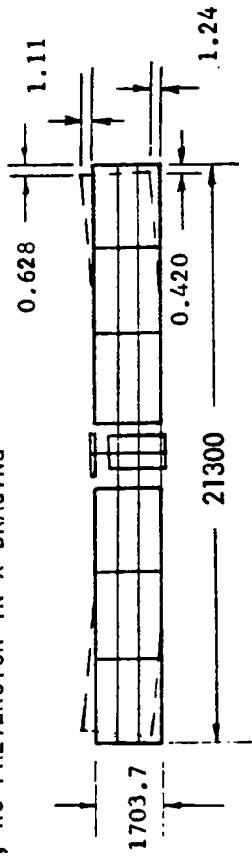
(b) CASE 2. COMPOSITE, PRETENSION IN X-BRACING
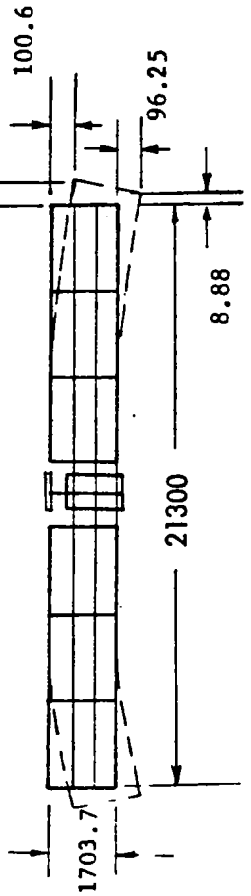
(c) CASE 3. ALUMINUM, PRETENSION IN X-BRACING

DEFLECTIONS ARE SEVERAL ORDERS
OF MAGNITUDE LARGER FOR
ALUMINUM AS FOR GRAPHITE MATERIAL.

Figure 2.3-13. Deflections - SPS Unit

NOTE:
ALL DIMENSIONS
IN METERS
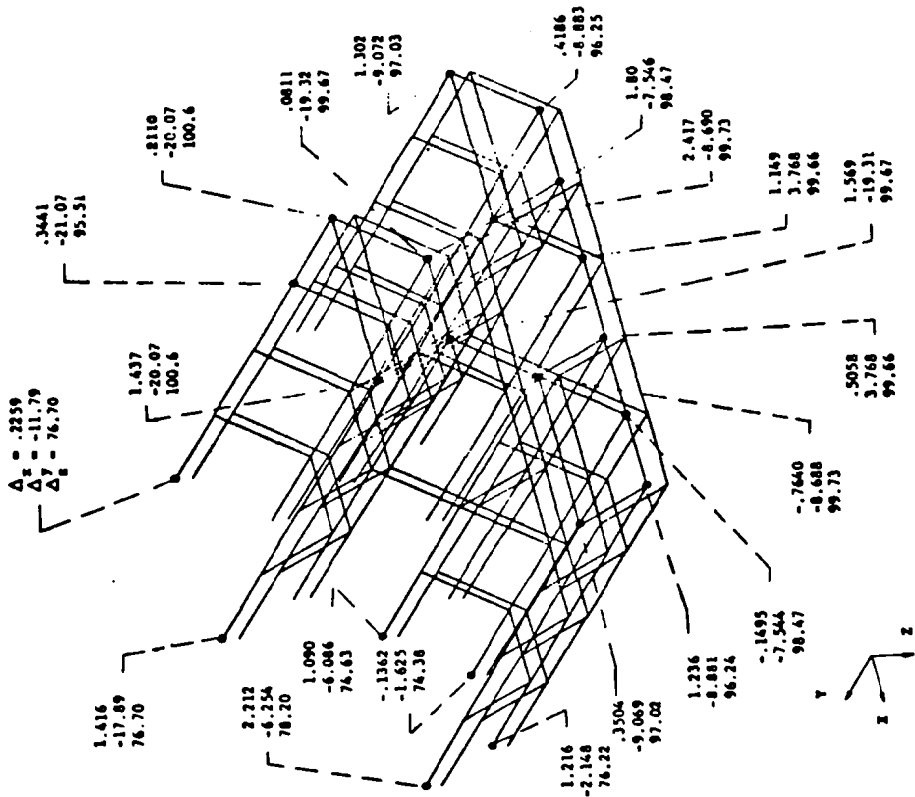
SUBSTRUCTURE NO. 1, CASE 3, DISPLACEMENTS
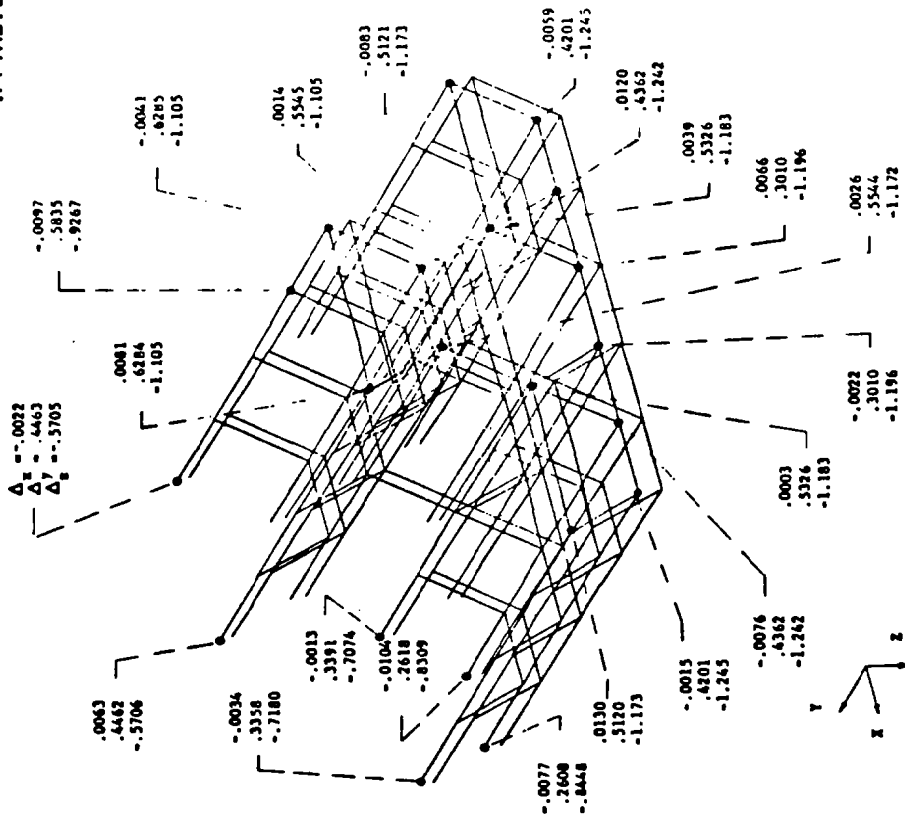
SUBSTRUCTURE NO. 1, CASE 2, DISPLACEMENTS

Figure 2.3-14. Deflections – End Mounted

NOTE:
ALL DIMENSIONS
IN METERS
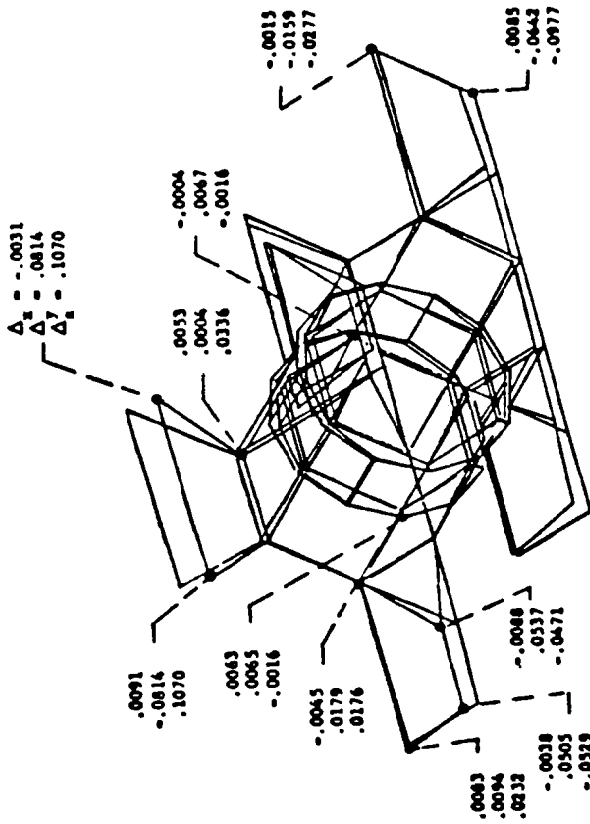
(a) CASE 2, COMPOSITE MATERIAL
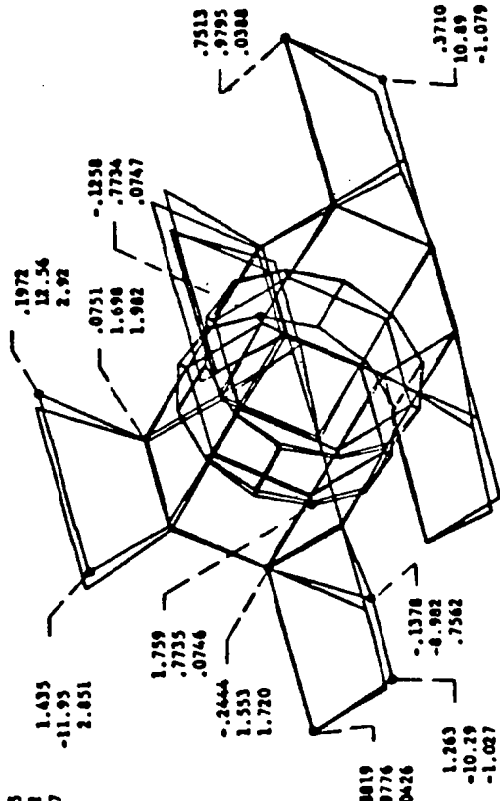
(b) CASE 3, ALUMINUM MATERIAL

Figure 2.3-15. Deflections – Center Structure

NOTE:
ALL DIMENSIONS
IN METERS

.5506
-1.473
.3222

.1926
.0005
-.0254

-.0653
-.0025
.0022

.0024
.0022
.0151

$\Delta_x = .0024$
$\Delta_y = -.0040$
$\Delta_z = -.0330$

.0065
.0016
-.0202

.0697
-.0027
-.0020

(a) CASE 2, COMPOSITE MATERIAL

-.2162
.3103
-2.123

-.2334
-.2467
.1212

.8167
-.0294
.8838

.5523
.4775
-.5100

.8161
-.2968
.1245

2.919
.3116
-1.476

1.868
-.2466
.1208

(b) CASE 3, ALUMINUM MATERIAL
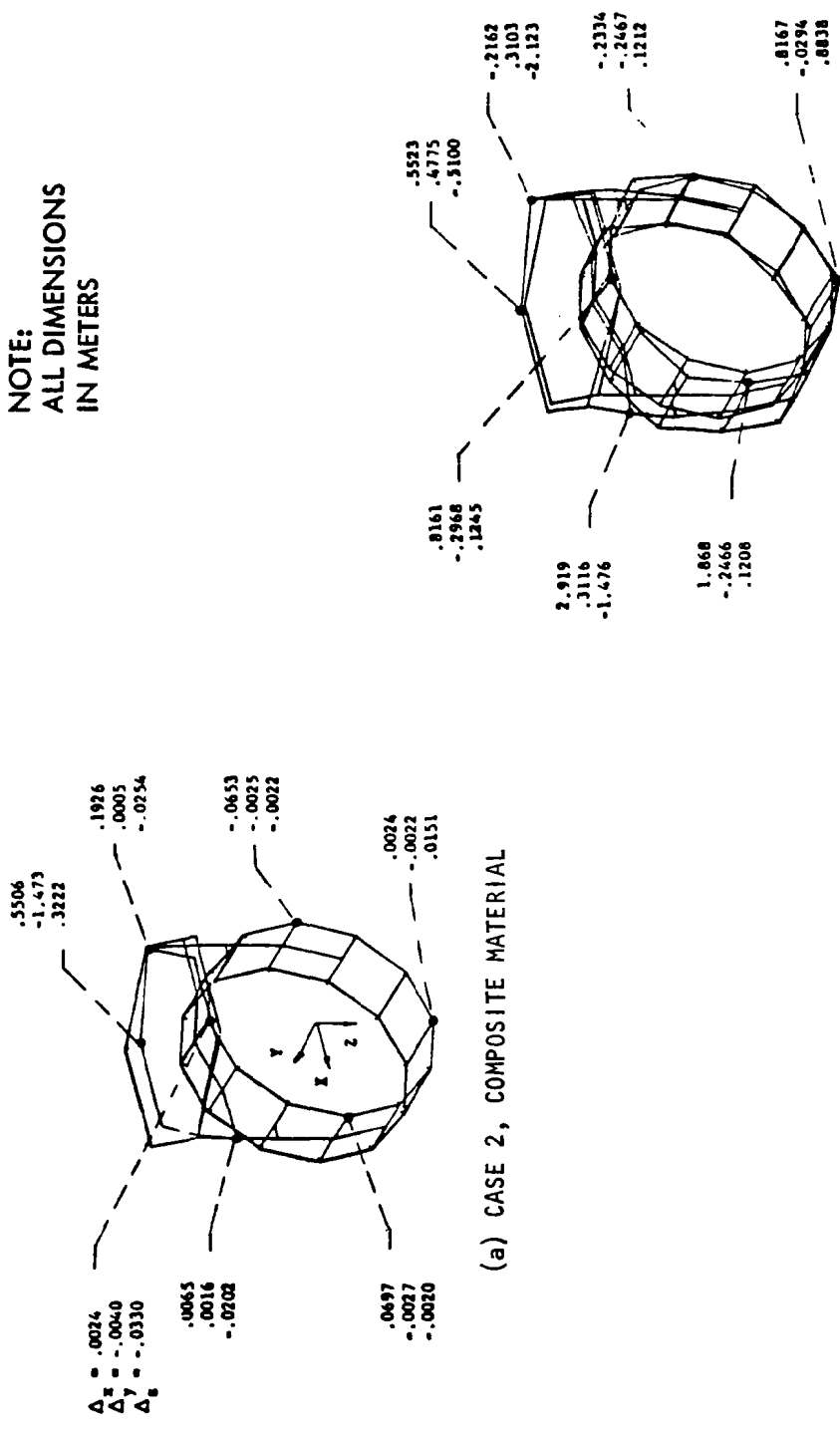
Figure 2.3-16. Deflections - Antenna and Rotating Ring

2-55

TABLE . COMPRESSIVE STRESS COMPARISON

ELEMENT NO.	CASE 2, COMPOSITE				CASE 3, ALUMINUM			
	AXIAL STRESS		MAX. BEND STRESS		AXIAL STRESS		MAX. BEND STRESS	
	MPa	(KSI)	MPa	(KSI)	MPa	(KSI)	MPa	(KSI)
101	-1.01	(-.14)	-8.72	(-1.26)	-5.88	(-.85)	-131.7	(-19.10)
102	-1.02	(-.14)	-1.89	(-.27)	-2.85	(-.41)	-58.4	(-8.47)
103	-0.87	(-.12)	-1.47	(-.21)	-9.54	(-1.38)	-72.7	(-10.50)
104	-1.02	(-.14)	-1.89	(-.27)	-2.85	(-.41)	-58.4	(-8.47)
105	-1.02	(-.14)	-8.72	(-1.26)	-5.88	(-.85)	-131.7	(-19.10)
106	-1.99	(-.28)	-4.98	(-.72)	-9.81	(-1.42)	-41.3	(-5.99)
107	-7.68	(-1.11)	-15.90	(-2.31)	-10.31	(-1.50)	-80.2	(-11.63)
108	-0.71	(-.10)	-2.21	(-.32)	-3.20	(-.46)	-8.4	(-1.22)
109	-7.68	(-1.11)	-15.92	(-2.31)	-10.03	(-1.45)	-80.2	(-11.63)
114	-0.21	(-.03)	-1.15	(-.16)	-2.74	(-.39)	-129.5	(-18.78)
115	-0.70	(-.10)	-2.60	(-.37)	-4.46	(-.64)	-22.5	(-3.26)
116	-7.65	(-1.11)	-16.59	(-2.41)	-15.70	(-2.28)	-110.1	(-15.97)
117	-0.21	(-.03)	-1.52	(-.17)	-2.74	(-.39)	-129.5	(-18.78)
118	-1.19	(-.17)	-3.85	(-.55)	-5.02	(-.73)	-59.5	(-8.63)
119	-7.61	(-1.10)	-1.52	(-.22)	-11.06	(-1.68)	-36.1	(-5.24)
1204	-2.08	(-.30)	-2.73	(-.39)	-8.26	(-1.20)	-80.7	(-11.70)
1206	-7.58	(-1.10)	-17.62	(-2.56)	-27.48	(-3.99)	-85.1	(-12.34)
1208	-7.01	(-1.02)	-18.09	(-2.62)	-8.66	(-1.26)	-49.6	(-7.19)
1210	-6.94	(-1.01)	-18.53	(-2.69)	-9.83	(-1.43)	-37.1	(-5.38)
1214	-6.90	(-1.00)	-16.22	(-2.35)	-12.71	(-1.84)	-17.7	(-2.57)
1213	-7.53	(-1.09)	-9.11	(-1.32)	-32.55	(-4.72)	-102.6	(-14.88)

STRESS MAGNITUDES ARE 3 TIMES
AND LARGER FOR ALUMINUM AS
FOR GRAPHITE MATERIAL.

ELEMENT NUMBER

ELEMENT IDENTIFICATION NUMBER

Figure 2.3-17. Results - Stress

NASTRAN Limitations

The thermal effects analysis of the SPS structure brought out several limitations in the NASTRAN computer program. For example:

1. Subelement level analysis of beam element is not practicable. The beam elements are themselves a structural subsystem.

2. Concentrated and/or distributed loadings capability for beam element not incorporated in NASTRAN. Equivalent joint loads must be used resulting in large manual effort.

3. Stress recovery for the beam elements is complex, requiring laborious error-prone manual operations.

4. Program cannot remove tension-only members which become compressive (negative) during solution.

Investigation into, and the corrections of, the defficiencies must be accomplished for further detailed stress/dynamic analysis of the SPS structure. Possible corrections may be through the use of pre- and post-processor programs in conjunction with the NASTRAN program and/or through the use of the DMAP feature of NASTRAN program.

Design Impacts

The impact of the results of this analysis upon the design of the SPS structure is summarized as follows:

1. Depending upon design methodology and ingenuity, there will be an increase in the aluminum gauge size (presently 10 mils) due to the crippling allowables with a corresponding increase in structural weight.

2. The larger deflections for the aluminum construction may present a more complex design problem for the reflectors and solar blankets attachments, brush design of the rotating ring, configuration control, and attitude/stationkeeping control.

3. Based on the thermal stresses and deflections, advanced composites are recommended for SPS structures as the basic structural material. For the rotating ring and the inner support ring, where power transfer is required, a combination of aluminum and composite may be appropriate and needs to be investigated. Although advanced composites are recommended, final resolution of this issue requires the long-term survivability issue to be resolved.

2.4 THERMAL CONTROL

The thermal analysis consisted of computing temperature profiles for the satellite structure, analyzing heat rejection options for the klystron installation concepts, and evaluating solid state alternative concepts.

2.4.1 TEMPERATURE PROFILES

The NASTRAN structural analysis of the SPS system was conducted to determine thermal effects comparison between a metal (aluminum) and an advanced composite (graphite) material design concept. The temperature profiles of the structure are shown in Figures 2.4-1 through 2.4-3 for three stages of the composite structure life. The end of life profile (Figure 2.4-3) is considered to be the most severe thermal gradient, and is used for the thermal structural analysis. Corresponding temperature profiles for coated aluminum were computed as part of work performed during Exhibit A/B and are shown in SD 78-AP-0023-4, SPS Point Design Definition.

Results of an analysis to define thermal control requirements for the switchgear and high voltage dc converters are shown in Figure 2.4-4. For the switchgear the waste heat can be rejected passively by increasing case size to the required dimension. The data shown on the figure is applicable to a cubic configuration. To cool the dc converters, an active loop is required.

COATED GRAPHITE COMPOSITE
(BEGINNING OF LIFE)

OPTICAL PROPERTIES
    $\alpha = 0.33$
    $\epsilon = 0.92$
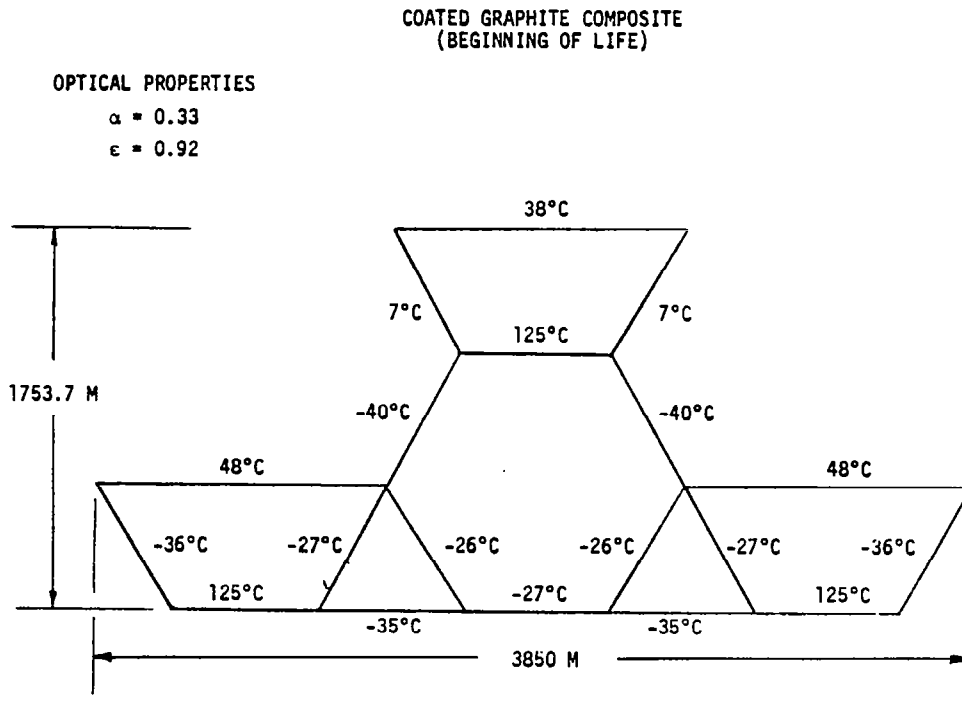
Figure 2.4-1. *Photovoltaic Structural Configuration Temperatures - Beginning of Life*

2-58

COATED GRAPHITE COMPOSITE
(INTERMEDIATE LIFE)

OPTICAL PROPERTIES

$\alpha = 0.67$

$\epsilon = 0.89$
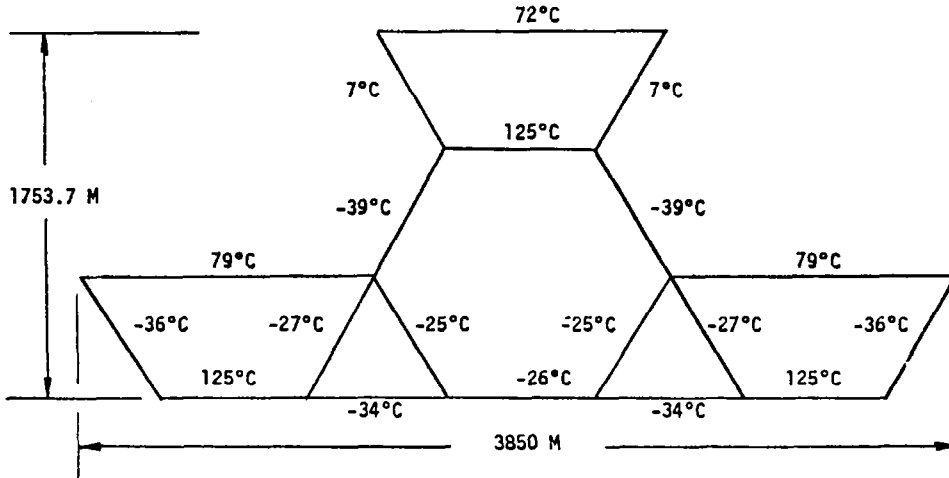
Figure 2.4-2. *Photovoltaic Structural Configuration Temperatures - Intermediate Life*

COATED GRAPHITE COMPOSITE
(END OF LIFE)

OPTICAL PROPERTIES

$\alpha = 0.89$

$\epsilon = 0.86$
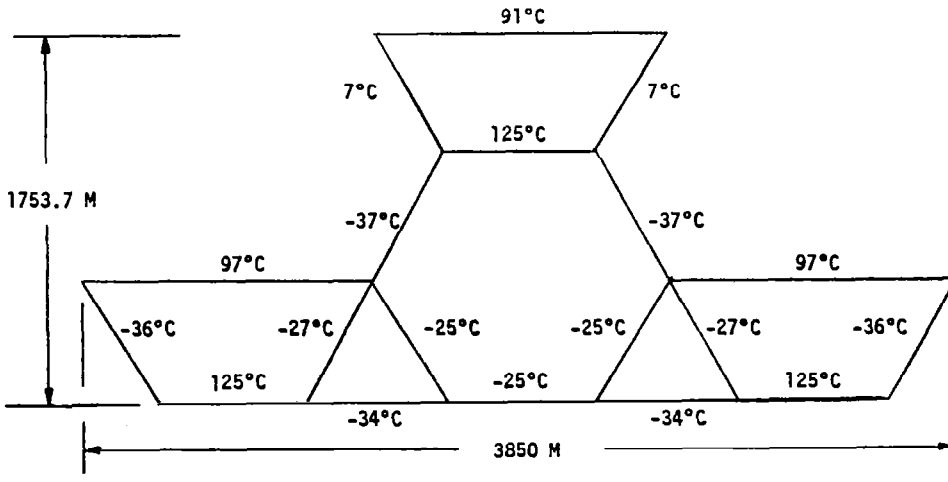
Figure 2.4-3. *Photovoltaic Structural Configuration Temperatures - End of Life*
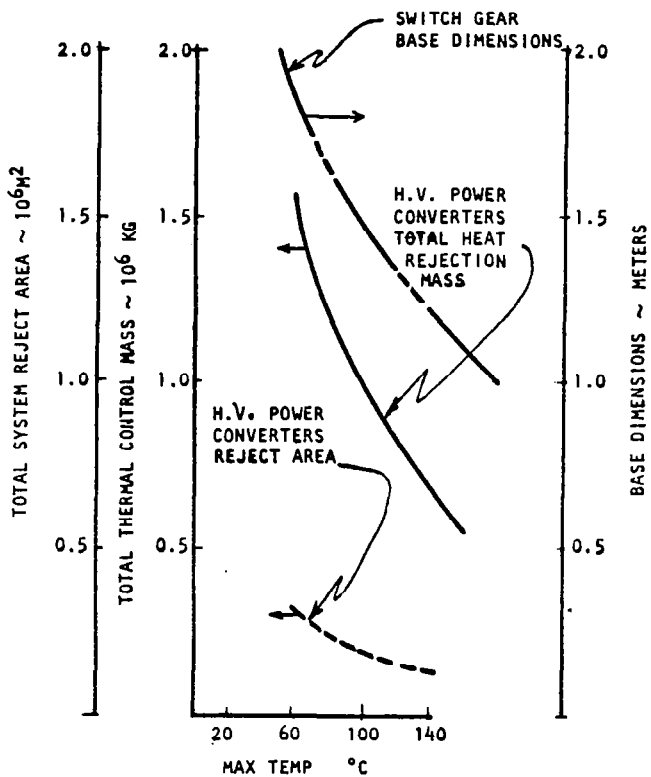
2-59

Figure 2.4-4. Power Distribution Component
Thermal Control

Due to their power level, thermal efficiency, and operating temperature re-
struction, relatively large radiator systems are required. Significant weight
reduction is required and advanced technology must be developed to reduce the
weight impact of these systems. System optimizations that offer potential for
weight savings include: disk configurations and/or hemispherical; heat pipe
integrated into the radiator; optimized radiator fin geometry; higher tempera-
ture electronics; and waste heat usage.

2.4.2 KLYSTRON HEAT REJECTION OPTIONS

The primary candidate klystron installation design concepts are illustrated
in Figure 2.4-5. The initial Rockwell baseline power module "poke through"
concept was selected during Exhibit A/B study because of thermal rejection
considerations relative to potential overheating of the slip rings, tempera-
ture limitations on the electronics, and the postulated requirement (later
deleted) for manned access to the antenna during operation. The alternate
Rockwell concept, which has since been adopted, eliminates the performance
uncertainty and efficiency losses resulting from poking the klystron tube
through the radiator. This selection follows from analysis which demonstrates
that the slip rings can be thermally protected and that the weight penalty
associated with controlling electronic component temperatures is relatively
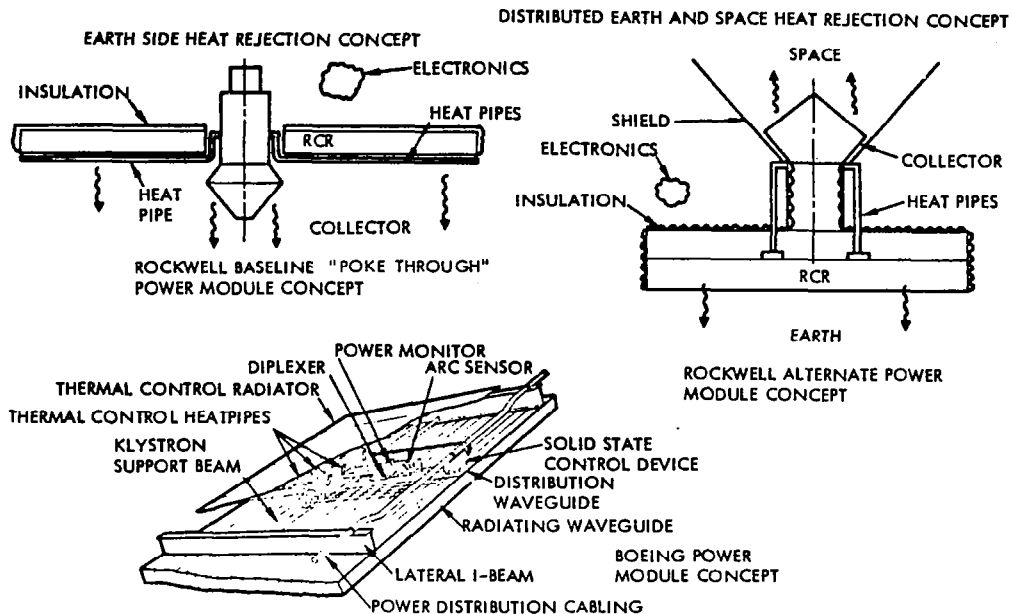
Figure 2.4-5. Klystron Design Concepts

small. This klystron installation concept appears more advantageous than the tubes sandwiched and on their sides as shown for the Boeing power module concept because of its less complex and lighter weight thermal control system. In addition, it appears more flexible in terms of distributing the heat to be rejected in both directions (space and earth).

The three options for the power tube installation were shown in Figure 1.1-9 with installation in a space frame configuration illustrated. Each of these concepts could be adapted to either the tension web or space frame antenna design.

If possible, utilization of low temperature composites (or aluminum) for the antenna structure is desirable to avoid increased complexity during the construction process and to preclude unnecessary additional program costs for the development of high temperature composite materials. Potential graphite fiber reinforced resin systems that might be utilized on large space structures are listed in Table 2.4-1. The maximum use temperatures shown are based upon General Dynamic quoted limits and Rockwell estimates. Further testing, including extended period outgassing determinations, could result in modifications of these values.

In the space frame configuration the primary structure is in close proximity to the high temperature, heat rejection surface of the klystron (assuming that the tube is not "poked through"). Independent studies by Rockwell, General Dynamics, and Grumman have demonstrated that temperatures in the central region of the antenna will exceed allowables for low temperature composites. For beam machine concepts this can complicate the construction scenario by potentially requiring the substitution of a different machine at some point in the assembly sequence.

2-61

*Table 2.4-1. Graphite Composite Materials
Temperature Limits*

MATERIAL	MAX. ALLOWABLE TEMP. °K
THERMOSETTING RESINS	
EPOXY	395
PHENOLIC	435
POLYIMIDE	
ADDITION	475
CONDENSATION	560
THERMOPLASTIC MATERIALS	
POLYSULFONE	380
POLYIMIDE	590

A temperature analysis was performed to compute thermal environments for the various installation options. A summary of the computed structural temperatures are given in Table 2.4-2. Results of this analysis show that for the space frame both the alternate and the sandwiched side installation concepts require high temperature composites for the structural materials. Low temperature polysufone materials are constructed to a 107°C (380 K) thermal environment. The thermal advantage of a tension web (compression frame) configuration is apparent from the tabulated summary. The tension web structural elements are distributed around the antenna periphery relatively distant from the power modules. The effect is further minimized due to the relatively small amount of energy intercepted from the high radiation area in the central portion of the antenna. Relatively low temperatures result. The tension web elements/cables could be manufactured simply from graphite filaments or possibly low temperature fibers (e.g., fiberglass) encased in a protective sheath. Temperature profiles and resultant thermal gradients will substantially influence antenna configuration, power module design and structural material selection.

Results of the thermal analysis suggests the continued use of the tension web (compression frame) structure and substitution of the improved, alternate Rockwell klystron concept. The center mounted antenna configuration, if modified to move the slip rings outward or reflector protected, is basically thermally equivalent to an end mounted antenna configuration. The space frame antenna concept requires the development of high temperature composite materials for all but the "poke through" klystron installation concept. The alternate Rockwell klystron installation concept is lightweight and permits a simple thermal control design. This also allows a flexibility in thermal design by being able to vary the percentage of waste heat rejected towards the earth, i.e., from ~10% to ~30%.

2.4.3 SOLID STATE ALTERNATIVE CONCEPTS

The concept initially studied for application of solid state dc/RF conversion assumed that 50 kW solid state power modules replaced 50 kW klystrons in an antenna configuration basically the same as that used for klystrons. In order to provide adequate efficiency and lifetimes, the temperature of the solid state devices need to be maintained $\leq$ 150 C. To achieve this low

Table 2.4-2. *Antenna Temperature/Materials Considerations*

CONCEPT	KLYSTRON POWER LEVEL KW	TEMPERATURES ~°C				STRUCT. SURFACE (COMP. MAX TEMP ~°C
		KLYSTRON		RCR SURFACE		
		COLLECTOR	BODY	EARTH SIDE	SPACE SIDE	
COMPR. FRAME						
"POKE THRU"	50	700	200	152	60	70
ALTERNATE	50	700	200	129**(140)	104**(60)	70
SPACE FRAME						
"POKE THRU"	50	700	200	152	60	<107
ALTERNATE	50	700	200	129**(140)	104**(60)	⊂127⊃
BOEING	70	500	300		>150*	⊂150⊃

KEY

⊂⊃ = EXCEEDS LOW TEMP. COMPOSITE LIMITS

* = THERMAL THIN CONTROL RADIATOR SURFACE

** = WITHOUT INSULATION

( ) = WITH INSULATION

• ALTERNATE CONCEPTS CAN BE MODIFIED TO ALLOW HEAT REJECTION FROM SPACE FACING SURFACE (I.e., WITH OR WITHOUT INSULATION)

• SPACE FRAME REQUIRES "POKED THRU" KLYSTRON FOR LOW TEMPERATURE COMPOSITE UTILIZATION

• COMPRESSION FRAME/TENSION WEB IS PREFERRED TO AVOID REQUIRE-MENT FOR HIGH TEMPERATURE COMPOSITES

temperature the radiator penalty was calculated to be ~5.5×10^6 kg (150 C) and 13.0×10^6 kg (60 C).

Alternative approaches that were judged to solve the thermal problem include: (1) a reduction of RF power in the center of the antenna to 12 kW/m^2 and radiation from both sides of the antenna; (2) redistribution of the center power module to increase their spacing and then using wave guides to direct RF energy to appropriate microwave radiators; and (3) increasing the antenna diameter to increase thermal and microwave radiation area while simultaneously reducing power output from the satellite.

The thermal problem can also be solved by locating the solid state power modules on the solar array. Wave guides would be used to direct the RF energy to a horn located on the end of the array that feeds a lens antenna. Studies of this wave guide approach have indicated very difficult technology problems related to RF mode control. A solution to the wave guide problem is to utilize a sandwich design which has the solar cells on one side and antenna on the other side and the use of reflectors to direct solar energy onto the solar cells.

2.5 ATTITUDE CONTROL AND STATIONKEEPING

During October 1978 the NASA recommended spacecraft configuration was specified to be coplanar with an end mounted antenna array. This configuration is illustrated in Figure 2.5-1. Because of the end mounted antenna the configuration has a large center of mass offset. This offset, when coupled to large effective solar pressure results in a substantial solar pressure torque about the axis perpendicular to the orbit plane.

SOLAR PRESSURE FORCE

ATTITUDE REFERENCE DETERMINATION
(7 LOCATIONS)
• CCD SUN SENSOR (1/SYSTEM)
• CCD STAR SENSORS (2/SYSTEM)
• ELECTROSTATIC OR LASER GYROS (3/SYSTEM)
• DEDICATED MINI PROCESSOR

REACTION CONTROL SYSTEM (RCS)

FEATURES:
• ARGON ION BOMBARDMENT THRUSTERS - LOCATED IN 4 MODULES
• CRYOGENIC PROPELLANT STORAGE - ELECTRIC REFRIGERATION FOR HEAT LOSS MAKEUP
• HEMISPHERICAL PLUME CLEARANCE
• SERVICEABLE IN PLACE

THRUSTER CHARACTERISTICS:
• THRUST - 13N
• SPECIFIC IMPULSE - 13,000 SEC
• POWER - 1275 KW
• APERTURE - 1M
• MASS (INCL. SUPPORTS & CABLING) - 120 KG
• RESTART TIME - 15 SEC
• OPERATING LIFE (GRIDS & CATHODES) - 8000 HR

CENTER OF MASS

GIMBALLED RCS THRUSTERS
(16 PER CORNER, 64 TOTAL)

$\theta_1 = +20.7°$
$\theta_2 = +1.8°$

Figure 2.5-1. ACSS Equipment Locations

A large solar pressure force acts on the structure because of the large surface area of the solar blankets and reflectors. This solar pressure force is the dominant orbit perturbation to be corrected by the stationkeeping system. For attitude control, the concern is how to accommodate the large unbalanced solar pressure torque and gravity gradient torque inherent in the coplanar configuration. Thus, for this configuration, these unbalanced torques have a larger impact on the design of the ACSS than for previous symmetrical Rockwell SPS configurations, (Final Report, SD 78-AP-0023, dated April 1978), which were designed to minimize these disturbance torques.

2.5.1 SOLAR PRESSURE MODEL

Because of the impact of the solar pressure force on the coplanar design, a more accurate model was necessary to describe the solar pressure force. To derive the model, it was assumed that solar energy was reflected specularly off the reflectors and diffusely off the solar cell blankets. Figure 2.5-2 shows
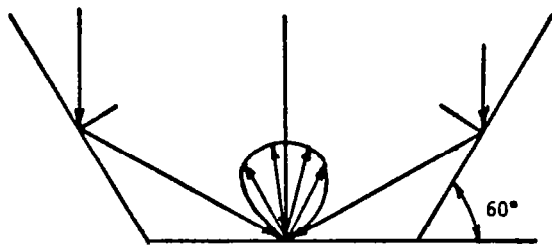
$A_b \overset{\Delta}{=}$ TOTAL AREA OF BLANKET

$A_c \overset{\Delta}{=}$ CAPTURE AREA OF BLANKET $= CR \times A_b$

$A_R \overset{\Delta}{=}$ TOTAL AREA OF REFLECTOR

$R_b \overset{\Delta}{=}$ REFLECTIVITY COEFFICIENT OF BLANKET $= 0.17$

$R_R \overset{\Delta}{=}$ REFLECTIVITY COEFFICIENT OF REFLECTOR $= 0.90$

$$\Sigma F_{sp} = \underbrace{P_s A_b (1+R_b)}_{\substack{\text{FORCE ON BLANKET} \\ \text{FROM DIRECT SUNLIGHT}}} + \underbrace{P_s A_R \cos 60°[(1-R_R)\sin^2 60° + (1+R_R)\cos^2 60°]}_{\substack{\text{FORCE ON REFLECTORS} \\ \text{FROM DIRECT SUNLIGHT}}} + \underbrace{2(1+R_b)R_R P_s A_b \cos^2 60°}_{\substack{\text{FORCE ON BLANKET FROM} \\ \text{REFLECTED SUNLIGHT}}}$$

$+$ REFLECTIONS FROM BLANKET BACK ON REFLECTORS (NEGLECTED)

$$\Sigma F_{sp} = P_s[A_b(1+R_b)(1+R_R/2) + A_R/2(1-R_R/2)]$$

FOR CR $= 2$, $A_c = 2A_b$ AND SUBSTITUTING $R_b = 0.17$ & $R_R = 0.9$

$$\boxed{\Sigma F_{SP} = 1.125 \, P_S \, A_C}$$

OVERALL COLLECTOR HAS EQUIVALENT REFLECTIVITY $= 0.125$

Figure 2.5-2.   Solar Pressure Force Model

the major steps that were taken in the derivation. The effects of secondary reflections from the solar cell blankets back onto the reflectors were found to be negligible and are not included. The result is a force expression as a function of the capture area of the blanket. The interpretation of this expression is that the overall collector has an equivalent reflectivity of .125.

2.5.2 RCS REQUIREMENTS

Attitude Control

The solar pressure and gravity gradient torques have been determined to be the dominant disturbances that will be encountered by the attitude control system. These torques are, therefore, the major factors driving the RCS propellant and thruster requirements. Argon ion bombardment thrusters have been assumed. The effect of these factors on the RCS requirements are shown in Figure 2.5-3. The data assumes the disturbance torques are balanced with torque couples and are obtained independently of the thrusters providing the stationkeeping forces.

Upon reviewing the data, the propellant requirements were found to be substantially larger than for the previous Rockwell symmetrical spacecraft (SD 79-AP-0023, dated April 1978). That vehicle had a total requirement of

FUNCTION	PROPELLANT MASS (% S/C MASS OVER 30 YEARS)	NO. OF THRUSTERS*		
		X	Y	Z
●SOLAR PRESSURE ⎫ ●ANTENNA RADIATION ⎬ PRESSURE ⎭	4.01			15.2
●GRAVITY GRADIENT				
• ABOUT X	0.124			1.66
• ABOUT Y	1.38			16.4
• ABOUT Z	0.124	1.6		
	1.62	1.6		18.1
TOTALS	5.63	1.6		33.3
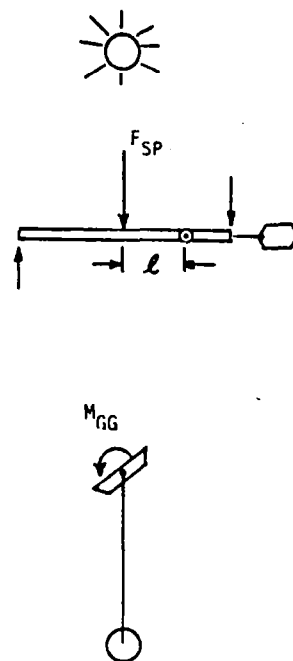
*TORQUE COUPLES ASSUMED

**100-CM ARGON THRUSTERS, $T = 13n$, $I_{SP} = 13,000$ SEC, $M_{S/C} = 36.6 \times 10^6$ KG, $I_{XX} = 9.86 \times 10^{14}$ KG-M^2,

$I_{YY} = 3.09 \times 10^{12}$ KG-M^2, $I_{ZZ} = 10.2 \times 10^{14}$ KG-M^2

(INCLUDING GROWTH)

*Figure 2.5-3. Attitude Control RCS Requirements***

less than 0.6% of the spacecraft mass over 30 years. Fortunately, attitude control and stationkeeping do not have to be considered independently. Appreciable savings can be realized by utilizing the thruster force for stationkeeping to provide the torques for attitude control.

Stationkeeping RCS Requirements and Correction Policies

For small contemporary spacecraft, the dominant stationkeeping ΔV is to correct the solar-lunar perturbations. However, Table 2.5-1 clearly shows that for an SPS vehicle the solar pressure perturbation dominates by a factor greater than five. To counter the solar pressure perturbation, two correction policies were considered for stationkeeping.

One stationkeeping policy considers the constant cancellation of the solar pressure force while the other policy for ΔV correction utilizes an approximate Hohmann transfer. Referring to Figure 2.5-4, the Hohmann transfer policy shows a potential propellant savings of 25%. However, this savings is not realized because during the coast periods large propellant consumption is required for attitude control. The preferred scheme is the continuous thrusting policy, and as will be subsequently shown, it virtually eliminates the propellant requirements for attitude control due to solar pressure and gravity gradient torques.

Table 2.5-1. Stationkeeping RCS Requirements * .

FUNCTION	ΔV (m/s/YR)	PROPELLANT MASS (% S/C MASS OVER 30 YRS)	THRUST REQUIRED (N)	NUMBER OF THRUSTERS
• SOLAR PRESSURE (E-W) • ANTENNA RADIATION PRESSURE (E-W) • EARTH TRIAXIALITY (E-W) • STATION CHANGE (E-W)	282.5	6.65	328	25.2
• SOLAR-LUNAR PERTURBATION (N-S)	53.3	1.25	124**	19.1**
TOTALS	335.8	7.90	452	44.3

* - 100 CM ARGON THRUSTER, T - 13 N, ISP - 13,000 SEC

** - THRUST ON 50% OF TIME

• UNCORRECTED LONGITUDE PERTURBATION - ΔA - ±2.52°

• PROBABLY NOT ACCEPTABLE WITH POST-2000 TRAFFIC IN GEO

• CORRECTION POLICIES:

CANCEL SOLAR PRESSURE FORCE

$T = -F_{SP}$

$$M_P = \frac{F_{SP} \, \Delta t}{I_{SP}}$$
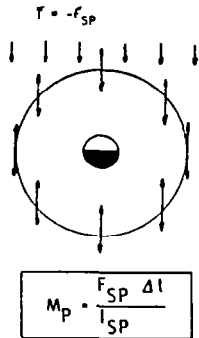
CORRECT AT APOGEE AND PERIAPSIS

$$M_P = \left(\frac{3}{4}\right)\frac{F_{SP} \, \Delta t}{I_{SP}}$$
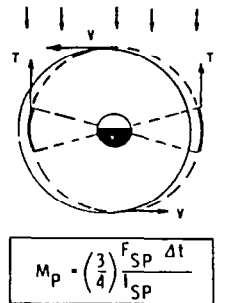
(PROPELLANT SAVINGS)

Figure 2.5-4. Solar Pressure Stationkeeping
Perturbation and Correction Policies

2.5.3 ACSS BASELINE DESIGN

Alternative Control Approaches

Figure 2.5-5 presents the RCS propellant and thruster requirements for
five possible cases including body mounted and gimbaled thruster configurations,
with and without complete correction of the solar pressure orbit perturbation,
and with the addition of two dimensional inertia balancing or the use of quasi-
inertial free drift attitude mode (QI – FDAM) to minimize the impact of large
cyclical gravity gradient torque. From the orbit perturbation considerations,

2-67

SYSTEM	THRUSTER CONFIGURATION		PROPELLANT MASS ($\%$ S/C MASS OVER 30 YR)	NO. OF THRUSTERS REQUIRED*			
	BODY FIXED	GIMBALED		X	Y	Z	TOTAL
COMPLETE STATIONKEEP-ING & ATTITUDE CONTROL	X		8.0	1.6	19.1	34.3	55.0
SAME		X	7.0			35.6	35.6
SAME BUT SOLAR PRESS. TRAJ. PERTURBATION NOT CORRECTED (TORQUE COUPLES FOR ATTITUDE CONTROL)	X		5.4	1.6	19.1	24.3	45.0
SAME BUT SOLAR PRESS. TRAJ. PARTIALLY CORRECTED (TORQUE COUPLES NOT REQ'D)	X		3.9	1.6	19.1	18.3	39.0
SAME BUT QIFDAM OR INERTIA BALANCING EMPLOYED (ELIMIN-ATES CYCLICAL G.G. ABOUT Y-AXIS)	X		8.0	1.6	19.1	26.1	46.8

*DOES NOT INCLUDE REDUNDANCY OR SPARES
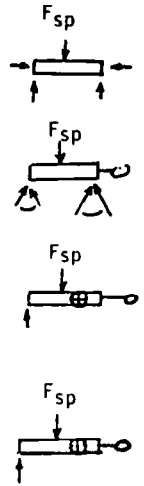
Figure 2.5-5. RCS Requirements for Alternative
Control Approaches

solar pressure stationkeeping correction is required and the preferred correction policy is a continuous force equal and opposite to the solar pressure force. The QI-FDAM approach with its $\pm 18°$ attitude excursions is applicable to a CR=1 configuration but is not appropriate to the current CR=2 design. Inertia balancing is not easily achieved in the present coplanar design concept. Based on these considerations, all the alternatives except the first two rows are rejected. The gimbaled thruster configuration (row 2) is seen to result in a small propellant savings and substantially less thrusters and is selected on that basis.

ACSS Baseline Description

In Figure 2.5-1, the SPS coplanar configuration is illustrated along with the pertinent features of the baseline ACSS. The baseline ACSS features an argon ion bombardment thruster RCS whose characteristics are enumerated on the figure. The system operates an average of 36 thrusters. A total of 64 thrusters are included to provide the required redundancy. The redundancy was based on an annual maintenance/servicing interval, 5000 hour thruster grid lifetime and 5-year thruster MTBF. Sixteen thrusters are located on the lower portion of each corner of the spacecraft. Each thruster is gimbaled individually to facilitate thruster servicing, to permit operation of adjacent thrusters during servicing, and to provide the redundancy. The thrusters nominally establish

a force vector approximately in the direction of the sun to counter the solar pressure force (stationkeeping) which is the dominant thruster requirement. The thrusters are gimbaled through small angles (as illustrated) and differentially throttled to provide the remaining forces and torques for attitude control and stationkeeping.

Also shown in Figure 2.5-1 are the locations and type of sensors that make up the Attitude Reference Determination System (ARDS). The mass properties of the ACSS are summarized in Table 2.5-2. The summary includes the mass of the individual elements and propellant mass. The system average operating power which is proportional to propellant mass is 33.87 megawatts.

Table 2.5-2. ACSS Mass Summary

ITEM	MASS $(x 10^{+3}$ KG)
ATTITUDE REFERENCE DETERMINATION SYSTEMS (7)	0.32
THRUSTERS - INCLUDING SUPPORT STRUCTURE, 64 @ 120 KG/THRUSTER	7.68
THRUSTER GIMBALS AND MOUNTING	TBD
TANKS, LINES, REFRIGERATION	15.07
POWER PROCESSING EQUIPMENT	TBD
ARGON PROPELLANT - ANNUAL REQUIREMENT	85.39
TOTAL (DRY)	23.07 *
TOTAL (WITH PROPELLANT)	108.46 *

* -NOT INCLUDING TBD ITEMS

2.5.4   BANKING FOR SOLAR POINTING

Previous ACSS concepts for SPS have employed a Y-POP reference orientation in order to minimize the RCS propellant expenditure due to the large gravity gradient torques for large bank angles. Collector cosine losses up to 8.2% result from this orientation.

Significant advantages can be realized if the spacecraft is pointed more directly toward the sun. The collector cosine losses would be reduced which reduces the sizing requirement for the solar collector, thereby achieving a reduction in spacecraft mass and cost. The ideal bank angle (roll) is 23.5° which is achievable with an increase in propellant and thrusters to the baseline ACSS. However, partial solar pointing with no propellant and thruster penalty is an advantageous feature. As illustrated in Figure 2.5-6, a roll angle of 9.0° can be realized with no propellant penalty or loss of control authority. Essentially, this is achievable by simultaneously countering the large gravity gradient torques and the solar pressure force through the use of the thrusters that are at one end of the spacecraft. With this bank angle, the collector cosine loss is reduced to 3.2% from 8.2% for a Y-POP orientation (net savings equal to 5%). The figure illustrates the steps and calculations
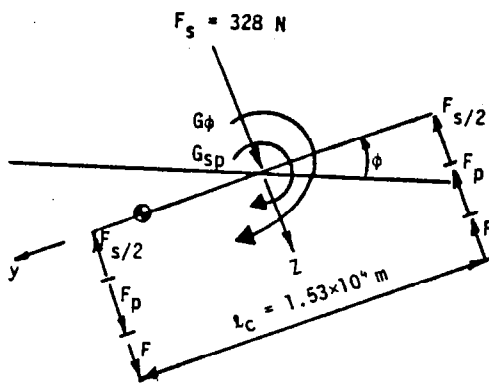
G_{SP} ≜ SOLAR PRESSURE TORQUE

G_ϕ ≜ GG TORQUE DUE TO BANK ANGLE ϕ
= $\frac{3}{2} W_0^2 (I_Z - I_Y) \sin 2\phi$

$F_S/2$ ≜ FORCE THAT CANCELS OUT SOLAR PRESSURE & TORQUE

F_P ≜ FORCE TO CONTROL GG TORQUE DUE TO .3° PRINCIPAL AXIS MISALIGNMENT = 5.4 N

F ≜ FORCE TO CONTROL G_ϕ

FROM PREVIOUS ANALYSIS ALL TORQUES EXCEPT G_ϕ ARE ACCOUNTED TO INSURE MODULATION $\Sigma F \geq 0$; $F_S/2 - F_P - F = 0$

$F = F_S/2 - F_P = 164 - 5.4 = 158.6$ N

F IS THE MAXIMUM FORCE AVAILABLE TO ROLL VEHICLE BY ANGLE ϕ

$$F\ell_c = 3/2 \, W_0^2 (I_Z - I_Y) \sin 2\phi \quad \text{AND} \quad \phi = \frac{1}{2} \sin^{-1} \left[\frac{F\ell_c}{\frac{3}{2} W_0^2 (I_Z - I_Y)} \right]$$

WITH THE VALUES OF F, ℓ_c AND $3/2 \, W_0^2 (I_Z - I_Y) = 7.84 \times 10^6$ NM

ϕ MAX = 9.02°
% COS LOSS = 3.16

Figure 2.5-6. Maximum Bank Angle

involved in deriving the bank angle. It is concluded that the ACSS configuration described herein will permit partial solar pointing (bank angles up to 9.0 degrees) which results in a substantial reduction in collector cosine losses, and hence a reduction in the solar collector size requirement.

2.6 MICROWAVE POWER TRANSMISSION

Existing analysis of the microwave transmission system (MPTS) have continued to leave certain basic questions unanswered. The fundamental concern, of course, is how to select an optimum approach to the transfer of energy to Earth located users. Five of these questions concerning:

- Beam formation,

- Microwave Power Amplifier selection,
    - Klystron
    - Solid State

- Solid state definition and design,

- Phase error control, and

- Antenna Array sidelobe variations and phase errors.

are discussed in the following section. Another, the question of the feasibility of laser energy transmission is partially discussed in Section 9, Volume V of this report. Other questions of this type will continue to be evaluated as they are identified, and as resources permit.

The analysis pertaining to the ground receiving station is discussed in Section 2.7.

2.6.1 BEAM FORMATION

The antenna configuration implemented in the present baseline consists of klystron power amplifier configured assemblies (subarrays) mounted in a planar configuration on the surface of the antenna structure. The klystrons are coupled to radiating wave guides in a selected energy pattern (beam). This beam is sized and shaped such that the ground receiving antenna (rectenna) portion of the ground receiving station intercepts better than 85% of the radiated energy.

Subarray configuration established in the baseline concept depends on the characteristics of the antenna beam efficiency, far field pattern and sidelobes. The beam efficiency is defined as the fraction of the total radiated power within the main beam. The beam efficiency is also a function of the far field pattern which is characterized by a main beam plus various sidelobes. The optimum aperture illumination distribution is one which places the most power within an angle subtended by the rectenna. Both Gaussian and Taylor distributions have been investigated to study the various parameters.

Gaussian Distribution

Although the analysis of the Gaussian shaped beam has been reported before, it is repeated here to afford the reader an opportunity to compare this analysis with the Taylor shaped beam analysis.

In the original Raytheon design, a Gaussian amplitude distribution with uniform phase distribution was used. The distribution is of the form

$$f(\ ) = e^{-0.115 \ (dB)\left(\frac{r}{r_o}\right)^2}$$

where r_o equals array radius, r = radial coordinate, and (dB) is the amount of taper from center to edge of the array in dB. Plots of the resulting antenna pattern and beam efficiency are shown in Figures 2.6-1 through 2.6-4. In these figures, the normalized angular parameter used is $\sqrt{A_T A_R}/\gamma D$, where A_T is transmitting array area, D is distance to measurement plane, γ is wavelength and A_R is the area of a disc whose radius subtends the pattern angle.
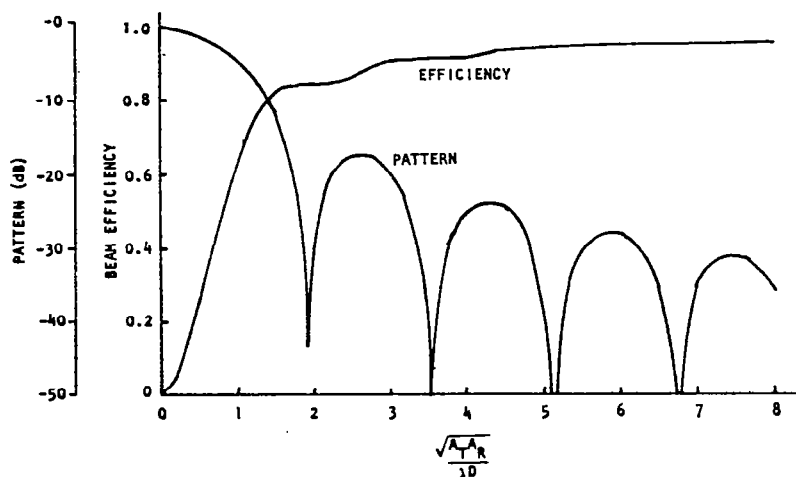
Figure 2.6-1. *Pattern Efficiency for Uniform Illumination*
(0 dB Taper)
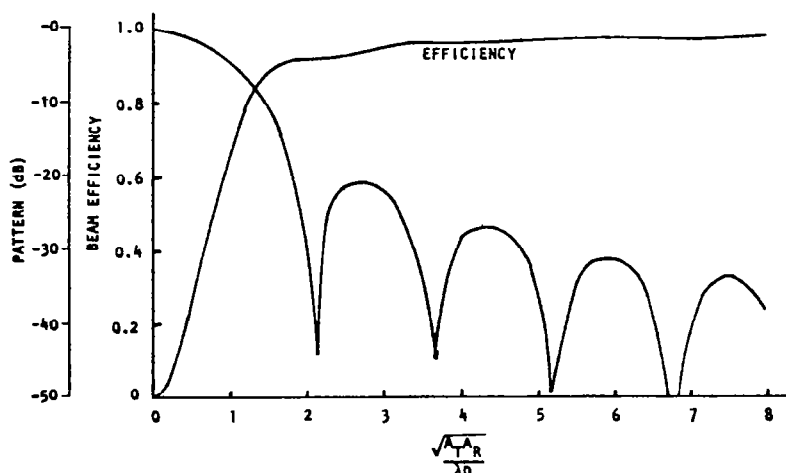
Figure 2.6-2. *Pattern Efficiency for Uniform Illumination*
(5 dB Taper)

2-72
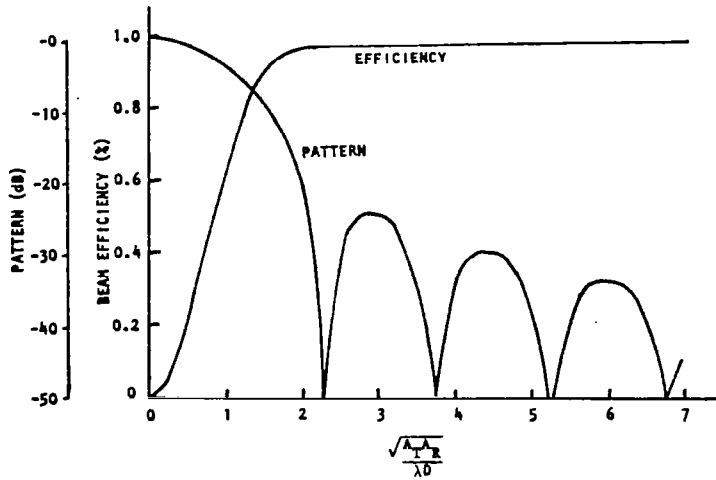
Figure 2.6-3.   Pattern Efficiency for Uniform Illumination
(10 dB Taper)
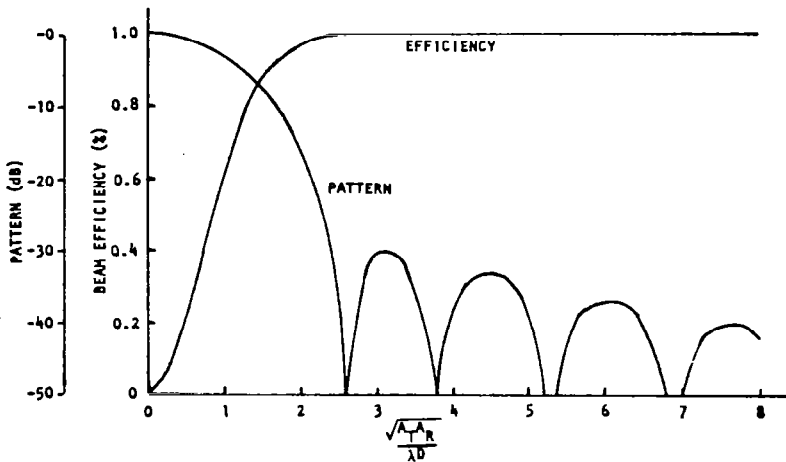
Figure 2.6-4.   Pattern Efficiency for Uniform Illumination
(15 dB Taper)

The taper was set by a permissible first sidelobe level to 10 dB. It may
be seen from Figure 2.6-5 that the corresponding first sidelobe level may be
about -23 dB. Figure 2.6-6 then shows equal beam efficiency contours plotted
on a taper/beam-radius plane. For a 95% efficiency the minimum rectenna radius
occurs for tapers of 10-15 dB. The least taper, 10 dB, is selected to minimize
the power density at the array center needed to obtain the required total power.
The corresponding rectenna radius is 5 km.

In actuality, 95% beam efficiency will not be obtained due to phase errors
over the array surface, quantization of the taper, and outage of power modules.
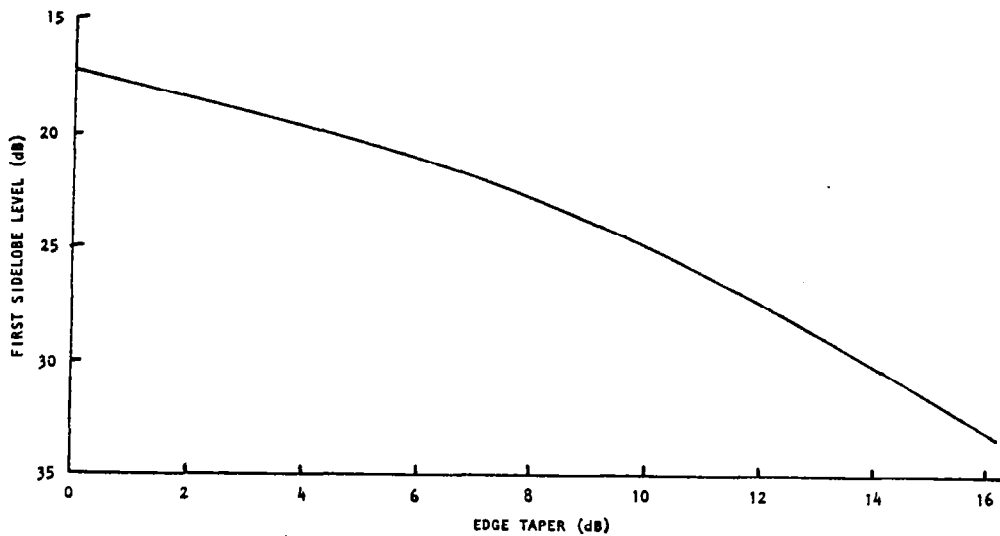
Figure 2.6-5. First Sidelobe Level Versus
Truncated Gaussian Taper
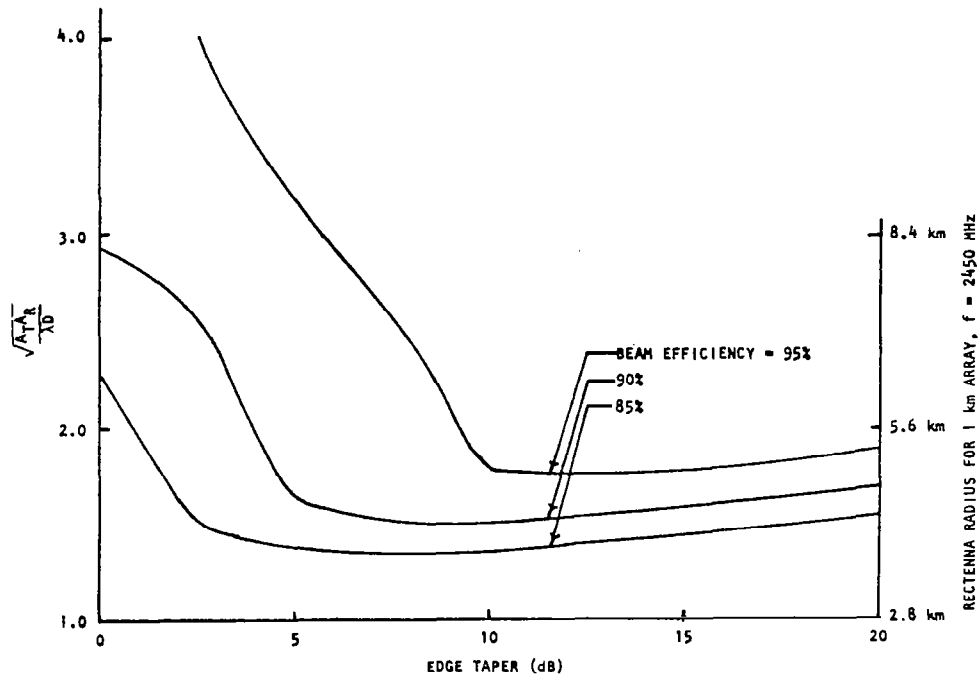
Figure 2.6-6. Antenna Sizes for Truncated
Gaussian Tapers

A ten-step quantization of the 10 dB taper was chosen in agreement with
the selection made in previous studies. A five-step taper would have given
1% less beam efficiency. Combining the effects of phase error, quantization
and outage, Figure 2.6-7 shows the resulting beam efficiency versus radius.
The results shown in Figure 2.6-7 represents the baseline configuration with
a rectenna collection efficiency of 88% for a 5 km radius.

2-74
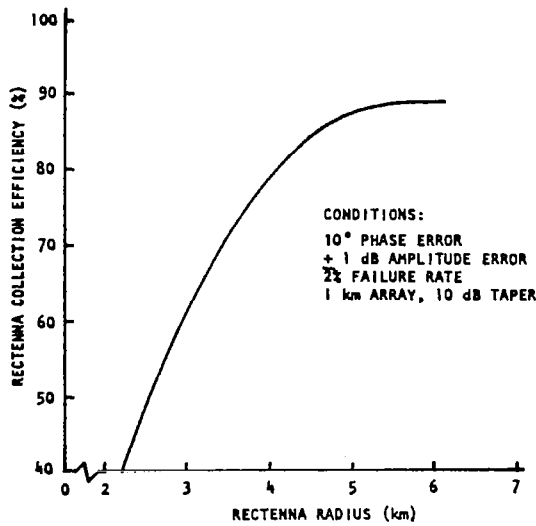
*Figure 2.6-7. Rectenna Collection Efficiency
for Baseline Configuration*

Taylor Distribution

An alternate way to investigate the antenna beam characteristics is through use of a Taylor distribution concept. Taylor distribution is defined by the equation

$$f(p) = \sum_{m=0}^{\bar{n}-1} \frac{2\, F\,(\mu m,\, A,\, \bar{n})}{\left[J_o\,(\pi\mu m) \right]^2 \pi^2}\; J_o\,(\mu m p)$$

and

$$F(\mu m,\, A,\, \bar{n}) = \begin{cases} 1 & m = 0 \\[2ex] J_o(\pi\mu m)\; \dfrac{\displaystyle\prod_{n=1}^{\bar{n}=1}\left[1 - \dfrac{\mu m^2}{\sigma^2\left[A^2 + (n-\frac{1}{2})^2 \right]} \right]}{\displaystyle\prod_{\substack{n=1 \\ n\neq m}}^{\bar{n}-1}\left[1 - \dfrac{\mu^2 m}{\mu n^2} \right]} & 0 < m < \bar{n} \\ & m > \bar{n} \\[2ex] 0 & \end{cases}$$

$$P = \frac{\pi}{a} \delta$$

δ = radial coordinate variable

a = antenna radius

μ_m = solution of $J_1(\pi\mu m) = 0$

A = $\cosh^{-1} \eta$

$\overline{n}$ = integer controlling the uniformity of sidelobes

$$\sigma = \frac{\mu\overline{n}}{\left[A^2 + (\overline{n}-\frac{1}{2})^2\right]^{\frac{1}{2}}}$$

= beam broadening factor

    Taylor Distribution provides a very attractive feature in that a circular source can be constructed with an optimum compromise between beamwidth and sidelobe level. Several cases have been investigated on a preliminary basis. These are presented in Figures 2.6-8 to 2.6-10. From these distributions, array configuration may be determined.

09/11/79 VER 9   *031650800
                        091178 0002
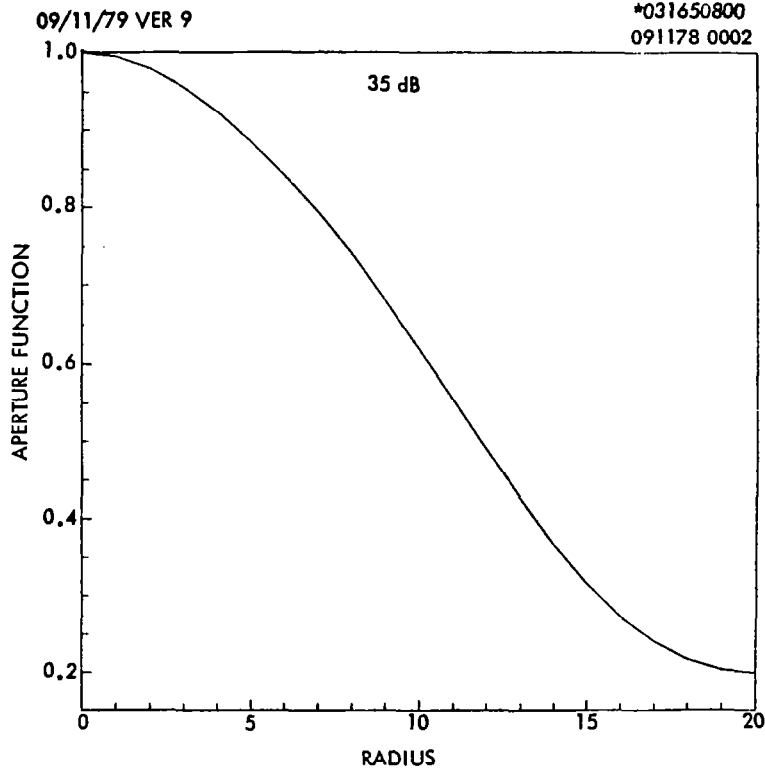
35 dB

Figure 2.6-8. Distribution Function
                - 35 dB

30 dB

APERTURE FUNCTION

RADIUS
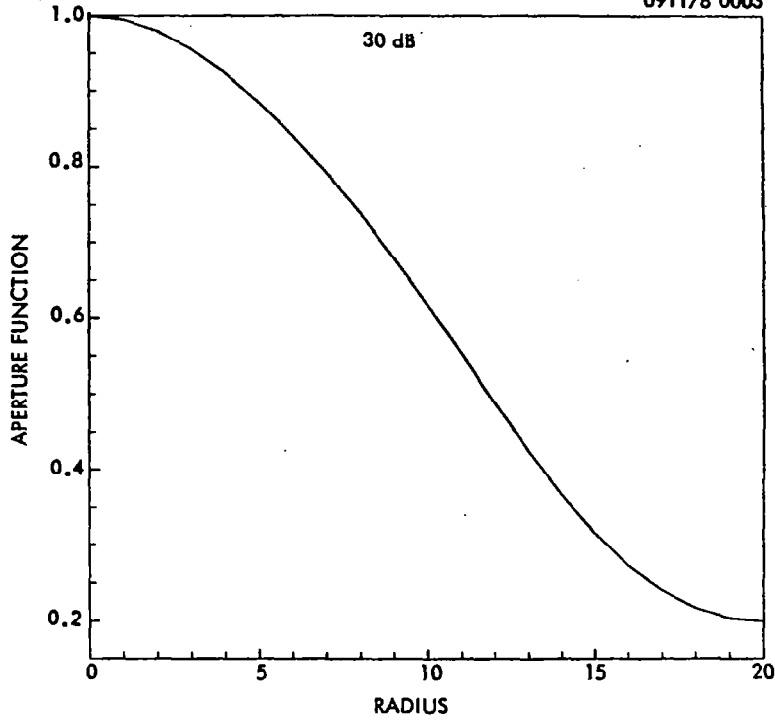
Figure 2.6-9.   Distribution Function - 30 dB

25 dB

APERTURE FUNCTION

RADIUS
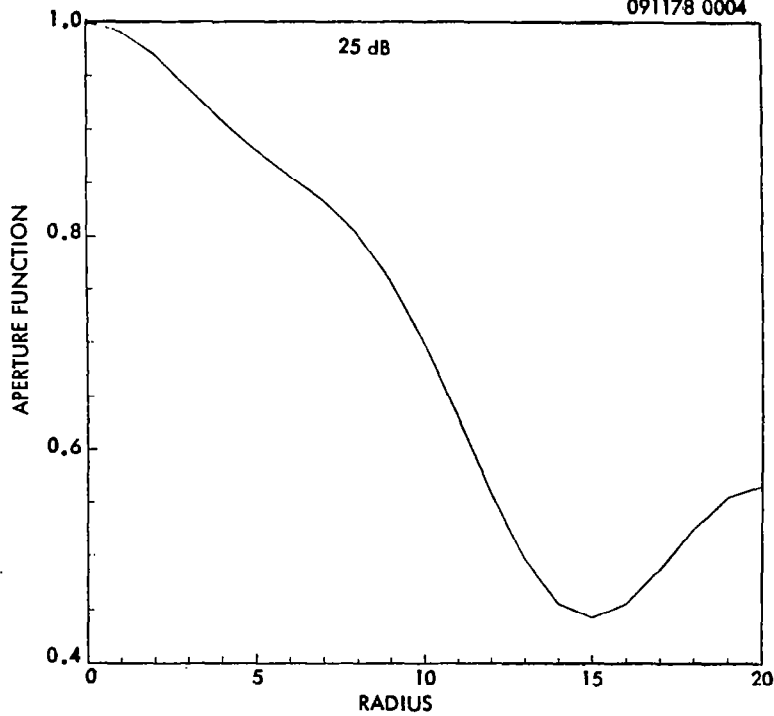
Figure 2.6-10.   Distribution Function - 25 dB

2-77

Additional data are required on far field pattern and beam efficiency. Also parametric comparisons must be made with the Gaussian Distribution to allow the determination of the optimum distribution from the antenna perform- ance point of view, as well as to determine the environmental impacts (if any).

Antenna Beam Interference

The Rockwell suggested alternative satellite concepts were defined in two configurations: an end mounted antenna version, and a second with the antenna located at the center of the solar array as shown in Figure 2.6-11. During earlier design analysis some concern was raised because of the possibility of beam energy losses due to structural interference. The following section describes the problem, the approach to the analysis, and the conclusions and corrections to alleviate and/or avoid the potential impacts.
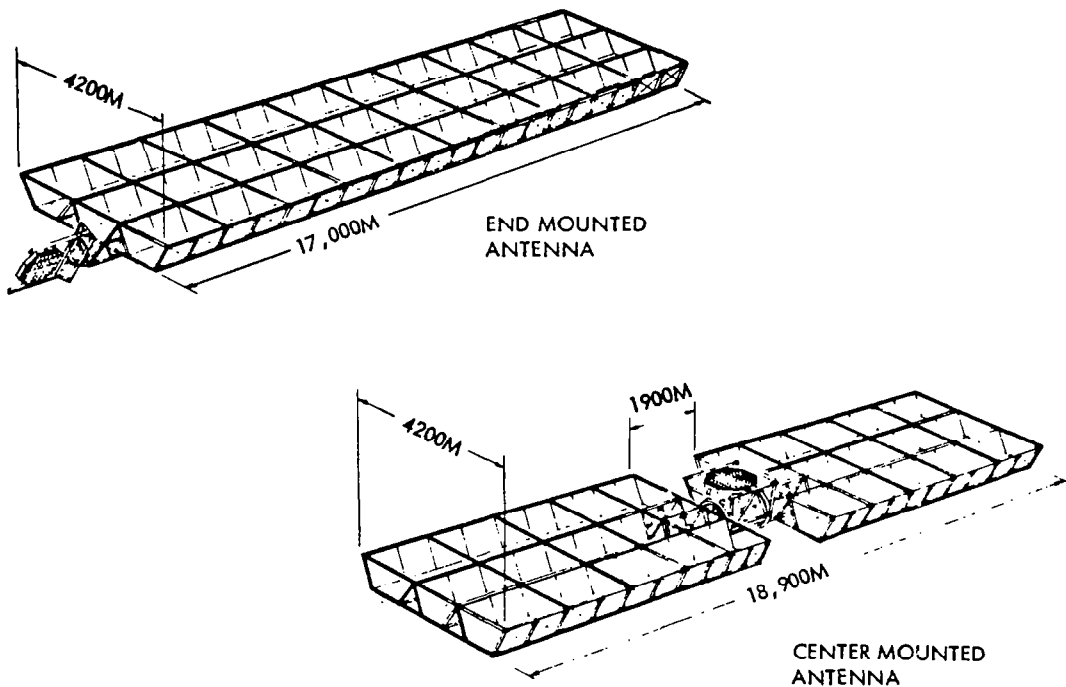
Figure 2.6-11. 3 Trough Coplanar Configurations

Procedure and Analysis. The problem geometry considered during the analysis is shown in Figure 2.6-12. The orbit selection (GEO), requires that to maintain the proper antenna pointing angle, the antenna must point such that at two times during the year the antenna centerline will be 17° off the vehicle axis. Furthermore, twice a day, the broad side of the solar panels lie in the plane of the antenna beam. When these two periodicities coincide the antenna aperture will be partially shadowed by the solar panels.

2-78
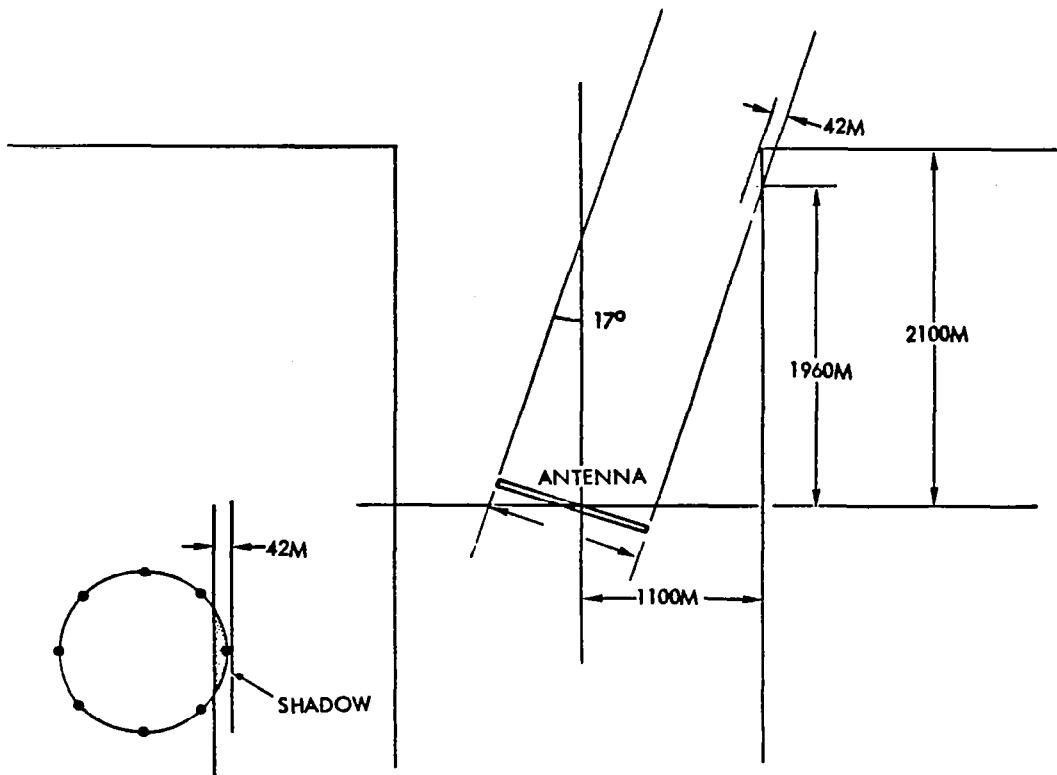
Figure 2.6-12. Problem Geometry

The assumptions, simplifications and procedures for the analysis are summarized in Figure 2.6-13. The assumptions considered for this analysis are:

1. The solar panels are considered an opaque absorbing screen so that reflections from the panels may be neglected.

2. The solar panels are sufficiently close to the antenna so that they may be considered to be at the antenna aperture. Figure 2.6-12 shows that the obstruction is about two antenna diameters from the aperture. Considering that the aperture is in the vicinity of 8000 λ across, this assumption is reasonable.

3. The rectenna is specified to be 42,000 km from the antenna, placing it in the Fraunhaufer region or far field, allowing the Fourier transform to describe the relationship between the aperture distribution and field distribution at the rectenna.

4. The aperture power distribution is Gaussian in shape, truncated at the one sigma point at the aperture edge and placed on a 10 dB pedestal. This is slightly different from the 10 dB Gaussian pattern being considered for the aperture, which would be closer to 1.6 sigma at the edge. The estimates given here for the main beam (unshadowed) thus have slightly higher side lobes and slightly narrower far field pattern than the 10 dB Gaussian pattern, as a result of a less tapered aperture distribution.

OBSTACLE IS AN OPAQUE FLAT SCREEN, NEGLECT REFLECTIONS

42,000 KM DISTANCE TO RECTENNA

PRIMARY PATTERN: 10 dB GAUSSIAN PEDESTAL,   AT APERTURE EDGE

λ = 0.1224 M,   APERTURE = 960 M

PROCEDURE

1.   PLOT APERTURE DISTRIBUTION (5 TERMS)—DETERMINE FAR-FIELD DISTRIBUTION

2.   DIVIDE AMPLITUDE INTO 50 LEVELS, DISTANCE INTO 10 M ΔR TO FIND DISC VOLUMES

3.   SUBTRACT SHADOW SECTORS FROM LOWER 9 DISCS, FIND SHADOW VALUE

4.   POWER LOSS DUE TO BLOCKAGE $\propto$ SHADOW VOLUME

5.   ESTIMATE SHADOW APERTURE SIZE, DISTRIBUTION—DETERMINE FAR-FIELD SHADOW

6.   NORMALIZE SHADOW PATTERN FOR BOTH TOTAL POWER AND SOLID ANGLE

7.   SUBTRACT FROM MAIN BEAM FIELD, COMPUTE TOTAL FAR-FIELD & POWER PATTERN

8.   SHADOW PATTERN SIMPLIFICATIONS:
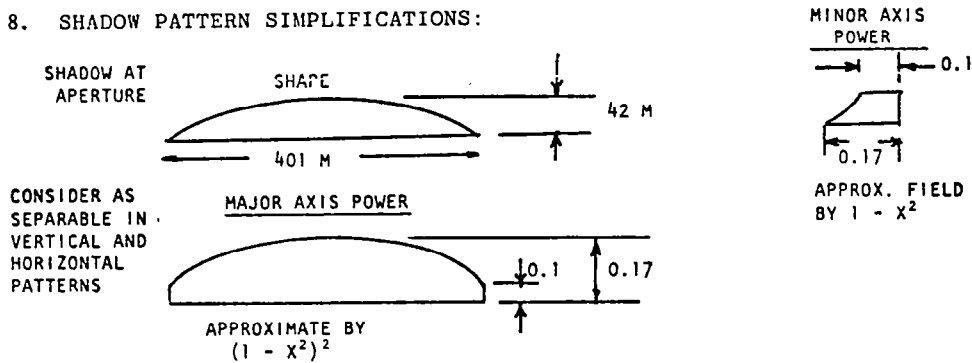
Figure 2.6-13.   Assumptions and Simplifications

5.   The antenna aperture is circular, 960 meters in diameter, and the wavelength is .1224 meters (2.45 MHz).

The procedure followed in making the shadow effect analysis is as follows:

1.   Express the aperture distribution in convenient analytic form, and determine the far field pattern from its Fourier transform. In this case, the aperture field distribution was expressed as the first five terms of an infinite power series representing the Gaussian power distribution, with an augmented first term to provide the 10 dB pedestal:

$$A(r) = \frac{233}{384} + \frac{116}{384} (1-r^2) + \frac{30}{384} (1-r^2)^2 + \frac{4}{384} (1-r^2)^2 + \frac{1}{384} (1-r^2)^4$$

(This is squared to determine the aperture power distribution.)

Use is made of the transform relationship:

$$\sum_n A_n (1-r^2)^n \longrightarrow \sum_n A_n \frac{\Lambda_{n+1}(u)}{n+1}$$

to obtain the corresponding far field pattern:

$$G(u) = \frac{233}{384} \Lambda(u) + \frac{58}{384} \Lambda_2(u) + \frac{10}{384} \Lambda_3(u) + \frac{1}{384} \Lambda_4(u) + \frac{1}{1920} \Lambda_5(u)$$

where $u = \frac{2a\Theta}{K\lambda}$, $\quad$ a = aperture radius

(This again is squared to determine the power pattern.)

2. Plot the aperture power pattern, and section into discs and radius increments for graphical integration. In this estimate, 50 power levels were used to form 50 discs, and the radius increment used was 10 meters.

3. Find the shadow power by graphical integration of the shadow volume of the power distribution. In this case, the shadow power was estimated at 0.47% of the main beam power.

The pattern distortion caused by the shadow is obtained by subtracting the field pattern that would be generated by the shadow from the field of the main beam, then squaring to obtain the resultant power pattern.

The following assumptions and simplifications were used in estimating the shadow pattern:

   a) The pattern is a sector of the 960 meter aperture circle 42 meters deep and 401 meters across.

   b) The pattern can be approximated by a rectangle of these dimensions, so that the two dimensional directions become separable. The physical taper of the shadow is approximated by a taper in field, the narrow direction by a distribution of $1 - X^2$, and the wide direction by $(1 - X^2)^2$.

   The transform relationship for the shadow yields a negative far field pattern of:

   $1 - X^2 \rightarrow \Lambda_{3/2}(u)$ $\quad$ Minor axis narrow shadow (vertical as viewed by rectenna)

   $(1 - X^2) \rightarrow \Lambda_{5/2}(u)$ $\quad$ Major axis wide shadow (horizontal as viewed by rectenna)

The shadow patterns are normalized so that the peak is the same, whether approached from the narrow side or the wide side. The shadow far field power, obtained by squaring, is normalized with the main beam power by the inverse of the solid angle subtended by each pattern, and by the amount of power in each pattern. The normalized shadow far field is then subtracted from the main beam far field. The power pattern at the rectenna with shadowing in both vertical (north-south) and horizontal (east-west) directions, is obtained by squaring the results.

2-81

Results. The resultant power patterns at the rectenna with and without maximum shadowing are shown in Figure 2.6-14 for the major axis at the rectenna (vertical) and Figure 2.6-15 for the minor (horizontal) axis.
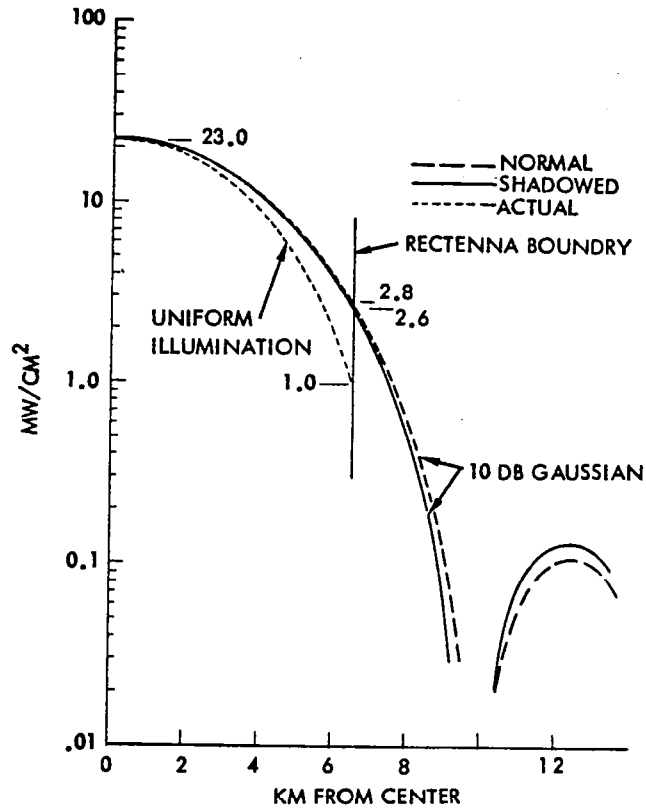
Figure 2.6-14. Rectenna Power Pattern - Major Axis

The figures show a slight narrowing of the beam (about 50 meters at the rectenna) due to the power reduction at the peak of the beam of 1.6%, a slight rise in the first sidelobe (and all other odd numbered sidelobes; from .11 mW/cm^2 to .13 mW/cm^2), and a slight shift of these sidelobes toward the main beam.

Also shown in Figures 2.6-14 and 2.6-15 is the beamwidth, at the rectenna, that would be produced by a uniformly illuminated satellite aperture with a diameter of 1 km. The uniformly illuminated aperture corresponds to previous computations for 1 mW/cm^2 at the edge of a 10×13 km rectenna. The Gaussian distribution should have a rectenna somewhat larger, about 11.6×15 km for 1 mW/cm^2 power density at its edge.

Recommendations. Although the power loss experienced during the twice yearly interference is seen to be very low ($\leq$1.6%), and falls within the initial system estimating uncertainty, this still represents unwanted (and unneeded) energy loss to the system. Furthermore the intercepted energy may cause additional thermal stress in the intercepting solar blankets and structure. The recommended approach was to remove the problem by adjusting the satellite geometry so that no interference could occur. The final dimensions, shown in Figure 2.6-11, satisfy this recommendation.

2-82
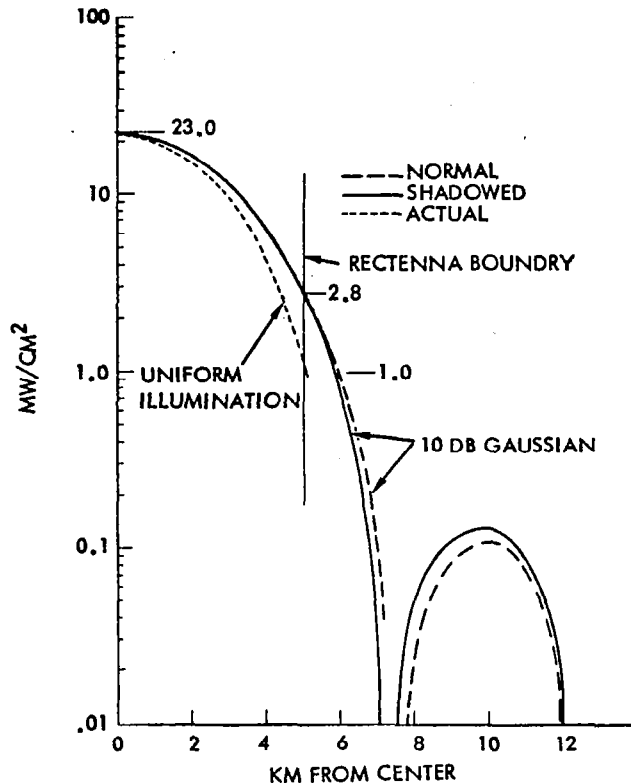
Figure 2.6-15. Rectenna Power Pattern - Minor Axis

2.6.2 MICROWAVE POWER AMPLIFIERS

The Microwave Power Transmission System (MPTS) array design is one of the most complex items in the Satellite Power System (SPS) concept primarily because of its demands upon the state-of-the-art in microwave power conversion devices, materials, system efficiencies and phase control.[1,2] Also, different MPTS array designs using each of the various dc-to-microwave power conversion candidates can have a significant overall system impact on both the spacecraft and the rectenna configurations and performance requirements.

One of the key tradeoffs in the SPS MPTS array study involves the use of tubes or solid state devices as the basic elements of the dc-microwave power conversion modules. In the tube area, a choice is required between the use of klystrons, amplitrons or magnetrons. In the solid state device area, a choice is required between the use of various types of bipolar or field effect transistors.

[1]SD 78-AP-007, Satellite Power System (SPS) Concept Definition Study, Rockwell International, June 21-22, 1978

[2]SD 78-AP-0023-4, Satellite Power Systems (SPS) Concept Definition Study - Final Report, Rockwell International, April, 1978

The primary difference between the use of the solid state devices or the microwave tube is that each will require a different SPS configuration due to dc-dc power conversion and thermal design impacts.[1]

Microwave Power Tube Tradeoffs

One of the basic decisions in the power conversion area is the selection of the type of microwave tube to be used in the SPS MPTS array. Klystrons and cross field amplifiers (amplitrons and magnetrons) are the only tubes with high enough efficiencies to be considered.[2,3]

Table 2.6-1 and 2.6-2 provide some insight into the area of power tube tradeoffs. The klystron appears to be the best choice from the standpoints of gain, stability and noise.[4,5,6]

Table 2.6-1. Comparison of Tube Lifetimes for Various Types of Cathodes

PARAMETER		OXIDE COATED	TYPE (NI MATRIX)	IMPREGNATED TUNGSTEN MATRIX
TEMPERATURE	• LABORATORY MODEL AT $3A/cm^2$	800°C	900°C	1080°C
	• COMMERCIAL	760°C	950°C	1080°C
LIFETIME FOR CATHODE TEMP. BETWEEN 700°C AND 1100°C UNDER LABORATORY CONDITIONS*		~10^4 HRS. (1.1 YRS.)	~4.10^4 HRS. (4.4 HRS.)	~10^5 HRS. (11 YRS.)
*LIFETIME IS SIGNIFICANTLY REDUCED BY SMALL AMOUNTS OF CHEMICALLY ACTIVE GASSES OR SULPHUR. ALSO, THE KLYSTRON LIFETIME IS TYPICALLY TWICE THE LIFETIME OF A MAGNETRON POWER AMPLIFIER WITH SIMILAR OUTPUT POWER LEVELS AND FREQUENCY RESPONSE.				

Tubes Versus Solid State

Comparing the electrical performance and size/weight differences between the reference SPS configuration using klystron power modules or solid state power module might not reveal dramatic differences. However, the solid state devices do provide advantages when such items as lifetime, manufacturability, off-on operation and maintainability are considered (Table 2.6-3).

[1] Ibid (1, page 2-83)

[2] G. Caryotakis, *State of the Power Tube Industry - 1976*, Microwave Journal, Pp. 31-34, August, 1976

[3] T. Walsh, *DoD and the Microwave Tube Industry*, Microwave Journal, Pp. 19-42, July 1977

[4] E. Lien, *Advances in Klystron Amplifiers*, Microwave Journal, Pp. 33-39, December 1973

[5] F. Johnson, *Interference Emission Filtering in High Power Microwave Transmitters*, Microwave Journal, Pp. 67-72, January 1970

[6] F. Voltaggio, Jr., *Why Not Crossed-Field Amplifiers*, Microwaves, Pp. 58-63, January 1970

Table 2.6-2. Performance Comparisons of
Basic Tube Candidates

PARAMETER	KLYSTRON	MAGNETRON	AMPLITRON
• PRESENT CW OUTPUT POWER LIMITATION	100 KW	50 KW	50 KW
• PRESENT EFFICIENCY LIMITATIONS AT 1% BW	≥ 70%	70%	60%
• NOISE LEVEL	130 dB/KHz BELOW CARRIER	35 dB/KHz BELOW CARRIER	40 dB/KHz BELOW CARRIER
• RF STABILITY	GOOD	POOR	FAIR
• GAIN	≥ 30 dB	10 dB-20 dB	7 dB-15 dB

Table 2.6-3. Comparison of Solid State and
Klystron Approaches for SPS MPTS

	SOLID STATE (TRANSISTOR)	KLYSTRON
• LIFETIME	LIFETIME POTENTIAL IS MUCH HIGHER FOR THE TRANSISTOR POWER MODULE.	CATHODE DEGRADATION AND HIGH VOLTAGE POWER SUPPLY BREAK-DOWN LIMIT LIFETIME.
• HIGH VOLUME PRODUCTION	THE SMALL SIZE OF THE SOLID STATE POWER MODULE PROVIDES MANUFACTUR-ING ADVANTAGES AND REPRODUCIBILITY POTENTIAL.	REQUIRES HIGH TOLERANCES. LARGE SIZES INVOLVED. SIGNIFICANT HIGH VOLUME TEST PROBLEMS.
• OPERATION	CAN BE SLOWLY SWITCHED ON AND OFF WITHOUT DEGRADATION.	PARTS OF KLYSTRON MUST REMAIN "ON" AT ALL TIMES.
• MAINTAINABILITY	NO X-RAY PROBLEMS. SMALL MODULE SIZES ALLOW EASY REPLACEMENT.	SIGNIFICANT X-RAY AND LEAKAGE PROBLEMS WHICH ARE HAZARDOUS TO PERSONNEL. SUSCEPTIBLE TO MAGNETIC DISTURBANCES. MANY INTERCONNECTS. AUTOMATED REPL. TECH. REQ.

Klystron

Klystrons have been proposed by Varian for the MPTS converters.[1] A total efficiency of 86% is predicted.[2] This is based on the performance of the VKS-7773, 50 kW, 2.45 GHz klystron previously built which obtained an efficiency of 74.4% without a depressed collector. Addition of a depressed collector with 55% beam power recovery efficiency plus other minor changes

[1]Ibid (1,2, page 2-83 and 2, page 2-84)
[2]Ibid (1, page 2-83)

leads to an 80% efficiency. Taking into account cathode heater and solenoid power, a final efficiency of 85% is used in the point design calculations.

The major drawback to the use of klystrons is the large number of electrode voltages which are required. The depressed collector design selected by Varian requires five unregulated voltages. In addition, two regulated power supplies are required to supply body current and establish the potential of the mod anode, which controls beam current. The present point design generates all these voltages from a single 40 kV bus by means of dc-dc converters.

Solid State Definition and Design

There are a number of possible solid state device candidates that could be considered for use on the SPS solid state power module. These include Electron Beam Semiconductor (EBS) devices,[1,2,3] TRAPATT diodes,[4,5,6] field effect transistors[7-11] and bipolar transistors.[12,13,14] Each have something to offer the SPS application. The EBS and TRAPP diode have upper efficiency limits of approximately 40-50%. This efficiency limitation makes them questionable candidates for the SPS Microwave Power Transmission System (MPTS). The various

[1]B. W. Bell, et al, *An EBS (Electron Beam Semiconductor) High-Current Pulse Amplifier*, IEEE Transactions on Electron Devices, Pp. 361-363, June 1975

[2]D. J. Bates, et al, *Current Reliability Results or Election Bombarded Semiconductor Power Devices*, IEEE Transactions on Electron Devices, Pp. 734-735, November 1974

[3]M. Weiner, et al, *Output Capability of Electron Beam Semiconductor Bandpass Amplifiers Using Large Area Diodes*, IEEE Transactions on Electron Devices, Pp. 308-310, May 1974

[4]H. Kawamoto, et al, *Advances in High-Power, S-Band TRAPATT-Diode Amplifier Design*, Microwave Journal, Pp. 41-44, February 1974

[5]R. J. Trew, et al, *The Operation of S-Band TRAPATT Oscillators with Tuning at Multiple Harmonic Frequencies*, IEEE Transactions on Microwave Theory and Techniques, Pp. 1043-1047, December 1975

[6]S. M. Sze and R. Ryder, *Microwave Avalanche Diodes*, Proceedings of the IEEE, Pp. 1140-1154, August, 1971

[7]M. Fukuta, et al, *Power GaAs MESFET with a High Drain-Source Breakdown Voltage*, IEEE Transactions on Microwave Theory and Techniques, Pp. 312-317, June 1976

[8]H. F. Cooke, *Microwave Field Effect Transistors in 1978*, Microwave Journal, Pp. 43-48

[9]H. F. Cook, *FETs and Bipolars Differ when the Going Gets Hot*, Microwaves, Pp. 56-61, February 1978

[10]C. Liechti, *Microwave Field-Effect Transistors-1976*, IEEE Transactions on Microwave Theory and Techniques, Pp. 229-300, June, 1976

[11]J. V. Dilorenzo, *GaAs FET Development-Low Noise and High Power*, Microwave Journal, Pp. 39-44, February 1978

[12]P. C. Parekh and J. Steenbergen, *The 3 Keys to Good Transistor Design*, Microwaves, Pp. 40-71, August 1973

[13]C. J. Nuese, et al, *GaAs Vapor-Grown Bipolar Transistors*, Solid State Electronics, Vol. 15, Pp. 81-91, 1972

[14]D. S. Jacobson, *What are the Trade-offs in RF Transistor Design?*, Microwaves, Pp. 46-51, July 1972

transistor candidates have efficiency potentials in excess of 80% and power output potentials in excess of 100 W. These capabilities place the transistor in the position of being the best semiconductor device candidate for the SPS solid state power module.

Design Drivers

Three basic solid state material/device limitations have a very significant impact on the spacecraft weight, MPTS array geometry, power distribution system configuration, overall efficiency and thermal profile. These three items are maximum breakdown voltage, output power and circuit efficiencies (Table 2.6-4) and they make up the three primary design drivers for SPS using solid state power converter modules. Figure 2.6-16 provides some insight into the supply voltage limitations caused by the transistor collector breakdown voltage. The high voltages in the kV range, required by the power tubes, are much more desirable from the standpoint of the spacecraft power distribution system in order to hold the size and weight of the power distribution system down to an acceptable level and to minimize I^2R losses. The low collector breakdown voltage limitation (<100 V) encountered with transistors is primarily due to the influence of semiconductor material doping and transistor device structure.

Table 2.6-4. Solid State MPTS Design Drivers

DESIGN DRIVER	IMPACT
1. MAXIMUM BREAKDOWN VOLTAGE (CAN PUT TWO TRANSISTORS IN SERIES TO INCREASE BREAKDOWN VOLTAGE BUT THIS WOULD REQUIRE A HIGH DEGREE OF TRANSISTOR REPRODUCIBILITY AND MATCHING AND COULD IMPACT EFFICIENCY -- WILL NOT HELP DC-DC CONV. PROBLEM SIGNIFICANTLY)	• COMPLETE REVISION OF POWER DISTRIBUTION SYSTEM • WEIGHT • COST • EFFICIENCY VERSUS LIFETIME
2. OUTPUT POWER LIMITATIONS	• WEIGHT • RELIABILITY • OVERALL EFFICIENCY • THERMAL PROFILE • ARRAY GEOMETRY
3. CIRCUIT EFFICIENCIES	• OVERALL EFFICIENCY • THERMAL PROFILE • WEIGHT • RELIABILITY • NOISE AND SPURIOUS • MATERIAL CANDIDATES (SEMICONDUCTOR AND STRUCTURAL

- THEORETICALLY, THE BASIC FORM OF BV_C SHOWS A FUNCTIONAL RELATIONSHIP BETWEEN BASE WIDTH (W_B), EPITAXIAL WIDTH (W_{EPI}) AND DOPING CONCENTRATION (N_A, N_0). IN GENERAL:

$$BV_C = \frac{e\, N_A\, W_B^2}{2\, \epsilon_r\, \epsilon_0} \qquad \text{(UNIFORM BASE ALLOY TRANSISTOR)}$$

$$BV_C = \frac{e}{\epsilon_r\, \epsilon_0}\left[N_A\, W_{EPI}\, W_B - \frac{N_D\, W_{EPI}^2}{2} + \frac{N_A\, W_B^2}{2}\right] \text{(DOUBLE DIFFUSED TRANSISTOR)}$$

- FOR OPTIMUM CONDITIONS WITH THE DOUBLE DIFFUSED TRANSISTOR:

$$W_{EPI\ (OPT)} = \frac{N_A\, W_B}{N_D}$$

$$BV_C \approx \frac{e\, N_A\, W_B^2}{2\, \epsilon_r\, \epsilon_0} \qquad (N_A \approx 2 \cdot 10^{19}/\text{CM}^3,\ N_D \approx 5 \cdot 10^{20}/\text{CM}^3)$$

- IF W_B IS APPROXIMATELY 4μ AND ϵ_r IS 12:

$$BV_C \approx 25V$$

- IT IS READILY APPARENT THAT THE TRANSISTOR BREAKDOWN VOLTAGE IS A FUNCTION OF DOPING AND DEVICE STRUCTURE.

Figure 2.6-16. Transistor Collector Breakdown Voltage
(BV_C)

Transistor Candidates

Of the many potential transistor candidates, the heterojunction bipolar transistor[1,2,3] and the Static Induction Transistor (SIT)[4,5] appear to be the most attractive from the standpoint of breakdown voltage, output power, gain and overall efficiency. The best material candidate for the heterojunction bipolar transistor appears to be a GaAs-(GaAl)As combination while the SIT might use GaAs.

Table 2.6-5 compares some critical physical properties for each transistor - semiconductor material candidate. Table 2.6-6 provides a sample of the crystal orientations associated with a few transistor semiconductor material/substrate material candidates. Table 2.6-7 shows some of the limitations and performance constraints associated with each of the primary transistor candidates.

[1]M. Konagai and K. Takahashi, *(GaAl)As-GaAs Heterojunction Transistors with High Injection Efficiency*, Journal of Applied Physics, Pp. 2120-2124, May 1975
[2]A. G. Milnes and D. L. Feucht, *Heterojunctions and Metal Semiconductor Junctions*, Academic Press, New York, 1972
[3]B. L. Sharma and R. K. Purohit, *Semiconductor Heterojunctions*, Pergamon Press, New York, 1974
[4]J. Nishizawa and K. Yamamoto, *High-Frequency High Power Static Induction Transistor*, IEEE Transactions on Electron Devices, Pp. 314-322, March 1978
[5]Y. Kajiwara, et al, *A New Microwave High Power Transistor (Static Induction Transistor)*, 1978 IEEE International Microwave Symposium Digest, Pp. 380-382, June 27-29, 1978

ITEM	SEMICONDUCTOR MATERIAL CANDIDATES	COMMENTS
BIPOLAR		
HETEROJUNCTION	- GaAs-(GaAl) As	- GOOD LATTICE MATCH, NO SEVERE MATERIAL INTERFACE PROBLEMS.
	- Si-InP	- THERMAL LIMITATIONS
	- Ge-GaAs	- MATERIAL INTERFACE PROBLEMS LIMITING CURRENT GAIN
HOMOJUNCTION	- GaAs	- EFFICIENCY POTENTIAL LOWER THAN HETEROJUNCTION
FET	- GaAs	- SURFACE STATE LIMITED, LOWEST BREAKDOWN VOLTAGE
STATIC INDUCTION TRANSISTOR	- GaAs	- HIGH BREAKDOWN VOLTAGE POTENTIAL, BULK MATERIAL CONDUCTION ADVANTAGES, LOW POWERS AT PRESENT

Table 2.6-6. Solid State Power Module Semiconductor/
Substrate Material Combination Candidates

SEMICONDUCTOR*	SUBSTRATE	COMMENTS
(111) GaAs	(COO1) SAPPHIRE	- SOME STRESS PROBLEMS CAUSING INTERFACIAL DEFECTS. (ROCKWELL ERC SOLAR CELL CANDIDATE)
(111) GaAs	(1011) BEO	- REPRODUCIBILITY PROBLEM
(100) GaAs	(1122) BEO	- BEST FOR BEO
(111) GaAs	(1011) BEO	- DEFECT AND IMPURITY PROBLEMS
(100) GaAs	(110) SPINEL	- SOME DEFECT PROBLEMS
(111) GaAs	(111) SPINEL	- LESS DEFECT PROBLEMS: BEST FOR SPINEL

*MANY OF THE CURRENT GaAs FET, HOMOJUNCTION BIPOLAR AND HETEROJUNCTION BIPOLAR DEVICES HAVE BEEN FABRICATED ON (100) GaAs N+ SUBSTRATES OR CHROMIUM DOPED SEMI-INSULATING (100) GaAs SUBSTRATES. (111) GaAs APPEARS TO HAVE A DEFECT/IMPURITY PROBLEM SIMILAR TO (111) SILICON.

GaAs Transistor Amplifier Performance Projections

Future performance levels anticipated for GaAs bipolar power transistor candidates can be based on present performance levels achieved with silicon bipolar transistors[1] (Figure 2.6-17). Also, future performance levels antic-ipated for GaAs field effect (FET) power transistor candidates (Figure 2.6-18) can be based on present GaAs FET performance[2,3,4].

[1]E. J. Colussi, *Internally Matched RF Power Transistors*, Microwave Journal, Pp. 81-84, April 1978
[2]_____, *GaAs FETs Market and Technology Review*, Microwave Journal, Pp. 22-31, February 1978
[3]D. Davis, *Microwave Power on the Rise*, Microwaves, Pp. 9-18, April 1974
[4]I. Drukier, *GaAs FETs Opening Gates on Power Reservoir*, MSN, Pp. 49-55, April 1978

Table 2.6-7. Solid State Amplifier Transistor*
Candidates

TRANSISTOR CANDIDATE	ADVANTAGE	DISADVANTAGE
GaAs BIPOLAR	- HIGH BREAKDOWN VOLTAGE (~ 40v)	- SLIGHTLY LOWER POWER & GAIN COMPARED WITH GaAs FET
GaAs FET	- HIGH POWER & GAIN	- LOWEST BREAKDOWN VOLTAGE (~ 25v) - SURFACE EFFECT LIMITATIONS
GaAs STATIC INDUCTION TRANSISTOR	- HIGHEST BREAKDOWN VOLTAGE POTENTIAL (~ 70v)	- OUTPUT POWERS ARE LOW WITH PRESENT DEVICES
HETEROJUNCTION BIPOLAR TRANSISTOR	- HIGHEST EFFICIENCY POTENTIAL - HIGH OUTPUT POWER POTENTIAL	- HIGHEST DEVELOPMENT COSTS

* APPEARS TO BE THE ONLY SOLID STATE DEVICE CAPABLE OF MEETING THE HIGH EFFICIENCY REQUIREMENTS.
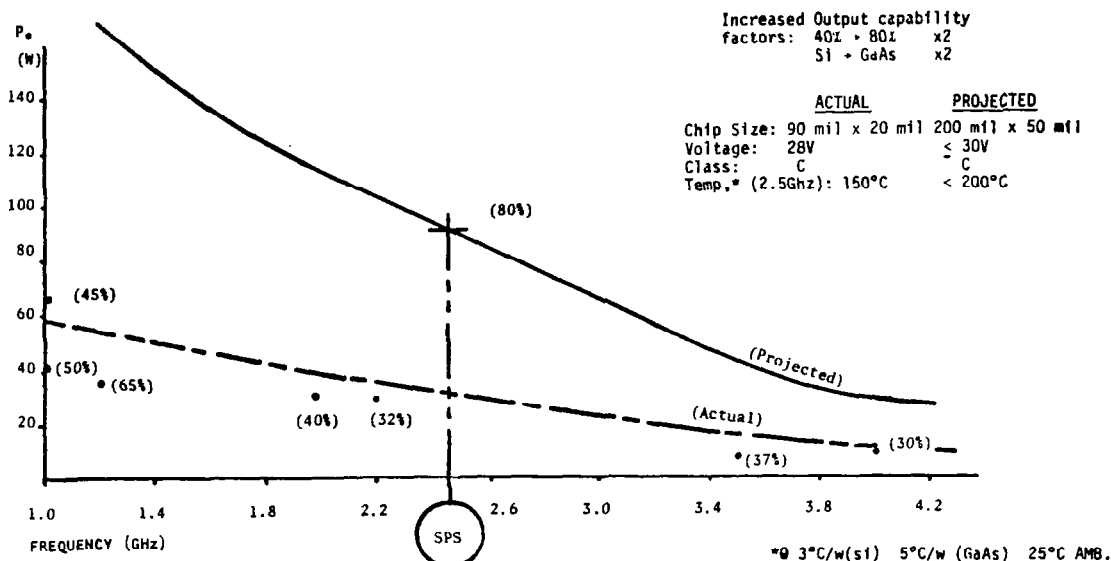
Figure 2.6-17. GaAs Bipolar SS Amplifier Projections on
Si Bipolar SS Amplifier Outputs and Efficiencies

A more complete list of projected transistor performance parameters can be found in Table 2.6-8. Table 2.6-9 provides a list of projected transistor physical parameters.

GaAs Transistor Chip Layout and Schematic

A common-base push-pull amplifier is a strong power amplifier candidate from the standpoints of power output, efficiency and RF stability.

2-90
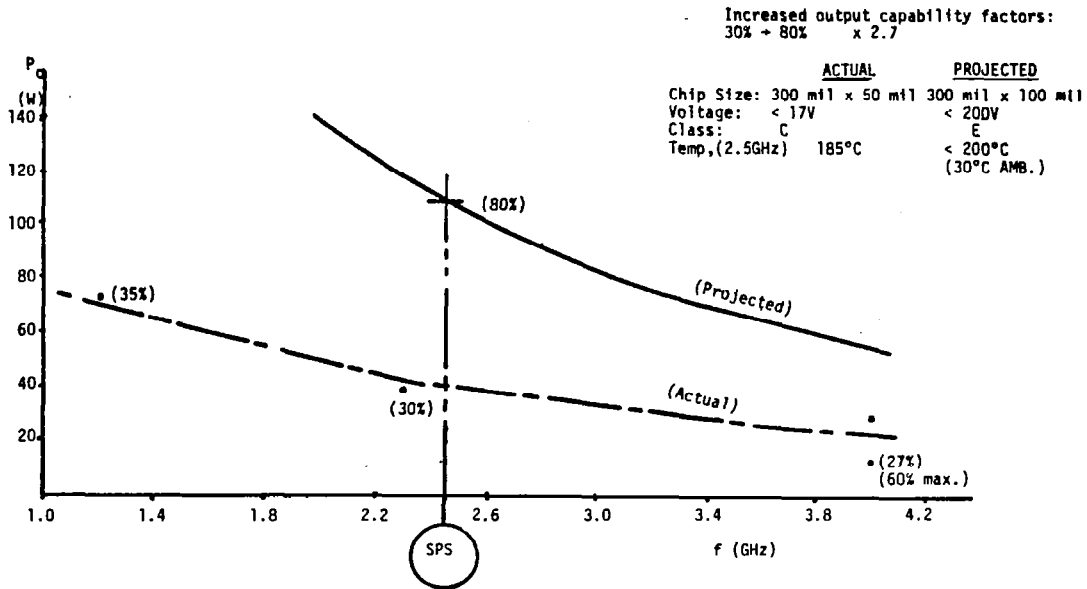
Figure 2.6-18. GaAs FET SS Amplifier Projections Based on Current GaAs FET Amplifier Outputs and Efficiencies

Table 2.6-8. Comparison of GaAs Bipolar and GaAs FET Projected Performance Parameters

ITEM	GaAs BIPOLAR	GaAs FET
. POWER OUTPUT	90W	108W
. EFFICIENCY *	≥ 78%	≤ 90%
. SPURIOUS OUTPUTS BELOW CARRIER	> 50 DB	> 50 DB
. GAIN	20 DB	22 DB
. VOLTAGE †	≤ 40 V	< 25 V
. JUNCTION TEMPERATURE $\begin{bmatrix} 180^{\circ}C \text{ AMBIENT} \\ \theta = 1^{\circ}C/W \end{bmatrix}$	$<200^{\circ}C \begin{bmatrix} 170^{\circ}C \text{ LIMIT} \end{bmatrix}$	$<200^{\circ}C \begin{bmatrix} 170^{\circ}C \text{ LIMIT} \end{bmatrix}$
. CLASS ≠	C	E
. MTBF	$<11 \text{ YEARS} \begin{bmatrix} J \leq 2 \cdot 10^4 \text{ A/CM}^2 \\ T_J = 200^{\circ}C \end{bmatrix}$	$<12 \text{ YEARS} \begin{bmatrix} J \leq 2 \cdot 10^4 \text{ A/CM} \\ T_J = 200^{\circ}C \end{bmatrix}$
. RADIATION HARDNESS ‡ RADS (SI) NEUTRON	$\leq 10^{15} \text{ N/CM.}^2$	
. 1 DB COMPRESSION POINT (P_0)	130W	140W

* TRANSISTORS WILL REQUIRE INTERNAL INPUT/OUTPUT MATCHING NETWORKS.
† HIGH FET SOURCE DRAIN BREAKDOWN VOLTAGE REQUIRES INLAID n^+ SOURCE - DRAIN.
≠ DEGRADATION IN FALL TIME DUE TO R-C (1-2 Ω & 3 - 10PF) FAVORS
  CLASS C FOR BIPOLAR AND CLASS E FOR FET.
‡ ABRUPT EMITTER-BASE JUNCTION & OPTIMUM BASE WIDTH WILL INCREASE BIPOLAR HARDNESS.

2-91

ITEM	GaAs BIPOLAR	GaAs FET
• SUBSTRATE MATERIAL	GaAs, SAPPHIRE, BeO OR SPINEL	GaAs, SAPPHIRE, BeO OR SPINEL
• CHIP SIZE	200 MIL x 50 MIL	300 MIL x 100 MIL
• CHIP THICKNESS	8 MIL (THICK GaAs)	10 MIL (THIN GaAs)
• GEOMETRY*	INTERDIGITATED	INTERDIGITATED
• METALIZATION PROFILE	CR/PT/AU, AU/GE TI/W/AU, AU/SN, AU/ZN	AUGE/PT (THERMAL AGING) NI/AU/GE, CR/PT/AU, AU/CR-PT AL (PER TI/W/AU (BURNOUT)
• EMITTER OR GATE LENGTH	1.5µ	2.0µ (4.5µ CHANNEL)
• EMITTER OR GATE WIDTH	60µ	≤ 5000µ
• JUNCTION	ION IMPLANT	INLAID N$^+$ SOURCE & DRAIN*
• DOPING	N$^+$ 2·10^{19} CM^{-3}(3µ) N 10^{17} CM^{-3} (5µ)	N$^+$ REGION 3 10^{18} CM^{-3} N REGION (0.2µ THICK) 10^{17} CM^{-3}
• DIE-PACKAGE (IF APPLICABLE)	BeO	BeO
• NUMBER OF INDIVIDUAL CELLS	200 (60µ)	100 (250µ)

* INTERDIGITATED CHOSEN FOR LOWEST r$_b'$, GOOD FREQUENCY RESPONSE AND OUTPUT POWER AND REASONABLE PROCESSING REQUIREMENTS.
+ 20 250µ WIDE FETs CONNECTED IN PARALLEL (λ/₁₀ LIMITATION CONSTRAINS INDIVIDUAL GATE WIDTHS.)
* FOR HIGH SOURCE-DRAIN BREAKDOWN VOLTAGE.

The GaAs transistor chip could be configured to contain two high power transistor stages for the push-pull amplifier configuration of Figure 2.6-19; with low power drive transistors and associated internal matching circuits as shown in Figure 2.6-20. One of the primary key to high efficiency amplifier operation will be the performance of the transistor internal matching circuits.
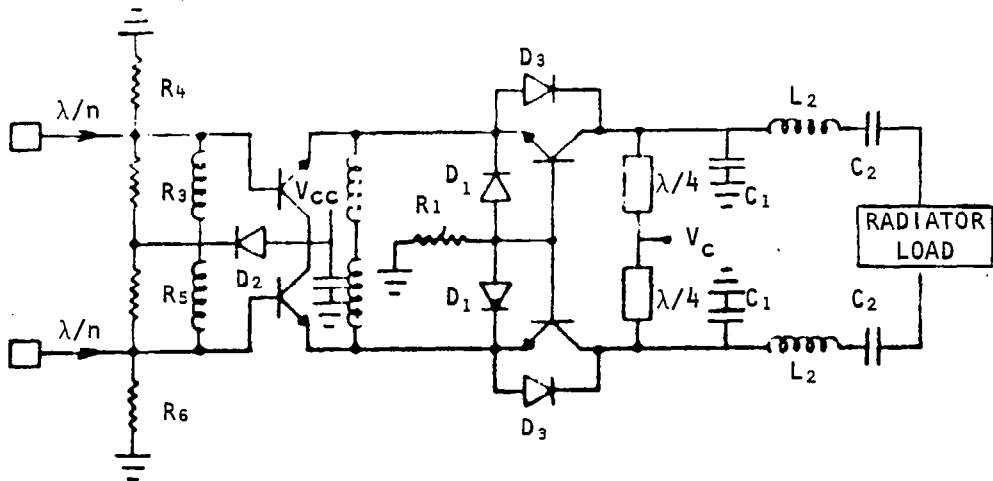
Figure 2.6-19. *Transistor Chip Schematic*

R₁ labels and circuit diagram
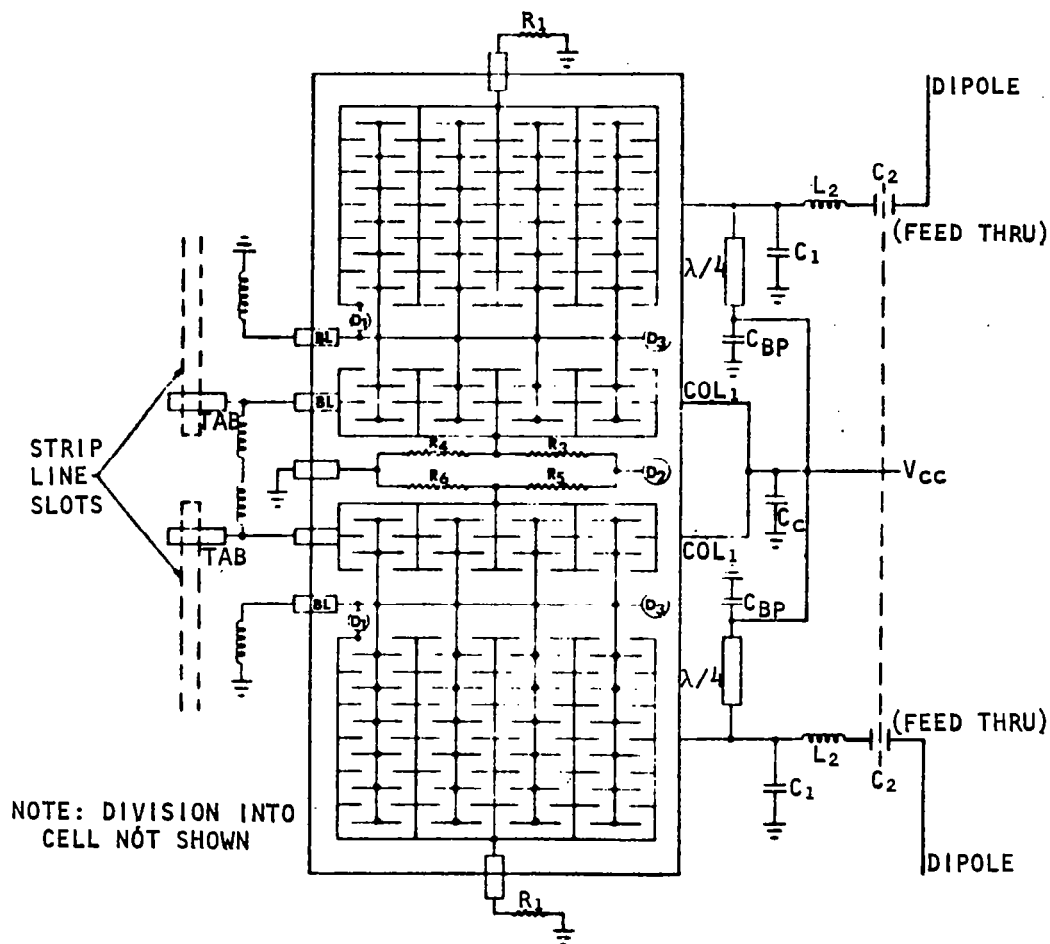
Figure 2.6-20. *Transistor Chip Layout*

     Low transistor output resistances combined with lead inductances, package
parasitics and ballast resistors will not allow optimum matching techniques to
be applied effectively at the external circuit level. The transistor output
resistance is too low and the output reactance is too high at the collector
port. Even considering the narrow bandwidths associated with the SPS MPTS
array, integral matching network constraints will introduce gain-bandwidth
limitations that will ultimately limit the maximum efficiency-gain-frequency
factors associated with class C or class E amplifier performance. Therefore,
internal matching at the transistor chip level (Figure 2.6-20) will be a de-
finite requirement in order to achieve high efficiencies with significant gains.

     Transistor chip sizes of 200 mil × 50 mil or 300 mil × 100 mil would be
necessary along with internal matching and an interdigitated transistor geo-
metry. High temperature tolerant bonds and alloy contacts must be developed.
Metallization combinations such as Au Ge/Pt, Ti/W/Au, Cr/PT/Au or Au-Ga

eutectic alloys must be developed. Metallization combinations, such as these, will help[1-5] improve the lifetime and reliability compared with the Au/Ge/Ni metallization currently used in GaAs FET devices.

Amplifier Power Modules

Large numbers of the transistors can be combined to form high power modules with output powers ranging from 1 kW to 5 kW and higher[6,7,8]. Amplifier designs with efficiencies in excess of 70% will be required (using narrow band Class C or Class E approaches) along with highly efficient power combining techniques.

Figure 2.6-21 provides some idea of how the solid state power module could be packaged. A single 2.5 in × 4.0 in power module package could provide output powers up to 2.5 kW. The individual MIC substrates lie flat on the module housing in order to provide a good heat sink for the power transistors.

Based on the previous transistor electrical performance and physical profile projections, a wide range of solid state power module options are available (Table 2.6-10). Current optimization estimates indicate that the 1 kW to 5 kW output power range appears to be the best for the SPS MPTS array solid state power module.

Table 2.6-11 and 2.6-12 provide an indication of the efficiency and weight for each of the solid state power modules. As the module output power increases, the total efficiency will decrease due to the impact of additional power combiners.

[1]D. Abbott and J. A. Turner, *Some Aspects of GaAs MESFET Reliability*, IEEE Transactions on Microwave Theory and Techniques, Pp. 317-321, June 1976
[2]M. Wittmer, *Investigation of the Au-Ge-Ni System Used for Alloyed Contacts to GaAs*, Solid State Electronics, Vol. 20, Pp. 433-439, 1977
[3]J. A. Higgins, R. L. Kuvas, F. H. Eisen and D. R. Ch'en, *Low Noise GaAs FETs Prepared by Ion Implanation*, Rockwell International Science Center, Final Report, 1978
[4]T. Moutouc, *Let's Take Another Look at Transistor Reliability*, Microwaves, Pp. 52-58, April 1973
[5]M. Flahie, *Reliability and MTF -- The Long and Short of it*, Microwaves, Pp. 36-44, July 1972
[6]A. Morse, *Modify Combiner Designs to Team High Power Amps*, Microwaves, Pp. 70-78, January 1978
[7]_____, *X-Band Planar Combiner Module Using GaAs FETs*, Microwave Journal, p. 34, February 1978
[8]S. Bearse, *Compact Radial Power Combiner Teams Up a Dozen Power GaAs FETs*, Microwaves, p. 9, October 1977

TO SECOND COMBINER OR ANTENNA

DC CONNECTOR

DIMENSIONS: 4" (DIAM) X 1.5" (HEIGHT)

TRANSISTOR BEO PACKAGE MOUNTED ON ALUMINUM BASE.

FIVE TO TEN SAPPHIRE MIC SUBSTRATES

ALUMINUM HOUSING WITH SAPPHIRE POWER DIVIDER/COMBINERS AT BOTTOM.

POWER MODULE STRUCTURE.

POWER MODULE BASE TEMPERATURE: 275°C TO 285°C (GAUSSIAN)
(PRELIMINARY CALCULATIONS)   160°C TO 170°C (UNIFORM-LARGER ARRAY)

*Figure 2.6-21.   Basic 500 W, 1 kW or 2.6 kW Solid State
Power Module Amplifier Configuration*

*Table 2.6-10.   SPS Solid State Power Module Candidates
Using Conventional Power Combining Techniques*

ITEM	POWER OUTPUT AT 2.45 GHz			
	500W	1KW	10KW	50KW
● BASIC AMPLIFIER CONFIGURATION	115W Single Stage Class C or E (≤ 90% Efficiency)	236W Push Pull Class C or E (≤ 86% Efficiency)	247W Push Pull Class C or E (≤ 79% Efficiency)	260W Push Pull Class C or E (≤ 78% Efficiency)
● COUPLER CONFIGURATION	5 Way-Radial Line (Fused Silica or Sapphire)	5 Way-Radial Line (Fused Silica or Sapphire)	10-1KW Modules on a 10 Way-Radial Line Coupler (Fused Silica or Sapphire)	12-2.6KW Modules on a 12 Way-Radial Line Coupler stacked with another 12 Modules (Sapphire)
● SUPPLY VOLTAGE	40V	40V	25V	40V
● TRANSISTOR CANDIDATE	GaAs Bipolar	GaAs Bipolar	GaAs FET	GaAs Bipolar
● NUMBER OF INDIVIDUAL SS POWER MODULES	13,586,400	6,793,200	679,320	135,864
● INDIVIDUAL SS POWER SIZE	4" Diam x 2"	4" Diam x 2"	17" Diam x 3"	20" Diam x 8"
● INDIV. SS PWR MOD WGT (with DC/DC Conv.)	2.5 lb.	2.7 lb.	22 lb.	83 lb.
● STATUS	Could be built now with push-pull @ 50%-60% eff. using 10-way combiner	Significant R&D required for transistor	Significant R&D required for circuit eff., combiner loss and transistor output	Significant R&D required for circuit eff., combiner loss, thermal management and transistor output

Table 2.6-11. Projected Solid State Power Module Efficiency Requirements to Achieve Overall Efficiencies of at Least 78%

ITEM	POWER OUTPUT AT 2.45 GHz			
	500 W	1 KW	10 KW	50 KW
BASIC AMPLIFIER CIRCUIT EFFICIENCY	92%	90%	90%	95%
OUTPUT RADIAL LINE COMBINER EFFICIENCY	95% (0.23DB)	95% (0.23DB)	94% (0.27DB)	93% (0.27DB)
MULTI-MODULE OUTPUT RADIAL LINE COMBINER EFFICIENCY	-	-	93% (0.31DB)	92% (0.03BDB)
STACKING EFFICIENCY	-	-	-	95%
OVERALL EFFICIENCY	90%	85.5%	79%	78%

Table 2.6-12. Projected Solid State Power Module Weights

ITEM	POWER OUTPUT AT 2.45 GHz			
	500 W	1 KW	10 KW	50KW
RF CIRCUITS AND COMBINERS	0.1LB	0.1LB	1.2LB	2.5LB
HEAT SINK	0.1LB	0.2LB	0.6LB	1.8LB
CONNECTORS	0.2LB	0.3LB	3.0LB	10.4LB
CASE	0.1LB	0.1LB	1.2LB	4.3LB
CONVERTER, REGULATOR CURRENT DISTRIBUTION CONTROL CIRCUITS	2.0LB	2.0LB	16.0LB	64.0LB
TOTAL WEIGHT (INCLUDES LOW VOLTAGE SIDE OF DC/DC CONVERTER)	2.5LB	2.7LB	22.0LB	83.0LB

Power Combiner Analysis

The analysis described in the previous sections resulted in a low power ($\leq$ 100 W) basic power module. If antenna phase control techniques were to be applied at this level the result would be the need to phase control more than 7.6×10^6 basic devices. It is therefore necessary to provide further power combination to provide a more realistic phase control interface. Earlier solid state concepts assumed a power module equivalent to a klystron based unit (50 kW). Accordingly this same power level was selected for use in the solid state antenna evaluation.

Present combiner designs assume that typical loss factors of 0.3 dB per combiner is realistic for a basic 2 way unit. Furthermore, the number of power combiners required may be approximated by the equation:

$$2^N P_i = Po$$

where: P_o = Power of amplifier module

Pi = Input power of individual amplifier device

N = Number of 2 way combiners.

Since the desired output power is 50 kW it is necessary to iterate the equation until the input power multiplied by the combiner efficiency satisfies the requirement. This occurs when 10 combiners are used in a cascade mode. Under this condition the combiner efficiency is estimated to be 50% (10×0.3 dB/comb = 3 dB).

The combiner analysis is summarized in Figure 2.6-22.
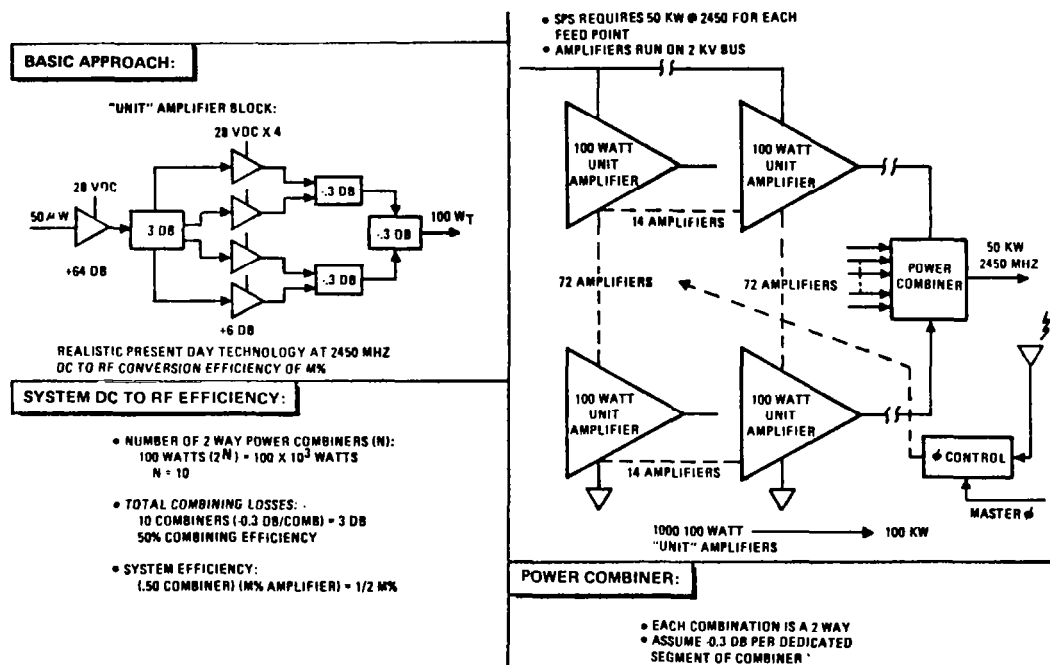
Figure 2.6-22. Bipolar Solid State SPS Option

Class E[1,2] and Class C[3,4] Amplifiers

Results of recent computer simulation studies[5,6] indicate that there is no significant difference between the efficiencies of the Class E amplifier and Class C amplifier for gains below 23 dB at 2.5 GHz. At gains of 23 dB, maximum efficiencies of 77.5% have been computed for the Class C amplifier and 82% for the Class E amplifier. These figures do not account for all circuit and transistor package parasitics. It appears that the Class E amplifier is more sensitive to the effects of parasitics and component variations than the Class C amplifier. In essence, the Class E amplifier efficiency may not be any better than the Class C amplifier efficiency under actual operating conditions.

From a solid state device standpoint, it appears that at 2.5 GHz, the GaAs bipolar transistor would be best for Class C amplifier operation and the GaAs FET would be best for the Class E amplifier.

Thermal

Considering thermal effects on transistor lifetime and efficiency. Upper limits of 160° to 170° are anticipated for both the GaAs bipolar and GaAs FET devices.

The original thermal limitations imposed upon the SPS MPTS array electronics may not be as low as originally anticipated (60°C - 100°C). Recent work on the performance characteristics of silicon devices for geothermal instrumentation indicate that discrete junction FET, MOSFET devices and integrated CMOS devices can be fabricated to perform at ambient temperature levels up to 300°C[7]. Certain CMOS devices can maintain useful characteristics at temperature levels approaching 275°C.

[1]F. Raab, *Effects of Circuit Variations on the Class-E Tuned Power Amplifier*, IEEE Journal of Solid-State Circuits, Pp. 239-247, April 1978

[2]N. Sokal and A. Sokal, *Class-E, A New Class of High Efficiency Tuned Single Ended Switching Power Amplifiers*, IEEE Journal of Solid State Circuits, Pp. 168-176, June 1975

[3]J. Vidkjaer, *A Computerized Study of the Class-C Biased RF Power Amplifier*, IEEE Journal of Solid-State Circuits, Pp. 247-258, April 1978

[4]O. Pitzalis and R. Gilson, *Broad Band Microwave Class-C Transistor Amplifiers*, IEEE Transactions on Microwave Theory and Techniques, Pp. 660-668, November 1973

[5]D. J. Roulston, I. N. Hajj and P. R. Bryant, *Evaluation of High Efficiency Microwave Power Transistors*, Report to Rockwell International, Space Division, September 10, 1978

[6]D. J. Roulston, I. N. Hajj and P. R. Bryant, *Evaluation of High Efficiency Microwave Power Amplifier Transistors*, Report to Rockwell International, Space Division, June 1, 1978

[7]J. L. Prince, *Performance of Silicon Devices at Very High Temperatures*, Digest, 1978 Government Microcircuit Applications Conference, November 14-16 1978

Impact of Solid State Power Module Concept on MPTS Array and Spacecraft Configuration

The solid state power module approach will require a significantly more complex power distribution system compared with the present SPS point design using klystrons. Weight increases of 40% to 90% are anticipated for the solid state power module approach using present point concepts. Efficiencies for the power distribution system associated with the solid state approach have been estimated to be 80% using the present point concept.[1] Increased complexities, higher costs, higher weights and reduced efficiencies associated with the SPS MPTS array solid state power module power distribution system indicates that an alternate SPS configuration will be required if the solid state approach is implemented. Table 2.6-13 summarizes some of the preliminary implications for the solid state approach.

Table 2.6-13. Preliminary Implications for SPS Solid State Power Module and MPTS Array Configurations

SOLID STATE POWER MODULE CONFIGURATION	DESIGN DRIVER	REASONS
● 1 KW TO 5 KW POWER MODULE	● POWER DISTRIBUTION DC/DC CONVERTER.	● CAPACITANCE LIMITATION ON TRANSFORMER WINDINGS.
	● THERMAL PROFILE	● TEMPERATURE LIMITATIONS ON STACKED MODULES.
	● EFFICIENCY	● LOWER POWER MODULES ARE MORE EFFICIENT
● HIGH TEMPERATURE (ALLOY) BONDING	● LIFE-TIME	● CONVENTIONAL BONDS WILL FAIL OVER 200°C.
● MATCHED SERIES TRANSISTOR PAIRS* (NOT A GOOD IDEA FROM EFFICIENCY STANDPOINT)	● LIFE-TIME	● TRANSISTOR FAILURES TEND TO INCREASE AS BREAKDOWN VOLTAGE IS APPROACHED.
● MPTS ARRAY SIZE AND POWER DISTRIBUTION CHANGE	● POWER MODULE & ELECTRONICS TEMPERATURE	● BASE TEMPERATURES IN EXCESS OF 250°C ARE ANTICIPATED. ⧧
● MICROWAVE POWER DISTRIBUTION SYSTEM MAJOR CHANGES.	● TRANSISTOR BREAKDOWN VOLTAGE	● LOW VOLTAGE (<100v) HIGH CURRENT PROBLEM.

*WHAT WE NEED IS A TRANSISTOR, CAPABLE OF DELIVERING 92% EFFICIENCY AT 2.45 GHz, WITH A SIMPLE STRUCTURE, HIGH TEMPERATURE CAPABILITY AND A BREAKDOWN VOLTAGE IN EXCESS OF 300v.

⧧ELECTRONICS ARE PRIMARY THERMAL DESIGN DRIVER (<100°C).

2.6.3 SOLID STATE/WAVEGUIDE CONCEPTS

The data presented in this section develop a series of ideas as to the feasibility of adapting the dc/RF, solid state, wave guide principles, developed by Aerospace Corporation GSSPS to the MSFC four-trough galium-arsenide SPS under study contract to Rockwell International.

General Description

The general arrangement of the Aerospace GSSPS and the Rockwell SPS systems is shown in Figure 2.6-23. In the spring and fall of each year, the solar collector panels of GSSPS obscure each other. Aerospace Corporation suggests a

---

[1] Ibid (item 1, page 2-83)

2-99
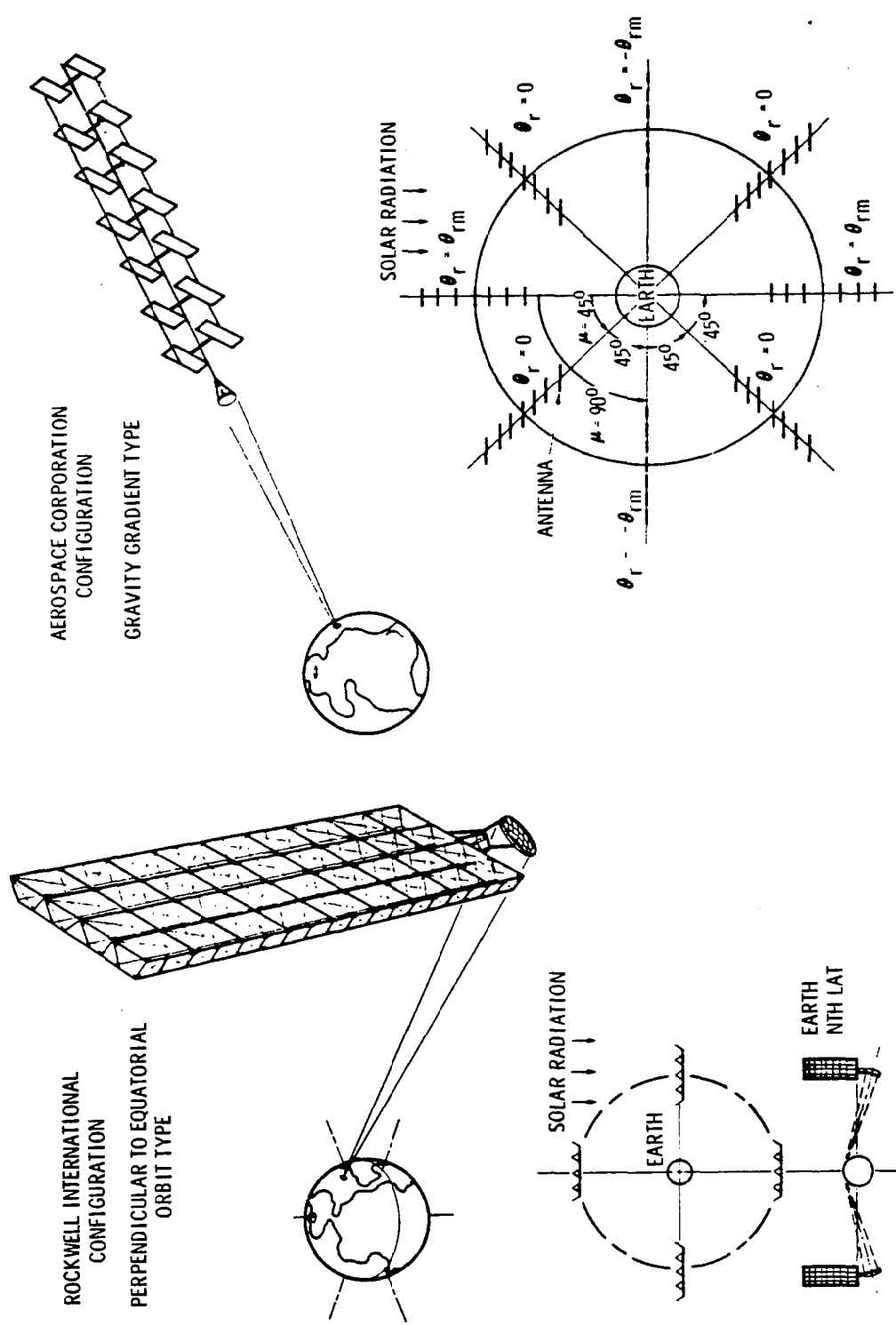
Figure 2.6-23. Dc/RF Solid State/Wave Guide SPS Concepts

twice-per-orbit libration about the satellite roll axis to minimize this
obscuration. In the winter and summer, the panels do not obscure each other
due to the 23.5-degree angle between the earth equatorial and ecliptic planes.
The libration cycles must be phased to cause a once-a-year precession if
synchronization with the changing sun angle is to be maintained. All of these
maneuvers may require a complex attitude control system for the 47 km long
string-like satellite to maintain sun-pointing of the solar panels and earth-
pointing (to latitudes not on the equator) of the lens antenna.

     The illustrated Rockwell configuration (Figure 2.6-24) simplifies sun-
pointing of solar cells and earth-pointing of the reflector-antenna using a
simple mechanical rotary joint and pivot system containing no electrical or RF
components. The satellite attitude is perpendicular to the equatorial orbit
plane with the antenna located on the South Pole end of the satellite pointing
toward northern earth latitudes. For south latitude antenna-pointing, the
antenna is mounted on the North Pole end of the satellite. Ion propulsion
units maintain active control over satellite attitude and either control-moment
gyros or simple electric motor drives maintain earth-pointing of the antenna.
The Aerospace Corporation GSSPS uses a three-layer (butterfly dipole/phase-
shifter/butterfly dipole) lens antenna to transmit energy, emitted from a horn
mounted on the end of the 47 km long main wave guide, in a coherent manner to
earth. Latitude pointing and minor longitude pointing is accomplished by wave-
front phasing and may require some mechanical pointing to maintain low sidelobe
requirements.
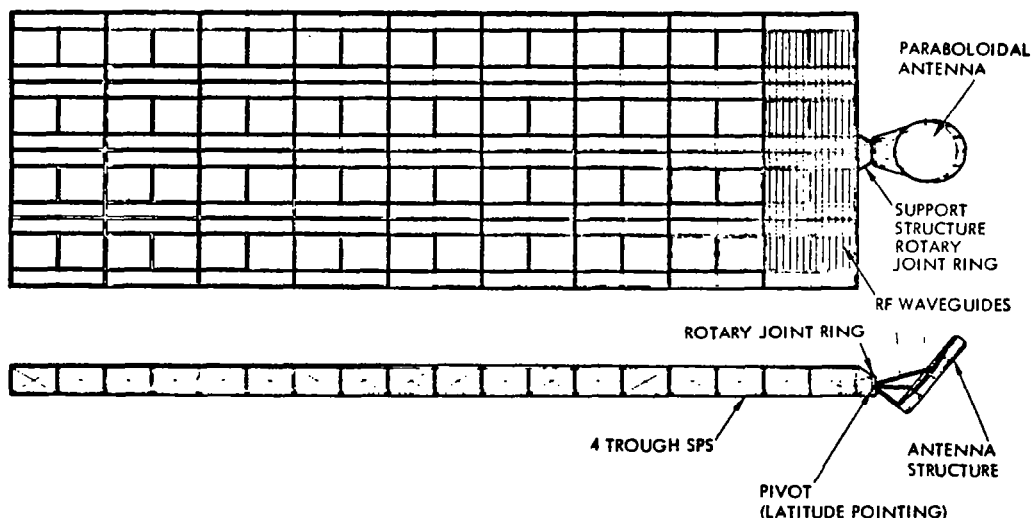
Figure 2.6-24. Solid State Satellite Power System

     The Rockwell configuration uses a paraboloidal wire mesh antenna to reflect
and collimate energy transmitted by a wave guide mounted transmitter horn that
is designed as a field lens to emit a spherical wave front. The wave guide
horn is located at the focal point of the paraboloidal, wire mesh mirror.

2-101

The general configuration of the Rockwell/MSFC four-trough SPS is shown in Figure 2.6-24. An antenna support structure is attached at the center line of the solar array structure. The support structure includes a rotary ring assembly and an antenna assembly attached by pivots to the rotating element of the ring assembly. The rotating ring (axis along SPS center line) permits the daily rotation of the antenna; the pivot permits latitude antenna pointing.

RF wave guides and solar cell panel in transverse orientation are shown.

Rockwell dc/RF Solid-State/Wave Guide Concept Details

Figure 2.6-25 shows the basic elements needed to adapt the Aerospace Corporation solid-state, wave guide RF power transfer concept to the Rockwell concept.
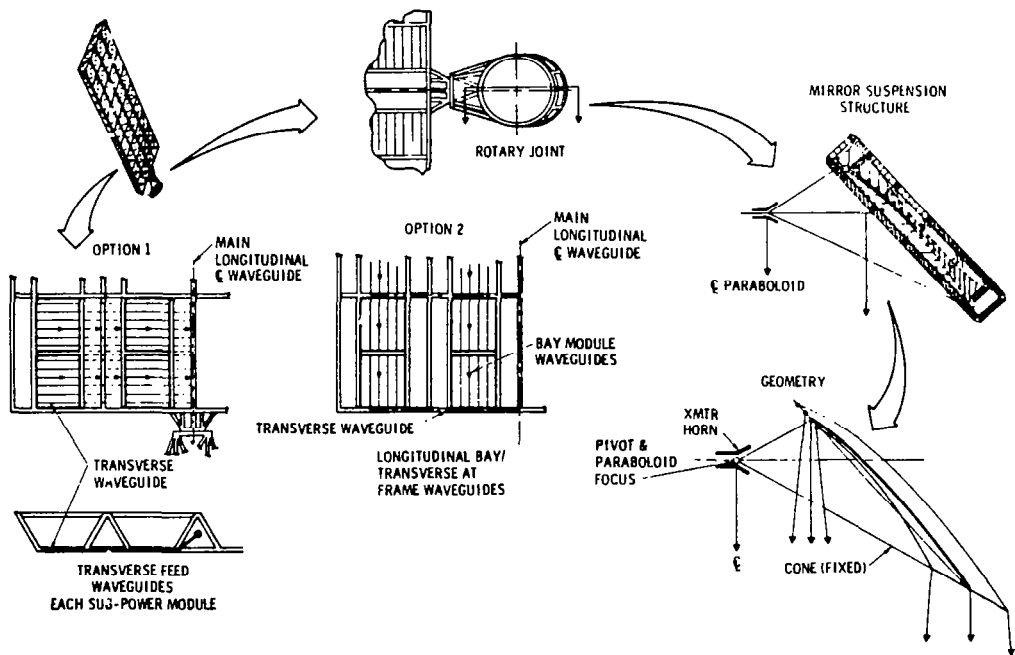
Figure 2.6-25. Rockwell dc/RF Solid-State/Wave Guide Concept Details

Two options for solar cell, wave guide orientation are shown. Option 1 illustrates a transverse orientation of solar cells and RF wave guide feeds. Solar cells on each side of the wave guide generate and conduct dc electrical power to solid-state devices mounted directly on the wave guide, that convert dc to RF power. The wave guides transmit the RF energy generated to a centrally located main wave guide where matching wave guide elements insert the lateral wave guide energy into the central wave guide connected to the transmitter horn.

2-102

Option 2 shows a longitudinal orientation of solar cells and waveguides. At the end of each structural bay, the longitudinal wave guides are connected to lateral wave guides which, in turn, are connected to the main longitudinal wave guide which feeds the transmitter horn. Power levels, wave guide matching, and system assembly procedures will determine which option is selected.

The antenna rotary joint shows the location of a section cut of the antenna illustrated at the right side of the chart. The geometry of the antenna, the relationship of the antenna horn to the antenna paraboloidal surface, and earth pointing of the collinated beam are shown below the section cut.

Geometry

The Aerospace Corporation lens antenna requires a diagonal mirror to permit attachment to the Rockwell SPS.

The case of a diagonal mirror pivoted at the intersection of the horn axis and the lens equatorial pointing axis is shown in the upper left-hand corner of the facing chart. For each degree the flat mirror rotates about the pivot point, the lens antenna must rotate two degrees about the pivot point remaining perpendicular to the fixed radial center line distance. Structural rigidity and alignment tolerance appear to be the key problems.

The case of two simple pivot motions is shown in the lower left-hand corner of Figure 2.6-26. As before, each degree of diagonal mirror rotation requires two degrees of lens antenna rotation. However, the lens in this case rotates around a fixed pivot point. The two pivot points thus may be rigidly attached to each other.

The pivot motion described accounts only for latitude pointing. Daily earth pointing (longitude fixed) of the lens/mirror assembly requires a rotary joint with its axis coincident to the wave guide/horn axis, rotating once every 24 hours. The overall structural complexity, mirror flatness, and lens tolerances make implementation of either of the lens/mirror suggestions difficult.

A third, reasonably simple, option is possible. If the transmitter horn is designed as a field lens to emit energy with a spherical wave front from the focal point of a paraboloidal mirror, the energy will be reflected parallel to the axis of the paraboloid and collimated into a flat wave front beam. In the near field, the energy profile will tend to be uniform.

In the far field, the energy profile will approximate a Gaussian sin x/x curve. A second mirror shape potential is an ellipsoid with one focus at the transmitter horn and the second focus at the center of the rectenna located on the earth. The ellipsoidal and paraboloidal contours are very nearly identical. Other antenna contours are possible if the lens horn has an apparent index of refraction as in coherent-light optics. The mirror index of minus one may be equated to the positive lens index to effect cancellation of mirror frequency aberrations of the system (if physical optics equivalence holds true). Wave shaping by the lens may also be used to correct for mirror surface anomalies to some degree. At issue in--How much?

FLAT REFLECTOR/LENSE
GEOMETRY
(FIXED XMTR HORN)

PIVOTABLE PARABOLOID
(FIXED XMTR HORN)
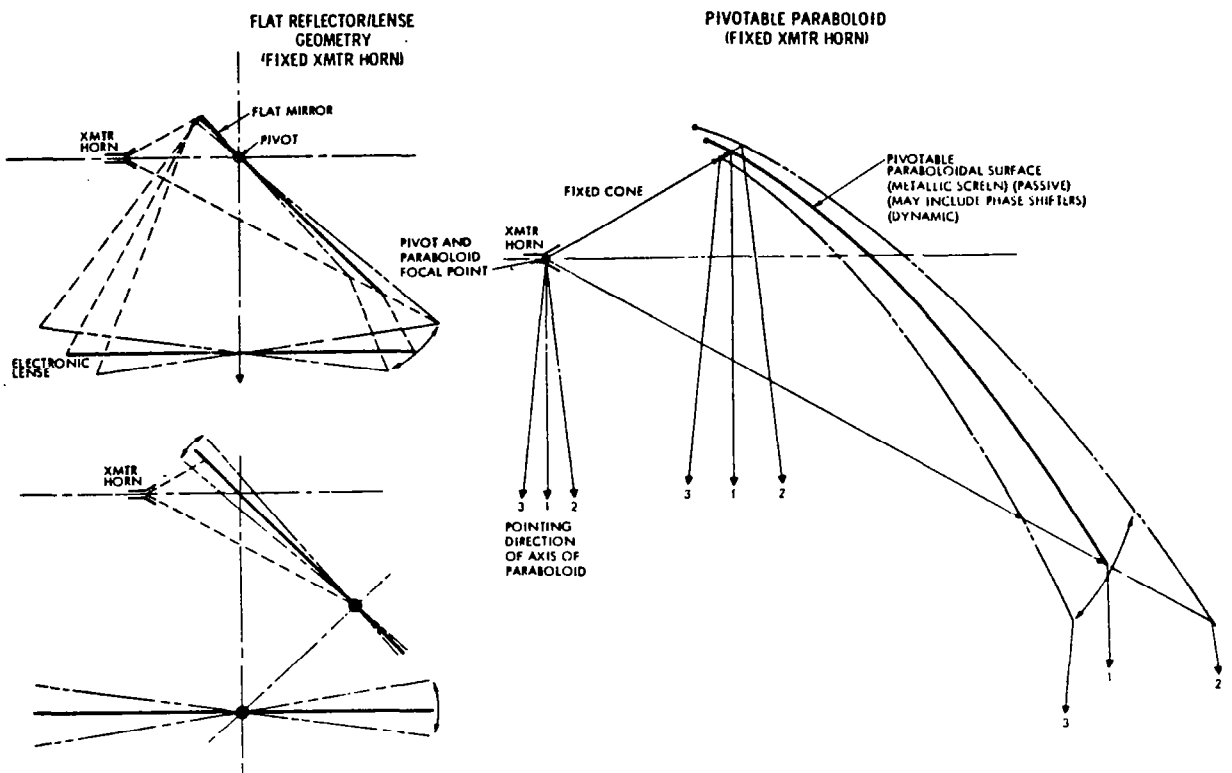
Figure 2.6-26. Geometry

To effect beam pointing for daily motion, a rotary joint with axis coincident to the wave guide and transmitter horn axis is required. The plane of rotation is located at the paraboloid focal point. To effect beam latitude pointing a pivot axis in the plane of the rotary joint is required. These two axes allow the paraboloid center line to be pointed at any required angle to place the transmitted beam at the earth rectenna.

A preferred pivot angle direction is identified by rays (3) shown on Figure 2.6-26. A smaller mirror surface results. This is the reason that the antenna is located at the South Pole end of SPS for north latitude pointing and, conversely, on the North Pole end of SPS for south latitude pointing.

Parabolic Antenna Details

Figure 2.6-27 illustrates how a frame and tension wire array might provide a close tolerance wire-mesh paraboloidal mirror.

It is possible to create a paraboloidal shape if a uniform force field oriented parallel to an axis is applied to a membrane perpendicular to the axis. If a system of meridian planes radiates from the axis, each contains a flexible member (contour members) anchored to a frame--in turn, pulled upon by close uniformly spaced flexible members (force members)--with each supporting equal loads, a segment of a parabola will be formed in each meridian plane. The

TRUE VIEW

ROTARY JOINT CUTAWAY
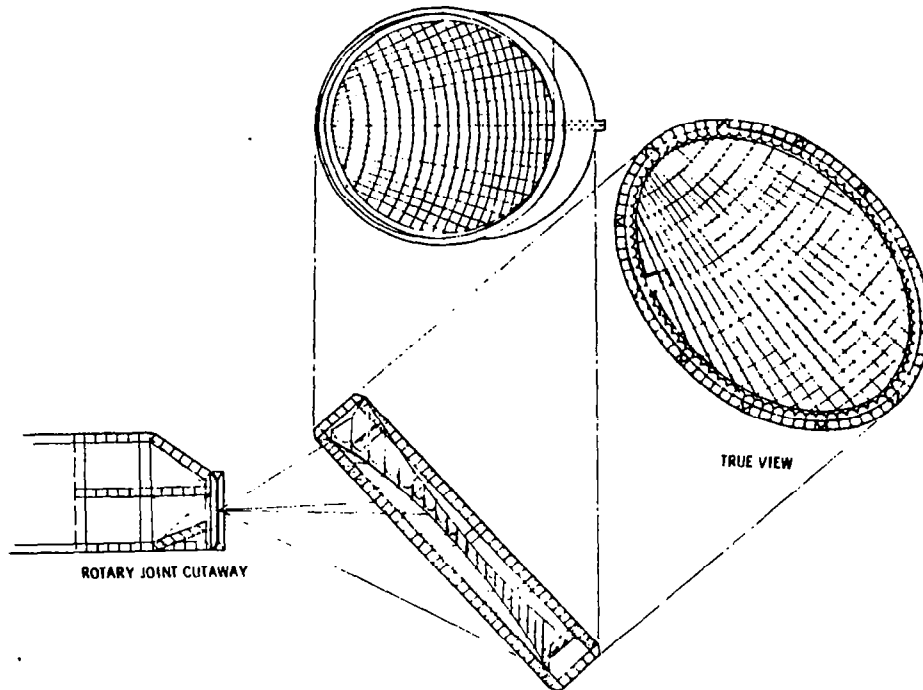
Figure 2.6-27. Parabolic Antenna Details

exact segment of the parabola formed is determined by the angular relationship
of the anchored meridian contour elements and the uniformly spaced elements
representing the uniform force. Other flexible members located orthogonally
to the meridian planes may be located to form concentric circles about the
paraboloidal axis. The degree of surface compliance is determined by the
closeness of the net pattern formed.

To effect the uniform force field upon the paraboloidal net, a system of
flexible members is required with the members pulling in opposition to the
previously described net. This second array of flexible members is connected
to the same frame. Since only one surface (the "mirror" surface) requires
shape compliance, the counter-pull member array may permit the accumulation of
the uniformly spaced members (force members) into fewer major strands reacted
by a single flexible member for each meridian plane formed. No concentric
circular counter force element members are required. Since all flexible members
are anchored on the same frame, and interconnected to each other, a complete
self-contained stable system of forces and nets will be established.

Figure 2.6-28 is an enlargement of solar cell/wave guide options described
in Figure 2.6-25. The heavy line in the lower left-hand figure illustrates the
transverse wave guide relative position to adjacent supporting structure.

Microwave Power Distribution Subsystem

Figure 2.6-29 shows the solid-state circuit diagram required for the
Rockwell concept, the transistor mounting concepts contained in the Aerospace
Corporation AIAA paper, and illustrates a conceptual transmitter horn mounted

2-105

TRANSVERSE
FEED

← MAIN
LONGITUDINAL
C_L WAVEGUIDE

TRANSVERSE
WAVEGUIDE

LONGITUDINAL BAY
TRANSVERSE AT FRAME

TRANSVERSE
WAVEGUIDE

MAIN
LONGITUDINAL
C_L WAVEGUIDE
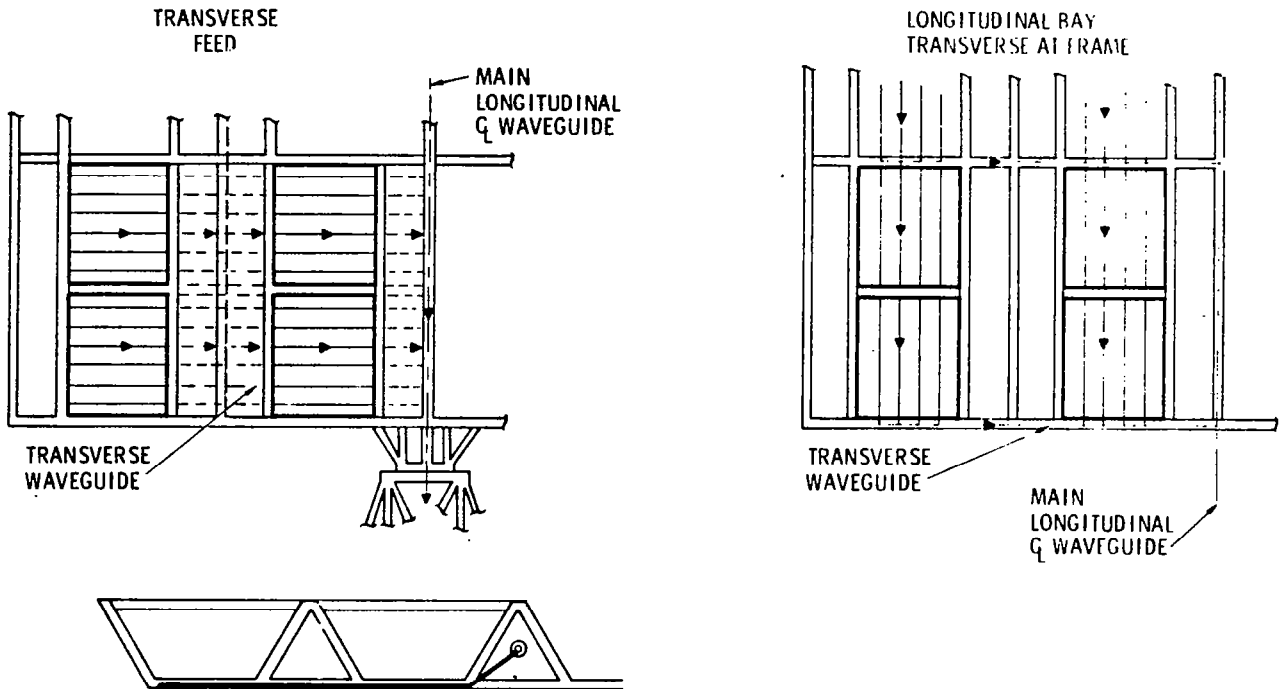
Figure 2.6-28.   RF Wave Guide Orientation Options

DC → TRANSISTORS MSTR-OSC → W/G → HORN FEED → PARABOLOIDAL ANTENNA → 6.6 GW

XMTR HORN

WAVEGUIDE

WAVE SHAPING
ELEMENTS

SPHERICAL
WAVE FRONT
PROPAGATION

SIDE LOBE SUPPRESSENT
CAVITIES
(LEAKAGE EXCITED)

(A) TRANSISTOR
MOUNTING
CONCEPTS

(B) COAXIAL CONDUCTOR
WAVES TO TE_{D1} WAVES
CONVERTER CONCEPT
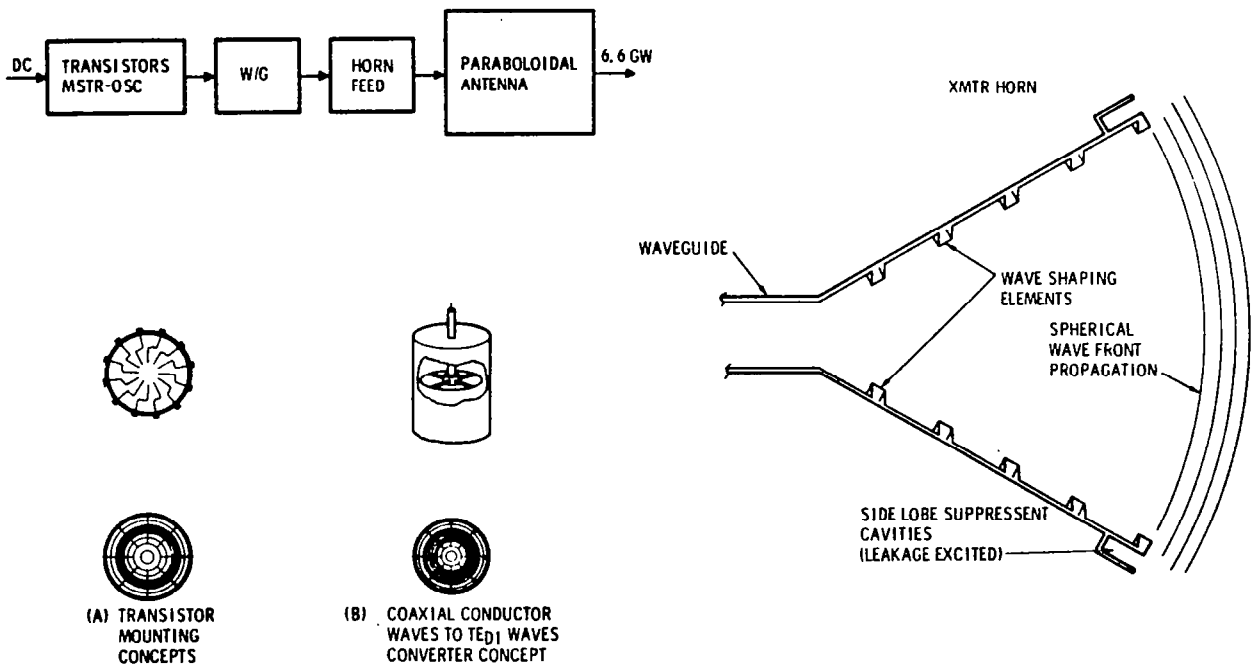
Figure 2.6-29.   Microwave Power Distribution Subsystem

2-106

on the end of the main wave guide. All RF rotary joints described in the Aerospace Corporation AIAA paper have been eliminated in the Rockwell concept. The lens property of the transmitter horn has been utilized on low-power (relative to SPS) radar antennas. The concept of self-excited, electrically tuneable sidelobe suppressant cavities may be new. Tuneable wave shaping of the emitted spherical wave front may also be new. The question as to whether horn spilling can be prevented and sidelobe suppression at the horn accomplished. Other questions are: What surface compliance must the paraboloidal mirror have? Will the paraboloidal mirror surface require a phase-shift property? Can the transmitter horn effectively control and phase-shift portions of the wave front (if required) to maintain the proper power distribution at the earth rectenna? Is it possible to transmit a unique wave shape such as to produce a uniform field intensity at the rectenna? This last question poses the possibility of a 5000- to 6000-m diameter rectenna.

The attendant potential for cost reduction of the SPS system and the earth rectenna warrants a "proof-of-concept" study.

2.6.4 PHASE ERROR CONTROL

Introduction

There are several key issues associated with maintaining accurate control of the transmitted phase front. These are as follows:

- Obtaining an accurate reference phase of the subarray level,

- Compensating for phase changes in the power amplifiers and feed system, and

- Compensating for subarray position errors and propagation effects.

The first two effects can be compensated internal to the satellite itself by measuring the phase shifts or deducing them by range measurements. The third effect requires either transmitting a pilot beam up from the ground and measuring the phase received at each subarray, or by making a number of field measurements on the ground and deducing the subarray phase errors from them. The pilot beam approach is defined as retrodirective phase control while the latter approach is called ground reference phase control.

Although the ground referenced phase control system is the simplest, (insofar as the antenna electronics are concerned), it does not correct well for ionospheric effects. The ground fields may not be related to the antenna aperture distribution by a simple Fourier transform because of the ionospheric and atmospheric perturbations between them. On the other hand, the retrodirective approach is very attractive because detailed field measurements on the ground are not required. As long as the propagation effects are equivalent at the pilot frequency and the power frequency, the retrodirective approach gives a direct and precise measurement of the subarray phases required and may also produce the correct reference phase by frequency conversion. Several previous retrodirective phase control systems were evaluated and found to have disadvantages from the standpoint of complexity, system errors, weight and cost. An

eclectic phase control system was chosen to combine the best properties of each previously derived retrodirective phase control system. The primary advantage of the eclectic system is that it reduces a significant amount of the error inherent with the other approaches.

Comparison of Certain Retrodirective Array Candidates

Some brief comments may be made in comparing the advantages and disadvantages of certain retrodirective array approaches.

1. Eclectic Retrodirective Array

Advantages

* Concept is proven on smaller scale systems

* Concept can be analyzed and simulated with resonable ease

* Concept provides the easiest approach for "add-ons" modification or subsystem growth items

Disadvantages

* Subsystem hardware is not well defined

* Certain subsystem interfaces have, as yet, not been defined

* Has significant interference problem without application of spread spectrum techniques to achieve processing gain

2. Spread Spectrum/Phase-Lock Retrodirective Array

Advantages

* Very good hardware definition

* Most hardware interfaces well defined

* SNR improvement with processing gain

* Bandwidth narrowing using phase-lock techniques

Disadvantages

* Concept had not been simulated or demonstrated to provide adequate proof that it will point accurately or point at all

* Concept requires cost as phase-lock loops which have significant problems with false lock and dropping out of lock

* Difficult to analyze but can be simulated

3. Mechanical Retrodirective Array

Advantages

* Concept is proven on smaller scale systems

* Concept can be analyzed and simulated

2-108

Disadvantages

- Mechanical tolerance limitations and aging will significantly inhibit the system's pointing accuracy

- Difficult to implement electronic "add-ons" or modifications

- This system has size/accuracy limitations

- This approach has a greater reliability problem as the result of containing a greater number of large moving parts

2.6.5 ANTENNA ARRAY SIDELOBE VARIATIONS AND PHASE ERRORS

Antenna Array Sidelobe Variations as a Function of Surface Perturbations

The effect of a surface perturbation on a basic n element antenna array can be approximated by assuming the perturbation effectively increases the array spacing by a small amount (Figure 2.6-30).

L = Array Spacing in Wavelengths
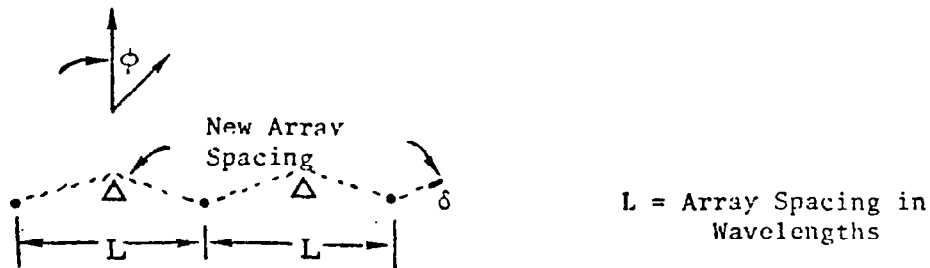
Figure 2.6-30. Effective Increase in Array Spacing by Surface Perturbation

The basic antenna array element expression for field intensity $[E(\phi)]$ as a function of L and ϕ:

$$E(\phi) = \frac{\sin (2\Pi \ n \ L \ \sin \ \phi)}{n \ \sin (2\Pi \ L \ \sin \ \phi)} , \tag{1}$$

where n is the number of elements in the array.

By differentiating $E(\phi)$ with respect to L, an expression can be derived which will show the fractional variation in $E(\phi)$ with respect to changes in ϕ:

$$\frac{d \ E(\phi)}{E(\phi)} = \frac{2\Pi \ \sin \ \phi}{\sin (n \ 2\Pi \ L \ \sin \ \phi)}$$

$$\times \left[n \ \cos(n \ 2\Pi \ L \ \sin \ \phi) - \frac{\cos (2\Pi \ L \ \sin \ \phi)}{\sin (2\Pi \ L \ \sin \ \phi)} \right] dL \tag{2}$$

By substituting in various values of ϕ, a plot of antenna sidelobe variations versus array perturbation can be obtained. Equation 2 indicates that a 2λ protrusion caused by a tube laying on its side or a solid state power module could cause first and second sidelobe variations of 8 dB and 14 dB, respectively.

2-109

This analysis makes a simplifying assumption. It takes a two dimensional problem and reduces it to one dimensional constraints. Although the assumptions in this analysis are over simplified, the results are reasonable enough to make some good approximations.

The results indicate that the perturbing effects of klystron tubes or solid state devices protruding from the surface of the MPTS antenna array could cause variations in sidelobe levels of at least 10 dB. For a uniform array with 0 dB Gaussian taper, this could result in a 0.7 dB reduction in main lobe power. For a uniform array of 10 dB Gaussian taper, the sidelobe variations could cause approximately 0.1 dB to 0.2 dB reductions in main lobe power. The effect on Taylor weighted antenna arrays would be similar.

Although not included in this analysis, it should be noted that Figure 2.6-30 implies a small variation in angle for Equation 1 where:

$$\psi = 2\Pi \, L \sin \phi \tag{3}$$

The perturbation introduced by the klystron will cause a small angular deflection:

$$\psi = 2\Pi \, L \sin \phi + \delta \tag{4}$$

and this will tend to introduce beam steering.

Phase Error Analysis

The principal consideration in establishing the phase error tolerance for an antenna array is the degradation of effective radiated power (ERP) which the antenna component and subsystem errors introduce. Results achieved with a retrodirective Van Atta array[1] can be extrapolated to estimate the phase error tolerances required for the retrodirective SPS MPTS antenna array. Figure 2.6-31 indicates the power degradation as a function of the uniform phase error distribution. Figure 2.6-31 shows an approximate ±29° phase tolerance allowed for each array element if an ERP degradation of 1 dB is allowed. This constrains each antenna element to the following phase error tolerances:

- Radiating Element   ±6°
- Amplifiers and Electronics   ±8°
- Feed Network   ±8°
- Phase Shifter   ±7°

Again, simplifying assumptions are being made because the retrodirective Van Atta array has significant differences when compared with the SPS retrodirective antenna array. However, the Van Atta results do provide a good source of tolerance and phase error estimates for the SPS MPTS array.

---

[1]J. M. Flaherty, *Microcircuit Phased-Array Electronic Countermeasures System*, Microwave Journal, Pp. 69-74, September 1969
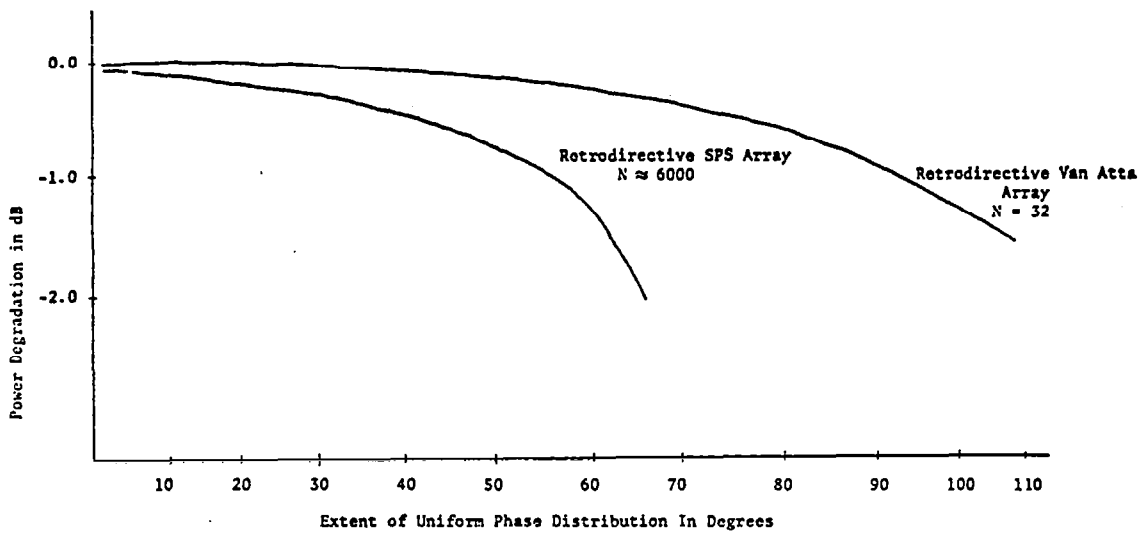
Figure 2.6-31. MPTS Array RF Phase Error

The estimates indicate that each basic antenna element can have an rms phase error tolerance of from +6° to ±8°. This requirement will place strict manufacturing requirements on each element, especially the phase shifters and feed networks.

2.7.1 INTRODUCTION

The microwave power transmission system (MPTS) has been described as consisting of two major elements: 1) the orbiting transmission antenna, and 2) the ground receiving antenna (rectenna). The ground receiving station (GRS) consists of the ground element of the MPTS, (the rectenna), and the power distribution, power conversion, data management, and other supporting subsystems required to collect, convert and route power to the utility interface tie lines.

The following subsections of this report address the rectenna and power distribution subsystems only. The other subsystems are not considered but may be evaluated in future studies.

2.7.2 RECTENNA

Siting

The rectenna siting analysis is discussed in Section 2.8 of Volume V of this final report. Summarizing the information discussed in that section, the GRS site requires approximately 35,000 acres. Figure 2.7-1 shows a layout of a typical site. The inner ellipse containing the rectenna panels, 10×13 km, is about 25,200 acres or 72% of the total acreage. The area surrounding the inner ellipse is utilized for maintenance facilities, access roads, converter stations and the two peripheral rows of towers which support the 40 kV dc and 500 kV ac cables. The outer perimeter of the area is fenced for security reasons. The towers which support the 500 kV ac cables are constructed of steel girders footed in concrete and are approximately 230 ft (70 meters) high. The inner towers are each comprised of four tapered steel columns 60 feet (18.3 meters) tall. Fifty-four of the larger towers and 401 of the smaller towers are required, the latter figure translating into 1604 tubular members because of the configuration.

Receiving Antenna (Rectenna)

The rectenna is postulated as being composed of many panels, nominally 9×15 meters, arranged to be perpendicular to the line of sight to the satellite as shown in Figure 2.7-2. In this section, the configuration of an individual panel and factors with respect to its location in the rectenna will be identified.

The portion of the panel initially under analysis is the structure of the microwave network that connects the individual antenna elements together and to a rectifier. The two major contenders for this network are stripline, for low cost; and wave guide, for low loss. However, there are other considerations in addition to the type of transmission line used. The main items among these are the rectifier operating point, and the type of antenna elements comprising the panel, and these will be discussed before comparing interconnect network types.
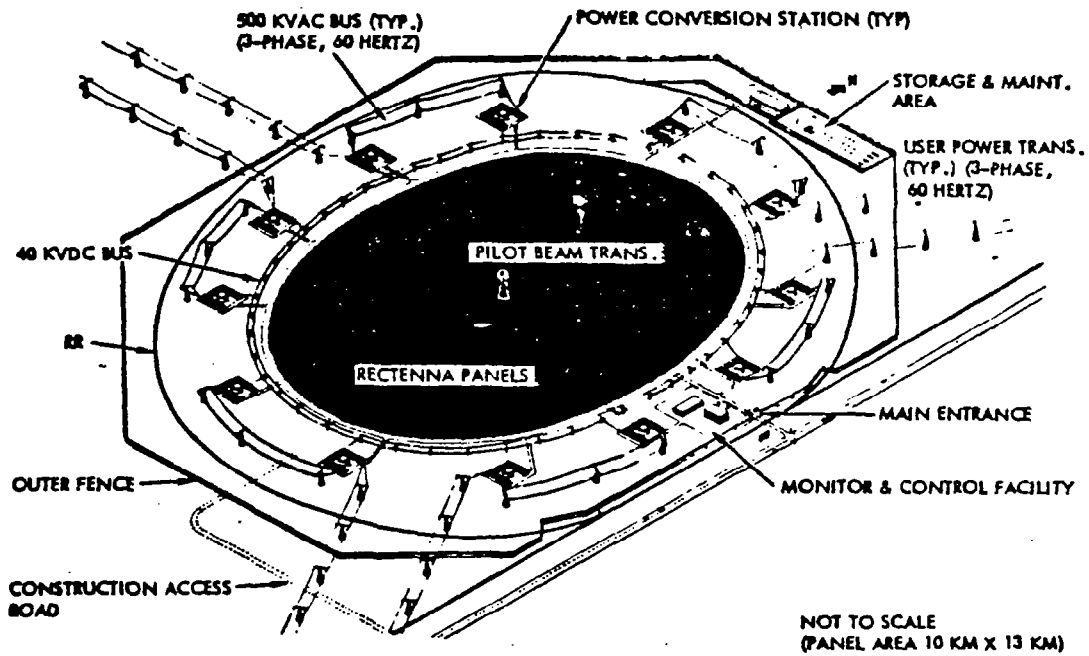
Figure 2.7-1. Operational Ground Receiving Facility
(Rectenna) - Typical
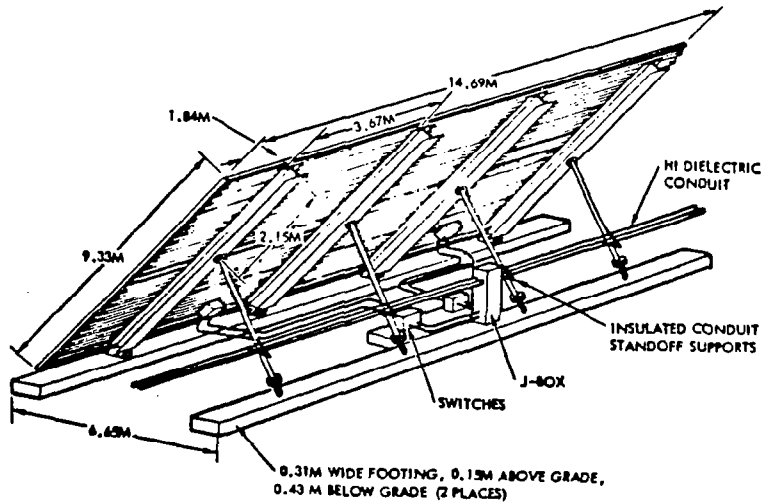
Figure 2.7-2. Rectenna Panel Assembly and Installation

2-113

Rectifier Operating Point. Efficiency of a solid state rectifier is a function of the power input level. This is illustrated in Figure 2.7-3.
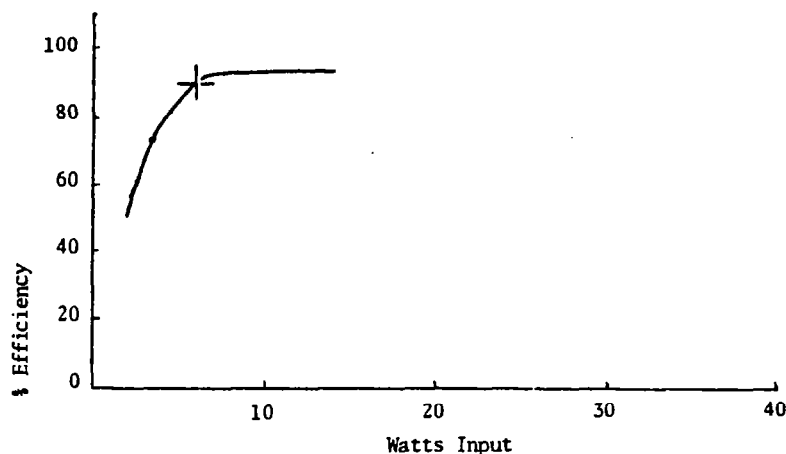
Figure 2.7-3. Rectifier Operating Proficiency

The curve shows that at 6 watts RF input, the efficiency is about 90%. This establishes the benefit of operating the rectifier at a reasonably high power; for the purposes of this analysis, above 6 watts. The maximum power handling capability of a rectifier is a function of many parameters encountered during its detailed design. Without pursuing these design problems further in this section, a maximum of about 45 watts has been assumed. Thus, it is desired to keep the RF power input as high as possible, but no more than 45 watts and no less than 6 watts.

The incident microwave energy from the satellite is estimated to total 5.53 GW within an elliptical area with major- and minor-axis of 13 km and 10 km respectively. The relative energy variation along the major-axis is illustrated in Figure 2.7-4. The rectenna area is arbitrarily divided into five concentric zones, with power received per unit area diminishing from the center to the edge. The chart of Figure 2.7-5 shows these zones plotted for the 10×13 km rectenna, along with some of the other assumed rectenna characteristics. Table 2.7-1 shows the average power density in each zone, and also the power density at the center and edge.

An area of .183 square meters was taken as a unit power gathering area. (this will be shown to be equivalent to a 7×7 element array with $\lambda/2$ spacing between elements.) If one rectifier is allocated to each unit power gathering area, Table 2.7-1 shows that for four out of five of the zones, the rectifier will have more than 6, but less than 45 watts input. For the fifth zone, a group of nine areas is assigned to each rectifier to maintain rectifier power in the efficient range.

By these choices of rectenna unit area, efficient rectifier operation is assured, and a baseline established to compare microwave interconnecting networks.
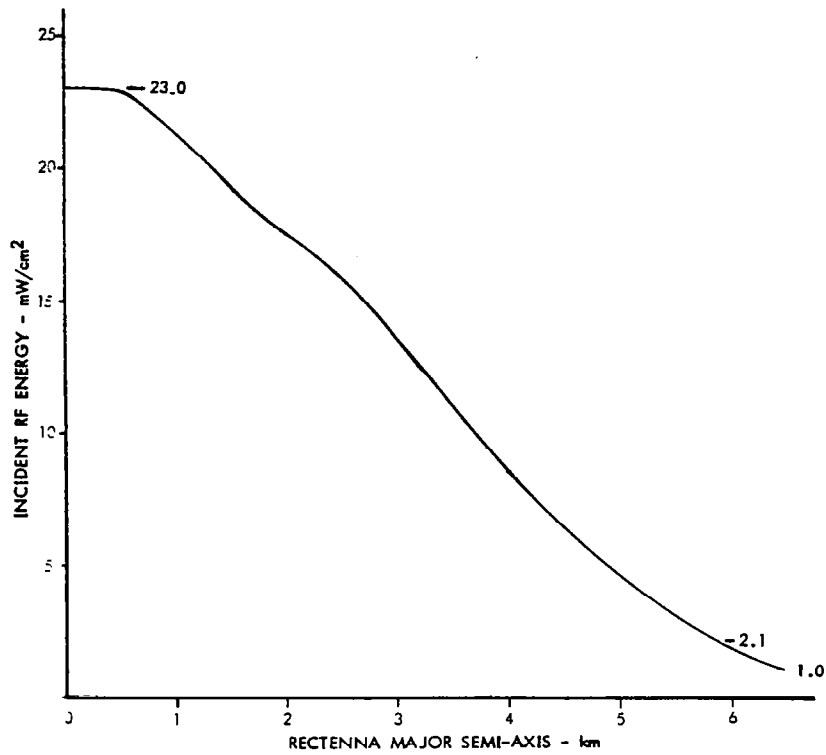
Figure 2.7-4. Power Density - Rectenna

PANEL AREA	79.56 KM^2
PANEL AREA	137 M^2
INCIDENT POWER	5.53 GW
NO. PANELS	580,500
NO. 40.5 KV/0.321A STRINGS	~329,000
NO. DIODES	~330 X 10^6

NO. PANELS

ZONE	NO.	AVERAGE PWR DENS
I	14200	220 W/M^2
II	58200	180
III	135400	100
IV	211000	52
V	161700	18

117.5 M

(100 PANELS)

150 M

N
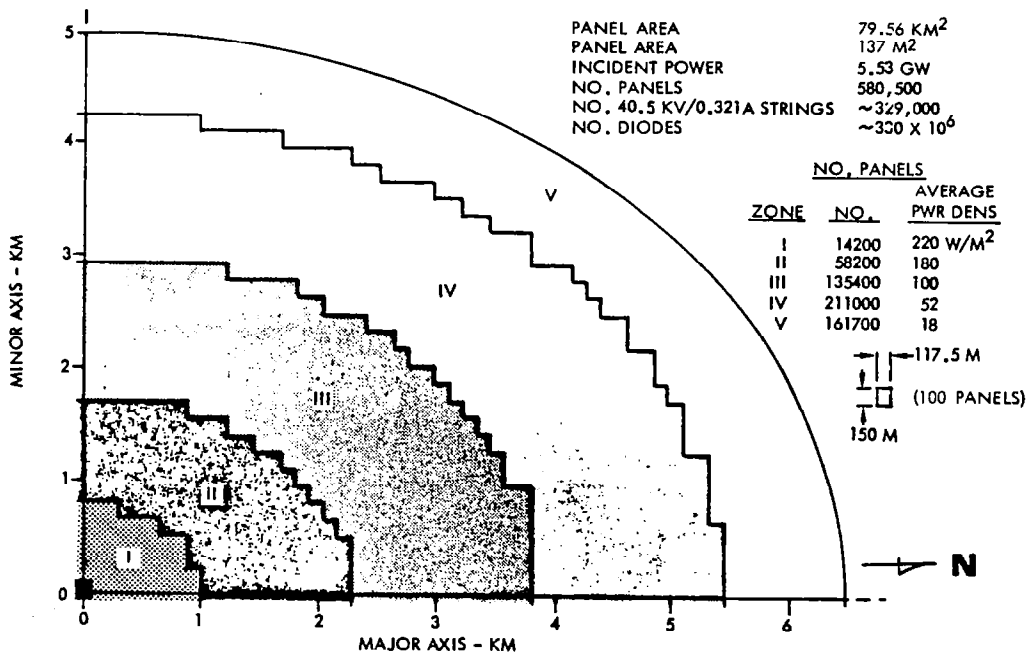
Figure 2.7-5. Rectenna Power Density Pattern
(34° N Latitude)

2-115

Table 2.7-1. Billboard Summary

.183 M^2/CLUSTER

REGION	NOMINAL POWER DENSITY	WATTS PER CLUSTER	TYPICAL ALLOCATION CLUSTERS (49 ELEMENTS) PER DIODE	WATTS PER DIODE
CENTER	230 W/M^2	42.1	1	42.1
I	220	40.3	1	40.3
II	180	33.0	1	33.0
III	100	18.3	1	18.3
IV	52	9.5	1	9.5
V	18	3.3	9 *	29.7
EDGE	10	1.8	9 *	16.2

* SATELLITE DRIFT < ± 0.2°

Type of Antenna

The 9×15 meter antenna panel can be anything between a dense (λ/2 spacing in both directions) array of radiating elements to a single antenna (9×15 meter parabola or horn, center or offset fed). The single element concept was discarded for a number of reasons: more power than could be handled by a single rectifier, too narrow a beam for ease in pointing and to accommodate satellite drift, and bulk that could cause complications in setting up the rectenna, were the major ones.

It was suggested that under certain conditions, the satellite might drift close to 3°. This is unlikely under most conditions, but the number provides a convenient unit for determining the fewest number of elements in a panel. If the beamwidth of an individual element is to be greater than 3°, and the pointing loss is to be held below 2%, the 3 dB beamwidth of that element must be broader than 19° or 20°, which is about .183 square meters.

Some general statements about antenna type and feed networks can be made at this point to illustrate trends in performance. Some of these statements can be modified through clever design, nevertheless they are valid over large regions of the design range.

Uniform illumination is approached (a desirable characteristic for the rectenna is uniform illumination. This means that the aperture efficiency is unity, all the energy impinging on the antenna is passed to the rectifier, and none is scattered back into space) most closely by a dense array. As the number of elements is reduced, the aperture efficiency drops. However, the drop in efficiency is not linear with the inverse of the number of elements, but rapidly stabilizes at about .7 as the number of elements decreases, provided that the detailed design has as its objective the maximization of aperture efficiency.

As the number of elements increases, more interconnecting transmission lines and matching devices are required, increasing network losses. From the performance point of view (neglecting rectenna structure economics) the antenna design should be a tradeoff between aperture scattering loss and network loss.

The antenna configuration baseline has been bounded by adopting a .183 square meter unit area, and allowing the design to range from a dense array of 7×7 elements spaced $\lambda/2$ to a square parabola of this same area with a single feed element. Configurations intermediate to these are a Yagi array of 12 elements, each with a capture area of about one square wavelength; a short backfire array either square or hexagonal, with a capture area of about four square wavelengths, and a parabolic trough. These configurations are illustrated in Figure 2.7-6.
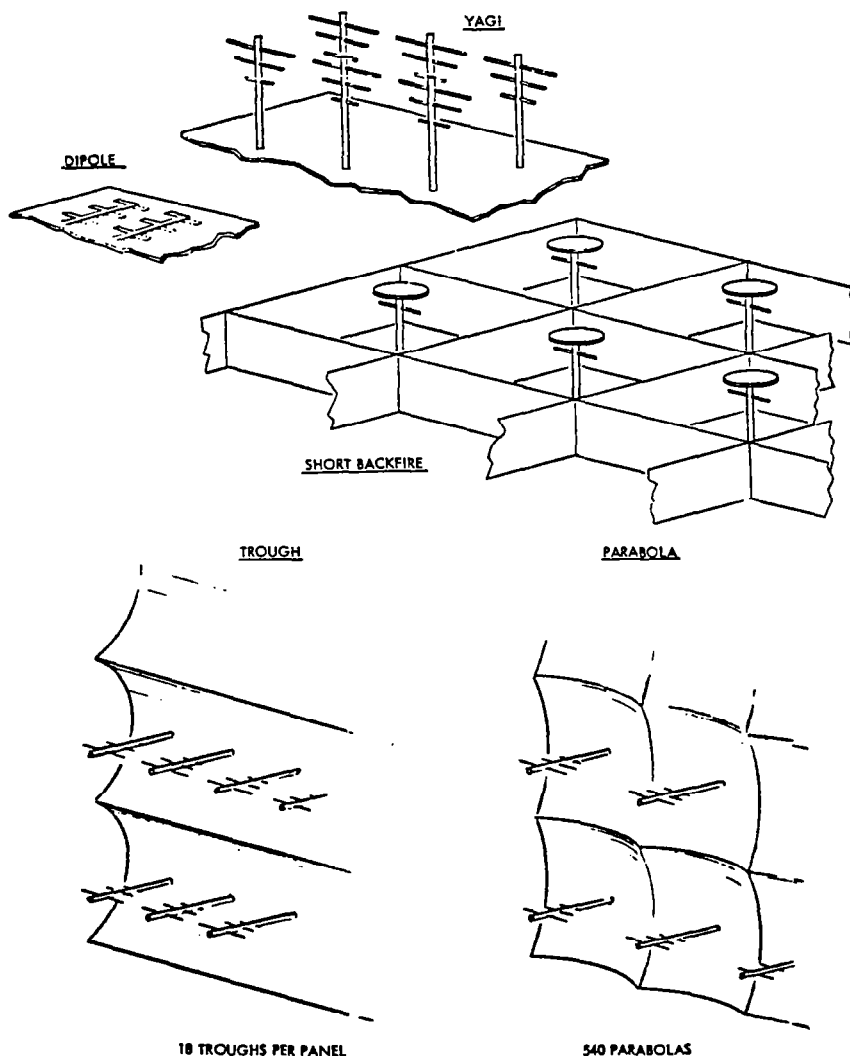
Figure 2.7-6. Panel Alternative

Estimated characteristics are shown in Table 2.7-2, which also indicates the number of elements required for each rectenna panel, and some comments on aperture efficiency and unknown parameters that require further study.

Table 2.7-2. Rectenna Concepts

CONCEPT	NUMBER OF ELEMENTS (9 x 15 M PANEL)	DESCRIPTION	COMMENTS
→ DENSE ARRAY (BILLBOARD)	36044	DIPOLES, $\lambda/2$ SPACING SQUARE CLUSTERS OF 49 ELEMENTS	STRIPLINE INTERCONNECT MATCHING LOSS \} EDGE EFFECTS \} NEEDS STUDY
YAGI ARRAY	9011	λ SPACING, RECTANGULAR CLUSTERS OF 12 ELEMENTS	MUTUAL COUPLING EFFECT NEEDS STUDY
SHORT BACKFIRE ARRAY	2254	2λ SPACING, SQUARE CLUSTERS OF 4 ELEMENTS	BEAMWIDTH SLIGHTLY TOO NARROW, NEEDS STUDY
→ TROUGH	2205	18 PARABOLIC TROUGHS YAGI FEEDS SPACED λ	APERTURE EFFICIENCY $< .8$
SQUARE PARABOLAS	540	540 PARABOLAS YAGI FED	APERTURE EFFICIENCY $< .7$

Interconnecting Network

In comparing the loss of stripline with wave guide interconnecting net-works, the approach taken was to interconnect 49 elements of a dense array arranged in a square, and show that the loss is tolerable. It is then assumed that any antenna configuration with a lesser number of elements will have less network loss. Following this, arrangements for interconnecting groups of .183 square meter unit areas are examined, for use in the fifth or outer zone of the rectenna, without regard for the consequent beam narrowing that will be experienced.

A stripline configuration is shown in Figure 2.7-7. If the square 7×7 element array has its central element connected to a rectifier, and other elements connected in series parallel, the average transmission line length may be shown to be $3/2$ λ_g. Figure 2.7-7 illustrates this method of connecting for one quarter of the 7×7 element array using connections λ_g long in serpentine form to fit the $\lambda/2$ spacing. A few places require $2\lambda_g$. This configuration appears to have the shortest average transmission line length but has some severe matching problems. These could introduce losses that dominate the normal transmission line loss, taken here as $.015$ dB$/\lambda_g$, but much could be done in rectifier design to avoid matching networks. Both of these factors are unknown at present. Simple line loss amounts to .02 dB or 0.5% for stripline.

A wave guide configuration is shown in Figure 2.7-8. The 49 element array consists of seven lengths of wave guide with either 7 slots or 7 dipoles in each length. The array is also center fed by another wave guide that couples at the center of each guide. This may not be the simplest feed arrangement, but it has the shortest average waveguide run between a rectifier located at

2-118

7 λ/2 = 0.428 M

7 λ/2

SQUARE CLUSTER 49 DIPOLES
19.5° BEAM AT 3 DB POINT
3.7° AT 2% POINT
(ALSO LOOKED AT HEXAGON, LINE)

1/4 CLUSTER
INTERCONNECT SCHEME

2 LINKS   2 λg LONG
ALL OTHERS λg LONG

2 λg

2 λg

OUTPUT
TERMINAL

DISTANCE - AVERAGE ELEMENT TO OUTPUT = 3/2 λg

• LOSS AT .015 DB/ λg = .0225 DB = 0.5%

• POTENTIAL DIFFICULTY - MATCHING LOSSES OF 17 PORT NETWORK
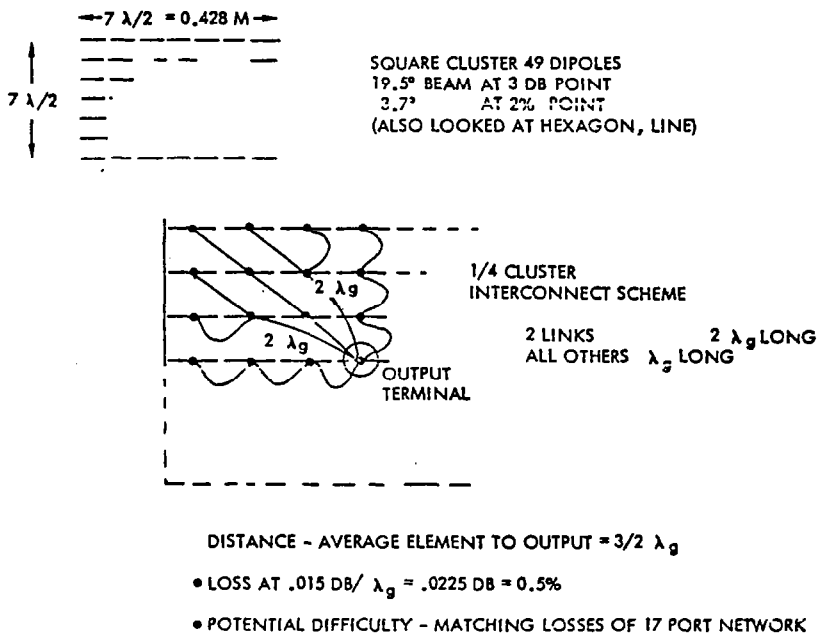
Figure 2.7-7.   Billboard Feed - Stripline

49 ELEMENT ARRAY

SLOTS

OR

DIPOLES

ASSUME CORREGATIONS TO
SHORTEN λg DO NOT CHANGE
DB/λg (OPTIMISTIC)

IF CENTER FED
AVERAGE ELEMENT PATH LENGTH
3/4λ + 3/4λ = 3/2λ

FOR λg = 1.2λ , 3 λg = .22 M
LOSS = .0044 DB = 0.1%

• ALUMINUM GUIDE .5 TO .75 DB/100'
  AVERAGE = .02 DB/M

• EFFICIENCY OF FEEDING ELEMENTS
  REQUIRES FURTHER STUDY
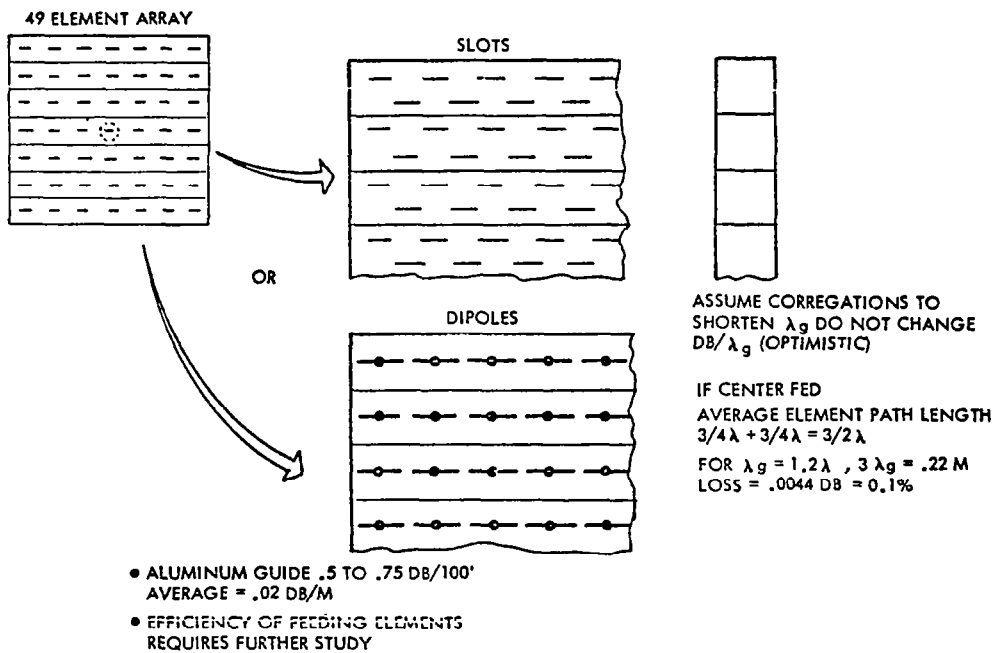
Figure 2.7-8.   Wave Guide Fed Billboard

the center of the array and any slot or dipole. The average path length is
again 3/2 λ_g, and loss for aluminum guide with λ_g = 1.2λ is .0044 dB or .1%.

Although wave guide has one fifth the loss of stripline, the stripline
loss is tolerable, and very much less costly to produce.

In Zone V, (of Figure 2.7-5) several .183 square meter (49 element) units
should be grouped to bring the power input to the rectifiers up to an efficient
operating point. Figure 2.7-9 shows four possible groupings, including the
grouping of 9 suggested earlier. Average loss using stripline interconnect is
computed for each of these groupings, this loss to be added to the transmission
loss within each .183 square meter unit. Loss for the grouping of 9 is comput-
ed at 1.8%, while because of the shortened path, the grouping of 6 has only
half this loss. Because of the group interconnect loss, and possible additional
matching losses, Zone V panels will have considerably more (estimated at four
times) interconnection loss of ungrouped panels in other zones.

DOES NOT INCLUDE MATCHING NETWORKS

PATH TO DIODE = 7/4λ	PATH TO DIODE = 7/4 $\sqrt{2}\lambda$	2 LINES 7/4 λ 4 LINES 7/2 λ	4 LINES 7/2 λ 4 LINES 7/2 $\sqrt{2}\lambda$
= 1.75λ	= 2.47λ	AVERAGE PATH TO DIODE = 2.91λ	AVERAGE PATH = 4.2λ TO DIODE

FOR λ_g = .8λ , LOSS = .015 DB/λ_g, LOSS TO BE ADDED TO CLUSTER LOSS

.033 DB	.046 DB	.041 DB	.079 DB
.8%	1.1%	.9%	1.8%
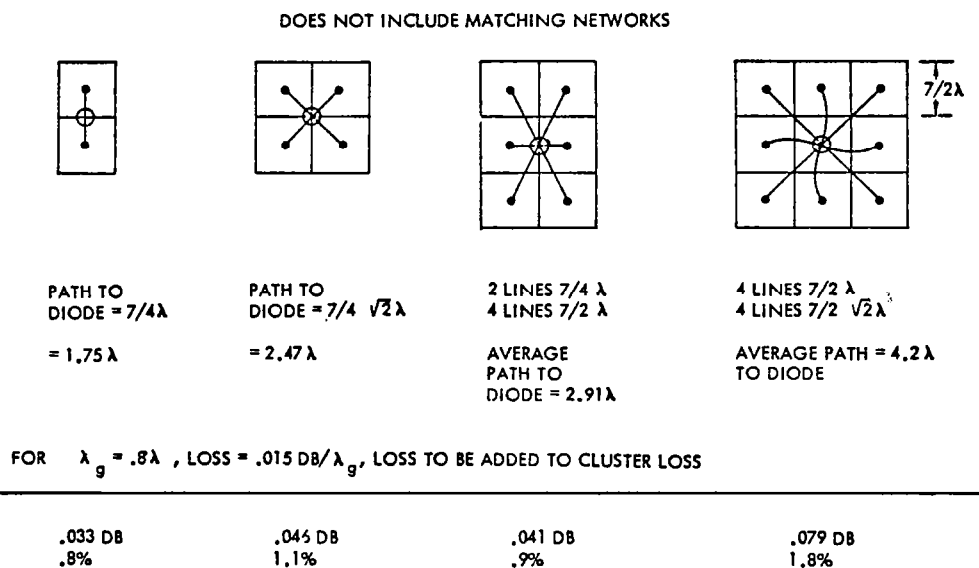
Figure 2.7-9. Cluster Interconnect

In considering the use of simple dipoles, the adequacy of linear polar-
ization under Faraday rotation was examined. Typical values of diurnal varia-
tion at 100 MHz were extracted from the "Handbook of Geophysics and Space
Environment". The variation to be expected under average conditions is 450°
to 3600°. Since variation is inversely proportional to the square of the
frequency, these typical values may be extrapolated to .75° to 6° at 2.45 GHz.
If linear polarization is used, this could result in 0.55% loss at 6°. This
is summarized in Figure 2.7-10. Should this problem be of concern, it should
be estimated for the specific geometry of the locations under consideration,
and also for the statistics on time that atypical conditions cause rotations
greater than typical.

FARADAY ROTATION (HANDBOOK OF GEOPHYSICS)
(AND SPACE ENVIRONMENT)

TYPICAL $\Omega = 450°$ TO $3600°$ AT 100 MHZ - DIURNAL VARIATION

$$\Omega \propto \frac{1}{f^2}$$

AT 2.45 GHZ
TYPICAL $\Omega = .75°$ TO $6°$

IF UNCORRECTED   LOSS $= .024$ DB $= .55\%$
POSSIBLY LARGER UNDER ATYPICAL CONDITIONS

Figure 2.7-10. Polarization Considerations

Conclusions

Several obvious conclusions can be drawn from the previous discussion.
Paramount is the conclusion that stripline losses are not excessive and there-
fore cannot be considered to eliminate this approach from consideration. Even-
though the losses beyond about 5 km exceed the 1% guideline used in efficiency
studies, the significantly better than guideline losses (0.5%) experienced in
the inner areas more than offset the average, and infact, the overall effect
may have been to improve the situation.

The use of waveguide concepts may provide improved conversion efficienc-
ies. However, the probable increase in manufacturing costs may be prohibitive.

The general recommendation is therefore to assume a stripline approach
but to continue with the analysis of alternative approaches.

Panel Installation

Figure 2.7-2 shows a panel in the installed position. The panels are
9.33×14.69 meters and are attached to continuous concrete footings at eight
points as shown. A trade-off which considered eight individual footings
versus continuous footings was made (Volume V). A maximum wind force of
90 mph was assumed. It was determined that the amount of concrete required
for either approach was essentially the same but that the continuous footing
concept was easier to install.

Threaded inserts are placed in the concrete during the pouring process
and provide the means for mounting the panel attach fittings which are capable
of longitudinal and lateral adjustment. Screw jacks are installed at each of
the four rear attach points to allow for panel adjustment and alignment.

Details of panel construction are shown in Figure 2.7-11. Four standard
size eight inch I beams, to which the attach fittings are secured, are spaced
in the lateral (14.69 meters) direction. Galvanized steel hat sections (thin
sheet, 0.020 inches thickness) of the dimensions as shown are mounted in the
longitudinal direction (14.69 meters) and provide the mounting for the sub-
strate containing the electronic components. The substrate (with components)
is delivered to the on-site assembly plant, in strips of 9.33×0.74 meters.
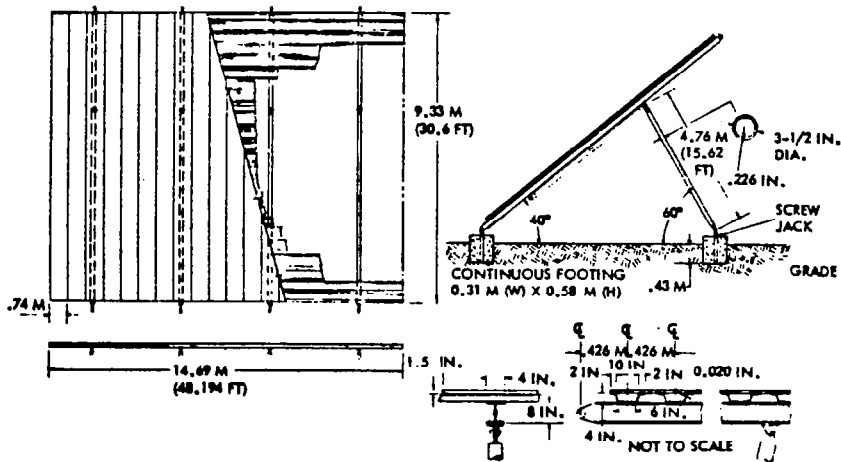
Figure 2.7-11. Rectenna Array Support Structure

The panels are supported in the inclined position by tubular steel members which provide an angle from the horizontal of 40° for this example, (latitude = 34°N). Each panel weighs 2080 kg, of which approximately 85% is steel.

Panel Hookup

From Table 2.7-2 it can be calculated that each panel can require approximately 735 diodes (in sectors I-IV, in sector V their will be approximately 82). Total number of diodes required in the farm is estimated to be approximately 330×10^6. The output of each cluster/diode rectifier are series connected so as to provide 40.5 kV "voltage strings", (13 kW @ 0.321 amp.). It is estimated that the rectenna farm will have available approximately 329,000 strings. The number of diodes per string will vary depending upon location in the rectenna farm area. The average number per string is estimated to be approximately 1000+.

2.7.3 POWER DISTRIBUTION

The power available from each "voltage string" on the rectenna panels must now be collected and distributed to various feeders and buses. From there the power is routed through interface converters and eventually converted to utility inter-ties. Figure 2.7-12 represents a simplified schematic of the basic station distribution subsystem.

2-122
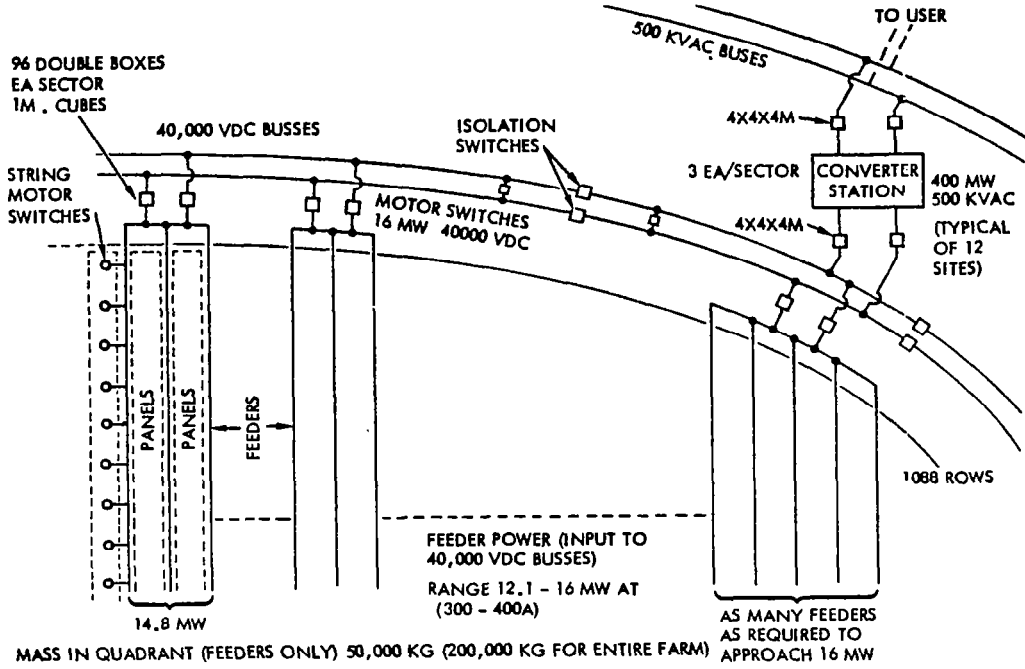
Figure 2.7-12. Receiving Station Power Distribution Schematic - Preliminary

3.0 POINT DESIGN

3.0 POINT DESIGN

3.1 INTRODUCTION

This section describes the Rockwell International Photovoltaic Satellite Based Satellite Power System (SPS) Point Design as it has been defined through March 1979. The point design to be presented is the result of a series of trade studies performed during the period January 1977 through March 1979 under contract NAS8-32475. The initial contract period effort is documented in Volume IV of report SD 78-AP-0023-4, Final Report, SPS Point Design Definition, dated April 1978. An updated version was released in July 1978 in document SD 78-AP-0113. The additional data established during the period August 1978 through March 1979 has been incorporated in this document.

The reader is cautioned that apparent inconsistencies may be observed during a review of this document. These inconsistencies result from the differing termination dates of the various subsystem trade and design activities. These inconsistencies will be identified whenever they exist in the text describing detailed subsystem point design(s).

The system relationship of the total Satellite Power System is depicted in Figure 3.1-1. This document discusses only the first two elements; the satellite and ground systems.

A summary of the primary program ground rules followed in development of this version of the photovoltaic (CR-2) satellite is as follows:

- IOC Date: 2000

- Program Size: 300 GW by 2028 (10 GW per year, average)

- System Life: 30 years

- Cost: 1977 constant dollars (7.5% discount rate)

- Systems Available in the 1980's: Shuttle 1980
                                    IUS   1981
                                    OTV   1987

This section covers the major subsystems of the satellite system including power conversion, power distribution and control, microwave, attitude control and stationkeeping, thermal control, structures, and information management and control. In addition, ground and space systems are described covering the rectenna and utility interface.
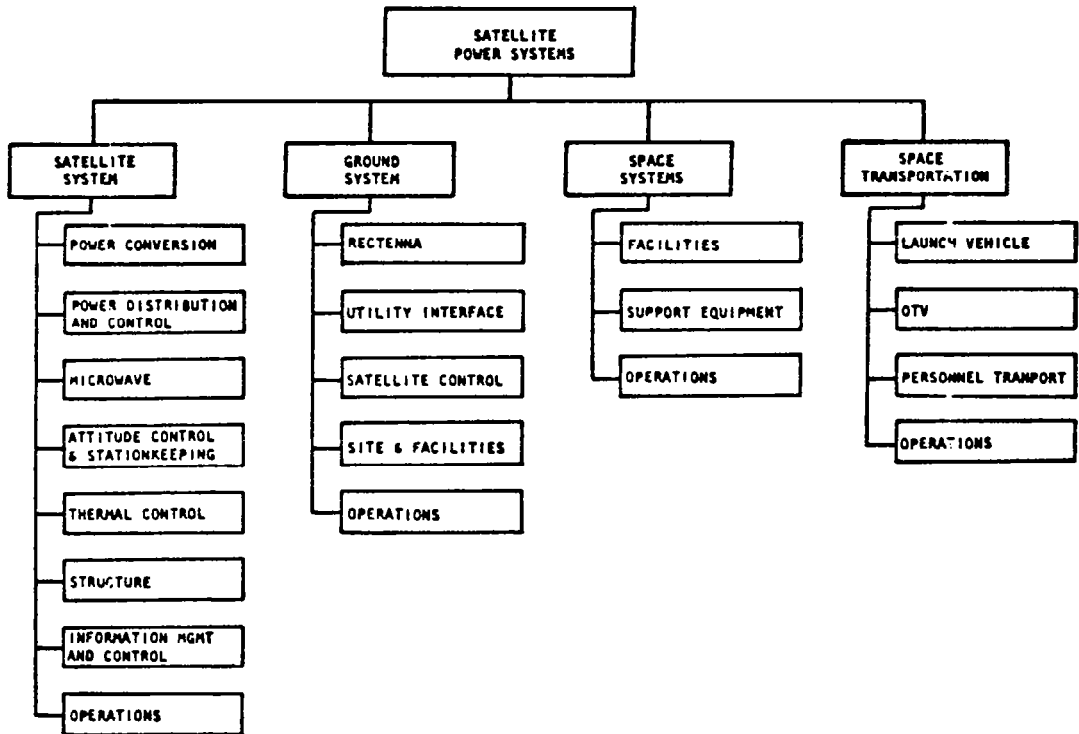
Figure 3.1-1. *SPS System Relationships*

3.2 SYSTEM DESCRIPTION

3.2.1 GENERAL

Figure 3.2-1 establishes the relationship of the Satellite Power System (SPS) program elements. Discussion in the following paragraphs is limited to a description of the satellite and the associated ground receiving station.

The satellite may be considered to be made up of a nonrotating section, (associated with the conversion of solar energy to electrical energy), and a rotating section, (concerned with the conversion of electrical energy into its RF equivalent and the transmission of the RF to the associated ground receiver). The ground receiving station is treated as a single unit.

The point design photovoltaic concept is shown in Figure 3.2-1 and was designed to supply 4.61 GW of electrical power to the utility grid on the ground. The SPS is a three trough configuration having reflective membranes at a 60° slant angle. It has a single microwave antenna, located in the center or at the end of the configuration. The overall dimensions of the SPS troughs are approximately:

- Length − 16 km
- Width − 3.9 km
- Depth − 0.564 km.
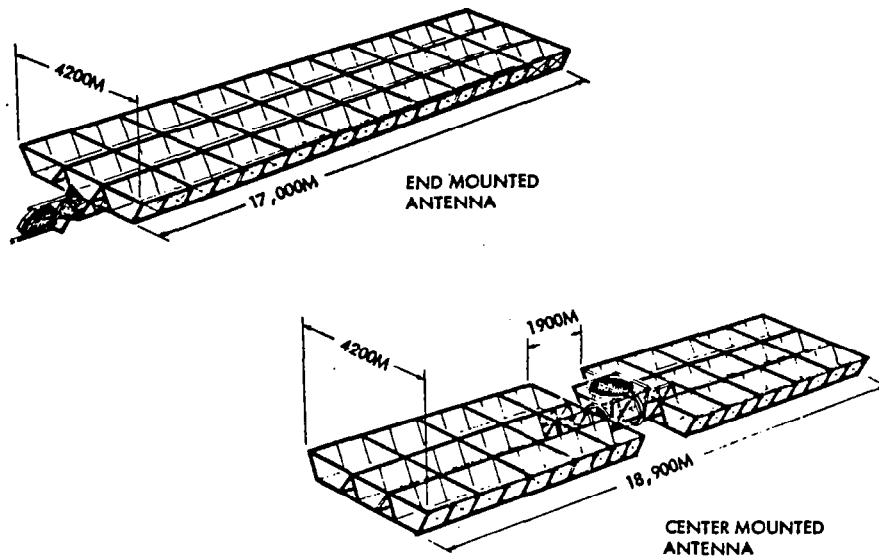
Figure 3.2-1. 5 GW Photovoltaic (CR-2)

The mass is estimated to be 30-33×10^6 kg and includes a 25% growth factor. In geosynchronous orbit the longitudinal axis of the SPS is oriented perpendicular to the orbital plane. The SPS design is based on construction in GEO.

Functional requirements for the photovoltaic SPS are summarized in Table 3.2-1. Primary operational requirements are summarized in Table 3.2-2.

Figure 3.2-2 presents the basic efficiency of the overall SPS and indicates the relative efficiencies of each of the major sub-elements of the system. Overall efficiency of the system is shown to be approximately 6.29%.

3.2.2 SATELLITE

The satellite is comprised of seven major subsystems (Figure 3.2-3). Attitude control directly affects power generation efficiency and includes satellite-rectenna pointing. Power generation, distribution and transmission are dominant mission functions, while thermal control is essential to dissipation of the large amounts of waste heat. Coordination of satellite operations is performed by the Information Management and Control Subsystem (IMCS) as shown in Figure 3.2-4.

All subsystems support the mission functions of power generation, distribution and transmission. Electrical power output from the solar panels is fed via switch gears into feeder buses and then into main distribution busses to the antenna (Figures 3.2-5 and 3.2-6). Power is also distributed to batteries so that critical functions, such as IMCS and thermal support, can be provided through solar eclipses.

The microwave power transmission subsystem (MPTS) (Figure 3.2-7) consists of dc-to-microwave conversion devices which feed an array antenna. Phasing control is maintained by use of a pilot beam originating at the rectenna and received at the satellite antenna.

3-3

*Table 3.2-1. Point Design Solar Array
Functional Requirements*

PROGRAMMATIC

ENERGY SOURCE	SOLAR
CAPACITY	5 GW DELIVERED TO UTILITY NETWORKS
LIFETIME	30 YEARS WITH MINIMUM PLANNED MAINTENANCE (SHOULD BE CAPABLE OF EXTENDED LIFE BEYOND 30 YEARS WITH REPLACEMENT)
IOC DATE	1998
OPERATIONS	GEOSYNCH ORBIT; 0-DEG INCLIN, CIRCULAR (35,786 km ALTITUDE)
RESOURCES	MINIMUM USE OF CRITICAL RESOURCES
COMMERCIALIZATION	COMPATIBLE WITH U.S. UTILITY NETWORKS
DEVELOPMENT	EVOLUTIONARY WITH PROVISIONS FOR INCORPORATING LATER TECHNOLOGY

TECHNOLOGY

OUTPUT POWER	POWER LEVEL IS DEFINED AS CONSTANT POWER LEVEL (EXCEPT DURING SOLAR ECLIPSE
WEIGHT GROWTH	25 %
ENERGY STORAGE	TO SUPPORT ON-BOARD SATELLITE SYSTEM OPERATIONS ONLY
FAILURE CRITERIA	NO SINGLE POINT FAILURE MAY CAUSE TOTAL LOSS OF SPS FUNCTION
ENERGY PAYBACK	LESS THAN 3 YR
COST	COMPETITIVE WITH GRND-BASED PWR GENERATION WITHIN LIFETIME OF SPS PROJECT
STORAGE	ONE YEAR ON BOARD WITHOUT RESUPPLY

*Table 3.2-2. Point Design Solar Array
Functional Requirements - Operations*

MODE	ASSEMBLY	FUNCTIONS
CONSTRUCTION	SUBSYSTEM	NONE
INTER-ORBIT TRANSFER	SUBSYSTEM	NONE
OPERATIONS	SUBSYSTEM REFLECTOR	STEADY-STATE OPERATION SIZED FOR EOL POWER RATING
ECLIPSE	SUBSYSTEM BATTERIES	SHUT DOWN BEFORE ENTERING ECLIPSE STANDBY (ZERO POWER) TURN ON AFTER LEAVING ECLIPSE & ARRAYS REACH EQUILIBRIUM TEMPERATURE SUPPLY POWER FOR ESSENTIAL FUNCTIONS
FAILURE/ MAINTENANCE	SUBSYSTEM PWR MODULE*	REDUNDANT OPERATION, AUTO SHUTDOWN, MANUAL STARTUP SHUT DOWN & ISOLATE FAILED MODULE; REPLACE SOLAR CELL BLANKET AND/OR REFLECTOR
CHECKOUT	SUBSYSTEM	FAIL-SAFE CHECKS; CONTROL RESPONSE

*SOLAR CELL/BLANKET/REFLECTOR MODULE

Figure 3.2-2. Solar Photovoltaic (CR-2) Efficiency Chain

$\eta_{SG} = .999^{14} = .986$

NOTE $.995^{14} = .932$

*POWER GEN. X POWER DIST. X MW ANT. X GROUND

(13.35%)   (93.81%)   (76.08%)   (67.91%)

6.47%
(5.6% BASED ON TOTAL INTERCEPTED AREA)
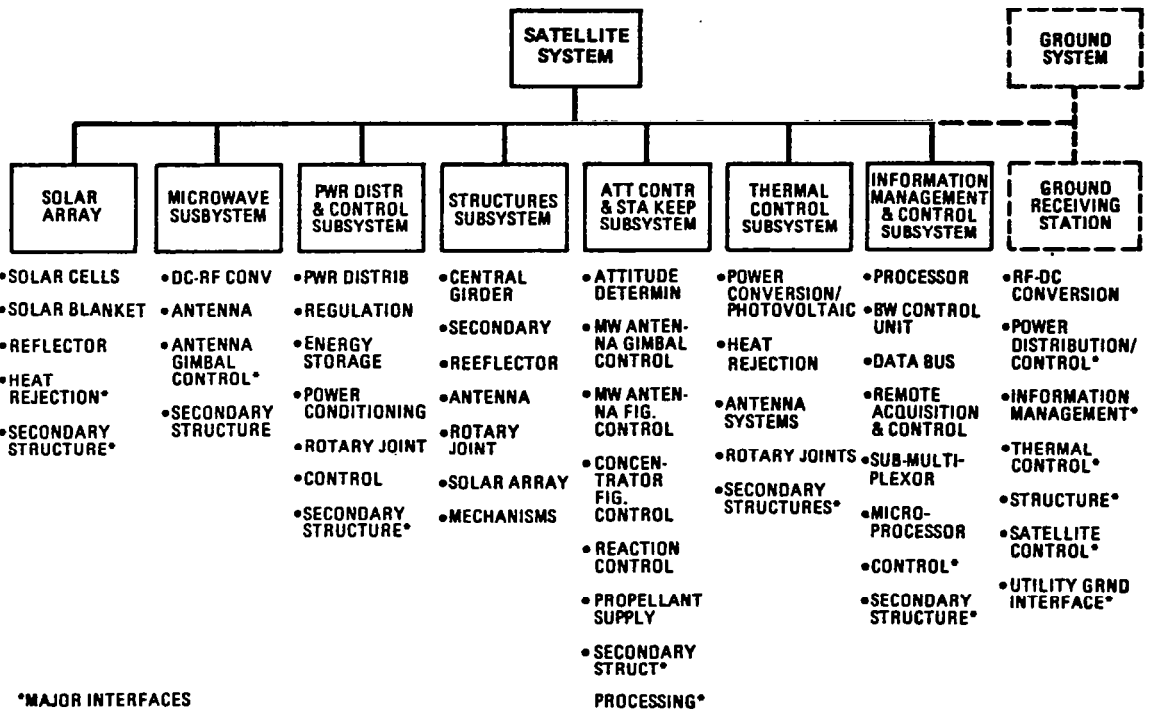
Figure 3.2-3.   Satellite Subsystems
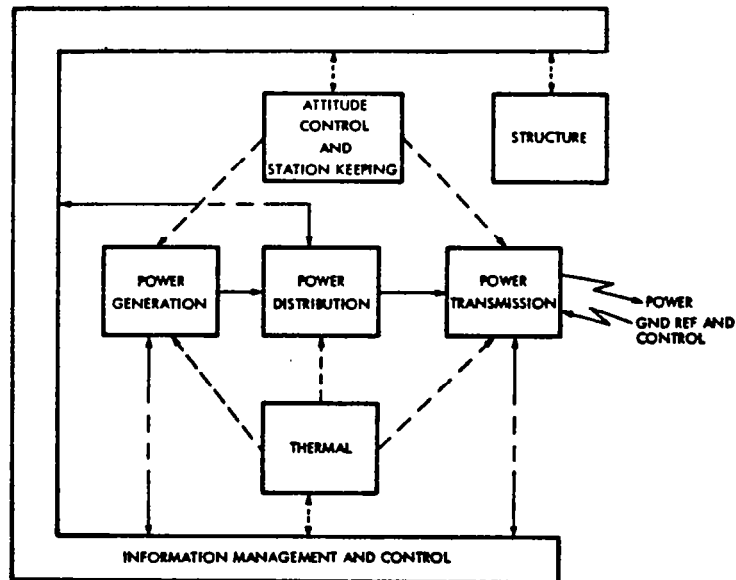
Figure 3.2-4.   Subsystem IMCS Relationships

3-6
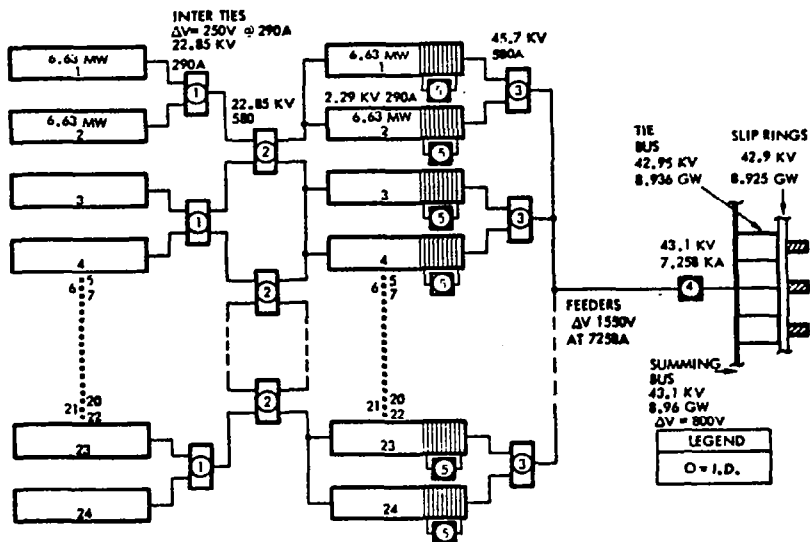
Figure 3.2-5. Power Generation Subsystem
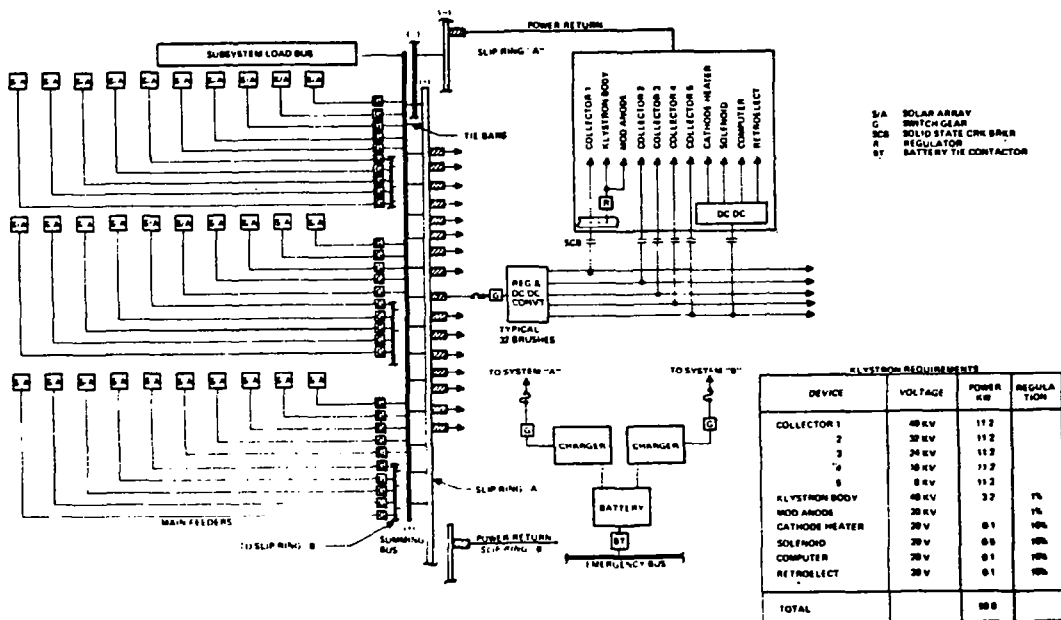
Figure 3.2-6. Power Distribution Subsystem

3-7
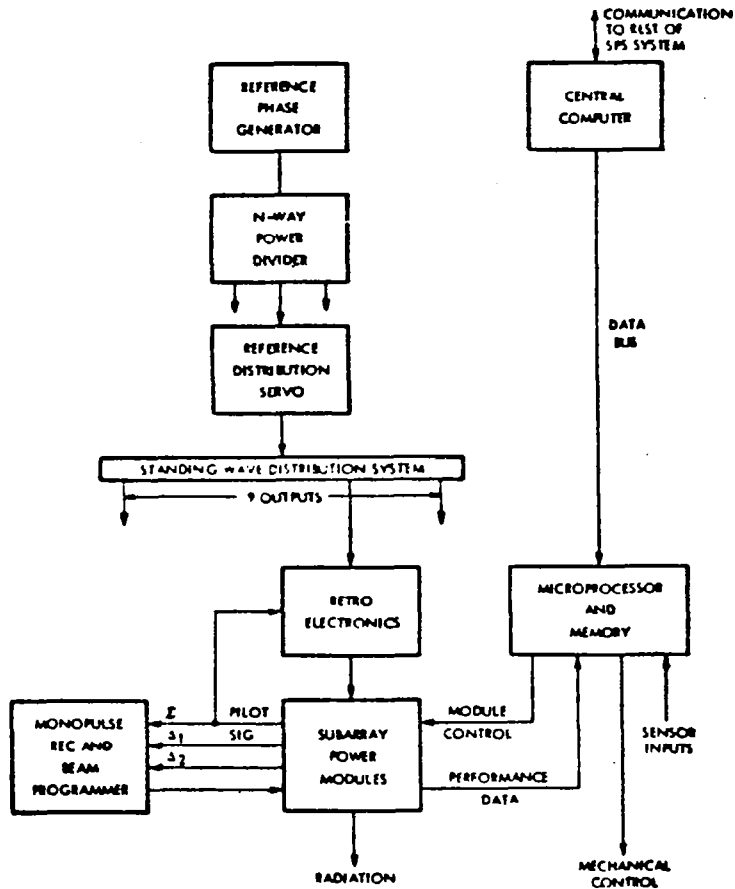
Figure 3.2-7. Microwave Transmission Subsystem

Microwave control and solar eclipses are two major areas of consideration because they are critical to SPS operations. Beam control is initiated from the rectenna through the pilot beam, which is used in a conjugation scheme to provide phase control signals for fine pointing.

Another factor which must be considered when evaluating operational requirements are the solar eclipses which occur during the spring and autumn and last for up to 1.2 hours. Figure 3.2-8 shows the expected ecliptic periods and their duration as a function of the calendar year. For rectenna sites in the northern hemisphere the eclipses will be centered about midnight.

A reasonable way to view the satellite system is to consider the entire satellite as being made up of two major on-orbit assemblies operating in concert at GEO. These on-orbit assemblies are the non-rotating, sun oriented solar arrays; and the rotating, Earth oriented power antenna.
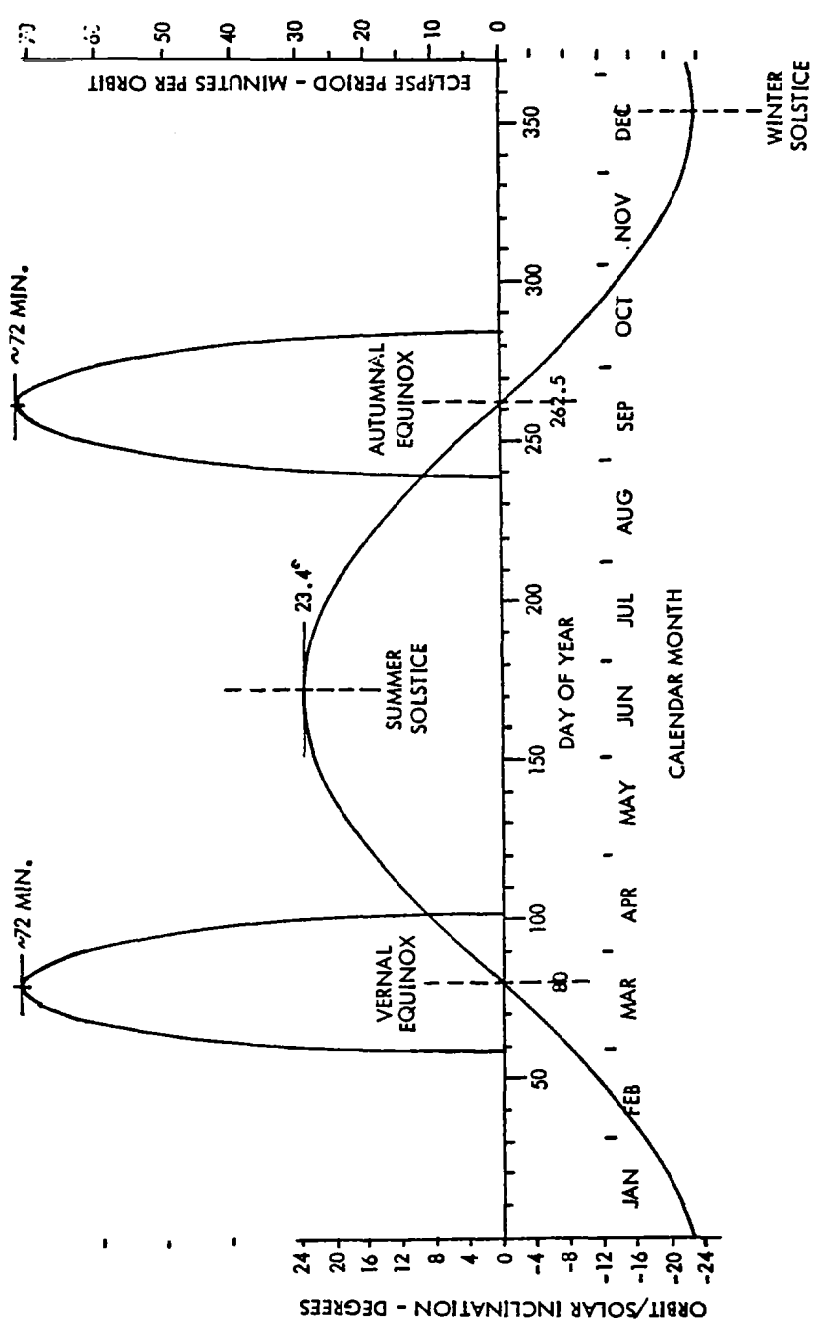
Figure 3.2-8. Eclipse Periods for Geosynchronous Circular Orbits

3-9

Non-Rotating (Solar Array)

The non-rotating subelement of the SPS satellite consists of the GaAlAs solar cells and the supporting subsystems required to operate the satellite in a sun oriented mode. Included in this subelement are Information Management and Control subsystem assemblies required to monitor and control the power generation devices; the power distribution network as well as all remaining subsystem functions. Figure 3.2-9 shows the basic energy flow path for one of the 1600×600-m electrical bays. The full satellite has 30 bays.

Rotating (Antenna)

The rotating subelement consists of the antenna primary and secondary structure, the microwave conversion and transmission assemblies and the elements of the various supporting subsystems required to operate the microwave transmission system. Figure 3.2-10 is a representation of the power distribution network on the antenna.

3.2.3 GROUND RECEIVING STATION

A major element in the SPS is the ground receiving station (GRS). This power receiver consists of a set of receiving antennas whose output is rectified, filtered and added to a summing network to form the system power output. The GRS is shown in Figure 3.2-11. The receiving antenna dipoles are constructed in striplines on dielectric material and assembled into panels tilted so as to be normal to the power beam from the satellite. Since the satellite is in synchronous orbit, it will be considered to be at a fixed location in space.

A large power collection grid subsequently gathers the power from all the panels and routes the collected power to large power conversion stations. The output of the conversion stations is then interconnected with one or more utility grids for consumer use.

3.2.4 OPERATIONS

Introduction

This section presents the considerations for a preliminary end-to-end operations scenario for a SPS system consisting of a single satellite and a single GRS. Where appropriate, requirements are identified for automated operations and for predicting and managing power outages.

Purpose

The purpose of this initial discussion is to outline startup and nominal functional operations for the satellite. This discussion is structured to develop a basic functional flow which can be expanded to cover the entire system, i.e., the space and ground elements, as the design evolves during the study.

Figure 3.2-9. Power Distribution – Nonrotating (Preliminary)
Typical Bay

KLYSTRON REQUIREMENTS			
DEVICE	VOLTAGE	POWER KW	REGULA- TION
COLLECTOR 1	40 KV	11.2	
2	32 KV	11.2	
3	24 KV	11.2	
4	16 KV	11.2	
5	8 KV	11.2	
KLYSTRON BODY	40 KV	3.2	1%
MOD ANODE	20 KV		1%
CATHODE HEATER	20 V	0.1	10%
SOLENOID	20 V	0.5	10%
COMPUTER	20 V	0.1	10%
RETROELECT	20 V	0.1	10%
TOTAL		50.0	

SA SOLAR ARRAY
G   SWITCH GEAR
SCB SOLID STATE CKR BRKR.
R   REGULATOR
BT BATTERY TIE CONTACTOR

3-11
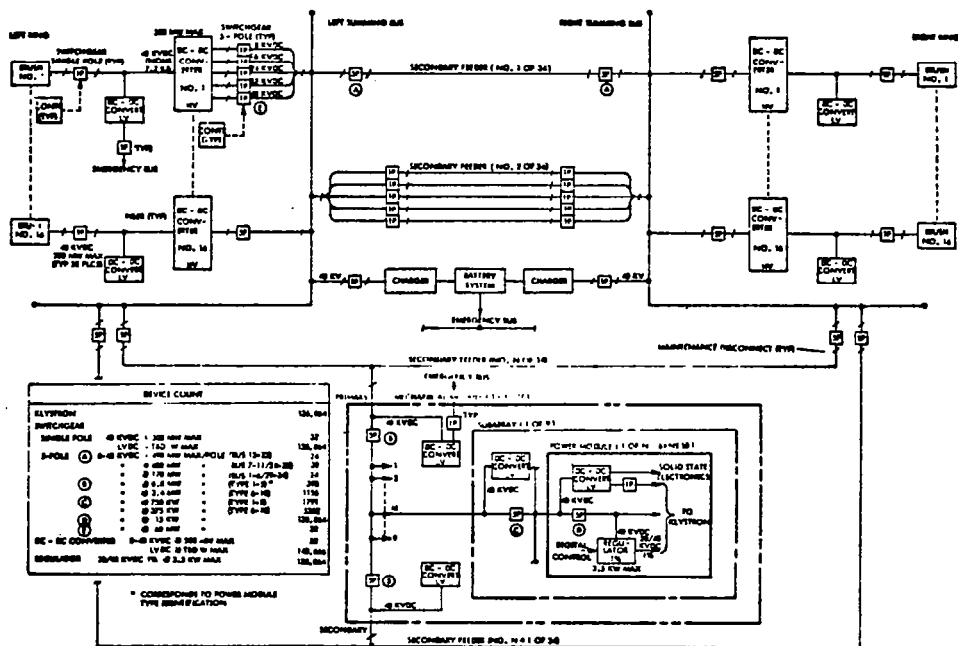
Figure 3.2-10. Power Distribution - Microwave Antenna
(Preliminary)
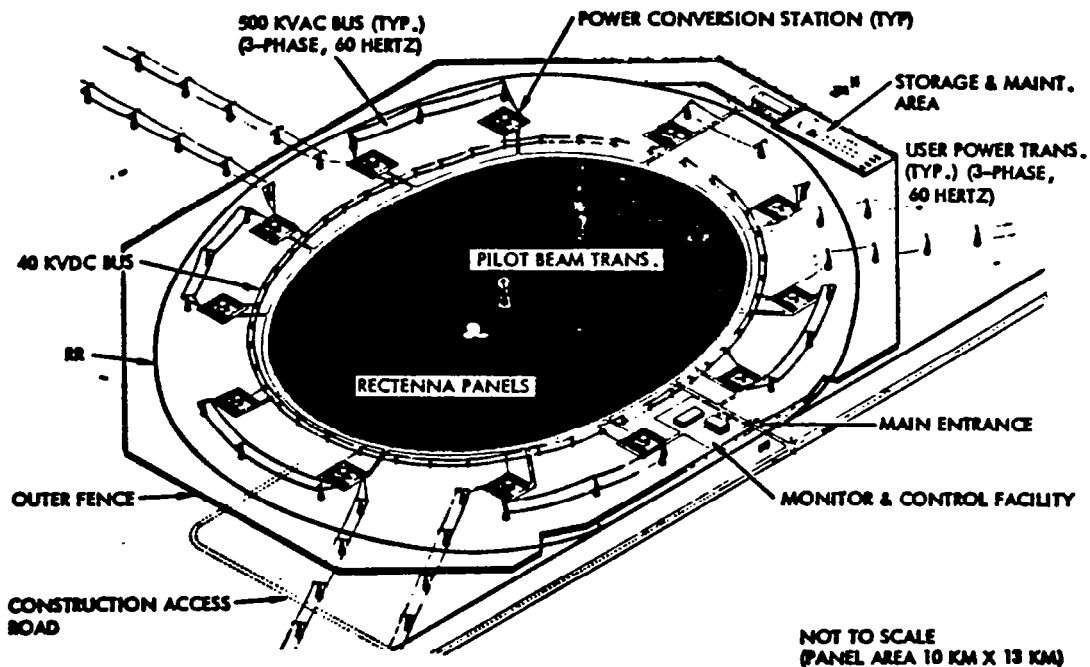
Figure 3.2-11. Rectenna Installation

3-12

Scope

This initial functional report covers only the satellite and its interfaces with the rectenna or its local control center. The scope is limited to identification and outlining of major operations areas for later verification and expansion. Ground-based functions, including the regional control center, are to be included in subsequent efforts.

Satellite functional descriptions are constrained to startup and nominal operations because of the limited time and resources available, and because these are fundamental operations areas affecting system feasibility and understanding.

Approach

Satellite control is functionally discussed from two perspectives: 1) nominal satellite and antenna control, and 2) startup and shutdown operations. These are then considered in a logical time/subsystem ordered sequence to facilitate development of a comprehensive operations scenario.

Operations Scenario

The operations begin with preliminary preparations for power generation and traces the power flow, enabling commands and system controls across the satellite-GRS/control center interfaces. The satellite is assumed to have been assembled and to have completed basic individual subsystems checkout. At this point it is expected to be ready for startup operations during which each subsystem is brought on line and integrated with other elements in logical order.

Start-Up. Start-up operations are divided between the satellite and its antenna.

Satellite Operations. Five major areas of satellite operations have been identified as follows:

- Status checking of all system components

- Attitude control to enable solar power conversion

- Power generation by the solar blankets

- Power distribution to the antenna rotary joint

- Voltage regulation to account for losses and aging

Status. Prior to start-up, all satellite subsystems must be checked for ready status. These include structure, attitude control, solar blankets, power distribution, thermal control and the information management and control system. A status check command or request would be expected to be received from the GRS control center indicating that the ground systems are ready for operations and that status of the satellite must now be checked. If the satellite is manned, this request might be a simple voice communications or a digital message displayed on a screen.

The IMCS is a central element in the checkout of all satellite subsystems. It is assumed to already be in an "on" status since it is required at all times for satellite operations, such as attitude control. However, it may be in a standby mode with only essential support functions operative. Control support to power generation, distribution, and microwave transmission may be in an "off" or standby status. Whatever the existing IMCS configuration and operational condition, the IMCS must be checked out. IMCS operative portions are placed into automatic sequencing checks and non-operating portions are brought on line and similarly status checked.

After IMCS checkout is complete, measurements data are accepted from the attitude control, structural, thermal, solar blanket and power distribution subsystems, and verified. These include temperatures, positions, pressures, voltages, etc. Next, limited control actions are issued to the various subsystems to check control loops and operating modes. Even though measurements and controls, as compared to the antenna, are relatively limited on the satellite, they still represent a hundred thousand or more data points which are sampled a number of times. Similarly over ten thousand control points are exercised. Such checkout sequences will be automatically implemented with human monitoring of test results on board the satellite in its master control center and/or on the ground in the rectenna control center. The time duration of such status checks may well be established by subsystem stabilization time constants rather than the actual time to automatically sequence through the various functions.

Attitude Control. Once all systems are checked out, the satellite must, concurrently, be oriented to its solar inertial attitude for power generation. For example, it may have been allowed to drift several degrees in attitude during the time since completion of assembly and basic checkout. Such drift errors must be corrected prior to initiation of power generation. Since stationkeeping is included in this function, the geographic location of the satellite centroid must be verified in relation to the rectenna location. Any undesirable drift must be eliminated and the satellite's longitude location refined.

The physical pointing angle of the microwave antenna is also controlled by this subsystem. Once the satellite achieves its proper solar orientation and longitude location with residual drift errors eliminated, the antenna gimbal drives are controlled to bring the antenna within boresight of the rectenna. This is likely to be a process that will take a significant period of time because of the large masses involved. Both support from the GRS site to assist boresighting, and power support from the solar blankets to the gimbal drives will be required.

Solar Blankets. The solar blankets are brought on line by closing switch gears between pairs of adjacent bay segments, each of which are 25×750-m and provide 276 amps nominal at 22.8 kV. Each bay has 24 segments. Two segments are connected to the first switch gear so that either one can be connected to corresponding segment pairs in the second panel, thus providing flexibility for current control and panel outages. Paired segments from the first panel nominally provide 552 amps to the 2nd bay panels which are then connected in series by a second set of switch gear to achieve the required voltage level of

45.7 kV. Bay segment pairs are sequentially brought on line from all 30 bays of the satellite until the power demands are met.

Power Distribution. Bay bus switch gears isolate each bay segment pair from the bay buses. As each bay panel pair is connected, it is tied to the main buses through closure of the related switch gear. During this connection process, bus temperatures and current measurements must be monitored to detect any shorts throughout the vast bus runs of the satellite so that controlled emergency disconnects can occur under IMCS or local breaker control to avoid catastrophic effects. Nominally, 208,000 amps at 42.9 kV are fed into the two antenna slip rings for transmission to Earth. During the startup sequence (as well as during nominal operations) it will be necessary to monitor ground power flows because of their possible influence on satellite procedures.

Voltage Regulation. Voltage regulation is obtained by selectively shorting module segments within the 2nd (series) panel. During the solar blanket connection process, voltage levels of each bay segment pair are monitored continuously to assure proper matching between outputs and the main antenna summing bus.

<u>Antenna</u>. Antenna startup operations are divided into status checking, power distribution, power storage, pointing initialization, thermal stabilization, acquisition of the rectenna and fine pointing including focus.

Status. The electronic and pointing status of the microwave antenna must be verified prior to power distribution for space-ground transmission. For example, the previously verified boresight of the antenna to the rectenna may have drifted so that updating may be required. This type of boresight support, from the GRS control center, may be required on a continuous basis.

Concurrently with boresight verification, the power distribution, thermal and phase control electronics must be checked. The switch gears on the antenna must be verified for proper positioning and functioning. The ability of the thermal control system to provide both heating and cooling is confirmed. Finally the phase control electronics are activated to ensure that all components are properly functioning. The reference phase generator is energized and the reference distribution servos are exercised to confirm that they are operating properly. Retro electronics are activated so that the pilot beams from the GRS can be received and processed through the monopulse receiver subsystem. The beam programmers are also checked through use of built-in test procedures.

Power Distribution. If the satellite is experiencing a solar eclipse, internal battery power is utilized to energize the satellite emergency distribution buses. The main power module switch gears are opened while switches at the subarray, mechanical module and bus levels may be left closed to provide power to antenna electronics for checkout and thermal stabilization.

If the satellite is leaving an eclipse, antenna electronic phase control must be reactivated and power fed to the klystrons for transmission to Earth. The satellite's power distribution system is reenergized and stabilized; the antenna ring brush switch gears are closed, allowing power to be distributed

to the 32 dc-dc central converters. These provide the 59 kW to each klystron collector at 5 voltage levels. Five-pole switch gears are then closed allowing the power to enter the primary and secondary feeders, where additional sets of 5-pole switches determine whether 1 or both secondary feeders may be activated (redundantly). In the same manner, the 5-pole switch gears at the mechanical and power module levels are sequentially closed until power flows through the klystrons and is transmitted to Earth.

Power Storage. Prior to the satellite entering an eclipse, the batteries are checked and brought up to full storage capacity to ensure IMCS, thermal, attitude control, communications, and other vital functions when photovoltaic power is lost. Closed loop control of the charging process is maintained through the IMCS until the batteries are fully charged.

When the satellite enters the eclipse, the photovoltaic supply buses are shut down and the emergency buses provide subsystem power. Prior to this time, the klystron power modules are switched off. Non-essential subsystems are shut down or placed in a standby mode to preserve power during the up to 1.2 hours eclipse time. GRS control center support is used to update orbit predictions for eclipses and generally support scheduling of satellite operations prior to predictable power outages.

Initialization. Initialization of antenna operations begins with activation of the reference frequency module and computation of coarse phase angles by the beam programmers, which command the digital diode phase shifters. Pilot signals are fed through the retro electronics to initiate the phase conjugation process. Cathode heater power is applied during initial startup to bring the klystrons up to a stabilized temperature for accurate phase control. This heater power is maintained through all eclipses and other scheduled standby situations.

Under IMCS control, the amount of power fed to the klystron is increased while monitoring phase and pointing stability. All scheduled klystrons are brought on line simultaneously with this gradual process to first establish pointing and then the required power levels. Klystron operation is carefully monitored and local arc detection circuits/circuit breakers disconnect any power module which malfunctions.

Thermal Stabilization. Thermal stabilization of klystron cathode temperatures is extremely important to accurate phase control and fine pointing. Phase control and fine pointing are achieved using pilot beam and reference phase comparisons through the monopulse bridge and monopulse receiver. Phase error signals are provided to the beam programmer for correcting the coarse phase angle which was computed at startup. The klystron output phase is also fed back into a phase bridge. Thus, individual klystron manufacturing irregularities and aging differences are automatically accounted for.

During eclipses when excessive cooling could occur, the battery storage subsystem provides cathode heating capability to prepare the system for restart as the satellite emerges from the eclipse.

Conversely; antenna array temperatures on the back side where control electronics are mounted must remain less than 100°C. The IMCS continuously monitors component temperatures and adjusts power levels or heater input power (if required) to maintain required temperatures consistent with the passive heat pipe cooling system used on the antenna.

Phasing. Once the MPTS acquires the rectenna by locking on to the pilot signals, the antenna must also be phased (focused) so that all down-linked power remains within the confines of the rectenna and is within given safe power levels. The beam programmer computes a phase gradient to be applied across each subarray. This, in turn, is locked to the reference phase which is generated at the reference subarray.

After lock-on to the rectenna is achieved, phase gradient corrections begin to achieve the required beam pattern. Signal strength is also monitored at the GRS and transmitted to the satellite to provide independent confirmation of beam location and focus.

Nominal Operations. At this point, the satellite has reached stabilized power production and transmission of that power to the GRS. Power demands are constantly monitored at the GRS and transmitted to the satellite so that system surges can be mitigated and scheduled maintenance can be planned. For example, as midnight is reached at the users' locations, power demands reduce. Solar blankets, antenna components or other related power production elements may be removed from the line for replacement or repair on a progressive basis to avoid future unscheduled shutdowns.

Satellite and GRS status are constantly monitored so that any unscheduled power production or distribution changes can be accommodated. Constant communications, voice, data, and commands, are required between the satellite and the GRS control center to achieve effective coordination.

Progressive maintenance inspections are performed on the satellite to insure reliable operation. The IMCS is constantly monitoring the status of components. As out-of-tolerance conditions are noted, the affected element is scheduled for repair or replacement before failure. As a statistical basis is developed for predicting problem conditions, inspections and replacements are pre-scheduled at convenient times before the problem occurs. The GRS control center is expected to provide some support through logistical scheduling and data base maintenance.

Scheduled outages occur during solar eclipses. These time periods can be utilized for minor repairs and replacements. Prior to each eclipse, coordinated planning occurs between the satellite and GRS control center crews to develop a master maintenance schedule. Since an eclipse may last for a maximum of 1.2 hours, careful planning is needed to capitalize on this time for component replacements. Once replacement parts are installed and safe conditions are verified, selective activation of the affected subsystems is implemented to check out replaced parts in preparation for startup subsequent to the eclipse.

Communications

While communications have not been specifically studied in this preliminary analysis, a number of implications have been drawn. The satellite must maintain continuous contact with the GRS control center. This includes voice, data, video, and commands in both directions. In addition, the dual uplink pilot beams from the GRS are crucial to acquisition and fine pointing (within 0.02 degrees). The high EMI environment in the near vicinity of the satellite imposes difficult conditions for communications. This requires primary emphasis and special design considerations.

Intra-satellite communications are highly dependent upon optical data buses to avoid the EMI problem.

Space-ground communications may have to be encrypted to avoid command intrusions and interference. Data compression may be required if data traffic becomes too heavy due to large data base updates, significant amounts of video traffic, or excessive interference.

3.2.5 MASS PROPERTIES

A detailed mass property summary is shown in Table 3.2-3.

Table 3.2-3. Satellite Mass Properties

SUBSYSTEM	WEIGHT (MILLIONS KG)	
	CENTER MOUNT	END MOUNT
COLLECTOR ARRAY		
STRUCTURES AND MECHANISMS	1.122	1.260
POWER SOURCE	7.855	7.855
POWER DISTRIBUTION AND CONTROL	0.882	2.603
ATTITUDE CONTROL	0.116	0.116
INFORMATION MANAGEMENT AND CONTROL	0.050	0.050
TOTAL ARRAY (DRY)	10.025	11.884
ANTENNA SECTION		
STRUCTURE AND MECHANISMS	0.977	0.977
THERMAL CONTROL	1.408	1.408
MICROWAVE POWER	7.012	7.012
POWER DISTRIBUTION AND CONTROL	4.505	4.505
INFORMATION MANAGEMENT AND CONTROL	0.630	0.630
TOTAL ANTENNA SECTION (DRY)	14.532	14.532
TOTAL SPS DRY WEIGHT	24.557	26.416
GROWTH (25%)	6.137	6.604
TOTAL SPS DRY WEIGHT WITH GROWTH	30.694	33.020

3.3 SUBSYSTEMS

3.3.1 SATELLITE

This section presents in some detail the selected subsystem concepts and characteristics of the various major satellite subsystems. The detailed subsystems are: 1) power generation; 2) power distribution and control; 3) microwave antenna; 4) information management and control; 5) attitude control and stationkeeping; 6) structures; and 7) thermal control.

Additional functional areas such as communications, safety, security, etc., have not been defined as of this time, and therefore although they are considered of major importance, are not included.

The relationships of the various subsystem elements onboard the satellite are shown in Figure 3.3-1.
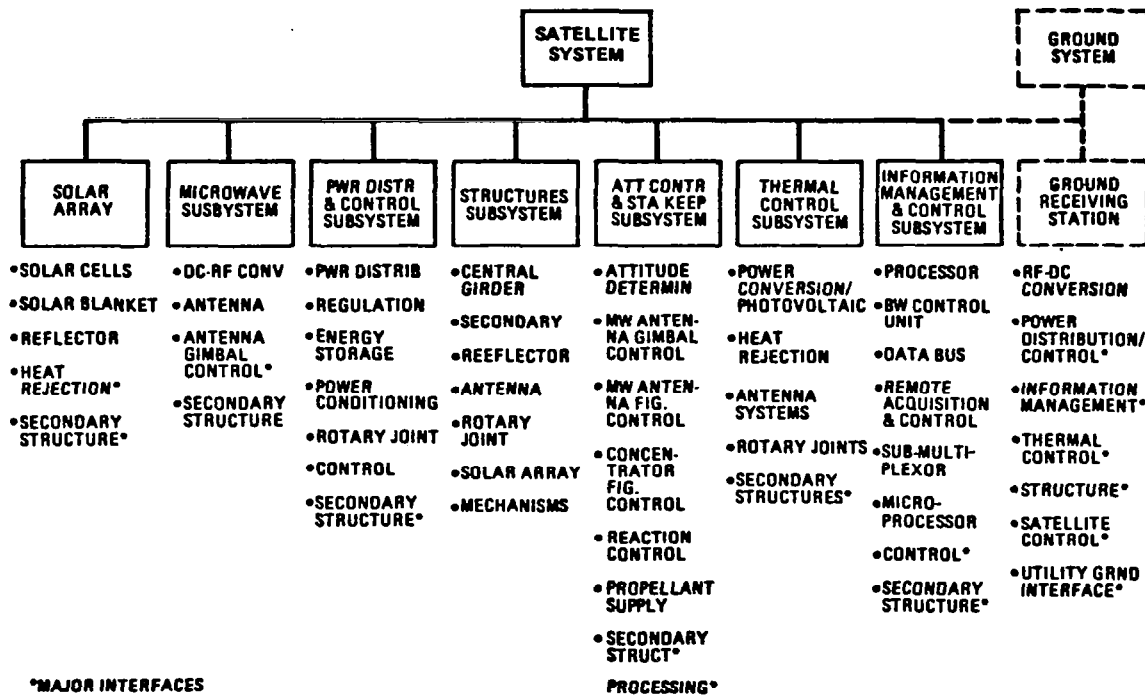
Figure 3.3-1. Total System

Power Generation

The solar photovoltaic power subsystem consists of the solar cells, blankets, attachment devices, and includes the reflector membranes and attachment devices. Gallium aluminum arsenide (GaAlAs) cells have been selected as the point design solar cell. The cell is fastened to a thin-film Kapton substrate with an FEP adhesive. The photovoltaic power conversion subsystem is designed for a geometric concentration ratio of 2.

The functional requirements for the photovoltaic power subsystems were listed in Tables 3.2-1 and 3.2-2. The system efficiency block diagram was shown in Figure 3.2-2. Shown in the figure are power levels, efficiencies, temperatures, degradation factors and solar cell area requirements. A simplified integrated block diagram for the CR-2 point design concept is presented in Figure 3.3-2. The major assemblies and components that are required for the photovoltaic subsystem are shown in Figure 3.3-3.
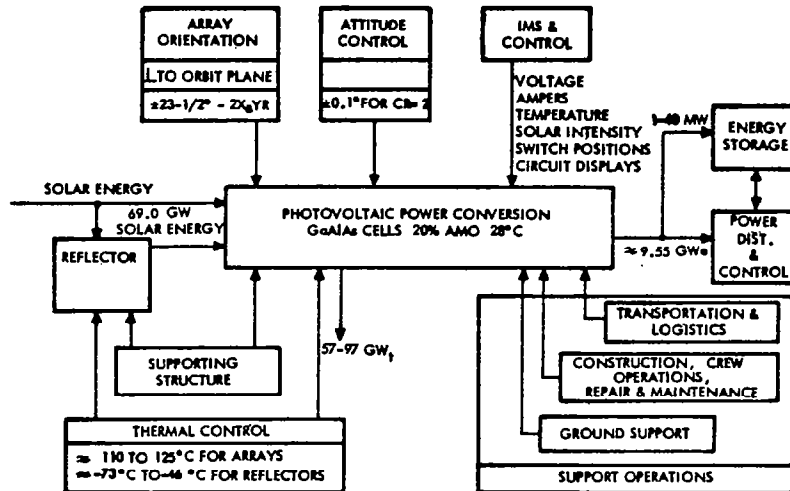
Figure 3.3-2. Simplified Integrated Block Diagram - Photovoltaic (CR-2)
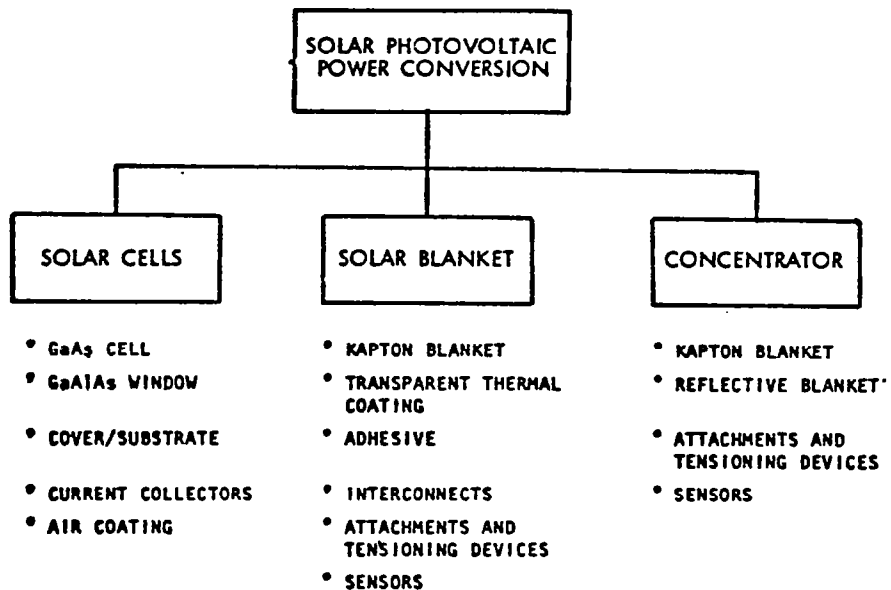
Figure 3.3-3. Assembly Tree - Power Generation

Solar Cells. The solar cell used in the SPS design is a GaAlAs cell having an efficiency of 18.2 percent at Air Mass Zero (AMO) and 113°C. The cell consists of the GaAlAs junction, GaAlAs window, cover/substrate, current

3-20

collectors, and an anti-reflection coating. The basic cell design is the inverted GaAs/sapphire design having a weight of 0.252 kg/m^2. The various cell designs that were investigated and the selected design are shown in Figure 3.3-4. The point design cell has a 20-μm sapphire substrate upon which is grown a 5-μm single crystal GaAs junction. A 500-Å GaAlAs window is then deposited on the 5-μm junction. The voltage and current characteristics of the cell as a function of operating temperature are shown in Figure 3.3-5.
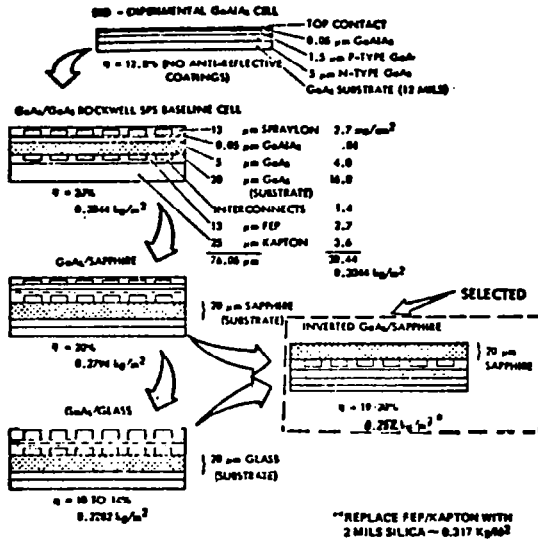
Figure 3.3-4. Solar Cell Design
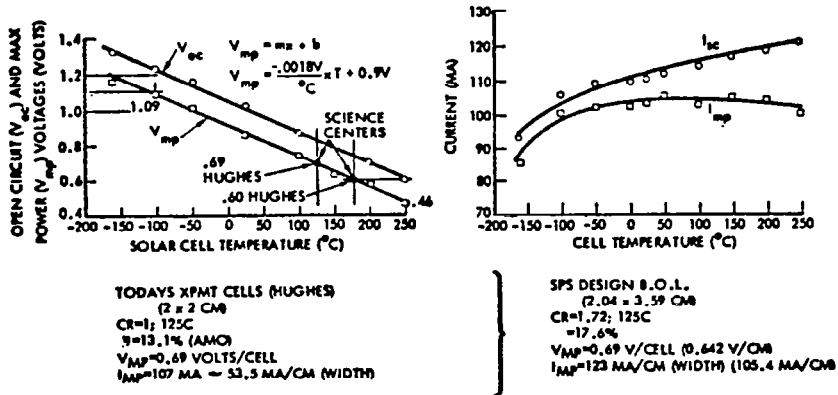
Figure 3.3-5. GaAlAs Solar Cell Voltage
and Current Characteristics

3-21

Solar Blanket. The solar blanket consists of a 25-μm Kapton membrane up-
on which the cells are fastened with a thermosetting FEP adhesive. Also includ-
ed in the blanket are the interconnects, transparent thermal coating required
for thermal control, attachments, tensioning devices, and sensors. The solar
cell blankets will be manufactured in blanket form and the solar cells attached.
This assembly will then be rolled up on a drum type canister. It is postulated
that the blankets will be 25 m wide by approximately 750 m in length. The can-
isters are then transported to orbit where the blankets are deployed via a roll-
out deployment-type operation.

The solar blanket layout for the GaAlAs point design configuration is
shown in Figure 3.3-6 and 3.3-7. The solar panel in each trough (effective
cell area) measures 600×750-m × 2 for 900,000-m^2. Twenty-four panels are re-
quired for the troughs. The total deployed solar area for the SPS is 27×10^6 m^2.
The basic building block is a 1 m^2 module configuration and the cells are con-
nected together in a series parallel arrangement. The module output is calcul-
ated to be 352.6 W/m^2 at the end of life. The cell characteristics and cell
design used to form a submodule for the solar blanket is shown in Figure 3.3-6,
the cell arrangement is illustrated in Figure 3.3-7.

SOLAR ARRAY DESIGN FACTORS	
SOLAR INPUT	1319.5 WATTS/M^2
ENERGY ONTO CELL (CR=1.83)	2414.7
OPS TEMP	113C
η(T)	438.5
DESIGN FACTOR (.89)	390.27
SEASONAL FACTOR (.968)	377.78
DEGRAD FACTOR (.96)	362.67
SG FACTOR(.997)	361.58
MARGIN(.975)	352.6

SOLAR ARRAY POWER OUTPUT = 352.6 W/M^2 X 27.0 (10^6) M^2
= 9.52 GW
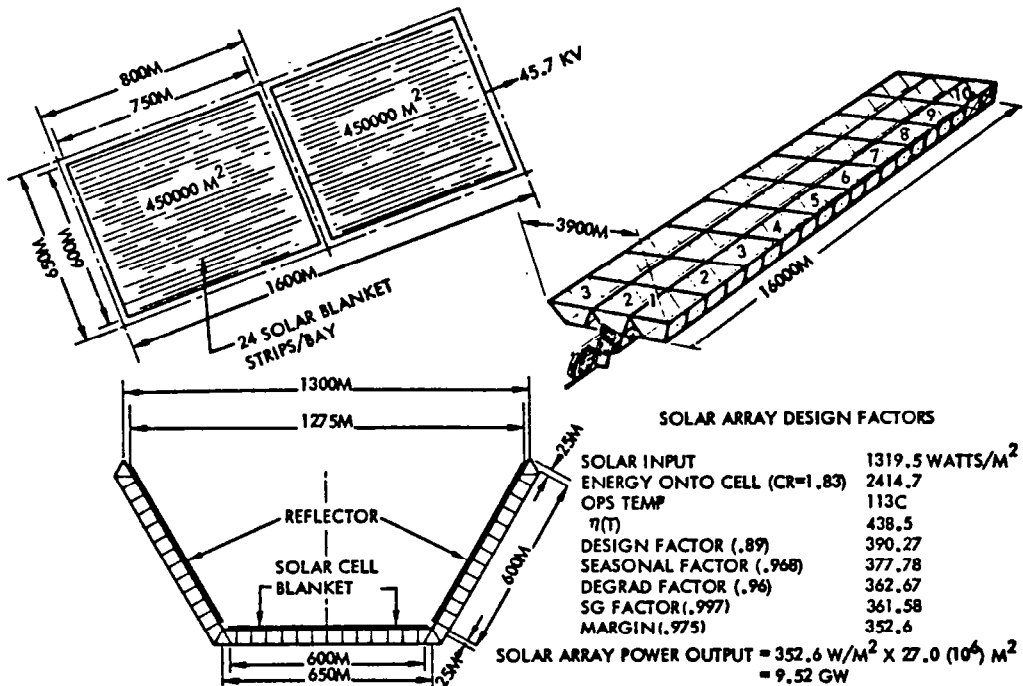
Figure 3.3-6. Solar Panel Power Output

Reflectors. Thin reflector membranes are used on the SPS to reflect the
sun onto the solar cell surfaces and obtain a nominal concentration ratio of
2. The reflector is made of 12.5 μm (0.5 mil) aluminized Kapton. Reflectivity
of the reflector was taken at 0.87 BOL and 0.83 EOL. The reflector membrane
has a mass of 0.018 kg/m^2. The reflective membranes are mounted on the struc-
ture using attachments and tensioning devices. Tensioning based on structural
limit of the existing beam design (with safety factor of 1.5) indicates that
tensioning of up to 75 psi can be used.
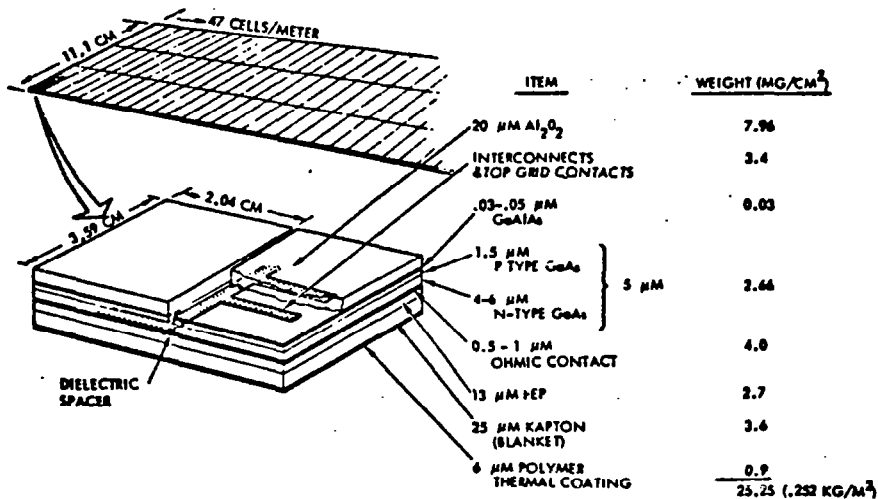
Figure 3.3-7. GaAlAs Solar Cell Blanket Cross Section

ITEM	WEIGHT (MG/CM²)
20 μM Al₂O₂	7.96
INTERCONNECTS & TOP GRID CONTACTS	3.4
.03-.05 μM GaAlAs	0.03
1.5 μM P TYPE GaAs / 4-6 μM N-TYPE GaAs } 5 μM	2.44
0.5 - 1 μM OHMIC CONTACT	4.0
13 μM FEP	2.7
25 μM KAPTON (BLANKET)	3.6
6 μM POLYMER THERMAL COATING	0.9
	25.25 (.252 KG/M²)

Reflectivity values for coated metal reflectors and thin film membranes are illustrated in Table 3.3-1. The thin film membranes utilizing an Aℓ coating has the potential of low weight and cost with high reflectivity. The table indicates that an aluminized film of at least 200 Å is required for a reflectivity of 0.87. In the study, a 500 Å coating was used on the Kapton film. The radiation dose rates for a geosynchronous orbit are presented in Table 3.3-2. Long term and on-orbit testing is required to verify the actual reflectivity values to use for the design of the SPS reflectors. The Kapton film properties such as ultimate strength, coefficient of thermal expansion and dielectric strength as a function of temperature are shown in Figure 3.3-8.

Table 3.3-1. Reflectivity

SILVERED GLASS ~ 0.83
3M SCOTCHCAL 500 ~ 0.85 (ALUMINIZED ACRYLIC)
SHELDAHL ALUMINIZED TEFLON ~ [0.87][1] (B.O.L.)

THIRTY YEAR DEGRADATION FACTORS
    METEOROID FACTOR • 0.995
    THERMAL CYCLING • 0.990   (DUE TO EXPANSION/CONTRACTION INITIATED BY ECLIPSE PASSAGE)
    RADIATION RESISTANCE • 0.965   (ALLOWANCE)
    30 YEAR E.O.L. REFLECTIVITY • [0.87]

[1]REFERENCE: R. B. PETTIT
    NASA A77-49074

Table 3.3-2.   Radiation Dose Rates
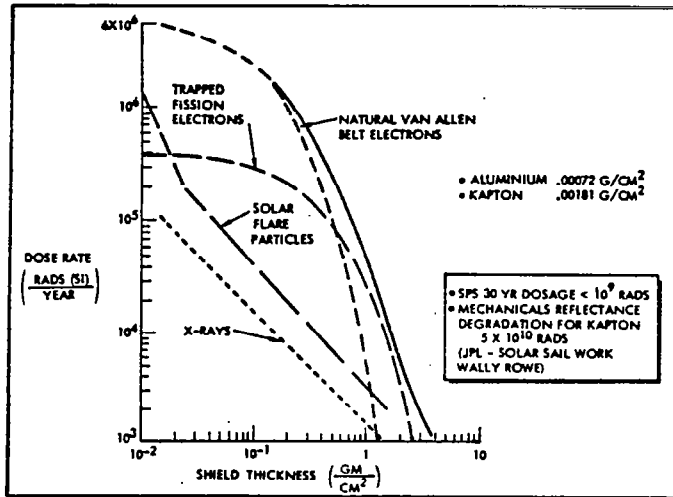
Results of analysis show weight savings with the utilization of concentrators. The selected design concept for the point design is the 60° Vee trough configuration. Weight, cost, on-orbit assembly and fabrication and design complexity were used in the selection of the 60° Vee point design configuration. Weight comparisons showed that penalties for ±1 degree misorientation in reflector oversizing at concentration ratios of 5 and penalties for 1000 psi tensioning are prohibitive. It appears that attitude control errors are controllable and that high membrane tensioning may not be a real requirement. Preliminary radiation tests indicate insignificant reflectivity degradation for aluminized thin film Kapton, e.g., MSFC tests at 10^{15} proton/cm^2 (2 MeV) and Rockwell tests at 10^{15} protons/cm (0.7 MeV). The point design solar array sizing model allows for 18% reflectivity degradation over 30 years which in view of some of the newer test data appears to be extremely conservative.

Subsystem Characteristics. The mass of the solar cells, solar blanket, and concentrator for the SPS are shown in Table 3.3-3. The mass of each component of the three major assemblies is defined. The total mass is 7.85×10^6 kg, (center mount) excluding the mass of the attachments and tensioning devices for the solar blanket and the concentrator, i.e., ~0.79×10^6 kg additional mass required for attachments and tension devices accounted for in secondary structure.

The GaAlAs solar cell arrays are designed to generate the electrical power for the SPS. The system is capable of delivering 5 GW of electrical power to the utility user on the ground. The end-of-life (EOL) output of the array is 9.52 GW, delivered to the distribution system. The overall system efficiency of the SPS is 6.47%. The solar cells are fastened on a 25-μm (1-mil) Kapton membrane which is mounted by tensioning devices or straps to the main structural members of the SPS. The array design parameters, efficiencies, materials of construction, area requirements, and mass are presented in Table 3.3-4.

(a) Ultimate Tensile Strength and Coefficient of Thermal Expansion
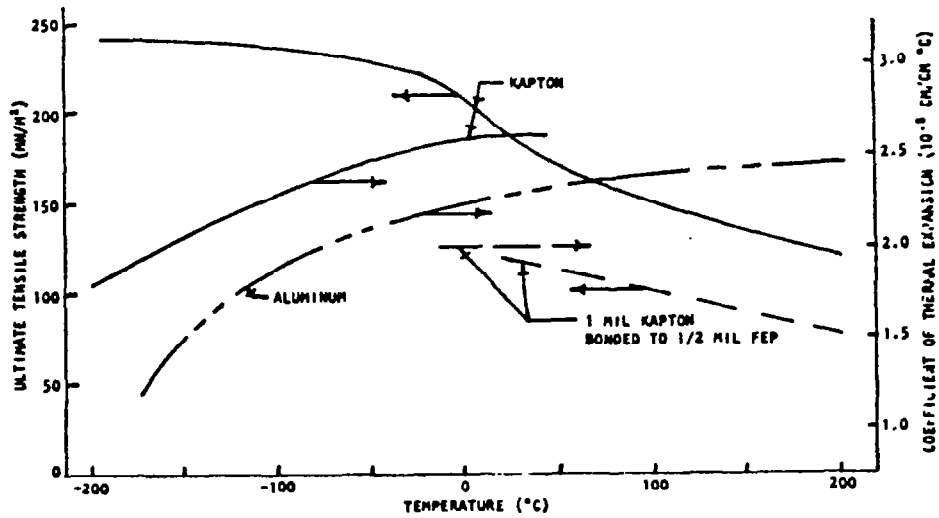
(b) Dielectric Strength
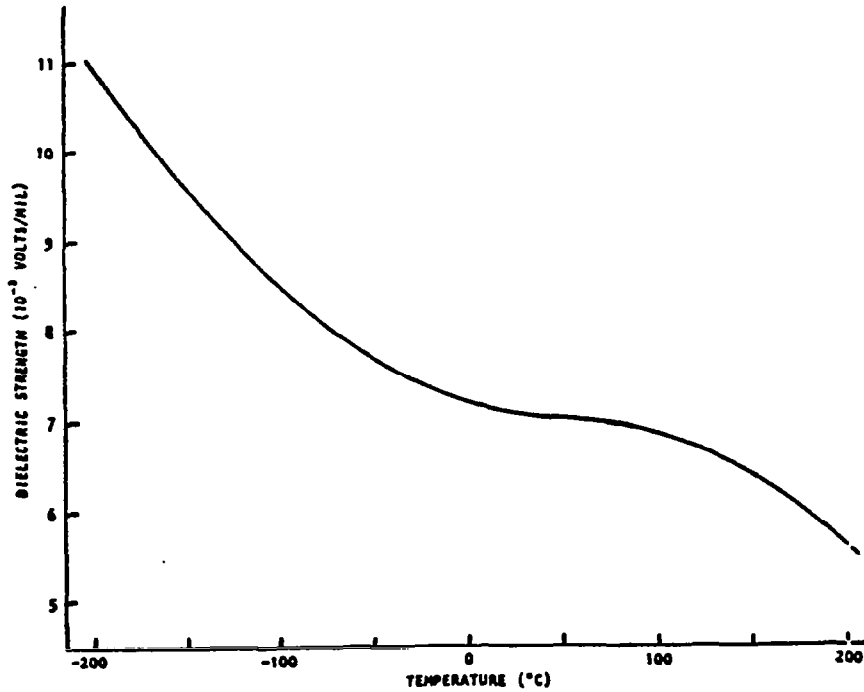
Figure 3.3-8. Kapton Type H

Table 3.3-3. *Solar Photovoltaic Power Conversion Mass*

	MASS (KG × 10^{-6})	
• **SOLAR CELLS**		
COMPONENT		
GaAs CELL	0.717	
GaAlAs WINDOW	0.007	
SAPPHIRE (COVER/SUBSTRATE)	2.150	
CURRENT COLLECTORS	1.622	
AIR COATING	0.002	
SUBTOTAL	4.492	
• **SOLAR BLANKET**		
KAPTON BLANKET	0.974	
TRANSPARENT POLYMER-		
THERMAL COATING	0.244	
ADHESIVES	0.730	
INTERCONNECTS	0.378	
SUBTOTAL	2.326	(6.818)
• **CONCENTRATOR**		
KAPTON BLANKET	1.031	
REFLECTIVE MATERIAL	0.006	
SUBTOTAL	1.037	
TOTAL WT: 7.855×10^{6} KG		

Table 3.3-4. *GaAlAs Solar Cell and Blanket Design and Performance Characteristics*

ITEM	CHARACTERISTIC
ARRAY INTERCEPTED ENERGY	69 GW
CELL η AT 28°C, AMO	20%
CELL η AT 113°C, AMO	18.15%
ARRAY OUTPUT TO DISTRIB. BUS EOL	9.52 GW
ARRAY OUTPUT VOLTAGE	45.7 kV
CELL OUTPUT VOLTAGE AT 113°C	0.7 V
CELLS IN SERIES	65,000
SOLAR CELL SUBPANEL SIZE	600×750 m
NUMBER OF BAYS PER SPS	60
ARRAY DESIGN FACTOR	89%
REFLECTIVITY & DEGRADATION	0.90 BOL, 0.72 EOL
CONCENTRATION RATIO	
GEOMETRIC	2
BOL	1.9
EOL	1.86
SOLAR CELL CONSTRUCTION	
COVER	20 μm SAPPHIRE
CELL	5 μm GaAlAs
INTERCONNECT	12.5 μm SILVER MESH
SUBSTRATE	
ADHESIVE	12.5 μm FEP
FILM	25 μm KAPTON
TRANSPARENT THERMAL COATING	6 μm POLYMER
SPECIFIC WEIGHT	0.2525 kg/m^2 (0.0516 lb/ft^2)
DEPLOYED CELL & BLANKET AREA PLANFORM	62.4 km^2
SOLAR CELL AREA	27 km^2
REFLECTOR SURFACE AREA	54 km^2
MASS	
SOLAR CELLS	6.818×10^6 kg
REFLECTORS	1.037×10^6 kg
TOTAL MASS	7.855×10^6 kg

Thin reflective membranes are used on the SPS to reflect the sun onto the solar cell surface and obtain a nominal concentration ratio of 2. The reflector is made of 12.5 μm (0.5-mil) aluminized Kapton. The reflectors are mounted on the main structural members at a 60° angle with respect to the solar blanket. The reflector design parameters, operating temperatures, area, and mass are presented in Table 3.3-5.

Table 3.3-5. *SPS Reflector Design and Performance Characteristics*

ITEM	CHARACTERISTIC
MATERIAL	ALUMINIZED KAPTON
KAPTON THICKNESS	12.5 KM
KAPTON SPECIFIC GRAVITY	1.42 (0.018 KG/M^2)
ALUMINIZED COATING THICKNESS	400 ANGSTROM UNITS
WEIGHT OF ALUMINIZED COATING	96 KG/KM^2
REFLECTOR SURFACE PROTECTIVE FILM COATING	QUARTZ OR CALCIUM FLUORIDE
REFLECTOR SUBPANEL SIZE	600×750 M
NUMBER OF REFLECTOR PANELS	120
REFLECTOR REFLECTIVITY/DEGRADATION	0.87 BOL, 0.83 EOL
CONCENTRATION RATIO GEOMETRIC	2.0
CONCENTRATION RATIO	1.9 BOL, 1.83 EOL
REFLECTOR SLANT ANGLE FROM HORIZ.	60 DEG
OPERATING TEMPERATURE	
TOP REFLECTORS	-52°C
INBOARD BOTTOM REFLECTORS	-46°C
OUTBOARD BOTTOM REFLECTORS	-73°C
TOTAL AREA OF REFLECTORS	108.0×10^6 M^2
TOTAL WEIGHT OF REFLECTORS	1.037×10^6 KG

Solar array switch gears as shown in Figure 3.3-9 are provided in each string of solar cells for isolation and maintenance. Voltage regulation of the solar array, power output, and beginning-of-life (BOL) excess power dissipation will be controlled by selective switching of isolation/regulation switch gears on array submodules. (Note: These switch gears are part of solar array assembly.) Optimum power output will be assured at all times by proper sizing and design of the submodules, their associated switch gear and IMCS control of the switching, in addition to control of the various loads. Voltages and currents being handled by the switch gears will be monitored by the IMCS to determine their status and to establish a need for the opening and closing of these switches. The switch gear and control are discussed in the power distribution and control and the IMCS sections of this report.

Power Distribution and Control

Introduction. The power distribution and control subsystem (PDS) receives power from the power generation subsystem, and provides the regulation and switching required to deliver power for distribution to the satellite power users. During the ecliptic periods, batteries will be utilized to supply the minimum required power to the various subsystems. Figure 3.3-10 illustrates the major assemblies comprising the PDS. Functional requirements are shown in Table 3.3-6. The subsystem consists of main feeders, secondary feeders, tie bars, summing buses, voltage converters, switch gear, circuit breakers,

KLYSTRON REQUIREMENTS			
DEVICE	VOLTAGE	POWER KW	REGULATION
COLLECTOR 1	40 KV	11.2	
2	32 KV	11.2	
3	24 KV	11.2	
4	16 KV	11.2	
5	8 KV	11.2	
KLYSTRON BODY	40 KV	3.2	1%
MOD ANODE	20 KV		1%
CATHODE HEATER	20 V	0.1	10%
SOLENOID	20 V	0.5	10%
COMPUTER	20 V	0.1	10%
RETROELECT	20 V	0.1	10%
TOTAL		59.8	

S/A SOLAR ARRAY
G   SWITCH GEAR
SCB SOLID STATE CRK BRKR.
R   REGULATOR
BT   BATTERY TIE CONTACTOR

Figure 3.3-9. Power Distribution – Nonrotating (Preliminary)
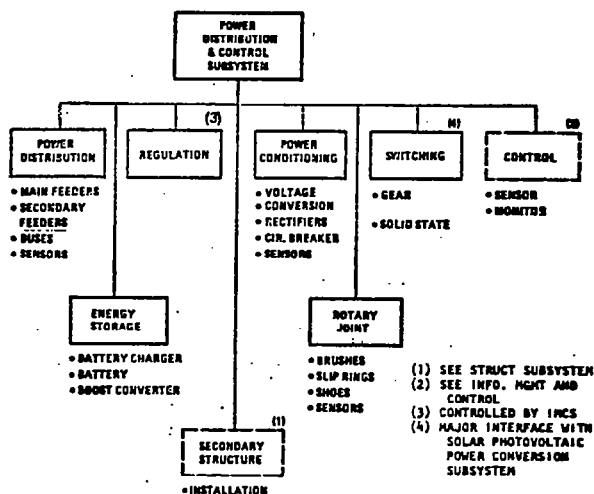Typical Bay – Each Wing

3-28

Figure 3.3-10. PDS Assembly Tree

Table 3.3-6. PDS Functional Requirements

LIFETIME	30 YEARS WITH MINIMUM PLANNED MAINTENANCE
OPERATIONS	GEOSYNCH ORBIT; 0° INCLIN, CIRCULAR (35,786 km ALTITUDE)
COMMERCIALIZATION	COMPATIBLE WITH U.S. UTILITY NETWORKS
OUTPUT POWER	STEADY-STATE OPERATION 42.5 kV @ 208.3 kA AT SLIP-RING INTERFACE; 5 GW AT UTILITY INTERFACE
WEIGHT GROWTH	25%
TOTAL WEIGHT	SATELLITE PDS APPROX .95 kg/kW
ENERGY STORAGE	BATTERIES INCLUDED TO SUPPORT ON-BOARD SATELLITE SYSTEM OPERATIONS ONLY DURING ECLIPTIC PERIODS (2-40 MW HRS)
FAILURE CRITERIA	NO SINGLE POINT FAILURE MAY CAUSE TOTAL LOSS OF SPS FUNCTIONS
DEVELOPMENT	EVOLUTIONARY WITH PROVISIONS FOR INCORPORATING LATER TECHNOLOGY
RESOURCES	MINIMUM USE OF CRITICAL RESOURCES
SUBSYSTEM CHECKOUT	CONTINUITY, INSULATION RESISTANCE, FUNCTIONAL SWITCHING OF SWITCH GEARS

manually operated switches, slip rings, brushes, and subsystem cabling.
Batteries, battery chargers, and boost converters are included for eclipse
operations.

The major requirements are to deliver power at specified voltages and
levels on a continuous basis throughout the solar seasons for a duration of
30 years. To assure 5 GW at the utility interface, the solar array will gen-
erate and deliver 9.52 GW [end of life (EOL)] at the power distribution and
control interfaces. Each solar array module is designed for 45.7 kV output.
The total array produces 208,300 A. Power delivered to the klystrons (major
power user) through power distribution is 8.32 GW, requiring 8.92 GW trans-
ferred across the rotary slip ring power interface.

Alternate Configurations. A number of power distribution configurations have been reviewed. Of the configurations reviewed, two were evaluated: 1) end mounted antenna and 2) center mounted antenna (Figure 3.2-1).

End Mounted Antenna. The electrical power distribution system for the 3 trough coplanar end mounted antenna configuration is illustrated by Figure 3.3-11. A split bus is provided and each bus is carried through the rotary joint by its own slip ring. The split bus concepts offers protection from losing total array power in event of catastrophic damage to a section of the array.

Center Mounted Antenna. The center mounted antenna configuration has two identical, 3 trough coplanar - 15 bay arrays as compared to a single, 3 trough coplanar - 30 bay array, (Figure 3.2-1). Electrically the configuration is the same. The power distribution system block diagram is the same as shown in Figure 3.3-11. Principle differences between the end mounted antenna and the center mounted antenna are: shorter main feeders and a larger slip ring for the center mounted antenna. Methods for calculations of each system were the same.

The rotary joint of the end mounted antenna has a 300 meter slip ring while the center mounted antenna has a 800 meter diameter slip ring. Each system utilizes a total of 32 brush assemblies. Materially each slip ring has an aluminum core with coin-silver cladding with the brushes being 70% MoS_2, 25 Mo+Ta with a current density of 7.75 amps/cm^2.

Sizing. A continuous review of subsystem efficiencies has been maintained in order to provide updated efficiency factors for sizing the SPS. The efficiencies of major components on the nonrotating solar array wing was shown in Figure 3.2-2. The major consideration for sizing the PDS is the power level (voltage and current) and line loss allowables. This subsystem was sized to handle EOL power levels of 9.52 GW at 45.7 kV.

Distribution. The power distribution subsystem utilizes flat (1 mm) aluminum (6101/T6) feeders at 20°C. These flat conductors are not considered part of the main structure; they will normally be passively cooled by radiation to free space. Main feeders are sized to an average transmission efficiency of 94 percent (determined to be optimum on a cost basis).

Conditioning. The power conditioning converts existing bus voltage to the subsystem voltage required for the various subsystem loads. Major requirements are shown in the table on Figure 3.3-11 (klystron requirements). Five basic voltages (40 kV, 32 kV, 23 kV, 12 kV, and 8 kV) - klystron body voltage (40 kV), mod anode voltage (20 kV) and low voltages for cathod heater (20 V), solenoid operation (20 V), computer (20 V) and retro-electronic (20 V) - are required to operate 135,864 klystrons. These voltages at the required power level are provided by centralized dc/dc converters as shown in Figure 3.1-11 and 3.1-12. The point design provides 32 converters, each sized for 290 megawatts (7.19 kA).

KLYSTRON REQUIREMENTS

DEVICE	VOLTAGE	POWER KW	REGULATION
COLLECTOR 1	40 KV	11.2	
2	32 KV	11.2	
3	24 KV	11.2	
4	16 KV	11.2	
5	8 KV	11.2	
KLYSTRON BODY	40 KV	3.2	1%
MOD ANODE	20 KV		1%
CATHODE HEATER	20 V	0.1	10%
SOLENOID	20 V	0.5	10%
COMPUTER	20 V	0.1	10%
RETROELECT	20 V	0.1	10%
TOTAL		59.8	

S/A SOLAR ARRAY
G SWITCH GEAR
SCB SOLID STATE CRK BRKR.
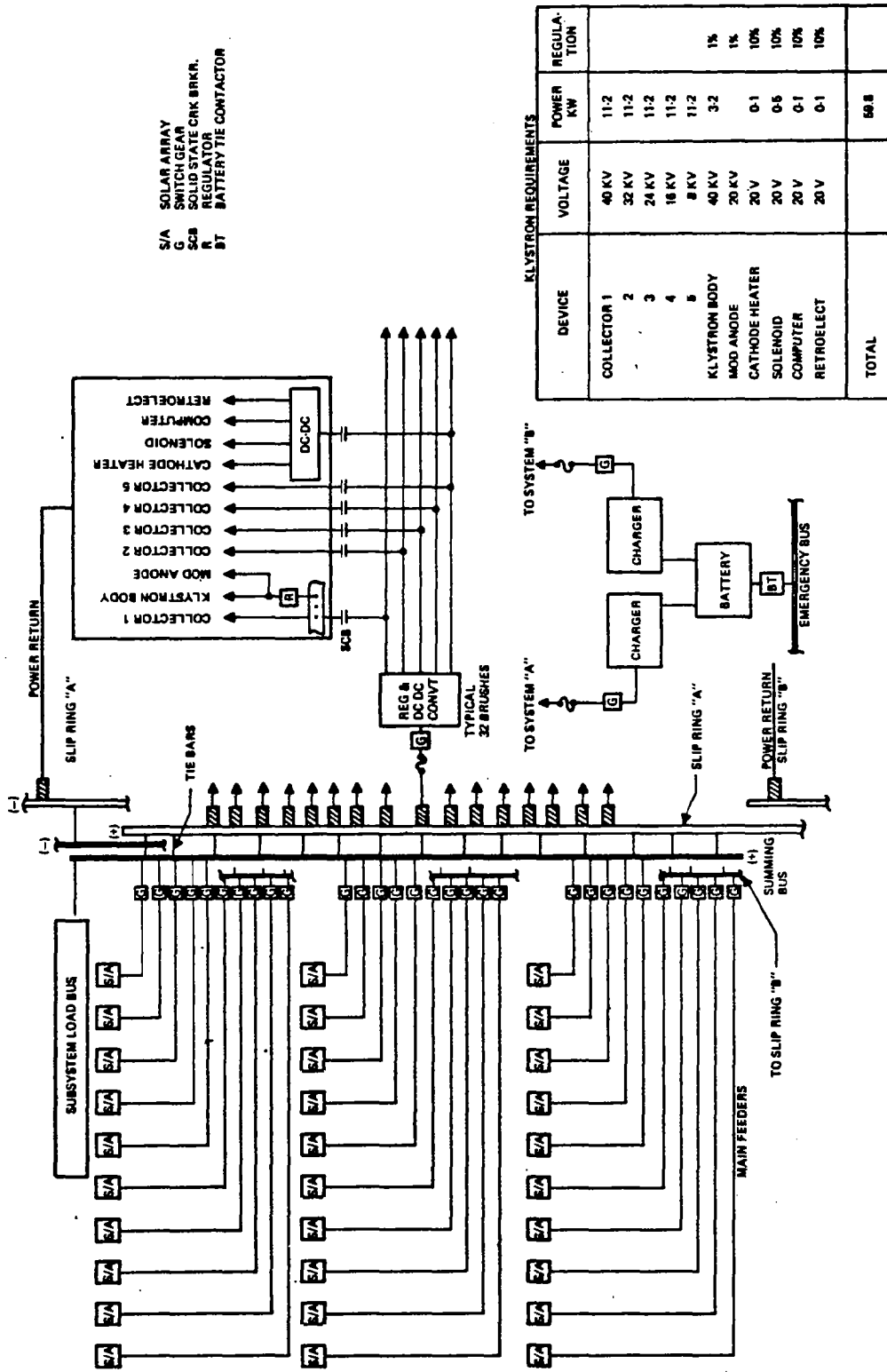R REGULATOR
BT BATTERY TIE CONTACTOR

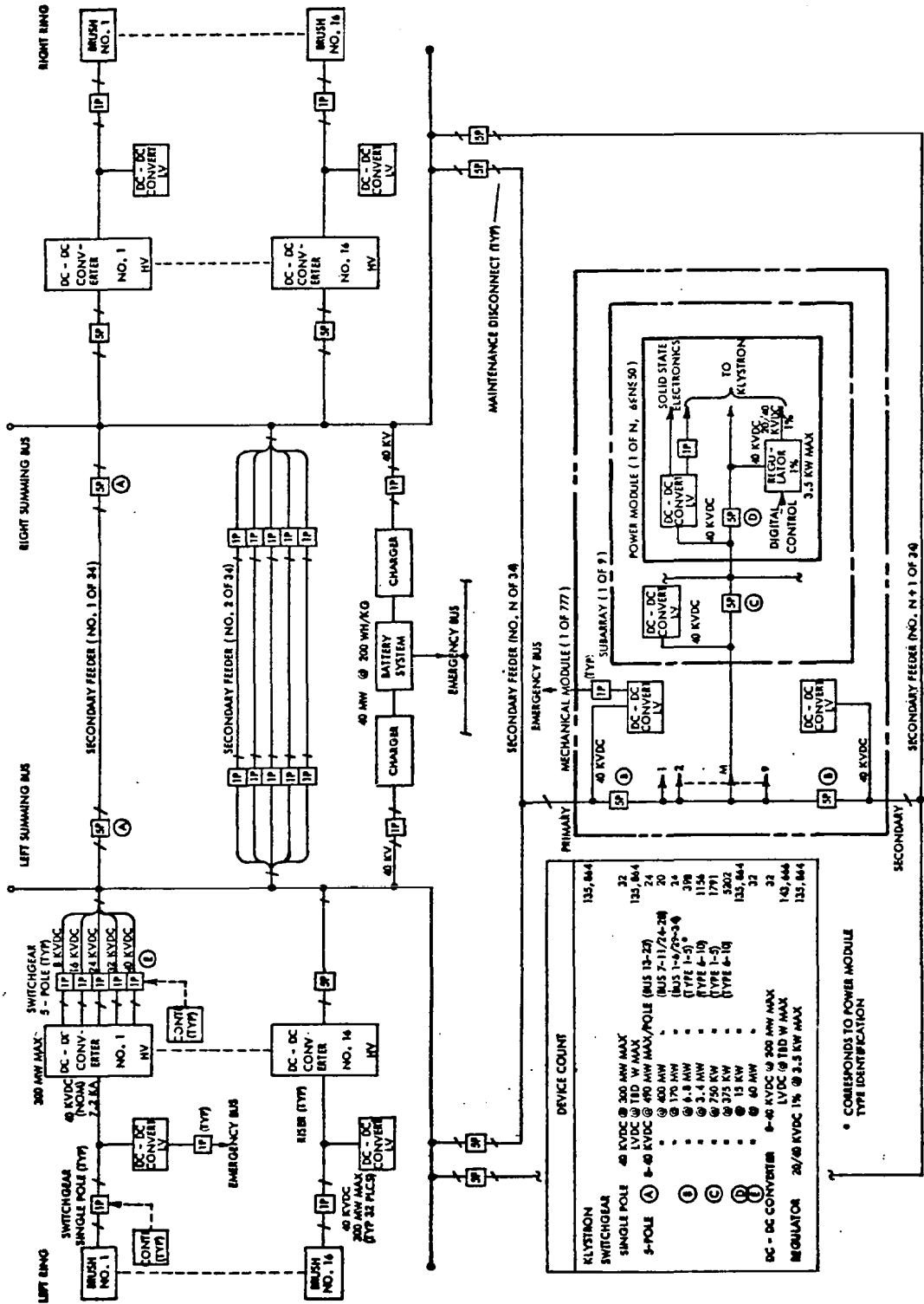*Figure 3.3-11. PDS Simplified Block Diagram*

3-31

Figure 3.3-12. Microwave Antenna – Power Distribution

Switching. Switch gears are provided at the end of each string of solar cells for isolation and maintenance. Voltage regulation of the solar array power output, as well as beginning-of-life (BOL) excess power dissipation will be controlled by selective switching os isolation switch gears on array sub-modules. (Note: These switch gears are part of solar array assembly.) Optimum power output will be assured at all times by proper sizing and design of the submodules, their associated switch gear and IMCS control of the switching, in addition to control of the various loads. Voltages and currents being handled by the switch gears will be monitored by the IMCS to determine their status and to establish a need for the opening and closing of these switches.

Rotary Joint. The rotary joint is utilized to transfer energy through slip rings and brushes from the satellite fixed member to the satellite rotating member upon which the microwave antenna is located. The rotary joint assembly design characteristics are given in Table 3.3-7.

Table 3.3-7. Rotary Joint Design Characteristics

TOTAL ASSEMBLY	
OPERATING VOLTAGE (kV)	42.9
AMPS PER RING ASSEMBLY	104.2
TOTAL MASS (kg)	TBD
SLIP RINGS (4)	
CORE	ALUMINUM
CLADDING	COIN-SILVER
CORE SIZE (cm^2)	41.3 (CROSS SECTION)
DIAMETER (km)	0.3
LENGTH (km)	0.94
SHOE BRUSH (16/SLIP RING ASSEMBLY)	
MATERIAL	75% MoS$_2$, 25 Mo + Ta
SHOE SIZE (cm)	12.7 W × 19 H × 68 L
CURRENT (A/cm^2) (MAX)	7.75
CONTACT AREA (cm^2)	864
QUANTITY	64 BRUSHES PER SHOE ASSY
GROUNDING	
SINGLE POINT - COPPER BUS (THERMAL ISOLATED FROM STRUCTURE)	

Rotating Antenna Power Distribution. A schematic of the power distribution system for the rotating antenna is shown in Figure 3.3-12. Riser's from the brushes are routed on the antenna supporting yoke, across the antenna pivot, with a loop, to the dc/dc centralized converters. Switch gears are provided to allow isolation when performing maintenance. Power from the dc/dc converters are tied to a multi-conductor summing bus for delivering the necessary voltages to the klystrons. Each slip ring feeds 16 centralized dc/dc converters situated near the antenna pivot. The Multi-conductor summing bus runs along the 2 sides of the antenna adjacent to the pivot. The other slip ring supplies power similarly to 16 dc/dc converters on the opposite side of the antenna along with its accompaning summing bus. Thirty-three feeders, isolated by switch gear at the summing buses, are interconnected between the summing buses. Mechanical modules of klystrons are then powered from adjacent feeders and are isolated from each feeder by switch gear. The feeder interconnect from the summing buses and the mechanical module feeder between adjacent feeders are for redundancy in the event of faults. The IMCS controls the power flow to each mechanical module so that a combination of one summing bus and one feeder is supplying power at any one time. There are 777 mechanical modules

on the antenna. Each mechanical module has 9 subarrays and each subarray is isolated through switch gear.

Energy Storage. Batteries will be utilized during ecliptic periods to provide 2-40 MW/hour energy. The batteries will be a sodium chloride type and have a density of at least 200 Wh/kg.

Subsystem Characteristics. A weight breakdown for the PDC subsystem is shown in Table 3.3-8. The PDC accounts for 9.802×10^6 kg (center mounted), and 11.677×10^6 kg (end mounted). This represents 31.9% and 35.4% of the total mass for the center and end-mounted antenna concepts, respectively.

Table 3.3-8. PDC Subsystem Mass Statement

ITEM	MASS 10^6 KG END MOUNTED	MASS 10^6 KG CENTER MOUNTED
NON-ROTATING		
SECONDARY FEEDERS	0.076	0.076
MAIN FEEDER	1.861	0.371
SUMMING BUS	0.220	0.114
TIE BUS	0.160	0.110
INSULATION	0.041	0.015
SWITCH GEAR	0.178	0.178
SECONDARY STRUCTURE	0.254	0.068
SLIP RING	0.043	0.049
SUBTOTAL	2.833	0.981
ROTATING		
RISERS	2.082	2.082
SUMMING BUS	1.426	1.426
FEEDERS	2.466	2.466
SECONDARY FEEDERS	0.005	0.005
INTER-TIES HIGH VOLTAGE	0.012	0.012
INTER-TIES LOW VOLTAGE	0.125	0.125
INSULATION	0.029	0.029
SWITCH GEAR	0.358	0.358
CONVERTERS & REGULATORS	1.639	1.639
SECONDARY STRUCTURE	0.668	0.668
BRUSH ASSY	0.017	0.011
SUBTOTAL	8.827	8.821
TOTAL	11.677	9.802

Microwave Power Transmission

Introduction. The microwave power transmission subsystem (MPTS) for SPS basically consists of two very large antenna array assemblies. An antenna 1 km in diameter serves as the transmitting array. A large number of power modules with 50 kW klystrons are mounted on the array structure. The klystrons serve as dc-to-microwave power converters and the microwave energy is beamed to an antenna array located on the earth's surface as part of the ground receiving station (GRS). The ground based antenna (rectenna) is defined in Section 3.3.2. Table 3.3-9 presents a summary of the MPTS and satellite antenna point design characteristics. The basis for the antenna analysis was a transmission capability of 6.96 GW. An assessed maximum klystron output of 50 kW (each) was established. If later, analysis shows a need for establishing a new beam distribution, the new power levels will be considered.

Table 3.3-9. *Point Design Microwave Power Transmission System (MPTS) Satellite Antenna Characteristics*

```
1.  MPTS SYSTEM (GAUSSIAN BEAM)

    • FREQUENCY (GHz)                                        2.45
    • MAXIMUM SATELLITE ARRAY POWER DENSITY (kW/m²)            21
    • POWER DENSITY AT IONOSPHERE (mW/cm²)                     23
    • MPTS EFFICIENCY (INCLUDES IONOSPHERE AND
          ATMOSPHERICS) (%)                                  59.3
    • DC INPUT POWER TO MPTS FROM SOLAR ARRAY (GW)           8.32
    • DC OUTPUT POWER TO UTILITY (GW)                        4.61

2.  SATELLITE MPTS ANTENNA ARRAY

    • SIZE (TRANSMITTING DIAMETER) (km)                         1
        - AREA (km²)                                        0.785
    • WEIGHT (kg)                                   14.532×10⁶
    • NUMBER OF MECHANICAL MODULES                            777
    • NUMBER OF SUBARRAYS                                   6,993
    • NUMBER OF KLYSTRON POWER MODULES                    135,864
```

14.532×10^6

  Design Configuration. The design data and analytical results for the 1 km diameter microwave antenna for the SPS is presented below.

  Subarray Description. The 50 kW klystrons, selected as power converters, are mounted in resonant cavity radiators (RCR) as shown in Figure 3.3-13. This assembly is defined as a power module. Its area varies so as to set the radiated power densities required over the array surface. There are ten density steps and corresponding module designs. These modules are assembled to form ten subarray types.
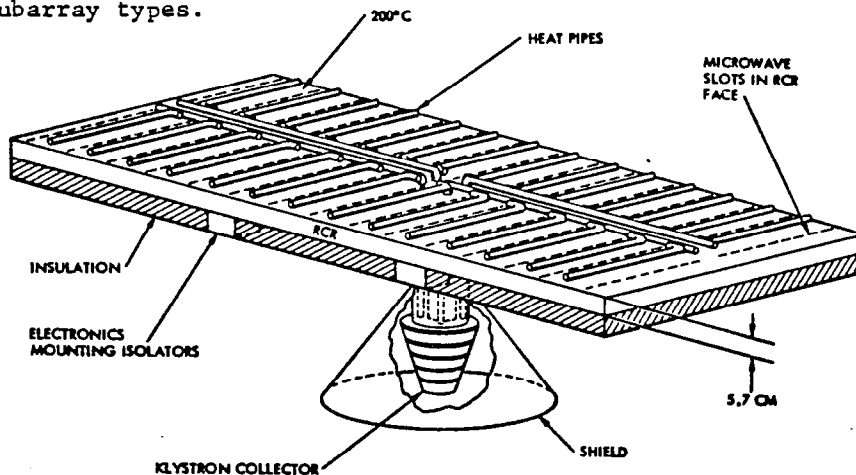

Figure 3.3-13. *Radiating Face of Power Module*

  When the klystrons are removed from their mounts, the subarray power modules can be stacked in a compact form for transport. The ten point-design subarray configurations and the dimensions of the stacked packages are shown in Figures 3.3-14, 3.3-15, and 3.3-16. The parameters associated with each subarray type are also given. The subarray coding is keyed to the coding of Figure 3.3-17 showing the total array.

3-35
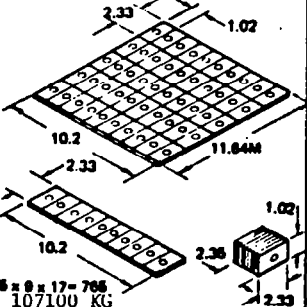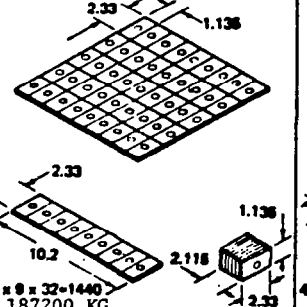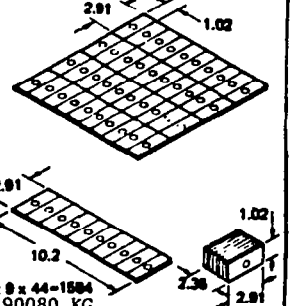
TYPE	PWR DENSITY	1.	21.06 KW/M2	2.	18.94 KW/M2	3.	18.94 KW/M2
NO. OF KLYSTRONS/ SUBARRAY & ARRANGEMENT		50	10 x 5	46	9 x 5	40	10 x 4
• PWR MOD SIZE • HINGED CONFIG • SHIPPING SIZE & WT.		1.02 x 2.33 10.2M x 2.33 2.36 x 1.02 x 2.33 140 KG		1.136 x 2.33 10.2 x 2.33 2.116 x 1.236 x 2.33 130 KG		1.02 x 2.91 10.2 x 2.91 2.36 x 1.02 x 2.91 120 KG	

| • TOTAL SHPG MODS & WT. | | 5 x 9 x 17= 765 107100 KG | | 5 x 9 x 32=1440 187200 KG | | 4 x 9 x 44=1584 190080 KG | |

Figure 3.3-14. Standard Subarray Size - Block 1
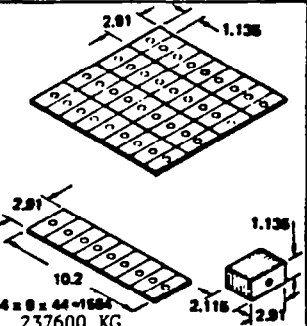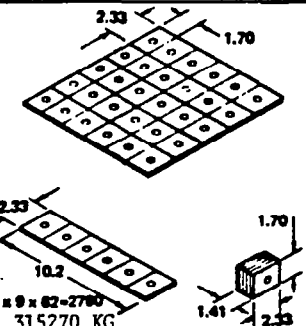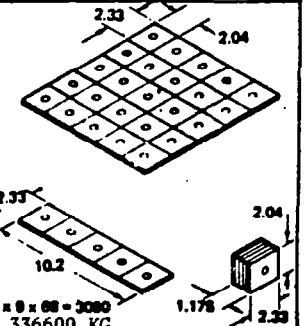
4.	15.16 KW/M2	5.	12.63 KW/M2	TYPE	PWR DENSITY	6.	10.52 KW/M3
38	9 x 4	30	6 x 5	• NO. OF KLYSTRONS SUBARRAY & ARRANGEMENT		25	5 x 5
1.136 x 2.91 10.2 x 2.91 2.116 x 1.133 x 2.91 150 KG		1.70 x 2.33 10.2 x 2.33 1.410 x 1.70 x 2.33 113 KG		• PWR MOD SIZE • HINGED CONFIG • SHIPPING SIZE & WT.		2.04 x 2.33 10.2 x 2.33 1.175 x 2.04 x 2.33 110 KG	

| 4 x 9 x 44=1584 237600 KG | 2.116 2.91 | 6 x 9 x 52=2760 315270 KG | 1.41 2.33 | • TOTAL SHPG MODS & WT. | | 5 x 9 x 68 = 3060 336600 KG | 1.175 2.33 |

Figure 3.3-15. Standard Subarray Size - Block 2

3-36
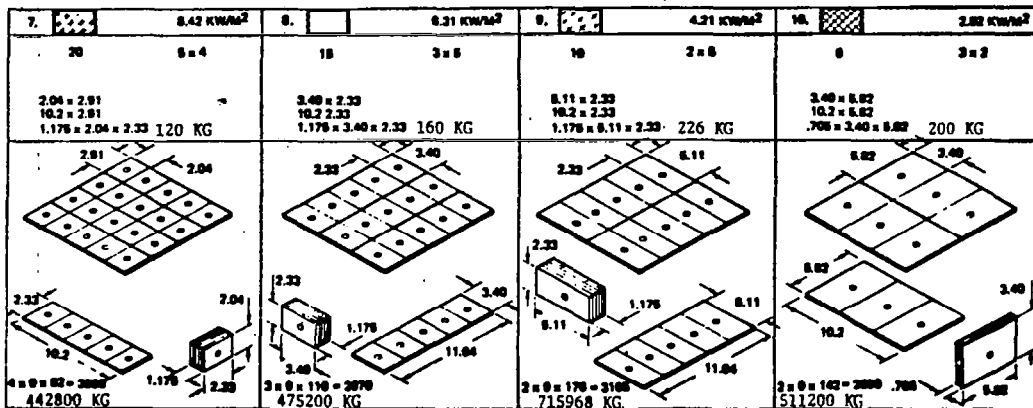
Figure 3.3-16. Standard Subarray Size - Block 3

Figure 3.3-17. Gaussian Beam Microwave Antenna

Subarray Configurations. A subarray is defined as a portion of the total antenna array which has the same phase over its radiating surface. This definition will be modified where the subarray beam is steered to point in the direction of the pilot beam. In this case, the center of the subarray has a phase, set by a single retroelectronics assembly. In addition, there is a phase variation across the array face used to steer the subarray antenna pattern.

The subarray size selected is 11.64×10.2 m. Sets of nine subarrays are then supported by a secondary structure to form a 34.92×30.6 m mechanical module. The module is supported by connections to the antenna secondary structure.

In order to keep costs down and make fabrication easy it is desirable that the subarray radiators be made of metal. However, neither the total mechanical module nor the subarrays can be a single metal structure due to thermal effects. As an example, for aluminum with an expansion coefficient of $2.5 \times 10^{-5}/°C$ and an operating temperature range of 100°C, the change in dimension for the mechanical module is 7.5 cm and for a subarray 2.5 cm. The resulting deviation from uniform spacing of the radiating elements in the subarray surfaces is too great.
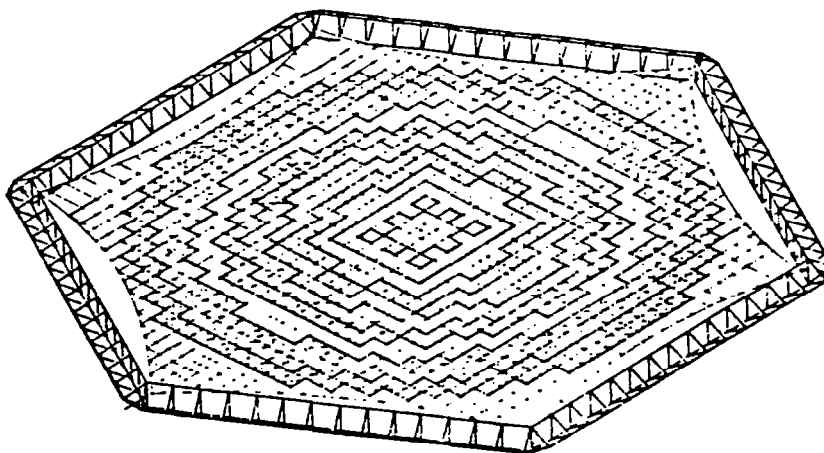
The subarrays are made up of power modules, each fed by a single microwave amplifier. These modules vary from about 1.0 m to 6.0 m on a side. The corresponding thermal dimension changes are ±0.13 cm to ±0.76 cm or ±0.010 λ to 0.062 λ around a design configuration. This is felt to be an upper limit on movement of the radiator elements. Therefore, the secondary support structure will be graphite-epon. Since the expansion coefficient of graphite-epon is an order of magnitude less than metals, only very small gaps between the mechanical modules are needed to accommodate thermal expansion.

The power level of all module amplifiers is the same. The size of the module radiating surface is varied to vary the power density weighting over the total array area. For instance, if 50-kW klystrons are used and the weighting is Gaussian, the number of modules per 11.96×10.2-m subarray varies from 50 at the array center to 6 at the array edge in the case of a 5-GW SPS system with a 1-km-diameter array. The module area then varies from 2.38 m^2 to 19.79 m^2. The layout of the ten subarray designs needed for a 10-step approximation to the Gaussian taper is shown in the section detailing the 5-GW microwave power transmission system (MPTS) point design. A ten-step quantization of a 10 dB taper (Figure 3.3-18) was chosen.

Resonant Cavity Radiator (RCR). The resonant cavity radiator selected is a modification of the basic slotted-guide radiator assembly. It is based on the observation that the traverse feeder forces loops in a standing wave field to appear at positions corresponding to the guide centers and nulls at positions corresponding to the guide walls. Therefore, if the guide walls are removed, we will still have the same field at the radiating slots as before and the radiated beam will be unperturbed.

However, we have gained several advantages. First, the radiator is now a shallow box with slots formed in one face. This is an easier structure to fabricate than the guide assembly. As a matter of fact, if we wish, we can make the box up out of two nesting trays as shown in Figure 3.3-19. If tray lips are a quarter-wave high, they form a choke joint which produces a short at crack formed by the lips making the RCR electrically continuous.
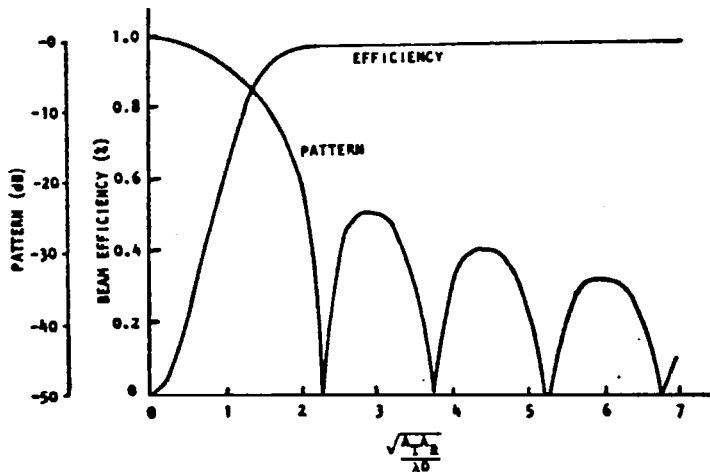
Figure 3.3-18.· Pattern Efficiency for
Uniform Illumination (10 dB Taper)
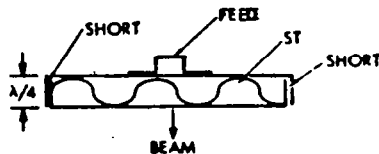
Figure 3.3-19. RCR Formed from Nested Trays

Next we have eliminated the weight of the guide walls. This is attractive since we are considering weight which must be transported to GEO.

Finally, we have decreased ohmic losses. The currents on the guide walls flow in opposite directions on the two sides of a partition. A portion of the top walls of two adjacent guides are cutaway in Figure 3.3-20 to show these currents. When the walls are removed these currents cancel and the ohmic loss associated with these currents is eliminated.

Klystron Amplifiers. Klystrons have been proposed by Varian for the MPTS converters[1,2,3]. An efficiency of 86% is predicted[3]. This is based on the performance of the VKS-7773, 50 kW, 2.45 GHz klystron previously built which obtained an efficiency of 74.4% without a depressed collector. Addition of a depressed collector with 55% beam power recovery efficiency plus other minor changes leads to an 80% efficiency. Taking into account cathode heater and solenoid power, a final efficiency of 85% is used in the point design calculations.

---

[1]*High Efficiency Klystron CW Amplifier for Space Applications*, A. D. LaRue, February 1976, Company Report
[2]*Personal Communication*, A LaRue to C. Tomita (11-24-76)
[3]*High Efficiency Klystron CW Amplifier for Space Power Applications*, A. LaRue, 1976 IEDM Tech. Digest
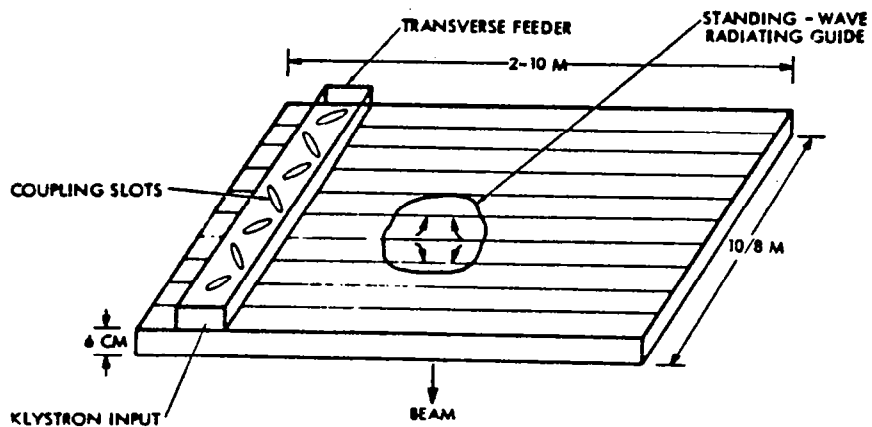
Figure 3.3-20. Klystron Power Module Guide Assembly

The major drawback to the use of klystrons is the large number of electrode voltages which are required. The depressed collector design selected requires five low regulation voltages. In addition, two regulated power supplies (1%) are required to supply body current and establish the potential of the mod anode, which controls beam current. The present point design generates all these voltages from a single 40 kV bus by means of switching converters plus precision regulators where required.

The collector can be run very hot and radiate directly to space, if it is made of a refractory material. Figure 3.3-21 shows that in such a collector assembly, made of pyrolytic graphite, the body cannot radiate directly to space as the collector can. The body cooling method selected is the use of heat pipes embedded in the klystron body walls and output drift tube. The heat-carrying pipes leave the klystron and carry heat to a set of pipes lying between the microwave slot radiators of the RCR face. This permits the disposal of klystron body waste heat downward toward earth and away from the satellite. A thermal blanket on top of the RCR prevents heat from traveling upwards. This makes it possible to keep electronics on the array back at 100°C. It also prevents radiated body heat from heating the satellite structure and slip rings.

In the array center there are 42 klystrons per 100 m^2 subarray. The radiator area per tube is then 2.37 m^2, if the microwave array structure is also used to radiate heat. The array face temperature is about 200°C for a power density of 21 kW/m^2.

Analysis of the latest efficiency chain, Figure 2.1-2, has indicated a need for a transmission power level of 6.79 GW. The nominal transmission capability of the 135,864 klystron amplifiers is calculated to be approximately 6.96 GW (klystrons operating at 50 kW nominal). This value was established at the time of the third quarterly report of the previous study and has been used for all layout and design effort for the satellite antenna as well as the ground receiving antenna (rectenna).

3-40
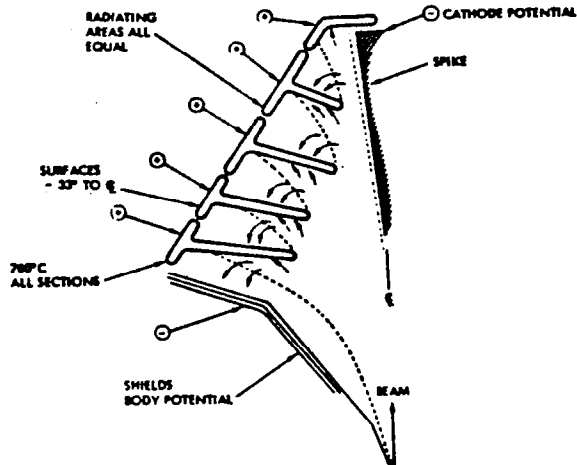
Figure 3.3-21. Collector Radiator

Klystron component masses and total mass are tabulated below:

COMPONENTS	MASS (kg)
PPM Magnet	2.0
Magnetic Poles	6.5
Electromagnet	13.0
Collector Assembly	5.5
Collector Heat Shield	0.1
Body Heat Shield	0.8
Copper Cavities	0.4
Heat Pipes in Tube	2.1
Electron Gun	0.6
TOTAL	31.0 kg
Specific Mass	0.62 kg/kW

Phase Array System - Eclectic Conjugate.

Introduction. A composite phase-conjugating system is proposed which embodies must of the good features of the systems already proposed. An over-all block diagram is given in Figure 3.3-22.

The reference phase distribution system is a modification of the system proposed by Seyl and Leopold of JSC. It uses a group of traveling wave feeders which distribute the reference source to a set of array regions. These feeders are servoed to produce the same phase at all outputs by means of signals fed back to the feeder inputs. The amplifiers in a given region are excited by a local feeder distribution system using resonant feeder elements.

Figure 3.3-22. Microwave Antenna – Beam Generation and Control

3-42

The pilot phase regeneration system is based on the JPL design. However, the transmitter signal is used as the local oscillator. This signal is of very high amplitude. It was feared that if the transmitter signal is not incorporated into the phase regeneration loop, it would produce so many spurious signals the design may fail. Elimination of transmitter phase noise forces us to a multiplier arrangement such as JPL used.

A pair of reference signals are used symmetrically placed around the operating frequency in order to eliminate ionospheric phase errors and errors due to filter detuning. The reference signal and the regenerated pilot are fed into the phase conjugating circuit shown in Figure 3.3-23.

f_R

OSC f_0

DIPLEXER

f_R+f_0 f_R-f_0

$(f_R+f_0)-f_p$

f_p IF AMP

$f_T = (f_R+f_0)-f_p + (f_R-f_0)$
$f_T = 2f_R-f_p$

BANDPASS FILTER
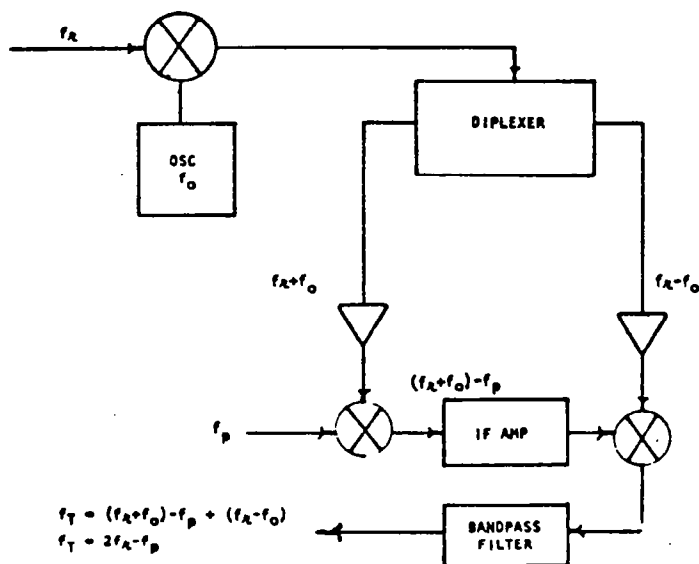
Figure 3.3-23. Phase Conjugating Electronics

Note that the output is $(2f_r - f_p)$. This is of the correct form to produce phase conjugation. If $f_r = f_p$, $f_T = f_p$; this is the most desirable condition. The only drawback is possible leakage of the high power transmitted signal into the phase reference distribution system. This is controlled by distribution of a reference at a frequency of $f_r/2$ which is converted to f_r by doubling at the point of usage.

The phase-conjugated signal, f_T, (which is what we wish to transmit) is fed to a transistor preamp and then to a power divider where the signal is distributed to the klystron amplifiers. The divider outputs are fed through analog phase shifters to the klystrons, where power generation occurs. The klystron outputs are used to drive the standing wave arrays which comprise the subarray.

The same subarray is receiving the pilot signals coming up from the earth station. Diplexers allow the klystron signals to flow into the standing wave radiators, while diverting the pilot signal coming from the cavity into a power

combining network which feeds a monopulse bridge. Since the pilot signals are equally displaced from the transmitted signal, the 180°C change in phase needed in the diplexer occurs for both pilots. Alternately the standing wave guide assembly or cavity can be fed from a separate feeder. The klystron signal at the bridge input is reduced by about 30 dB. The pilot signals are about 1 mW at this point. The pilot signals are then fed to a monopulse bridge. The sun signal is fed to the pilot phase regeneration circuitry. This sum signal and also the difference signals are fed to a monopulse receiver as shown in Figure 3.3-24. Just as in the pilot phase regeneration circuits, the transmitted signal is used as the local oscillator.
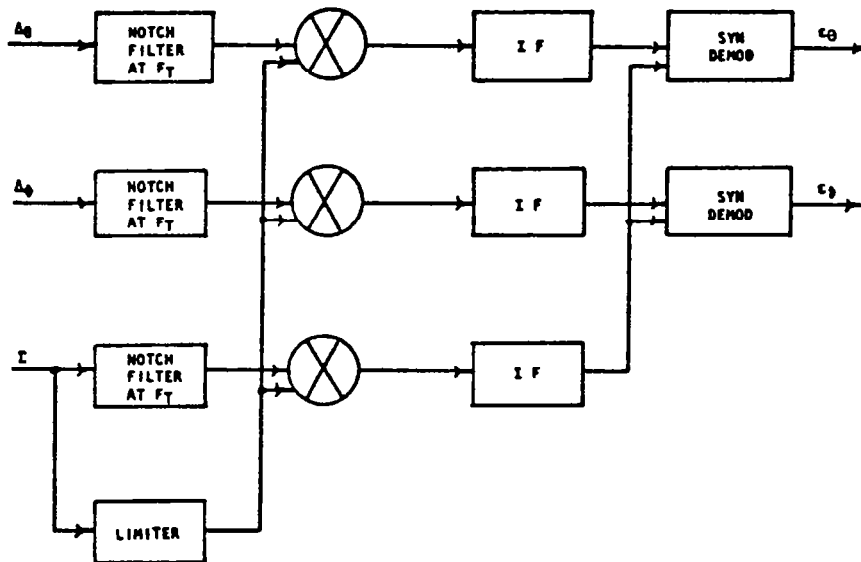
Figure 3.3-24. Monopulse Receiver

The monopulse receiver outputs $\varepsilon\theta$ and $\varepsilon\phi$ are a measure of the angular deviation of the direction of reception of the subarray from the direction of arrival of the pilot beam. The same signal f_T which was fed to the klystrons is fed to a second power divider. The outputs of this divider are fed through a set of phase shifters to an array of phase bridges.

The other set of inputs to these bridges is from taps which sample each klystron output in the standing wave radiators fed by the klystrons which comprise the subarray. These signals would be f_T, except that they have suffered phase shifts in the klystrons. They will be called f'_T. The first input to the phase bridges is f_T at the center bridge corresponding to the center of the subarray. The other members of this set are F_T shifted by the phase shifters so as to point the subarray pattern in the direction of arrival of the pilot beam. The phase shifters are set by a beam programmer which uses $\varepsilon\theta$ and $\varepsilon\phi$ from the monopulse receiver to make the correction. The phase bridge outputs are amplified and used to control the analog phase shifters at the klystron inputs. These servo loops then remove phase shift errors caused by the klystrons and introduce a phase gradient across the subarray face which corrects for subarray tilt.

3-44

At the edge of the array, subarrays will have only about six klystrons. As a result the subarray beam can only be steered about one beamwidth before the rms phase error of the subarray becomes too great. However, even angular control of one beamwidth greatly reduces the angular tolerances in mechanical orientation of the subarrays.

Reference Frequency Distribution. The basic organization of this distribution system is shown in Figure 3.3-25. Since each region supplied by a primary feeder is fed directly from the phase reference system, there is no buildup of phase error due to repeated processing at the primary feeder output points. A feedback servo is used to hold the phase of the feeder outputs with respect to the source to a fixed value. This servo is shown in Figure 3.3-26.
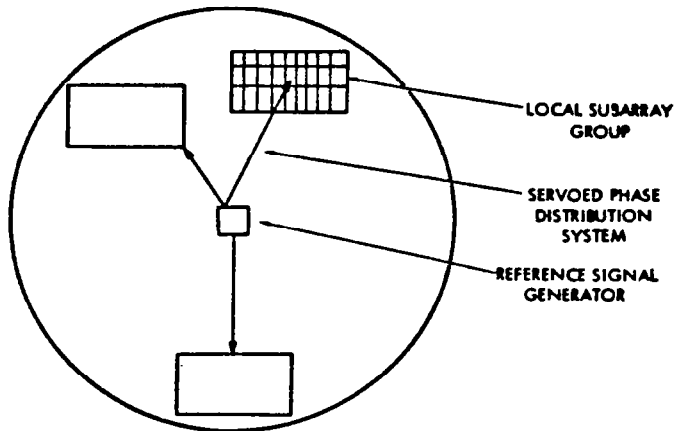
Figure 3.3-25. Array Reference Signal Distribution System
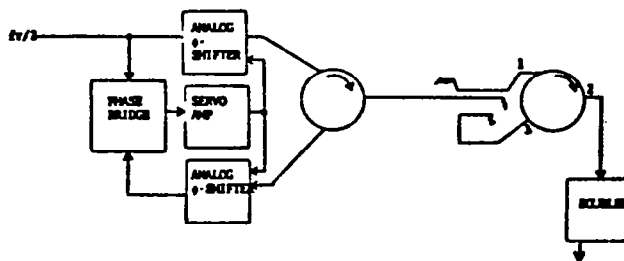
Figure 3.3-26. Reference Phase Distribution Servo

The reference source is at half the actual reference frequency. This signal enters the feeder through a diode phase shifter and a circulator. After reflection from the short at the other end of the feeder, it arrives back at the input and directed by the circulator into the output port. It then passes through a second phase shifter to a phase bridge. The other input to the bridge is the original reference signal.

The phase bridge output is an error signal which changes the phase shifter settings until the input to the feeder and the reflected signal from the feeder are in phase. The path delay through the shifters and feeder is then an integral number of wavelengths, since the forward and backward path delays are of equal length. Since the forward and return paths are of equal length, the forward path is an integral number of halfwaves long. This forward-path signal is sampled by the directional coupler/circulator arrangement. At port 2 of the circulator part of the signal is reflected back to the central station and part is fed to the doubler. When the signal is doubled to form f_r in the harmonic multiplier driven by the probe the doubler output phase delay with respect to f_r at the source will be twice the phase delay of $f_r/2$ or an integral number of full wavelengths. Therefore, the phase of the doubler output is the same as the phase of the source.

Each coax feeder serves an array region which is small enough to use a phase distribution system based on resonant feeders. Such regions are shown in Figure 3.3-25, designated as local subarray groups. The resonant feeder distribution concept depends on the fact that the phase at all points in a resonant cavity is approximately the same. The phase variation from point to point depends on the attenuation a wave experiences in traveling across the cavity. If the resonant feeder cavity is not too long, the cavity can be trapped along its length at the standing wave loops to obtain the reference phase. The accuracy with which the signals tapped from the feeder reproduce the reference phase depends on the total loss in the feeder.

If the resonant feeders are made of graphite-epox coated with metal or thin-wall invar, their thermal expansion coefficient can be of the order of 10^{-6} per °C or 10^{-4} for a 100°C change. The elongation is 2.4×10^{-3} m for a 25 m feeder. The corresponding change in electrical length at 2.45 GHz or 0.122 m wavelength is 7°. This small change will not destroy resonance, so it is felt that a servo to hold resonance is not required.

A servo to maintain resonance is required, if guide materials with larger expansion coefficients are used. An error signal for such a servo can be obtained by use of a loop and a dipole probe in the guide. At resonance, the electric and magnetic fields are in exact phase quadrature. These fields are sampled with a probe and a loop respectively and compared in a phase bridge to generate an off-resonance error signal. This signal can then be used to change the effective length of the line till it is exactly in resonance. Figure 3.3-27 shows such an arrangement.

Since the signal is removed from the feeder and then reinserted, it can be amplified to make up for losses in the phase shift loop and some of the guide losses.

Pilot Signal Regeneration. The pilot signal required should be at the same frequency as the transmitted signal. However, it could not be detected in the presence of the very high power transmitted signal, if it were at the same frequency. Therefore, it must be offset in frequency. It turns out that in order to control phase errors due to filtering and the ionosphere it is best to have two pilot signals displaced by equal amounts upward and downward from the transmitter frequency. Also since the transmitted signal is at such a
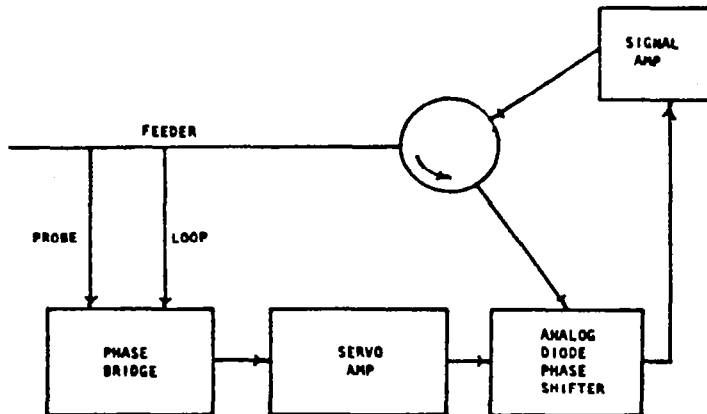
Figure 3.3-27. Electronic Servo Loop to Hold Feeder at Resonance

high power level, transmitter phase noise can be the dominant noise in pilot signal reception, if the pilot regeneration system is not planned with this in mind. The transmitter signal can also cause spurious frequencies by beating with other signals which can cause trouble.

The solution appears to be to include the transmitter signal in the regeneration process in such a way it cannot cause harm, rather than suffer its presence as an extraneous signal. This is done in the regeneration circuit shown in Figure 3.3-28. Since the output of the frequency quadrupler is the basic quantity, any change in phase in the multiplier will be divided by four. The multiplier should be two halfwave rectifier frequency doublers, rather than high efficiency multipliers using snap-back diodes. This will reduce phase errors due to the multiplier.

Information Management and Control

Introduction. The information management and control subsystem (IMCS) provides the interconnecting elements between and within all the varous satellites and ground-based operational subsystems. The IMCS also provides operational control of both the satellite and ground systems as well as providing all subsystem processing support for all but very special functions.

The IMCS consists of the on-board and ground-based processing equipment [central processing units (CPU) and memories], the inter- and intra-subsystem data network (data busses), the man-machine interfaces (display/control), and inter-system communication links, including RF, but excepting those specifically provided for the control and transfer of primary power, and all elements provided to accommodate activities related to system security, safety, or any other operation necessary to the continuing operation of the SPS.

Because of the early stage of program analysis, only those requirements imposed upon the IMCS by a limited number of satellite operations have been identified. The identified requirements generally are limited to those associated with the immediate operations of an active satellite. Auxiliary
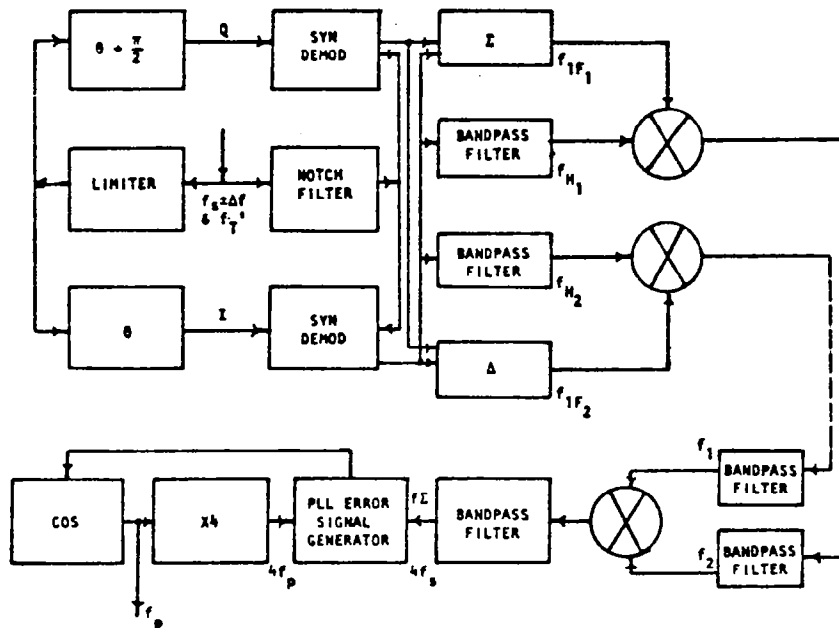
Figure 3.3-28. Pilot Signal Regeneration Circuit

functions such as ground/space communications, display/control, safety, security, etc., will be added when data become available.

Design Approach. The IMCS design selected for the baseline study is shown as a top level block diagram in Figure 3.3-29. This diagram illustrates a simplex (non-redundant) system. Local computer centers are envisioned to be located at substations located at selected sites in each trough and at the end sections. The end sites would house attitude control support centers. Processing support to structure alignment, microwave antenna beam pointing control, and additional attitude control functions would be housed in the center section near the antenna.

Three levels of data processing are illustrated in Figure 3.3-29: Master, Supervisory, and Remote. Subtiered to this hierarchy are microprocessors, Remote Acquisition and Control Units (RAC), and Submultiplexors (SM). Micro-processors as stand-alone processors have only been identified for the micro-wave antenna beam pointing function.

The IMCS hierarchy applicable to the microwave antenna subsystem, attitude control and stationkeeping subsystem, and power distribution subsystems is presented in Figure 3.3-30 through 3.3-32, respectively. These hierarchies are established to the level at which the IMCS and the using subsystem inter-faces are apparent (e.g., physical/electrical interface).

Table 3.3-10 summarizes the estimated number of data interfaces (not measurements) that must be accommodated by the IMCS. Note specifically that the microwave antenna subsystem is by far the major contributor to the determi-nation of the complexity of the IMCS electrical interface. Table 3.3-11 provid-es a very preliminary estimate of the control interface that must be accommodated
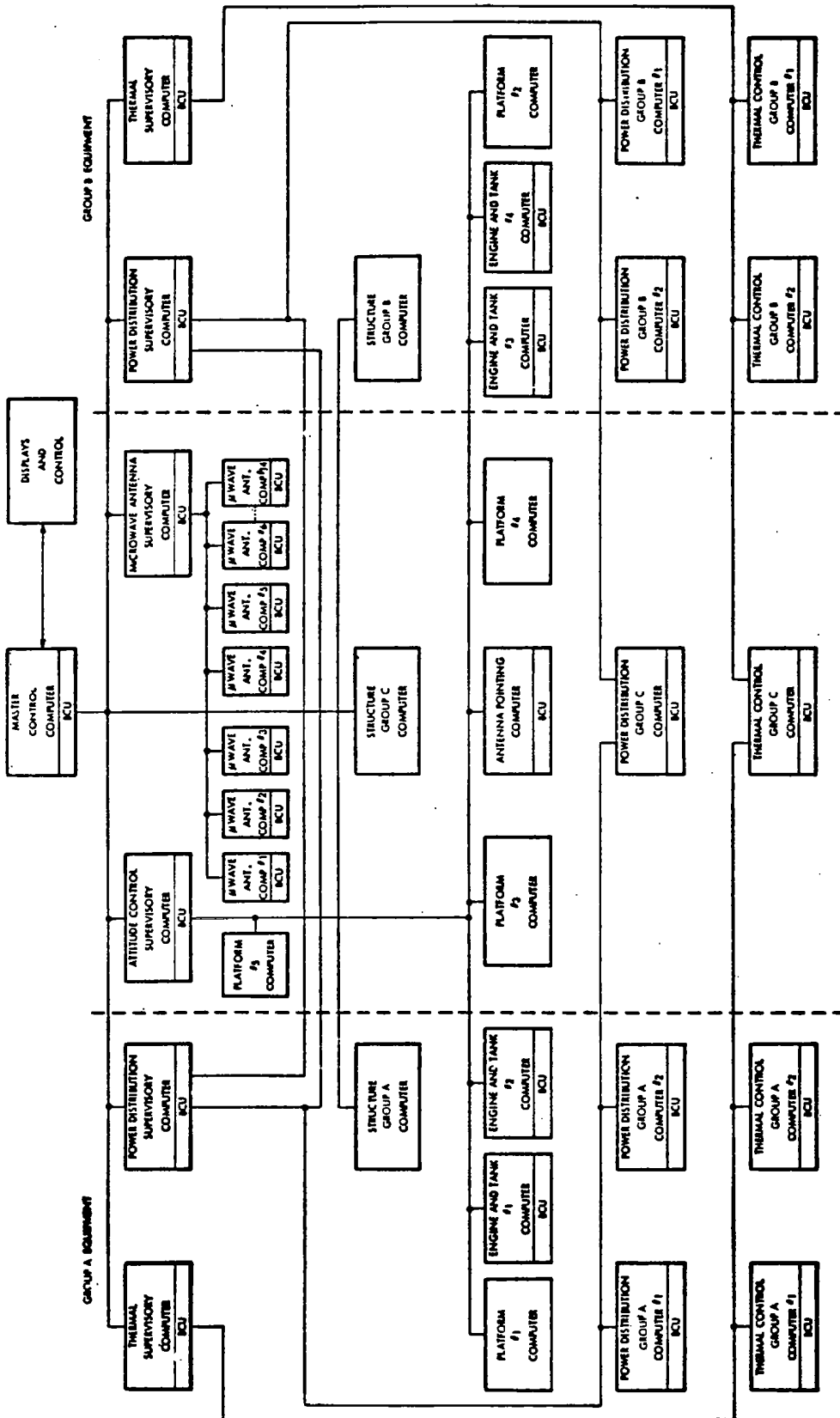
Figure 3.3-29. SPS IMCS Top-Level Block Diagram

Figure 3.3-30. IMCS - MW Antenna
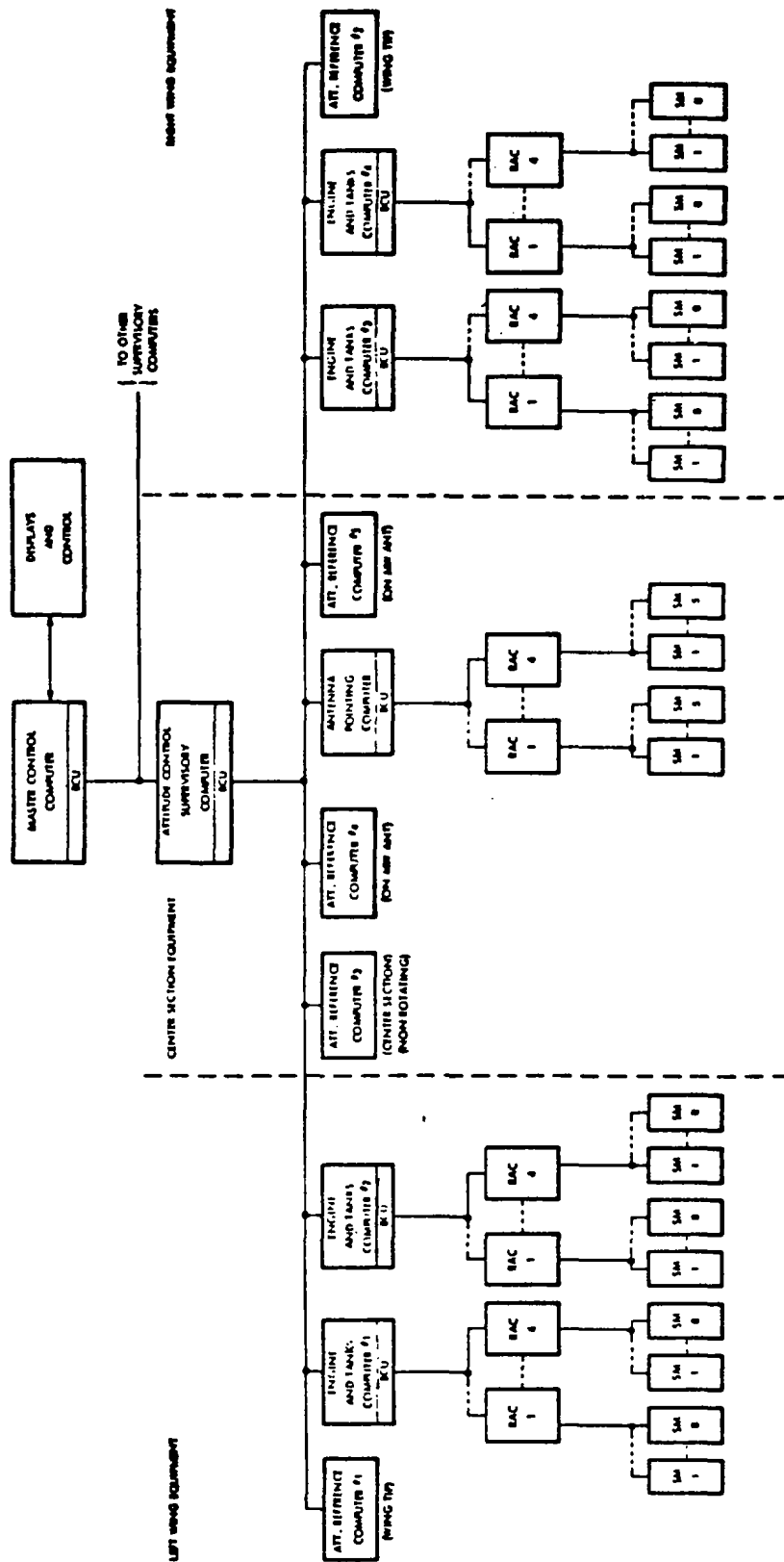
Figure 3.3-31. IMCS - Attitude Control
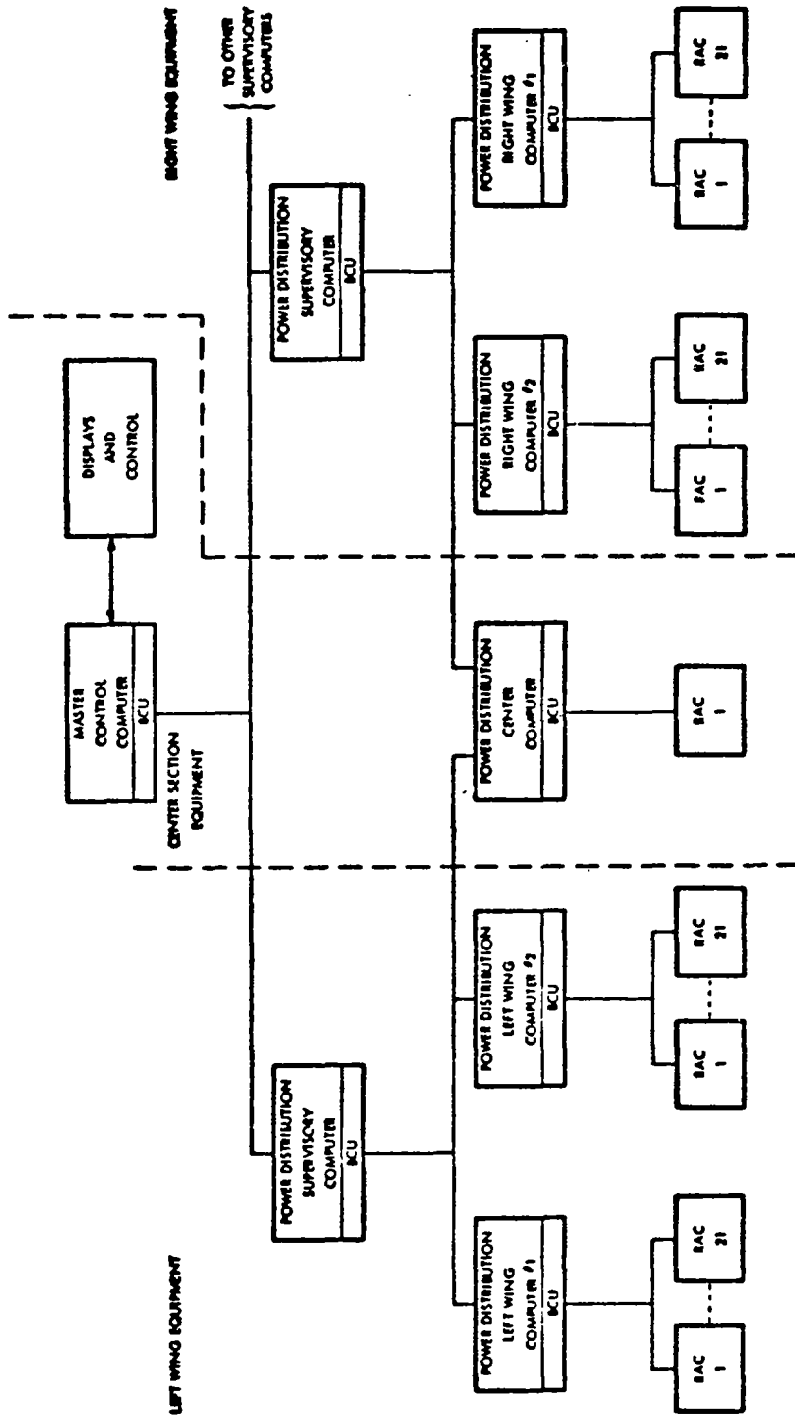
Figure 3.3-32. IMCS - Power Distribution

Table 3.3-10. *Preliminary Data Interface Summary -*
Photovoltaic (CR-2) Configuration

	ANALOG	DIGITAL	EVENT	TOTAL
MICROWAVE ANTENNA	6×10^6	1×10^6	2.1×10^6	$>9 \times 10^6$
OTHER SUBSYSTEMS				
STRUCTURE	35	35	35	>100
ATT. CONTROL & STATIONKEEPING	900	800	1000	~3000
POWER DISTRIBUTION	1000	100	2000	~3000
INFORMATION MANAGEMENT	-	~19,000	-	~19,000
THERMAL	16,000	-	-	16,000
LIFE SUPPORT	TBD	TBD	TBD	TBD
SAFETY AND SECURITY	TBD	TBD	TBD	TBD

Table 3.3-11. *Preliminary Control Interface Summary -*
Photovoltaic (CR-2) Configuration

	PROPORTIONAL	EVENT	TOTAL
MICROWAVE ANTENNA	$<13.6 \times 10^4$	30×10^4	$<44 \times 10^4$
OTHER SUBSYSTEMS			
STRUCTURE	~35	~35	<100
ATTITUDE CONTROL & STATIONKEEPING	~100	>300	<500
POWER DISTRIBUTION	-	>300	>300
INFORMATION MANAGEMENT	-	>3000	>3000
THERMAL	-	-	-
LIFE SUPPORT	TBD	TBD	TBD
SAFETY AND SECURITY	TBD	TBD	TBD

by the IMCS although the estimates are not supported by an in-depth analysis.
Again, the microwave antenna system predominates.

Major Assemblies. Figure 3.3-33 identifies the major assemblies that form
the IMCS. Six major assemblies have been identified at this time: (1) proces-
sors, (2) bus control units (BCU), (3) data bus, (4) remote acquisition and
control units (RAC), (5) submultiplexers (SM), and (6) microprocessor (μp).

Processors. The satellite Master Control Computer (Figure 3.3-30) will
operate with a 16-32 bit word format and have a 64K-128K word active memory
plus a TBD billion word bulk storage facility. Second- and third-level pro-
cessors (supervisory or local) will be 16-bit word assemblies and be limited
to 16K-32K memories. In special cases, memory capacity may be increased to as
much as 128K words. Assemblies or subassemblies identified as microprocessors
(normally those units incorporated directly within the associated electronics)
will incorporate an 8-bit-word format and use active 8K-64K word memories.
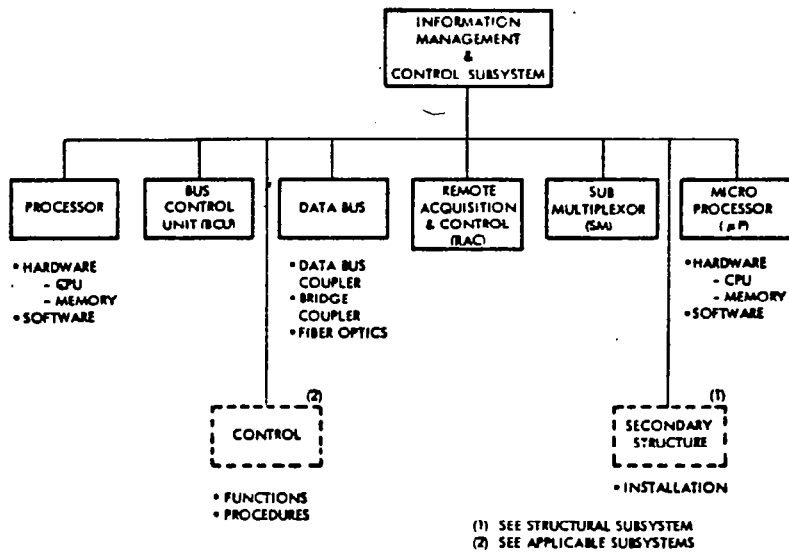
Figure 3.3-33. Assembly Tree - IMCS

Bus Control Unit. The bus control unit (BCU) provides the control neces-
sary for data/command transfer over the subsystem data bus network. The BCU
accepts instructions and data (or commands) from its associated processor and
translates these data from a processor-compatible format to one compatible
with the data network. It also accepts bus-compatible data and converts these
data to processor formats. In addition, the BCU monitors the data traffic--
performing bit and word checks as well as health/status checks.

In addition to data bus control, the BCU will provide a computer-to-
computer link where appropriate.

Data Bus. The data bus network accommodates multiplexed, digital data
transmitted between the BCU and all other remotely located data acquisition
and central devices associated with a specific processor/BCU combination. The
bus link may utilize conventional wire techniques for short runs in low EMI
areas or fiber-optic technology for long paths or through high EMI areas. Basic
bit rate within the bus assembly is assumed to be 1.0 Mbps. Included in the
data bus assembly are the data bus coupling devices used to connect the various
remote units (one required per remote) as well as the bridge coupler required
to transfer data across the microwave antenna rotary joints; the latter element
is presently TBD.

Remote Acquisition and Control. The remote acquisition and control (RAC)
assembly is the basic interface between the IMCS and the various operating sub-
systems. The RAC provides for data format conversion from the preconditioned
analog, digital or event voltage/impedance levels, and converts these data into
8-bit digital, serial, equivalents. The RAC also accepts digital data words
and outputs commands in a format compatible with the receiving subsystems.

3-54

Basic conversion (input/output) is assumed to be ±1% (e.g., 7-bit and sign). Voltage ranges and impedances are TBD.

Submultiplexers. The submultiplexer (SM) provides a means of expanding the capability of the RAC. The SM thus contains all of the capabilities of an RAC, but can only communicate with a single RAC rather than a given data bus. The number of SM's that can communicate with an RAC is presently TBD.

Microprocessor. The microprocessor (µp) elements provide local, front-end processing of data obtained from the various using systems. These processors will handle the bulk of the system's monitoring and control task, sending raw data up through the computer hierarchy only when the task-levels exceed pre-established limits, or when detected out-of-tolerance conditions exceed local control boundaries. These devices are solid state and could normally be integrated within the user electronics. When necessary, the µp can be located within the RAC's or SM's to provide local performance monitoring and control.

Subsystem Summary. Table 3.3-12 summarizes the number of IMCS elements required for the photovoltaic configuration. Table 3.3-13 summarizes the physical (weight, power, volume) requirements for this system.

Table 3.3-12. Hardware Summary - IMCS

HARDWARE ELEMENT	FUNCTION							
	MASTER CONTROL COMPUTER	DISPLAY AND CONTROL	SUPER-VISORY COMPUTER	REMOTE COMPUTER	MICRO-PROC	BUS CONTROL UNIT	REMOTE ACQUIS. AND CONTROL	SUB-MUX
SATELLITE CONTROL	2	1	-	-	-	2	-	-
THERMAL CONTROL	-	-	2	5	-	7	85	1,352
STRUCT. ALIGN.	-	-	-	3	-	3	-	-
ATTITUDE CONTROL	-	-	1	10	-	11	28	148
POWER DISTRIB.	-	-	2	5	-	7	85	-
MICROWAVE ANTENNA CONTROL	-	-	1	14	777	792	787	29,500
TOTAL	2	1	6	37	777	822	985	31,000

Attitude Control and Stationkeeping (ACSS)

Introduction. The ACSS functional requirements include the pointing and stabilization of the solar collector, the microwave antenna, and geosynchronous orbit stationkeeping for the overall spacecraft. The point design performed is a relatively simple ACSS concept featuring argon ion electric thrusters for attitude control and stationkeeping, the Y-POP orientation (long axis perpendicular to the orbit panel) and partial inertia balancing of the spacecraft to minimize reaction control system (RCS) propellant consumption. An equatorial geosynchronous orbit (GEO) was selected over other alternative orbit inclinations to minimize the ground rectenna size (and cost) impact.

Table 3.3-13. Mass/Power/Volume Summary - IMCS

NON-ROTATING

HARDWARE ELEMENT	QUANTITY	UNIT MASS (Kg)	TOTAL MASS (Kg)	UNIT POWER (KW)	TOTAL POWER (KW)	UNIT VOLUME (m³)	TOTAL VOLUME (m³)
MASTER CONTROL COMPUTER	2	500	1,000	2	4	0 4	0 8
DISPLAY & CONTROL SET	1	200	200	0.9	0 9	0.72	0 72
SUPERVISORY COMPUTER	5	14	70	0.07	0 35	0.01	0 05
REMOTE COMPUTER	23	14	322	0 07	1 61	0.01	0.23
MICRO-PROCESSOR	-	5	-	8 02	-	0.003	-
BUS CONTROL UNIT	30	5	150	0 02	0.6	0 005	0.15
REMOTE ACQUISITION & CONTROL	198	5	990	0 02	3 96	0 005	0 99
SUB MULTIPLEXOR	1,500	3	4,500	0 01	15 0	0 003	4 5
SUBTOTAL			7,232		26 42		7 44

ROTATING

HARDWARE ELEMENT	QUANTITY	UNIT MASS (Kg)	TOTAL MASS (Kg)	UNIT POWER (KW)	TOTAL POWER (KW)	UNIT VOLUME (m³)	TOTAL VOLUME (m³)
MASTER CONTROL COMPUTER	-	500	-	2	-	0 4	-
DISPLAY & CONTROL SET	-	200	-	0 9	-	0 72	-
SUPERVISORY COMPUTER	1	14	14	0 07	0 07	0 01	0 01
REMOTE COMPUTER	14	14	196	0 07	0 98	0 01	0 14
MICRO PROCESSOR	777	5	3,885	0 02	15.54	0 003	2 331
BUS CONTROL UNIT	792	5	3,960	0 02	15 84	0.005	3 96
REMOTE ACQUISITION & CONTROL	787	5	3,935	0 02	15 74	0.005	3.935
SUB MULTIPLEXOR	29,500	3	88,500	0 01	295 0	0 003	88 5
SUBTOTAL			100,490		343 17		98 876
TOTAL			108,000		369 6		106 3

CABLE

NON ROTATING-WIRE (22GA)	1,200 KM	12 0/KM	14,000			2×10^{-5}/KM	
FIBER OPTICS	90 KM	0 14/KM	12			2×10^{-6}/KM	
ROTATING-WIRE	23,000 KM		279,000				0 48
FIBER OPTICS	350 KM		50				
TOTAL			293,000				0 48

The ACSS dedicated subsystem elements are the RCS and the attitude reference determination system (ARDS). The principal features of these subsystem elements is summarized in Figure 3.3-34. The information management and control subsystem (IMCS) provides the interconnecting data paths for the ACSS components as well as the mini-processors for computation of the control algorithms. The mass properties requirements of the ACSS is summarized in Table 3.3-14. Passive figure control has been determined to be adequate for the CR=2 collector. Active figure control is employed for the microwave antenna. This utilizes laser figure sensing and three actuation systems at alternate corners of the antenna frame in order to maintain coplanarity of the antenna web to the three fixed attach points (tension web concept).

Reaction Control System (RCS). The RCS thruster configuration and thruster characteristics are shown in Figure 3.3-34. These thrusters are identical to those employed on the electric orbit transfer vehicle, except that they are operated in a throttled mode for ACSS application. The thruster configuration is similar on each corner of the spacecraft. The configuration minimizes contamination of reflectors and solar blankets due to ion engine sputtering. Sixty-four thrusters (16 in each corner) are mounted in two axis gimbals to provide proper thrust vectors. During the stationkeeping ΔV, thrusters are throttled differentially to obtain yaw control torques. These thrusters provide the solar pressure stationkeeping correction (E-W) continuously except when in the earth's shadow. These thrusters also correct the other E-W stationkeeping perturbations. Roll and pitch attitude control torques (about the X and Y axes) are obtained by gimballing and throttling these thrusters at each of the four corners as required.
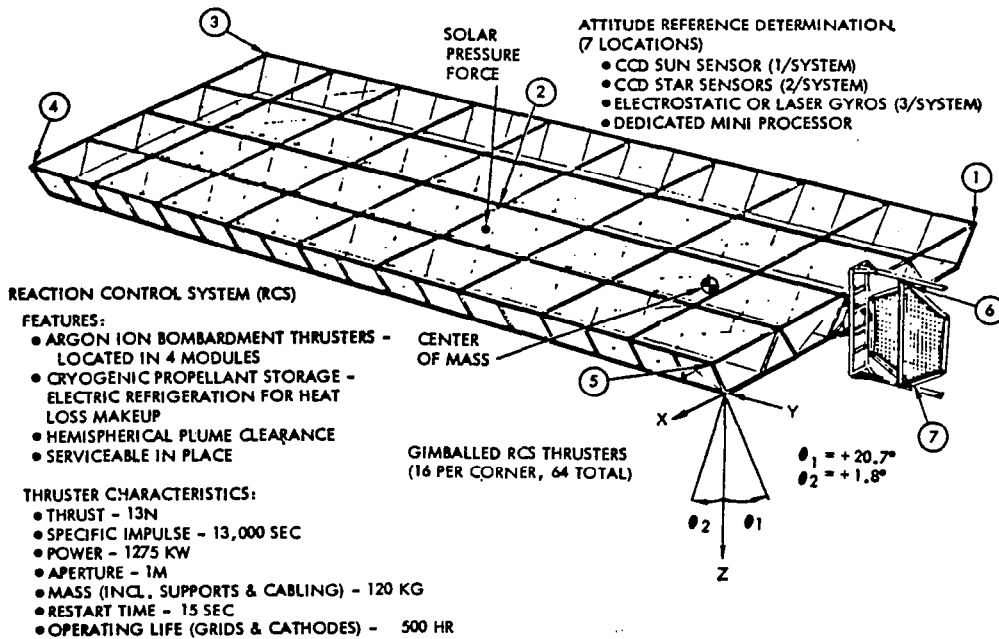
3-56

REACTION CONTROL SYSTEM (RCS)

FEATURES:
- ARGON ION BOMBARDMENT THRUSTERS – LOCATED IN 4 MODULES
- CRYOGENIC PROPELLANT STORAGE – ELECTRIC REFRIGERATION FOR HEAT LOSS MAKEUP
- HEMISPHERICAL PLUME CLEARANCE
- SERVICEABLE IN PLACE

THRUSTER CHARACTERISTICS:
- THRUST – 13N
- SPECIFIC IMPULSE – 13,000 SEC
- POWER – 1275 KW
- APERTURE – 1M
- MASS (INCL. SUPPORTS & CABLING) – 120 KG
- RESTART TIME – 15 SEC
- OPERATING LIFE (GRIDS & CATHODES) – 500 HR

ATTITUDE REFERENCE DETERMINATION (7 LOCATIONS)
- CCD SUN SENSOR (1/SYSTEM)
- CCD STAR SENSORS (2/SYSTEM)
- ELECTROSTATIC OR LASER GYROS (3/SYSTEM)
- DEDICATED MINI PROCESSOR

SOLAR PRESSURE FORCE

CENTER OF MASS

GIMBALLED RCS THRUSTERS (16 PER CORNER, 64 TOTAL)

$\theta_1 = +20.7°$
$\theta_2 = +1.8°$

Figure 3.3-34. RCS Thruster Configuration

Table 3.3-14. ACSS Mass Summary

ITEM	MASS ($\times 10^{+3}$ kg)
ATTITUDE REFERENCE DETERMINATION SYSTEMS (5)	0.32
THRUSTERS – INCLUDING SUPPORT STRUCTURE, 64 @ 120 kg/THRUSTER	7.68
TANKS, LINES, REFRIGERATION	15.07
POWER PROCESSING EQUIPMENT	TBD
ARGON PROPELLANT – ANNUAL REQUIREMENT	85.39
TOTAL	23.07*
TOTAL (WITH PROPELLANT)	108.46*
*NOT INCLUDING TBD ITEMS	

The SPS spacecraft is nominally designed to operate in a Y-POP orientation (i.e., long axis, Y-axis, perpendicular to orbit plane). Major advantages can be realized if the spacecraft is pointed more toward the sun. The collector cosine losses would be reduced which reduce the size of the solar collector, and thus a reduction in spacecraft mass and cost. The ideal maximum bank angle is 23.5 degrees which is achievable with an increase in propellant and thrusters. However, partial solar pointing with no propellant and thruster penalty is an advantageous feature. As illustrated in Figure 3.3-35, a roll angle of 9.0 degrees can be realized with no propellant penalty or loss of control authority.

FROM PREVIOUS ANALYSIS ALL TORQUES EXCEPT G_ϕ ARE ACCOUNTED TO INSURE MODULATION $\Sigma F \geq 0$: $F_S/2 - F_p - F = 0$

$F = F_S/2 - F_p = 164 - 5.4 = 158.6 N$

F IS THE MAXIMUM FORCE AVAILABLE TO ROLL VEHICLE BY ANGLE ϕ

$$F\ell_c = 3/2 \, W_0^2 \, (I_Z - I_Y) \sin 2\phi \quad \text{AND} \quad \phi = \frac{1}{2} \sin^{-1} \left[\frac{F\ell_c}{\frac{3}{2} W_0^2 (I_Z - I_Y)} \right]$$

WITH THE VALUES OF F, ℓ_c AND $3/2 \, W_0^2 \, (I_Z - I_Y) = 7.84 \times 10^6$ NM

ϕ MAX = 9.02°	
% COS LOSS = 3.16	

Figure 3.3-35. Maximum Bank Angle

Essentially this is achievable by simultaneously countering the large gravity torques and the solar pressure forces through use of thrusters that are predominatly at one end of the S/C. With this bank angle the collector cosine loss is reduced to 3.2% from the 8.2% for the Y-POP operation (net savings equal 5%). Figure 3.3-35 shows the steps and calculations involved in deriving the bank angle.

The number of thrusters required to perform the various functions is summarized in Table 3.3-15. A number of thrusters are added as spares to accommodate the 5000-hour operating life of the thruster grids and random failures (assuming a 5-year MTBF). The system results in approximately 44 thrusters being operated on a time-averaged basis. The total number of thrusters including spares in the system is 64. The thruster configuration (Figure 3.3-34) has been designed with adequate spacing (10 m) to permit servicing (primarily grid replacement) of a thruster with a servicing cab while adjacent thrusters are operated.

The mass properties of the RCS is given in Table 3.3-14. The argon propellant is stored as a cryogen to prevent the large tank mass penalty that would result if the argon were stored as a gas. A small electric refrigeration system is located at each tank for heat loss makeup. Four argon tanks are provided at each of the four thruster modules (total of 16 tanks) in order to prevent loss of function for single point failures. The tank outer diameters are approximately 2.4 m. The tank sizing is based on annual propellant resupply.

The annual propellant requirements for attitude control and stationkeeping are presented in Tables 3.3-16 and 3.3-17.

Table 3.3-15. Summary of Thruster Requirements

Function	Number of Thrusters Required/Corner		
	F_x	F_y	F_z
Attitude Control			
Roll (M_x) and Pitch (M_y) Yaw (M_z)	1.6		18.1
Stationkeeping			
Lunar/solar (N-S)			19.1
Solar pressure (E-W)			25.2
Total required/corner*	2		7
Spares	7		6
Total/corner (with spares)	3		13
Total thrusters/spacecraft	64		
*Rounded up to even number			

Table 3.3-16. Attitude Control Propellant Requirements

FUNCTION	PROPELLANT MASS (% S/C MASS OVER 30 YEARS)
SOLAR PRESSURE ANTENNA RADIATION PRESSURE	4.01
GRAVITY GRADIENT	
ABOUT X	0.124
ABOUT Y	1.38
ABOUT Z	0.124
SUBTOTAL	1.628
TOTAL	5.638
100-cm ARGON THRUSTERS T = 13n ISP = 13,000 SEC	

Table 3.3-17. *Stationkeeping RCS Propellant Requirements*

FUNCTION	ΔV/YR. (~M/SEC)	RCS PROPELLANT REQ'D* OVER 30 YR (% S/C MASS)	THRUST REQ'D (N)
• EARTH TRIAXIALITY (E-W)	282.5	6.65	328
• SOLAR PRESSURE PERTURBATION (E-W)			
• STATION CHANGE MANEUVERS (E-W)	1.0	0.03	
• M.W. ANTENNA RADIATION PRESSURE (E-W)	NEGLIGIBLE		
• SOLAR/LUNAR PERTURBATIONS (N-S)	53.3	1.25	124**
TOTAL	335.8	7.9	452

* I_{SP} = 13,000 SEC, 100 CM ARGON THRUSTER, T = 13 N
** THRUST ON 50% OF TIME

Attitude Reference Determination (ARDS). There are seven separate ARDS units on the spacecraft (Figure 3.3-34). The seven units are located on the collector (5) and the microwave antenna (2) to permit accurate control in the presence of structural bending without the use of complex autocollimation equipment working across large expanses of structure and across the microwave antenna rotary joint. Each ARDS unit consists of strapdown sun, star, and gyro sensors operating in conjunction with a dedicated mini-processor (provided by the IMCS) to yield three-axis attitude state data with an accuracy better than 1 arc-minute. Charge-coupled device (CCD) sensors are selected for the sun star sensors and are representative of the highly reliable, low-cost, sensor technology available in the near future. Electrostatic or laser gyros are representative of the gyro technology that may be commonplace in the SPS time frame.

Control Algorithms. No major problems are anticipated in stabilizing structural bending. In order to minimize structural dynamic interaction with the control system, the following features appear to be desirable for incorporation in the control algorithms:

• Weighted averaging of the attitude data from the five ARD's located on the solar collector body is a power means of decoupling or stabilizing the bending.

• Bending-state observers (or estimators) are also a powerful method of accomplishing the same objective.

• The use of a "quasi linear" thrust command policy can minimize structural vibration excitation as well as permitting the attitude control system to actively damp modal bending. A means of achieving such a policy is illustrated in Figure 3.3-36.

• THROTTLING PLUS ON-OFF SWITCHING POLICY PRODUCES APPROXIMATE LINEAR TORQUES

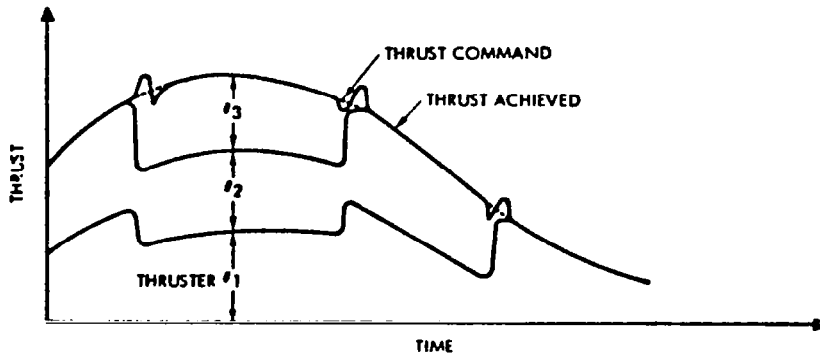• CAN TAKE ADVANTAGE OF BEST FEATURES OF LINEAR CONTROL

Figure 3.3-36. Quasi-Linear Thruster Control Policy

A statistical estimation scheme (Kalman filter) should be employed to provide optimal estimates of the principal axis of inertia orientation error. This parameter is observable and directly affects the RCS propellant consumption for roll and yaw control.

A relatively simple ACSS featuring argon ion electric thrusters for stationkeeping and attitude control torques has been defined. Reasonably small RCS propellant resupply requirements (and costs) are possible as a result of the Y-POP orientation (long axis perpendicular to the orbit plane) and the spacecraft design requirement for two-dimensional inertia balancing.

Structure

Introduction. This subsystem consists of the primary structure for the solar array, antenna, and rotary joint; secondary structure; and mechanisms. The primary structure assemblies are made up, basically, of the tribeam girders, tension cables, and joints. The fabrication and assembly of these structures are accomplished on orbit by beam machines and supporting auxiliary equipment.

Tribeam Girder. The general configuration and detailed breakout of the tribeam girder are illustrated in Figure 3.3-37.

The girder is 50 m on a side, and each bay is 50 m in length, stabilized by X-tension ties. Three longitudinal elements and the transverse struts, are formed by basic beam elements fabricated on orbit by a beam machine. The basic beam element is 2 m on a side with transverse structs every 2 m and modified triangular cap sections at the vertices. The cap sections, transverse struts, and X-tension braces are made from 60% graphite fiber composite sheets with approximately 88% cutouts, which is roll-formed, flanged, and welded by the beam machine to form a basic beam element 2-m on a side.
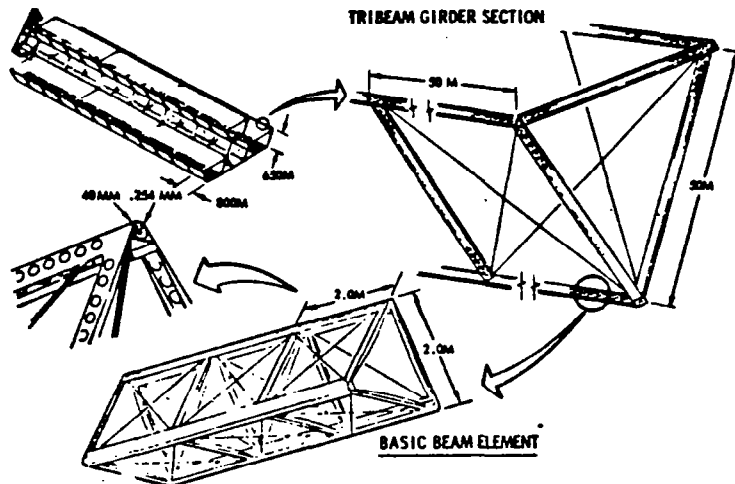
Figure 3.3-37. Photovoltaic Wing Structure Tiering

The pertinent physical properties of the tribeam girder basic beam element, cap section, and tension ties determined by this preliminary sizing analysis are listed in Table 3.3-18.

Table 3.3-18. Solar Array and Rotary Joint Tribeam Girder Characteristics

ITEM NO.	PARAMETER	CAP SECTION	BASIC BEAM ELEMENT	TRIBEAM GIRDER	TENSION TIE
1	A_{EM} = EFFECTIVE AREA FOR MASS CALCULATIONS IN M^2	0.035×10^{-3}	0.21×10^{-3}	0.21×10^{-3}	3.17×10^{-5}
2	A_{EI} = EFFECTIVE AREA FOR MOMENT-OF-INERTIA CALCULATIONS IN M^2	0.064×10^{-3}	0.19×10^{-3}	0.19×10^{-3}	3.17×10^{-5}
3	ρ = RADIUS OF GYRATION (M)	28.28×10^{-3}	820.78×10^{-3}	20.236	1.59×10^{-3}
4	I = GEOMETRIC MOMENT OF INERTIA (M^4)	5.1×10^{-8}	0.128×10^{-3}	237.5×10^{-3}	7.9×10^{-11}
5	E = MODULUS OF ELASTICITY - P_a (2)	9.65×10^{10}	9.65×10^{10}	9.65×10^{10}	2.34×10^{11}
6	α = COEFFICIENT OF THERMAL EXPANSION - M/M-°C	0.18×10^{-6}	0.18×10^{-6}	0.18×10^{-6}	0.4×10^{-6}
7	μ = POISSON'S RATIO	0.40	0.40	0.40	0.32
8	F_n = NATURAL FREQUENCY (Hz)	254	8.3	0.57(1)	$8.4 \ 10^{-3}$
(1)	TRIBEAM GIRDER LENGTH = 800 M				
(2)	MATERIAL IS GRAPHITE COMPOSITE, 60% FIBER, VOLUME, MADE UP AS (0, ◈, 0)				

Antenna Structure. The tension web compression frame antenna structure concept, shown in Figure 3.3-38, consists of three major elements (1) the tension web to which the dc-to-RF conversion and transmission hardware is attached, (2) a catenary rope system which is attached to the perimeter of the tension web, and (3) a hexagonal compression frame. The tension web resists the lateral pressure loading described in Figure 3.3-39. The loading is transmitted to the vertices of the hexagonal compression frame via the catenary rope system. The compression frame members are loaded in pure compression and can be analyzed as columns. Three of the six catenary-to-compression-frame vertice attachments are fixed. The other three attachments at every other intersection have lateral adjustment jacks. The three fixed attachments describe a plane perpendicular to the desired boresight, and the adjustable attachments maintain the tension web as a flat surface. All six catenary rope/compression frame attachments have in-plane tensioning devices which maintain the tension web flat within the design limits. Antenna elevation (north-south) adjustments are accomplished by gimbals in the trunnion structure which attaches the antenna to the rotary joint. Azimuth adjustments are made by the rotary joint.
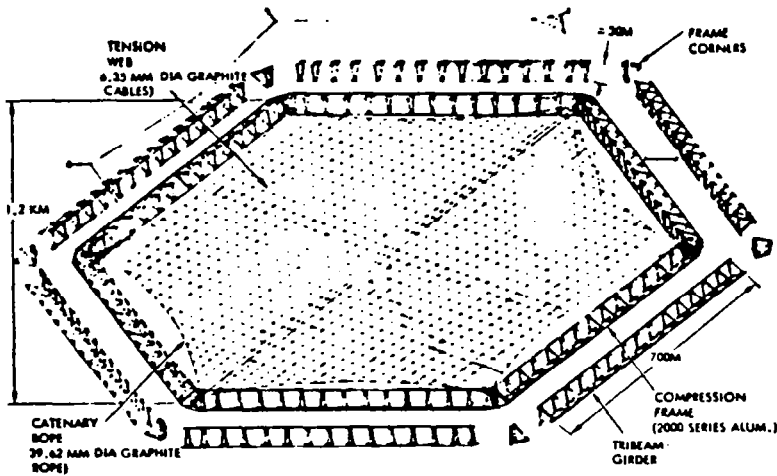
Figure 3.3-38. Microwave Antenna Structure
Selected Design Concept

The basic requirements for the compression frame tension web concept are as follows:

- 1-km-diameter surface (or equivalent)

- Web angular misalignment: ±0.08° under environmentally and operationally induced loads and temperatures

- Optimize for light weight

- Compatible with on-orbit fabrication and assembly

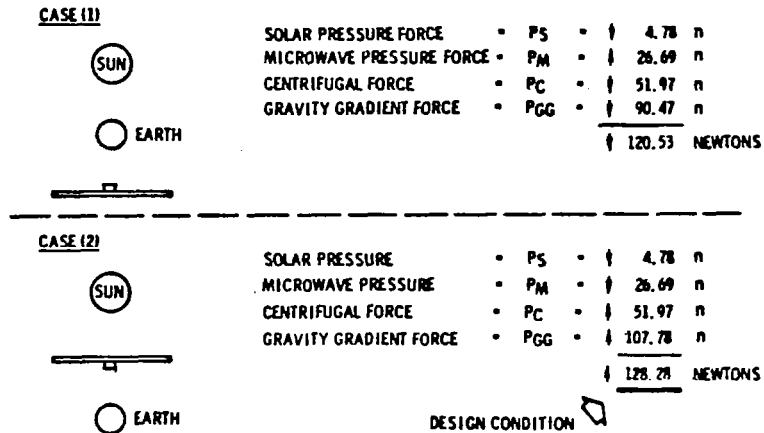- Compatible with operatonal equipment

- Service life: >30 years

CASE (1)

SOLAR PRESSURE FORCE $= P_S = \downarrow$ 4.78 n
MICROWAVE PRESSURE FORCE $= P_M = \downarrow$ 26.69 n
CENTRIFUGAL FORCE $= P_C = \uparrow$ 51.97 n
GRAVITY GRADIENT FORCE $= P_{GG} = \uparrow$ 90.47 n
$\uparrow$ 120.53 NEWTONS

CASE (2)

SOLAR PRESSURE $= P_S = \downarrow$ 4.78 n
MICROWAVE PRESSURE $= P_M = \downarrow$ 26.69 n
CENTRIFUGAL FORCE $= P_C = \downarrow$ 51.97 n
GRAVITY GRADIENT FORCE $= P_{GG} = \downarrow$ 107.78 n
$\downarrow$ 128.28 NEWTONS

DESIGN CONDITION

Figure 3.3-39. Microwave Antenna Structure Design Condition

The antenna structure was subjected to a sizing analysis based on the environmentally and internally induced loads and the pressure forces indicated on Figure 3.3-39, as well as the design requirements listed above. This resulted in the physical properties for each of the three structural elements listed in Table 3.3-19. The tribeam girder side dimension and bay length dimension are 30.57 m. The catenary cables and tension web cables are woven graphite, 0.0396 m (1.56 in.) and 0.0064 m (0.25 in.) in diameter, respectively.

Table 3.3-19. Antenna Structure Elements Physical and Mechanical Properties

ITEM NO.	PARAMETER	COMPRESSION FRAME			CATENARY CABLE	TENSION WEB CABLE
		CAP SECTION	BASIC BEAM ELEMENT	TRIBEAM GIRDER		
1	A_{EM} = EFFECTIVE AREA FOR MASS CALC. (M^2)	0.05×10^{-3}	0.3×10^{-3}	1.8×10^{-3}	1.2×10^{-3}	3.167×10^{-5}
2	A_{EI} = EFFECTIVE AREA FOR MOMENT-OF-INERTIA CALCULATIONS (M^2)	0.09×10^{-3}	0.27×10^{-3}	0.81×10^{-3}	1.2×10^{-3}	3.167×10^{-5}
3	ρ = RADIUS OF GYRATION (M)	23.68×10^{-3}	0.47	12.48	1.58×10^{-5}	1.53×10^{-11}
4	I = GEOMETRY MOMENT OF INERTIA (M^4)	5.15×10^{-8}	0.6×10^{-6}	0.126	1.2×10^{-7}	7.9×10^{-11}
5	E = MODULUS OF ELASTICITY (P_a)	9.65×10^{10}	9.65×10^{10}	9.65×10^{10}	13.79×10^{10}	13.79×10^{10}
6	α = COEFFICIENT OF THERMAL EXPANSION (M/M-°C)	0.18×10^{-6}	0.18×10^{-6}	0.18×10^{-6}	0	0
7	μ = POISSON'S RATIO	0.4	0.4	0.4	TBD	TBD
8	MATERIAL	*	*	*	**	**

*GRAPHITE COMPOSITE, 60% FIBER VOLUME, MADE UP AS (0, ◈, 0)
**WOVEN GRAPHITE

The space frame antenna structure concept is shown in Figure 3.3-40. This concept consists of two basic elements: the space frame primary structure, and the space frame secondary structure. The primary structure is an open truss structure, 138-m deep, with a quasi-square shape approximately 60-m on a side. The outer structure is modified to conform to the shape shown in Figure 3.3-38. The secondary structure consists of an open truss structure, 8-m deep, with a rectangular shape 30×33-m on the two sides. The material used on this concept is the same as that used on the compression frame approach.
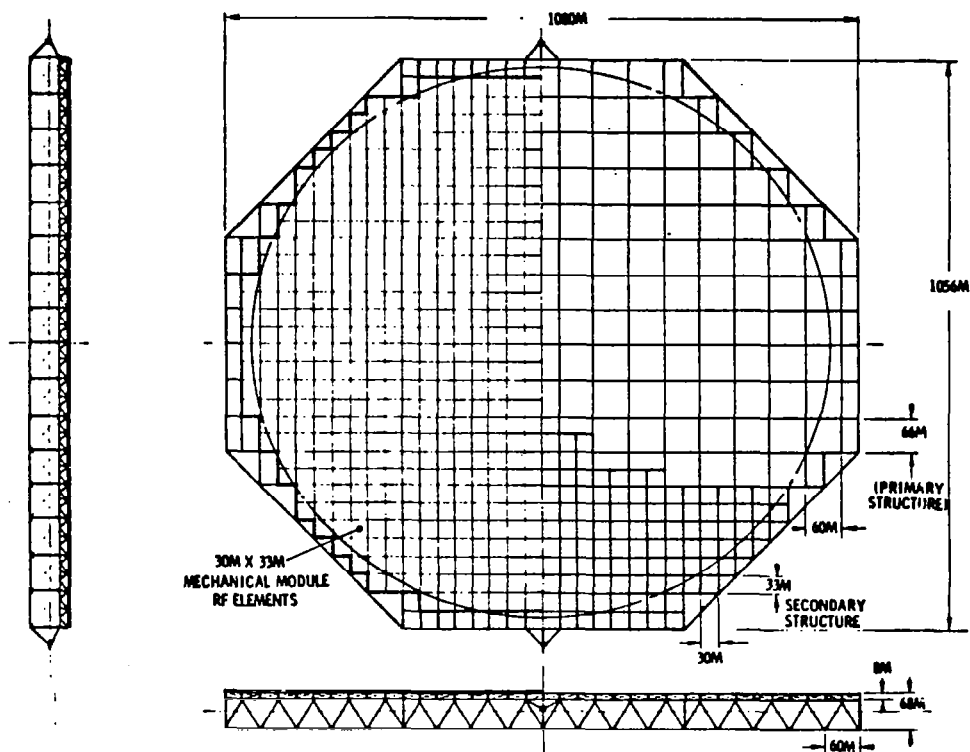

Figure 3.3-40. Space Frame Antenna Configuration

Rotary Joint. The rotary joint attached to the hexagonal center carry-through structure is illustrated in Figure 3.3-41 for the center mount concept. The joint consists of a double set of inner stationary and out-rotating rings. The rings are modified 50-m tribeam girders fabricated on orbit by beam machines. Rotary joint dimensions are noted in Figure 3.3-42. The power transfer slip rings, etc., are discussed in the Power Distribution section. This concept can be termed "large structure/large power transfer rotary joint" configuration. The end mounted concept is illustrated in Figure 3.3-43.

Thermal Control

Introduction. The design of a solar power satellite is significantly influenced by thermal control considerations. The importance of this subsystem may extend well beyond the designation of specific thermal control components
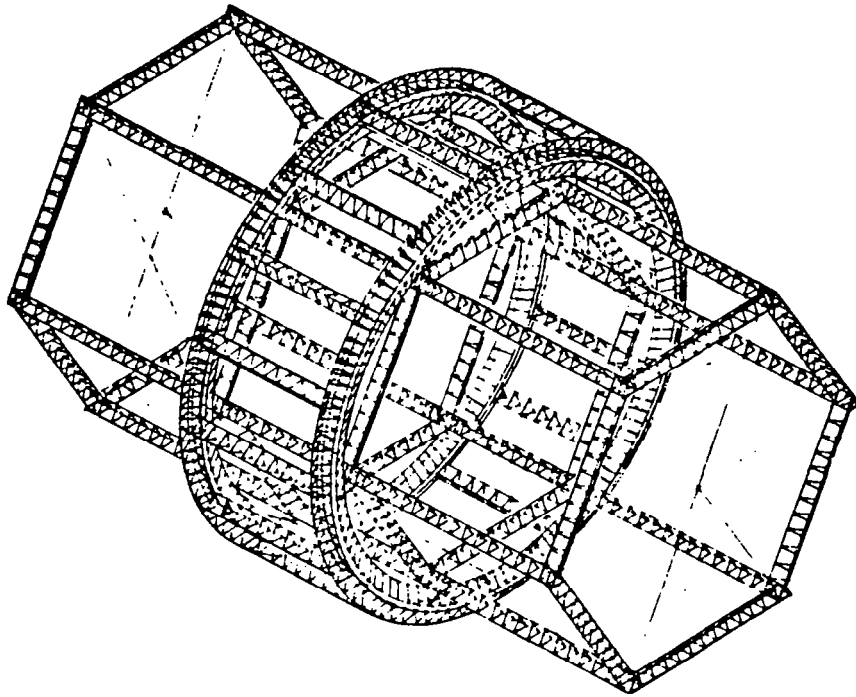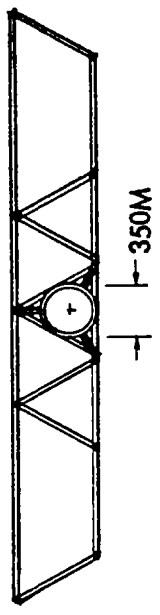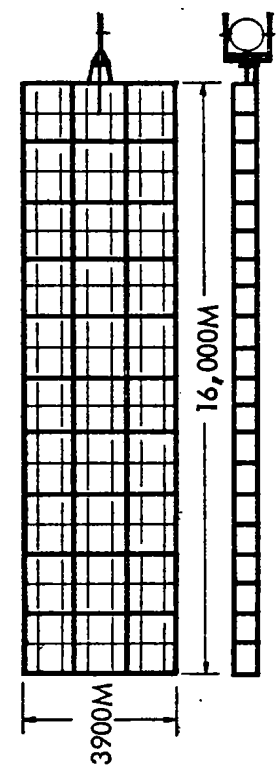
Figure 3.3-41. Rotary Joint Structural Concept
(Center Mount)

inasmuch as it is a major contributing element in the selection of structural
configuration, power distribution network orientation, antenna power levels/
layout, and number and location of rotary joint slip rings.

This description includes those aspects of the SPS point design for which
the thermal control subsystem elements tend to stand alone. In other areas
supported by thermal control, thermal response effects are incorporated into
the individual summary.

The thermal discussion documented here is presented relative to specific
SPS system elements. It covers power conversion, the microwave antenna, and
the rotary joint.

Power Conversion. A model of the photovoltaic baseline design was con-
structed to determine the adequacy of the design to meet blanket operating
temperature specifications, and to identify the effect of coating optical
properties on thermal gradients for incorporation in structural response
analyses. The cross-sectional aspect of the modeled array is shown in
Figure 3.3-44. Preliminary NASTRAN computations were based on the assumption
that the basic material is anodized aluminum with values of $\alpha = 0.4$ and $\varepsilon = 0.8$
for absorptivity and emissivity respectively.
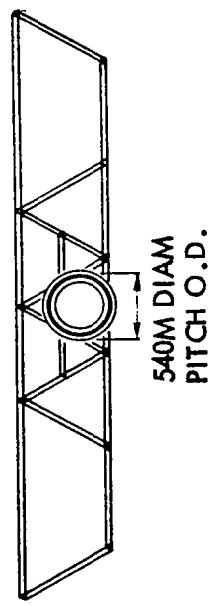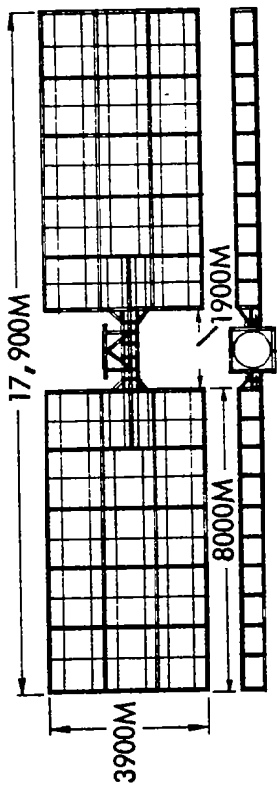
Figure 3.3-42. Rotary Joint Preliminary Dimensions
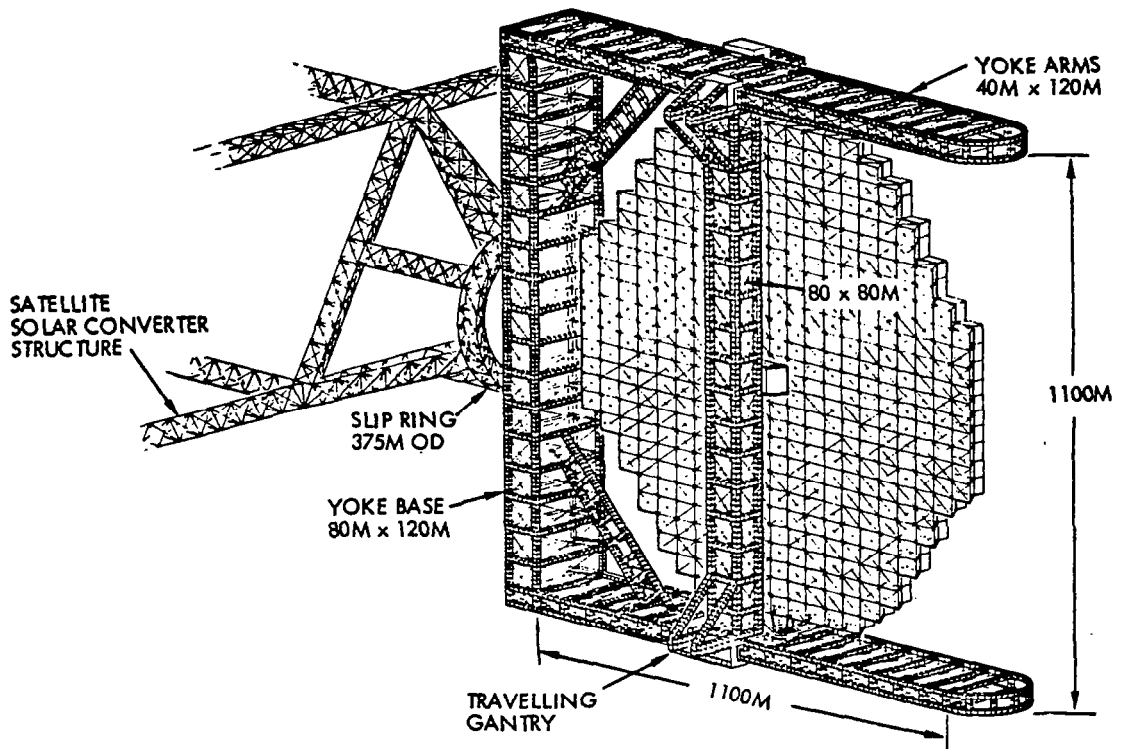
END MOUNT

CENTER MOUNT

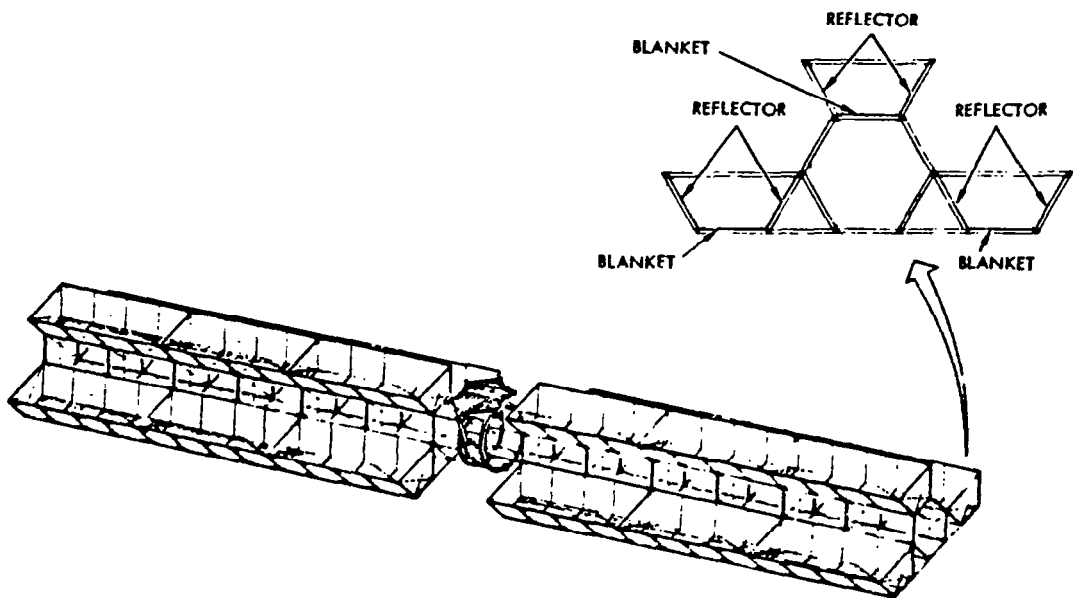Figure 3.3-43.   Rotary Joint Structural Concept
(End Mount)

Figure 3.3-44.   Photovoltaic Structure Model

Anodization can also be used to provide a higher α/ε ratio (≈1.0) if desired. Computer thermal profiles for aluminum are shown in Figure 3.3-45.
The thermal profile for a composite based structure is shown in Figure 3.3-46.
The temperatures shown for the structure, blanket, and reflectors are based
upon a solar constant of 1355 W/m². Optical properties for the solar cells
and concentrators were based upon nominal inherent values for the materials
of construction, i.e., selective coatings were not assumed. There may be
some concern over the use of anodization to provide desired optical properties
due to possible degradation which might occur during reforming or joining
operations in space. It appears that bending operations, such as brake form-
ing, would affect the surface properties if the length change were significant.
Degradation would result from cracking or crazing which would expose the under-
lying base material. The extent of emissivity reduction would also depend on
the original thickness of the anodized film. Although some local hot spots
could occur, it is not expected that the degree of additional heating would be
excessive. Welding operations through an anodized layer are possible, but
would likely result in poor attachment. Welding side to side would require an
initial grinding or cutting operation. If the joining is end to end, a pre-
liminary shearing step to remove the edges and expose the bare metal could be
used.

COATED ALUMINUM
OPTICAL PROPERTIES
α = 0.4
ε = 0.8
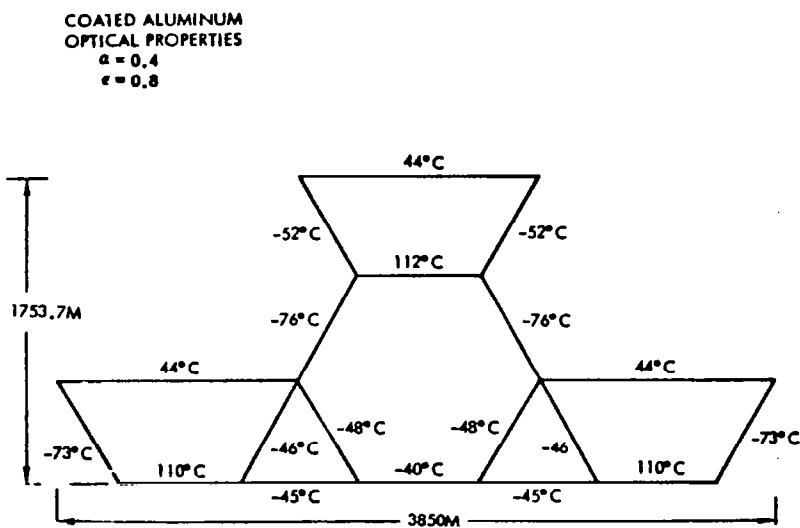
Figure 3.3-45. Photovoltaic Structural Configuration
Temperatures (Aluminum)

Several graphite fiber composites were considered as candidates for the
satellite. Table 3.3-20 summarizes the estimated maximum temperature (based
upon General Dynamics quoted data and on Rockwell estimates) for the various
candidates.

The temperature of the solar blankets is 110°C to 112°C. As it is desired
to operate at a temperature between 113-125°C to promote the GaAlAs self-
annealing characteristic, some modification to the blanket design is expected.
Because of the temperature uniformity of the three blanket sections, any changes

Figure 3.3-46. Photovoltaic Strutural
Configuration Temperatures
(Graphite Composite)

Table 3.3-20. Maximum Estimated Temperatures
(Graphite Composite)

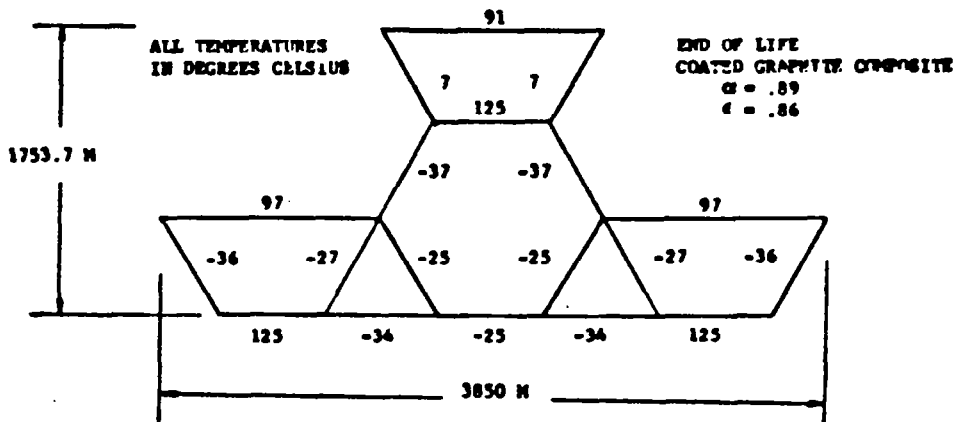| MATERIAL	MAX. ALLOWABLE TEMP. $^{\circ}K$
THERMOSETTING RESINS	
EPOXY	395
PHENOLIC	435
POLYIMIDE	
ADDITION	475
CONDENSATION	560
THERMOPLASTIC MATERIALS	
POLYSULFONE	380
POLYIMIDE	590

introduced would be common to the array. The simplest approach is to reduce the rear surface emissivity from the design value of 0.68 to 0.36; this can be achieved at a negligible weight impact by the somewhat complex approach of vapor depositing a mosaic grid of several hundred angstroms of aluminum, or more simply by adding approximately 1/4 mil of Kapton (or Mylar) rear-surface-coated aluminum to the blanket. The required emissivity reduction would be moderated if self-annealing could be satisfied by periodic shutdown of individual bays to increase thermal loads through elimination of electrical conversion. The selected approach was to add the thin aluminized plastic layer.

Switch Gear. At 99.9% efficiency, thermal losses per unit are 12,000 watts and this level is accommodated by appropriate sizing to permit passive rejection. Relative base dimension requirements as a function of design temperature are shown in Figure 3.3-47 for a cubic configuration. At a postulated allowable temperature of 60°C a length of 2 meters is adequate and consequently it is expected that any mass additions relative to the previous design concept of a 1 meter cubed casing will be minimal.
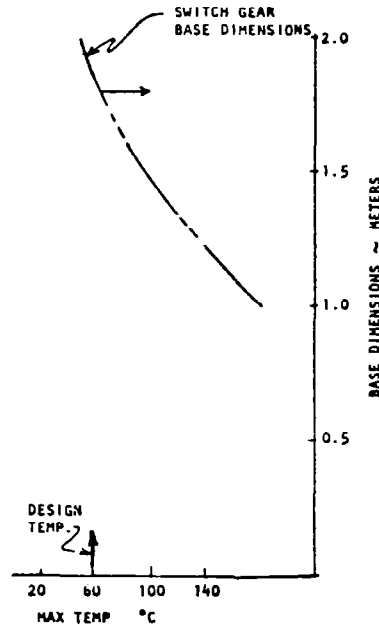
Figure 3.3-47. Power Distribution Component
Thermal Control - Switch Gear

Microwave Antenna. Thermal control of the microwave antenna includes protection of the klystrons and associated electronics, the antenna structure, and consideration of the impact of antenna thermal response on the rotary joint.

The antenna structure configuration can experience minimal distortions/deflections due to imposed thermal gradients/stresses. A thermal model of the hexagonal frame/web structure for the center mounted configuration was

developed for variable solar orientations to determine peak operating temperatures and thermal gradients, and to support dynamic structural response computations. The model, shown in Figure 3.3-48, assumed that the earth side of the web could be treated as an isothermal section at T = 200°C, and the space side of the web could be fixed at an isothermal temperature of 60°C. This represents a simplification because the hot side of the web will vary with time due to solar loading and will vary with distance from the center due to RCR density and size variation. There may also be some influence by the higher temperature collector radiators (≈700°C) on structural temperature. The space side of the antenna changes temperature with sun loading also, and will probably operate between 0°C and 60°C (effective temperature).
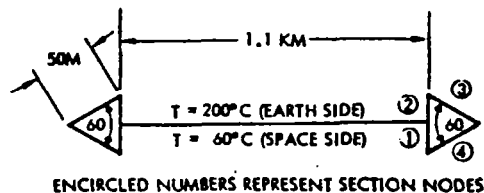

ENCIRCLED NUMBERS REPRESENT SECTION NODES

Figure 3.3-48. Antenna Frame/Web Model

Nodal points were selected as shown (Figure 3.3-48), and the thermal analysis was conducted assuming that each section was represented as a uniform node at a single temperature. View factors to space and from element to element were determined from an exact representation of the section by using the CONFAC computer code.

Due to variation in solar incidence during each orbit, the sections of the frame will experience time-varying temperature. Temperature profiles are shown in Figure 3.3-49 for a typical orbit representing the response of a low α/ε anodize structural coating and, in Figure 3.3-50, for a degraded coating condition. (If could also represent a "dark" or high α/ε anodize structural coating.) For an eclipse condition, the minimum temperature levels and thermal profiles would markedly change. Temperature gradients during construction would also influence the structural design.

In the space frame configurations the primary structure is in close proximity to the high temperature, heat rejection surface of klystrons. Independent studies by Rockwell, General Dynamics, and Grumman have demonstrated that temperatures in the central region of the antenna will exceed allowables for low temperature composites. For beam machine concepts this can complicate the construction scenario by potentially requiring the substitution of a different machine at some point in the assembly sequence. This problem is illustrated in Figure 3.3-51 for the candidate polysulfone resin assuming a "worst case" condition. In this environment the temperature could exceed the allowable maximum even if the klystron heating is neglected.
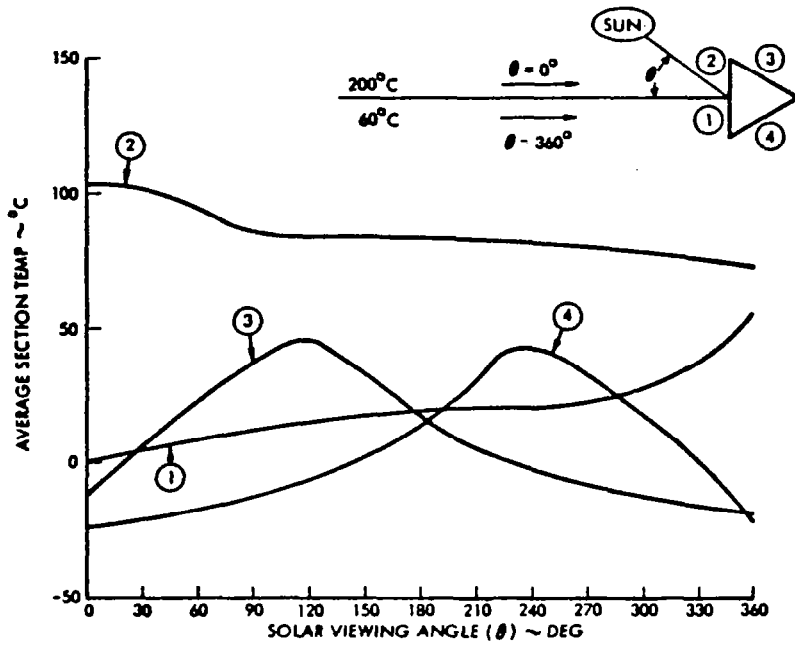
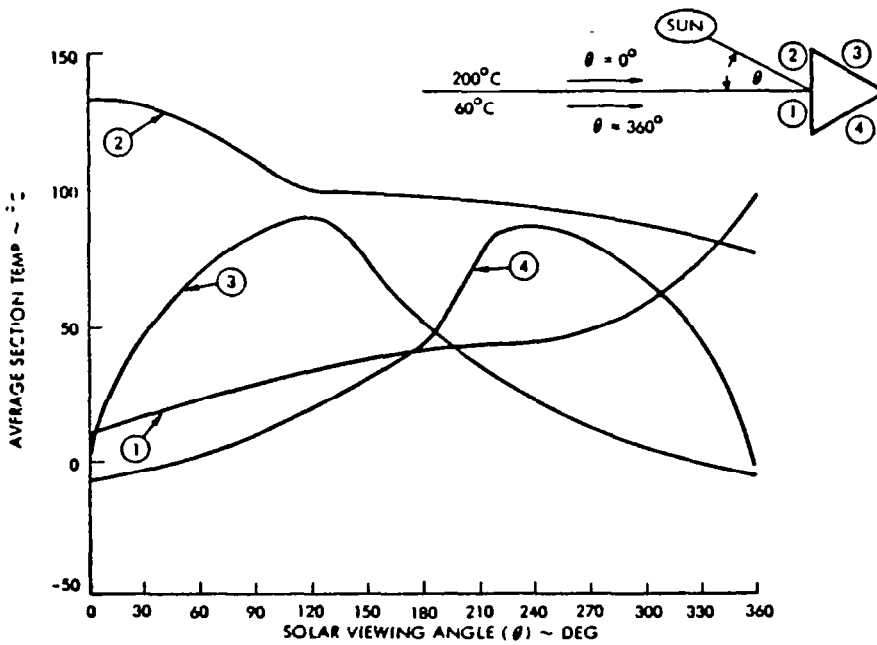Figure 3.3-49. Frame Temperature Variation with Solar Orientation (BOL)

Figure 3.3-50. Frame Temperature Variation with Solar Orientation (EOL)

● ASSUME MAX. ALLOWABLE TEMP. = 380°K; α_s = .9 ϵ = .8

FOR THESE PROPERTIES THE MAXIMUM ALLOWABLE EFFECTIVE
ANTENNA TEMPERATURE IS (APPROXIMATELY):

$$(.9)\ (1352) + .8\sigma\ (T^4_{MAX} - 400^4) = .8\sigma\ 400^4 \quad OR \quad T_{MAX} = 395°K$$

● FOR "WORST CASE" SOLAR LOADING ON ANTENNA (EVEN IF KLYSTRON
EMITS ZERO POWER) ASSUMING RADIATOR HAS BLACK COATING AND
ZERO CAPACITANCE STRUCTURE.

$$(.93)\ (1352) = .85\sigma\ T^4 \quad OR \quad T_{MAX} = 402°K$$

∴ UNDER WORST CASE ASSUMPTIONS LOW TEMP. COMPOSITES MAY BE
MARGINAL FOR ZERO POWER KLYSTRONS.

*Figure 3.3-51. Space Frame Configuration Limitations
of Low Temperature Composites*

For compression frame-tension web structures this situation can not occur. The frame will experience relatively low temperatures and the secondary structure is sufficiently removed from the center of the antenna to permit application of low temperature composites. This represents a substantial thermal advantage for tension web structures.

A thermal control design was developed for the klystron tubes to dissipate the waste heat levels and minimize interactions with the antenna structure and rotary joint. The thermal rejection requirement includes a cavity heat load of 3.267 kW and a collector heat load of 7.454 kW. It was determined that a heat pipe radiator for the cavity tube would provide a high-confidence/low-mass system. The relative orientation of the slots and the heat pipes in the baseline RCR is shown in Figure 3.3-52, along with the relative location of the insulation and electronics.

The primary candidate klystron study designs are illustrated in Figure 3.3-52. The initial Rockwell baseline power module was selected during Phase 1 because of thermal rejection considerations relative to potential overheating of the slip rings, temperature limitations on the electronics and the postulated requirement (later deleted) for manned access to the antenna during operation. The alternate Rockwell concept, which has been adopted during Phase 2, eliminates the performance uncertainty and efficiency losses resulting from poking the klystron tube through the radiator. This selection follows from analyses which demonstrate that the slip rings can be thermally protected and that the weight penalty associated with controlling electronic component temperatures is relatively small. This klystron concept appears more advantageous than the Boeing concept because of its less complex and lighter weight thermal control system. In addition, it appears more flexible in terms of distributing the heat to be rejected in both directions (space and earth).

The RCR design as shown (Figure 3.3-52), is representative of a unit near the center of the antenna. Modules will vary in size and heat pipe spacing/number throughout the antenna. A top view exhibiting relative orientation of the klystron pipes for the "poke through" concept is presented in Figure 3.3-53. The rear mounted approach is shown in Figure 3.3-54. The heat pipes all use

EARTH SIDE HEAT REJECTION CONCEPT

DISTRIBUTED EARTH AND SPACE HEAT REJECTION CONCEPT

INSULATION

ELECTRONICS

HEAT PIPES

RCR

HEAT PIPE

COLLECTOR

ROCKWELL BASELINE
POWER MODULE CONCEPT

SPACE

SHIELD

ELECTRONICS

INSULATION

COLLECTOR

HEAT PIPES

RCR

EARTH

ROCKWELL ALTERNATE POWER
MODULE CONCEPT

POWER MONITOR
DIPLEXER   ARC SENSOR
THERMAL CONTROL RADIATOR
THERMAL CONTROL HEATPIPES
KLYSTRON
SUPPORT BEAM

SOLID STATE
CONTROL DEVICE
DISTRIBUTION
WAVEGUIDE
RADIATING WAVEGUIDE

BOEING POWER
MODULE CONCEPT

LATERAL I-BEAM

POWER DISTRIBUTION CABLING

Figure 3.3-52.   Klystron/RCR Configurations

ARTERIAL WICK HEAT PIPE
28" LENGTH, 1/2 IN. O.D.
4 REQ'D

AXIAL GROOVE HEAT PIPE
25 IN. LENGTH, 3/8 IN. O.D.
28 REQ'D

ΔT_1

ΔT_3

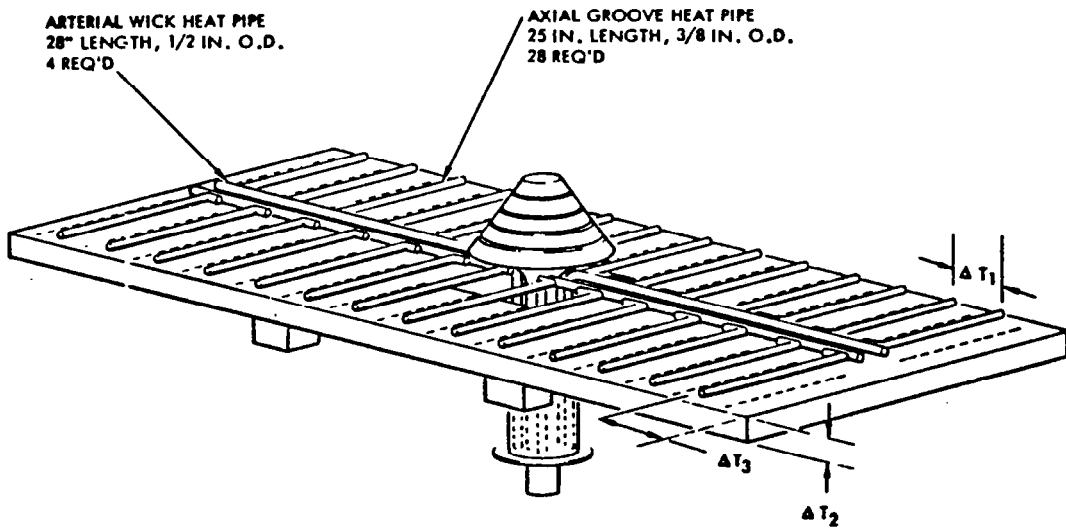ΔT_2

Figure 3.3-53.   Klystron Raidator Configuration
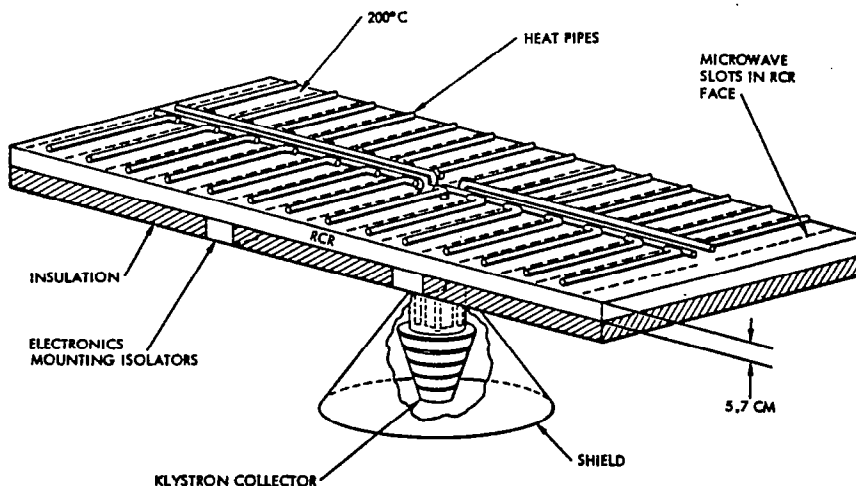(Poke Through)

*Figure 3.3-54. Klystron Radiator Configuration
(Rear Mounted)*

water as a working fluid encased in a copper liner. The outer tube is aluminum
to eliminate the single-point contact of dissimilar metals. The spacing of the
axial groove heat pipes is 11.4 cm. Any one of the arterial wicked pipes can
fail and the system will still reject the incident heat load and maintain
allowable temperature limits, although the structural response for this mode
must be evaluated. There are four of these arterial wick pipes, each 1/2 inch
O.D.; and 28 axial groove pipes, each 3/8 inch O.D. The layout of the pipes
is dictated by the microwave slots which will not permit a more optimal radial
distribution. Total mass of this subsystem is 6.18 kg.

Thermal distortions may occur as a result of various temperature gradients
occurring in the RCR as shown in Figure 3.3-55. The temperature drop across
the fin length will be about 40°C. Thermal gradients from one face of the RCR
to the other face are shown as a function of internal emissivity. The value
of 0.9 corresponds to the use of a high emissivity coating (e.g., black anodize)
and the lower limit of 0.1 is representative of bare aluminum. Gradients at
the end of the RCR depend upon the fraction of the surface that is used for
radiator, and the view factor variation to the collector radiator. The value
shown (63°C) is an average value for the high-density portion of the antenna.

The collector radiator (Figure 3.3-56) is required to dissipate the 7.5 kW
of waste heat dissipated due to beam inefficiencies. The pyrolytic graphite
structure must have a relatively high fin efficiency to maintain local temper-
ature below 700°C. If required, radiation shields can be used to isolate the
collector from the cavity radiator. This would reduce the effective rejection
capability and require higher temperature operation on thicker fins. The
effect of fin efficiency on radiator temperature is shown in Figure 3.3-57.
It can be seen that the minimum possible operating temperature is only slightly
below 700°C. This assumes that the waste heat distribution can be controlled
and is rejected equally from the radiator segments.

ΔT_1 • TEMP DROP BETWEEN HEAT PIPES
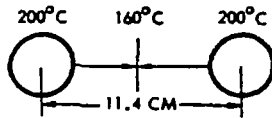
ΔT_2 • TEMP DROP FROM TOP OF RADIATOR TO BOTTOM OF RADIATOR

EMISSIVITY OF OPPOSITE SURFACE	ϵ	ΔT ^{0}C
	0.9	3^0
	0.5	5^0
	0.1	21^0

ΔT_3 • TEMP DROP FROM END OF HEAT PIPES TO END OF KLYSTRON RCR - $200^0C \longrightarrow 137^0C$

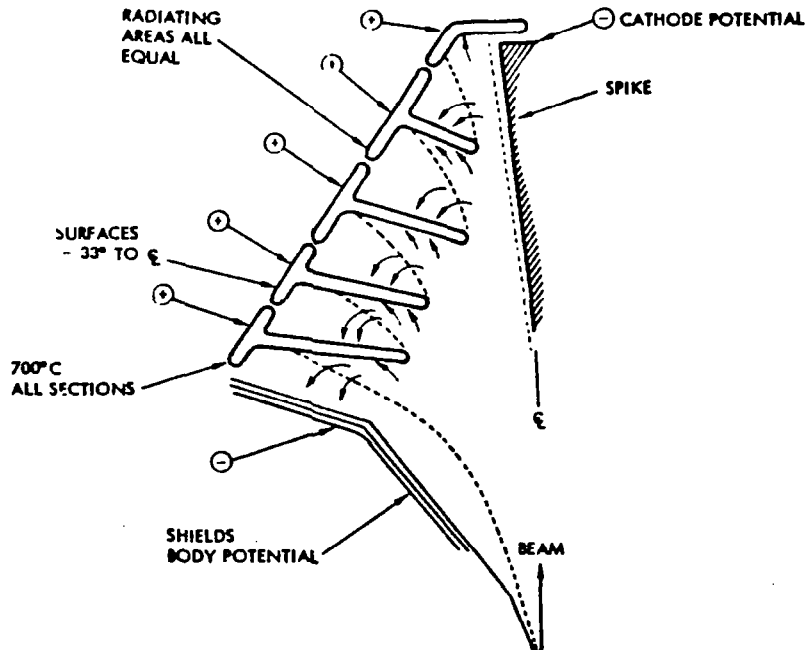*Figure 3.3-55.   Related Design Configurations*

Figure 3.3-56.   Collector Radiator

- ASSUME RAD FIN IS PYROLYTIC GRAPHITE

- COLLECTOR AREA IS 0.173 M^2

  (8 IN. HIGH CONE, r_1 = 7 IN., r_2 = 1.75 IN.)

  ASSUME ALL SECTIONS EQUAL

  ASSUME α = ϵ = 0.9

  ASSUME SOLAR FLUX (EFF) = 35 WATTS

FIN EFFICIENCY η	TEMP ^{0}C
1.0	687
0.9	712 ← BASELINE DESIGN
0.8	742
0.7	776
0.6	818
0.5	868
0.4	934

Figure 3.3-57. Collector Radiator Analysis

Insulation is required for the back surface of the cavity radiator to restrict waste heat leaks which could increase temperature of the electronics to unacceptable levels. This insulation must be coated externally with low α/ϵ materials to limit the absorbed solar flux to which the surface is exposed during part of the orbit. Although many materials with low absorptivity/emissivity ratios are available, they typically experience substantial degradation as a function of solar exposure time. To limit the rear surface to 60°C (maximum allowable temperature of electronics), it is seen in Figure 3.3-58 that the maximum α/ϵ ratio is about 0.5, which is below values typically obtained for extended-life inexpensive insulations. If refurbishment of degraded blanket is not possible, the electronics could be protected by isolation in finned containers or by use of active cooling. Alternatively, advanced blankets using more expensive external surfaces (e.g., quartz microsheet) could be applied at some cost penalty.

Temperature extremes across the antenna (center to edge) are presented in Table 3.3-21 for the Phase 1 baseline and improved klystron concepts. The edge values assume that the total allowable radiator area is used. Temperatures at the center were calculated for no rear surface insulation or collector shield. If the shield is used then the maximum value would be approximately 100°C. The high proportion of waste heat that can be rejected from the earth side (≈30%) represents a significant advantage of this concept.

Additional sources of heat generation on the antenna are the high voltage dc-dc converters. The 32 units on the antenna operate at 96% efficiency and dissipate 300 megawatts each. To maintain a 60°C design limit active cooling must be provided. Figure 3.3-59 illustrates the required radiator area and associated system penalties at different temperature levels. For 60°C the antenna mass must be increased by about 1.3×10^6 kg for the purposed cooling system which utilizes an integrated heat pipe radiator design that incorporates optimized radial fin geometry.
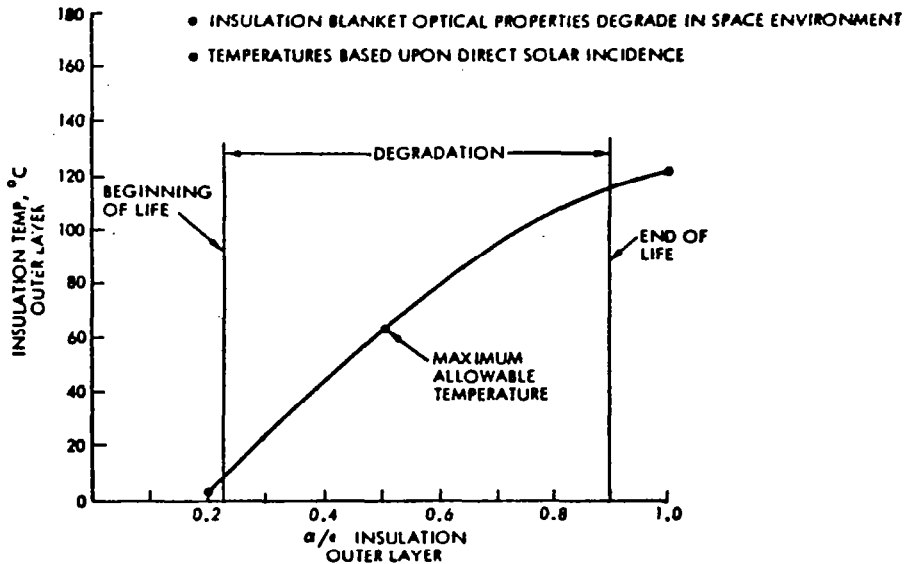
Figure 3.3-58. Rear Surface Cavity Radiator
Thermal Response

Table 3.3-21. 50 kW Klystron Radiator
Thermal Levels

		ANTENNA CENTER	ANTENNA EDGE
BASELINE KLYSTRON (TUBE POKED THROUGH) EARTH SIDE RADIATOR		152°C	-4°C
IMPROVED KLYSTRON (COLLECTOR RADIATES IN SPACE DIRECTION)	EARTH SIDE SPACE SIDE	129°C 104°C	-14°C -23°C

Rotary Joint. The orientation of the rotary joint relative to the photo-voltaic structure and the antenna is shown in Figure 3.3-60. Proximity to the space-facing side of the antenna substantially influences both the antenna design and the rotary joint thermal environment. Temperature levels for the slip rings and brush boxes were computed for the design configuration. The slip rings were assumed to be aluminum-core/coin-silver cladding of 1.1 km diameter, and I-beam shape with a current/wing design value of 112,500 A.

The temperatures shown in Figure 3.3-61 represent average values for the inner slip ring based on a voltage loop of 20 V across the slip ring-brush interface. For aluminum, the maximum allowable operating temperature is about 150°C. To provide assurance of structural integrity, it is necessary to de-monstrate the excessive stresses do not result from the thermal gradients developed in the rings. Both rings were thermally modeled to include the

3-79
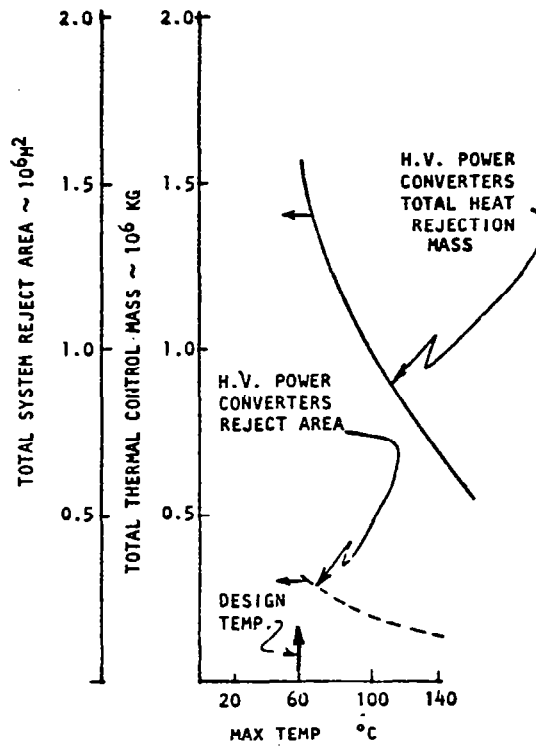
Figure 3.3-59. Power Distribution Component
Thermal Control - HV Converters
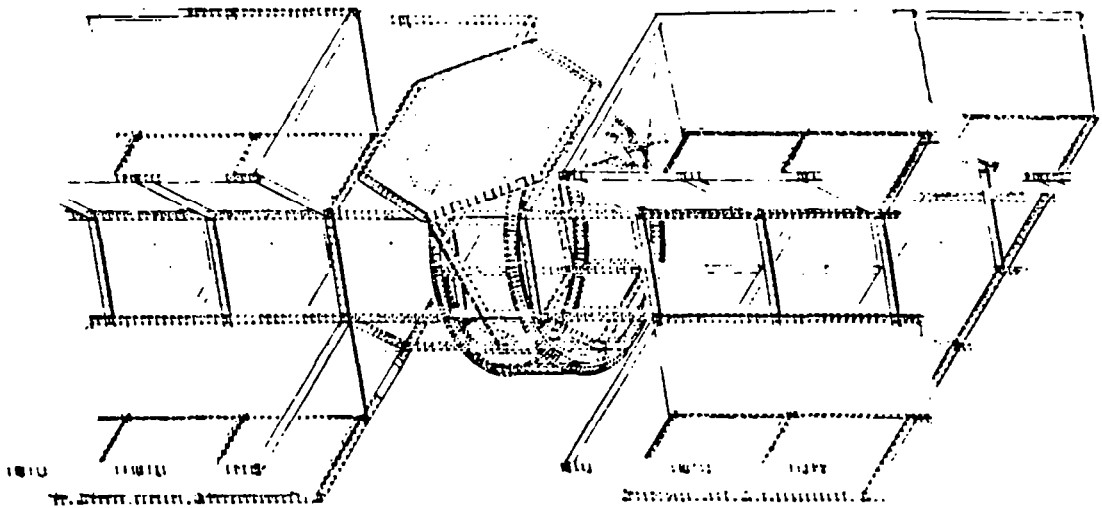
Figure 3.3-60. Rotary Joint Installation
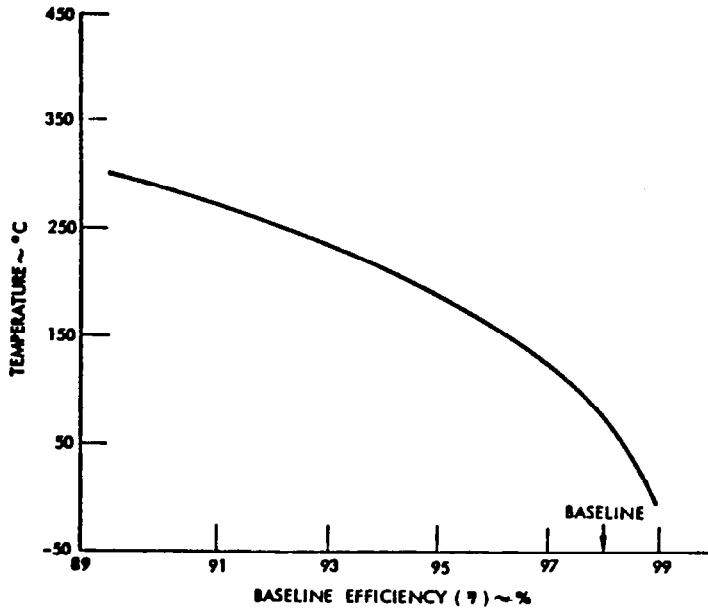
*Figure 3.3-61. Slip Ring Temperature Variation
With Efficiency*

effects of electrical inefficiencies, antenna interactions, and solar heating. Temperature levels are shown in Figure 3.3-62. The outer ring can reach a higher temperature because it shields the inner ring from the sun. Brush assembly temperatures will approximate the slip ring values due to conduction across the contact area. Additional electrical losses are relatively negligible. During eclipse, the klystrons must be kept warm and thus some relatively large gradients may occur because radiation from the antenna is the sole heating source.

- INNER RING $65^{\circ}C$ TO $115^{\circ}C$

- OUTER RING $65^{\circ}C$ TO $130^{\circ}C$

- BRUSH ASSEMBLY TEMPERATURES SIMILAR
  TO SLIP RING VALUES

- FOR ALTERNATE KLYSTRON DESIGN RING
  TEMPERATURE CAN EXCEED $370^{\circ}C$

- ECLIPSE PROFILES NOT YET DETERMINED -
  MAY BE VERY SEVERE

*Figure 3.3-62. Rotary Joint
Temperature Gradients*

3.3.2 GROUND RECEIVING STATION

The ground receiving station (GRS) consists of two major system elements and several additional supporting subsystems (Figure 3.3-63). The first is the receiving antenna/rectifier circuit (rectenna) portion of the Microwave Power Transmission System. A second element consists of the power distribution subsystems required to collect, switch, converter, and transfer the received/ rectifier power to the associated utility power network. The remaining subsystem will only be touched upon.

```
                    ┌──────────────┐
                    │   GROUND     │
                    │  RECEIVING   │
                    │   STATION    │
                    └──────────────┘
```

| RECTENNA | POWER DISTRIBUTION AND CONTROL | POWER CONVERSION | THERMAL CONTROL |

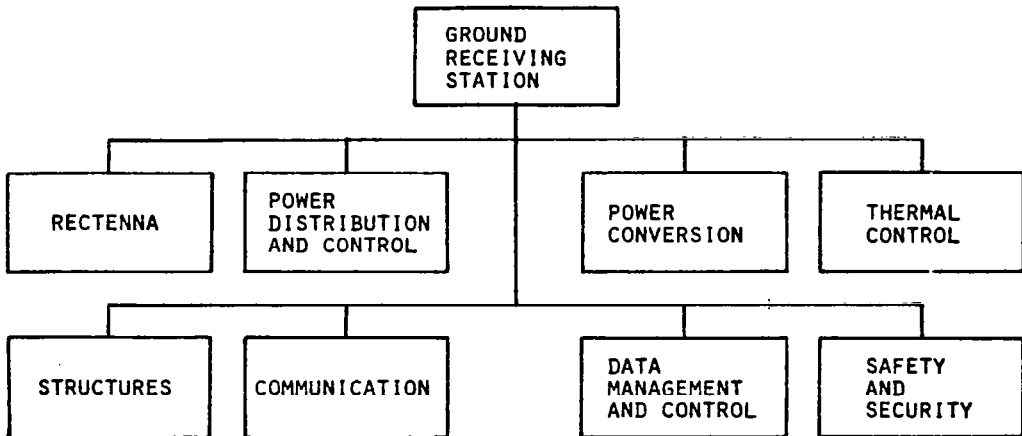| STRUCTURES | COMMUNICATION | DATA MANAGEMENT AND CONTROL | SAFETY AND SECURITY |

Figure 3.3-63. Ground Receiving Station Subassembly Relationships

Each rectenna is designed to accept power from a single satellite and provide 5.5 GW (nominal) at the interface to the power distribution subsystem. As shown in Figure 3.3-64, the typical GRS site located at 34° N latitude includes an elliptical rectenna area, 13 km in the N-S direction by 10 km in the E-W direction. The overall GRS encompasses approximately 35,000 acres. The rectenna area consists of approximately 25,200 acres or 72% of the total acreage. The area surrounding the inner ellipse is utilized for maintenance facilities, access roads, converter stations and the two peripheral rows of towers which support the intermediate (40 kV dc) and high voltage (500 kV ac) transmission wires.

A summary of the GRS point design specification is provided in Table 3.3-22.

Rectenna

The rectenna subsystem consists of microwave receiving elements (dipoles), rectifiers, regulators and isolating motor switches (Figure 3.3-65). The dipoles are fabricated using a multilayer (sandwich) construction of copper and dielectric insulators formed into panels. A rectification element consisting of a GaAs diode and filters is added to convert the received microwave energy into dc. Conversion efficiency is estimated to be 89%.
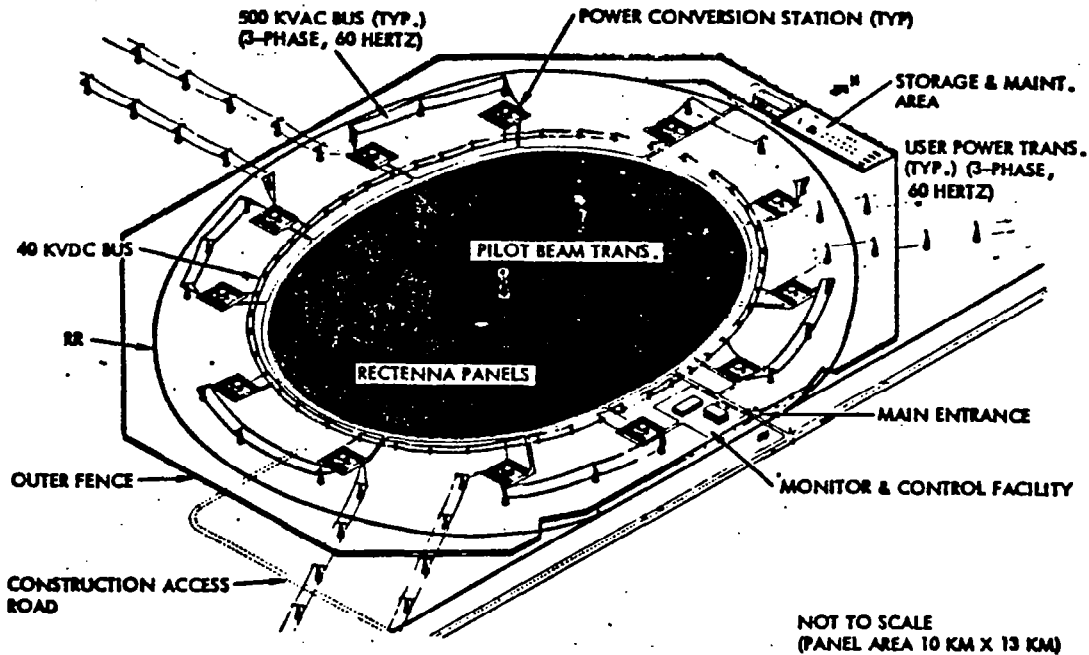
Figure 3.3-64. Operational Ground Receiving Facility
(Rectenna) - Typical

Table 3.3-22. GRS Point Design Summary

FREQUENCY (GHz)	2.45
INTERCEPTED ENERGY (GW)	5.53
RECTENNA EFFICIENCY (%)	89
DIPOLE CLUSTER AREA (m^2)	
INNER AREA (R = 0 TO 5.5 km)	0.186
PERIMETER (5.5-6.5 km)	1.674
DIPOLE CLUSTER OUTPUT (W)	6-42
VOLTAGE STRING OUTPUT	
VOLTAGE (kV)	40.5
CURRENT (A)	0.321
POWER (kW)	13.0
RECTENNA OUTPUT (GW)	4.93
PANEL DIMENSIONS (m)	9.33 H × 14.69 W
RECTENNA CONFIGURATION	ELLIPSE
RECTENNA DIMENSIONS (km)	10×13
NUMBER OF PANELS IN RECTENNA	580,500
PANEL AREA (km^2)	79.56
GROUND AREA (km^2)	102.1
GRS GROUND AREA (ACRES)	35,000

Incident Radiation. The energy transmission pattern at the transmitting
antenna is specified to be 10 dB Gaussian (modified). The received energy
levels in the rectenna area is approximated along the rectenna major axis
(13 km N-S) in Figure 3.3-66. The limit of 23 mW/cm^2 at the center, reducing
to 1.0 mW/cm^2 at the perimeter is compatible with present environmental limits
as stated in the program guidelines.

```
                    ┌──────────────┐
                    │  RECTENNA    │
                    └──────┬───────┘
        ┌────────────┬─────┴──────┬─────────────┐
  ┌───────────┐ ┌──────────┐ ┌───────────┐ ┌───────────┐
  │  ANTENNA  │ │RECTIFIERS│ │ REGULATORS│ │ SWITCHING │
  └───────────┘ └──────────┘ └───────────┘ └───────────┘
```

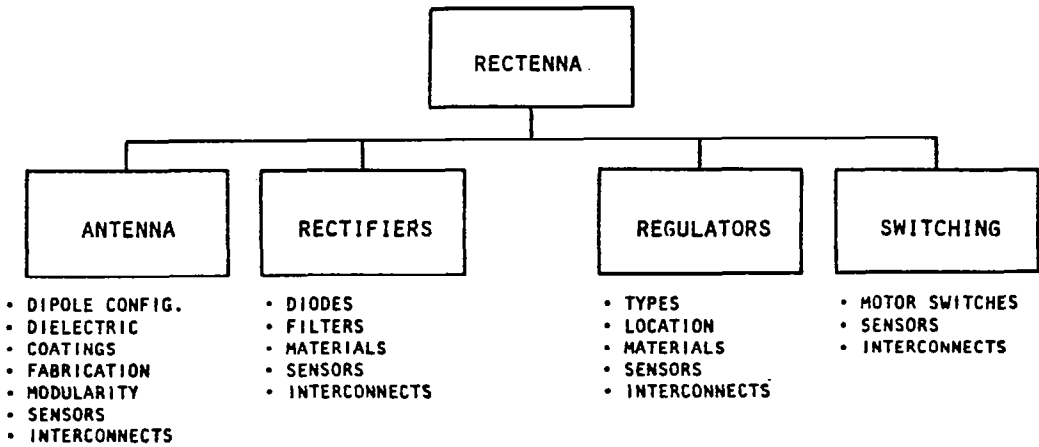|			
• DIPOLE CONFIG.	• DIODES	• TYPES	• MOTOR SWITCHES
• DIELECTRIC	• FILTERS	• LOCATION	• SENSORS
• COATINGS	• MATERIALS	• MATERIALS	• INTERCONNECTS
• FABRICATION	• SENSORS	• SENSORS	
• MODULARITY	• INTERCONNECTS	• INTERCONNECTS	
• SENSORS			
• INTERCONNECTS			

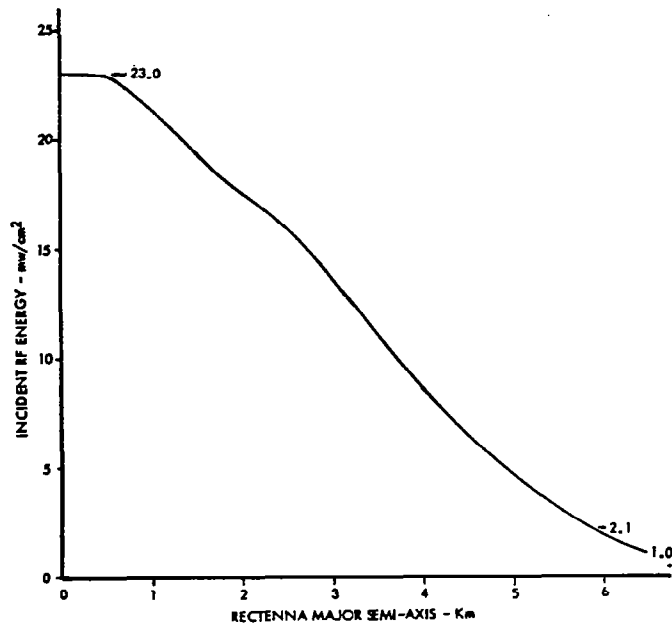*Figure 3.3-65.   Assembly Tree - Rectenna*

Figure 3.3-66.   Rectenna Incident Power Density

To further reduce the complexity of the design analysis it was decided to consider the incident energy as consisting of five doughnut shaped energy zones as illustrated in Figure 3.3-67. The average energy level within each zone was then estimated. The average level was then stated to exist at all points within the stated zones. The established average power density levels used to determine the various design parameters is identified in Figure 3.3-67.

Antenna. The receiving antenna is a multilayer copper/dielectric sandwich panel as shown in Figure 3.3-68. The total antenna system consists of 580,500 9.33×14.69 m panel assemblies. Each panel assembly is prepared by assembling and interconnecting 20 - 0.735×9.33 m subpanels and mounting on a steel structure. The full panel assembly is illustrated in Figure 3.3-69. Also included on the antenna panel assemblies are the associated rectifier elements. The
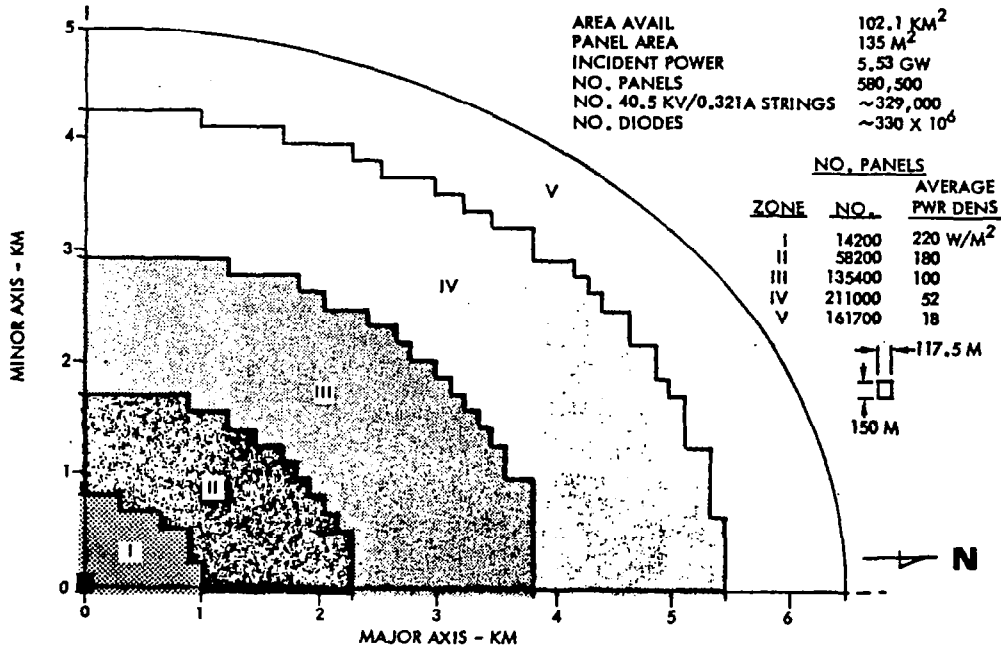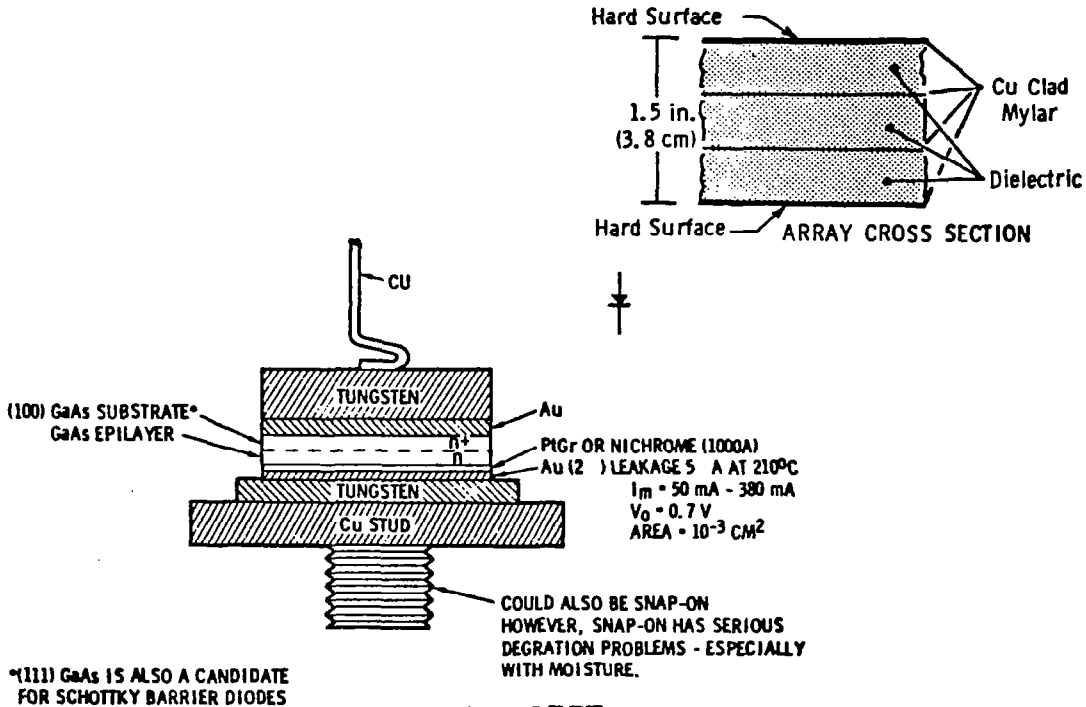
AREA AVAIL   102.1 KM^2
PANEL AREA   135 M^2
INCIDENT POWER   5.53 GW
NO. PANELS   580,500
NO. 40.5 KV/0.321A STRINGS ~329,000
NO. DIODES   ~330 X 10^6

ZONE	NO. PANELS NO.	AVERAGE PWR DENS
I	14200	220 W/M^2
II	58200	180
III	135400	100
IV	211000	52
V	161700	18

V

IV

III

II

I

MINOR AXIS - KM

5
4
3
2
1
0

MAJOR AXIS - KM
0   1   2   3   4   5   6

117.5 M

150 M

N

Figure 3.3-67.   Rectenna Power Density Pattern (34° N Latitude)

Hard Surface
1.5 in.
(3.8 cm)
Hard Surface
Cu Clad Mylar
Dielectric
ARRAY CROSS SECTION

CU

TUNGSTEN
Au
(100) GaAs SUBSTRATE*
GaAs EPILAYER
n+
n
PtGr OR NICHROME (1000A)
Au (2) LEAKAGE 5 A AT 210°C
I_m • 50 mA - 380 mA
V_0 • 0.7 V
AREA • 10^{-3} CM^2
TUNGSTEN
Cu STUD

COULD ALSO BE SNAP-ON
HOWEVER, SNAP-ON HAS SERIOUS
DEGRATION PROBLEMS - ESPECIALLY
WITH MOISTURE.

*(111) GaAs IS ALSO A CANDIDATE
FOR SCHOTTKY BARRIER DIODES

DIODE CONCEPT

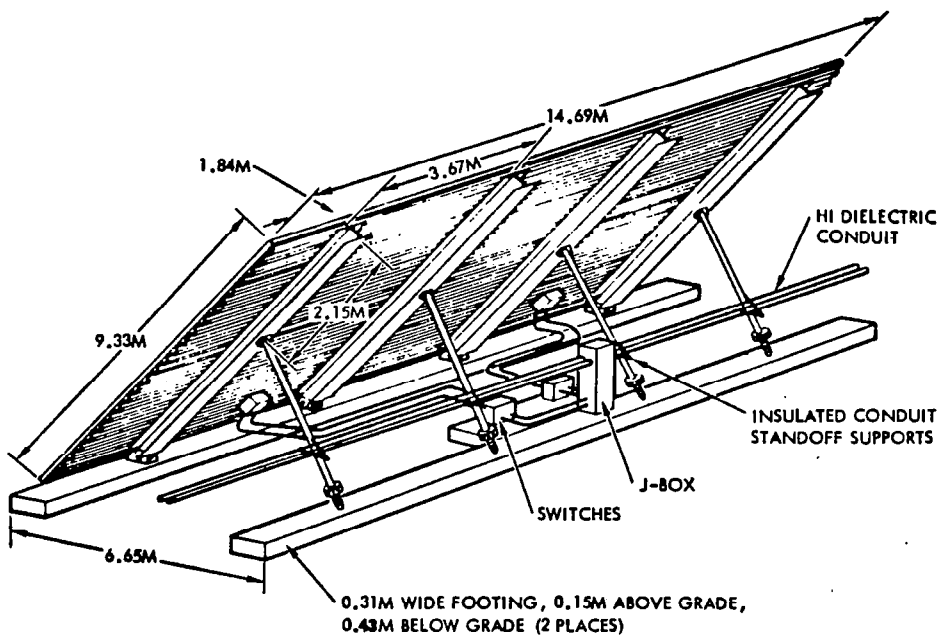Figure 3.3-68.   Rectenna Systems Major Assembly/Component

3-85

Figure 3.3-69. Rectenna Panel Assembly and Installation

equivalent schematic of the antenna electrical schematic is shown in Figure
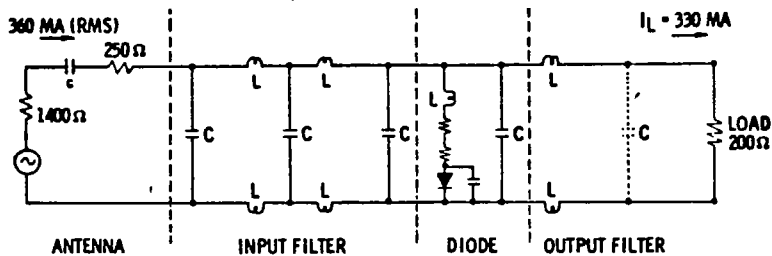3.3-70.

Figure 3.3-70. Simplified Schematic - Rectenna

The use of subarrays can cause problems if they are too large and become
too directional. Motion of the satellite due to imperfect stationkeeping can
produce unacceptable losses due to movement of the satellite off the peak of
the subarray beams. However, if the rectenna is operated in conjunction with
a single satellite, the directions of arrival of the power beam will be re-
stricted to a small solid angle. The solid angle dimensions are set by the
satellite orbit and the stationkeeping scenario. The subarray can then be
sized so that only a small budget loss results due to pointing error, say 1%.
By tilting the subarrays to various directions this loss can be made constant
over the solid angle. Diodes can then be designed to have optimum efficiency
at the power levels produced by the subarray at each location within the
rectenna. Even a very moderate amount of subarraying can dramatically decrease
the number of rectifiers.

3-86

The total rectenna efficiency budget is given in Table 3.3-23.

Table 3.3-23. Rectenna Loss Budget

LOSS	TYPICAL VALUE %
POINTING, L_P	1.0
SUBARRAY, L_{SA}	0.5
DIODE, L_D	3.0
JUNCTION, L_J	3.0
CIRCUIT, L_C	1.5
MISMATCH, L_R	1.0
COLLECTION BUS LOSS, L_B	1.0
TOTAL LOSS, L_Σ	11.0
RECTENNA EFFICIENCY	89.0

The installation pattern used in the rectenna area is illustrated in Figure 3.3-71. The special equipment shown in the figure is representative of one approach to the installation/maintenance equipment design considered during the course of the study.
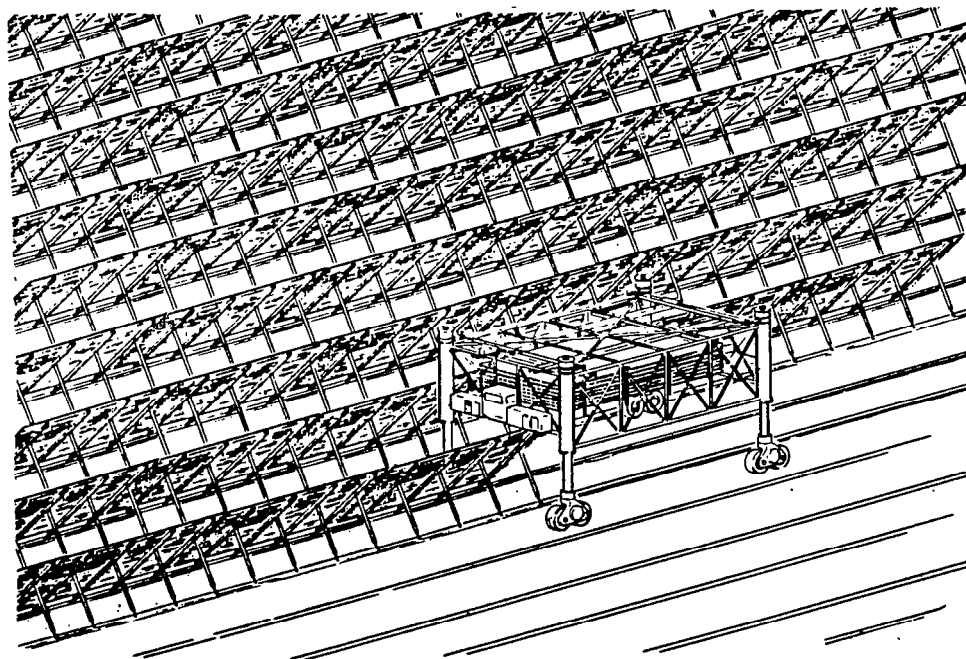

Figure 3.3-71. Panel Installation Operations

Rectifier. The rectifier assembly consists of a GaAs diode and input/output filters. An illustration of a possible diode configuration is shown in Figure 3.3-68. The equivalent schematic of the rectifier/filter circuit is shown in Figure 3.3-70.

3-87

The individual rectifier outputs must be connected to form the panel output. The rear-most layer of the copper/dielectric sandwich provides the major interconnection path. Each of the 0.186 m^2 antenna dipole/rectifier assemblies are series connected so as to establish a 40.5 kV/0.321 A (13 kW) "voltage string". The number of cluster assemblies comprising each string will vary depending upon its location within the rectenna area, however, on the average their will be approximately 329,000 such strings. Each string will consist of approximately 1000 cluster assemblies, or in other words the rectenna farm area will contain approximately 330×10^6 rectifier/diode subassemblies.

Panel Configuration

The rectenna panel consists of a multilayer copper-dielectric sandwich sub-panel containing dipoles tuned for 2.45 GHz, interconnects, ground plane and diode rectifier assemblies. These multilayer subpanels, shown in cross-section in Figure 3.3-68 are 9.33 m high by 0.735 m wide by 3.8 cm thick. The rectenna panels are comprised of steel I-beams and steel hat sections supporting these subpanels. The overall width of the rectenna panel is 14.69 m (20 of the sub-panels per rectenna panel). The panels are mounted on pre-pour concrete foundations and inclined approximately 40° with respect to the ground. The general construction features are shown in Figure 3.3-72.
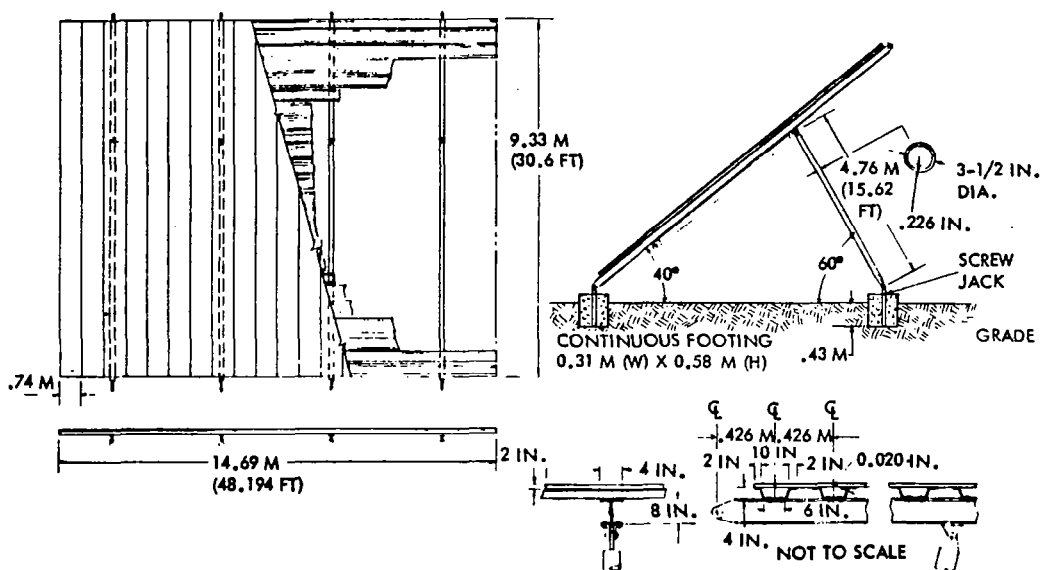

Figure 3.3-72. Rectenna Array Support Structure

Each panel (Figure 3.3-69) is secured to continuous footings at eight locations by fixtures which are imbedded in the concrete during pouring operations. Mounting attachments which provide for longitudinal and lateral adjustments are secured to the fittings. Screw jacks on each of the rear attach points provide for panel adjustment and alignment. Design of the fittings and foundation assumed a continuous wind force of 90 m/hr.

The panel switch gears and feeder lines are mounted above ground behind each panel as shown, although it is recognized that either above or below ground runs for the feeders is feasible.

Regulators/Motor Switches. The regulator units (not shown in schematic) accept and modulate the voltage string outputs to prevent current reversal. The motor switches (shown in Figure 3.3-73) provide isolation for each established voltage strong and are not considered part of the power distribution subsystem. These switches will be designed to open only under no-load conditions (with emergency override capabilities).

Power Distribution

Figure 3.3-73 illustrates the major assemblies comprising the power distribution and control subsystem. The power distribution assembly consists of the main feeders, secondary feeders, 40 kV dc and 500 kV ac buses, tie bars and power interface cabling for the various operating subsystems. The main feeders are sized to handle gradually increasing current loads starting at the center of the rectenna array and continuing to the perimeter. The feeders are grouped in each quadrant of the array to permit systematic maintenance and to avoid catastrophic system failures. The main feeders utilize TBD cm round aluminum cables, uninsulated, mounted on insulated standoffs or in insulated raceways. Other feeders, tie lines, buses, etc., are sized to handle maximum estimated loads, at specified voltages. All cables are passively cooled by radiation to local environment.
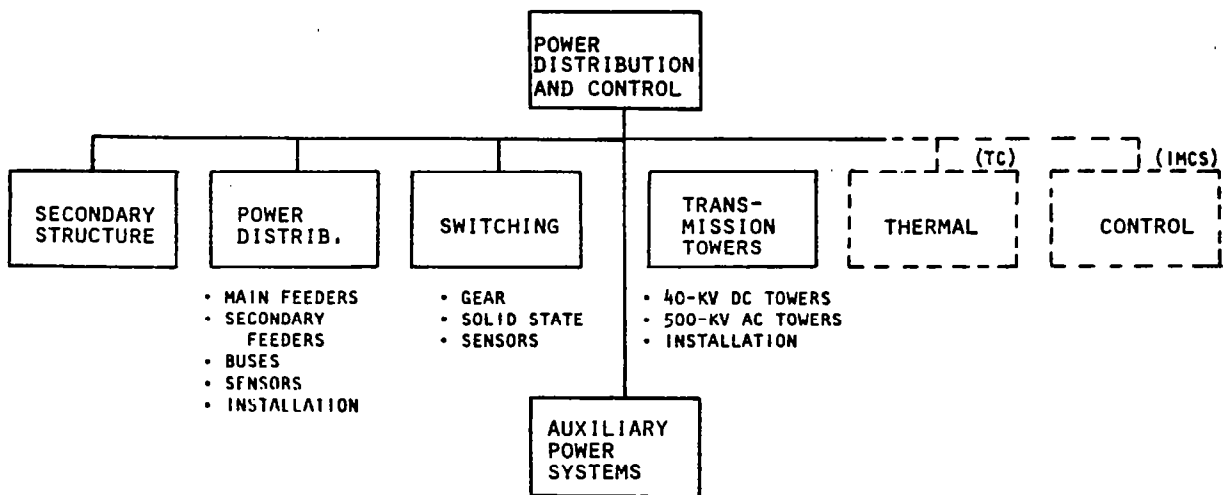

Figure 3.3-73. Assembly Tree - Power Distribution and Control

The power distribution and control subsystem receives power from the rectenna subsystem and provides the switching required to deliver the power to the power conversion stations, and then delivers the power station outputs to interconnected utility interfaces. Power transmission, (high tension cabling), from the designated interface at the perimeter of the ground receiving station are the responsibility of the power utility. The grounding, electromagnetic interference control, and all shielding requirements are also included. The life expectancy of the power distribution system is 30 years.

The outputs from each voltage string motor switch is connected to feed-lines which are routed behind each row of rectenna panels. The interconnection concept is illustrated in Figure 3.3-74.
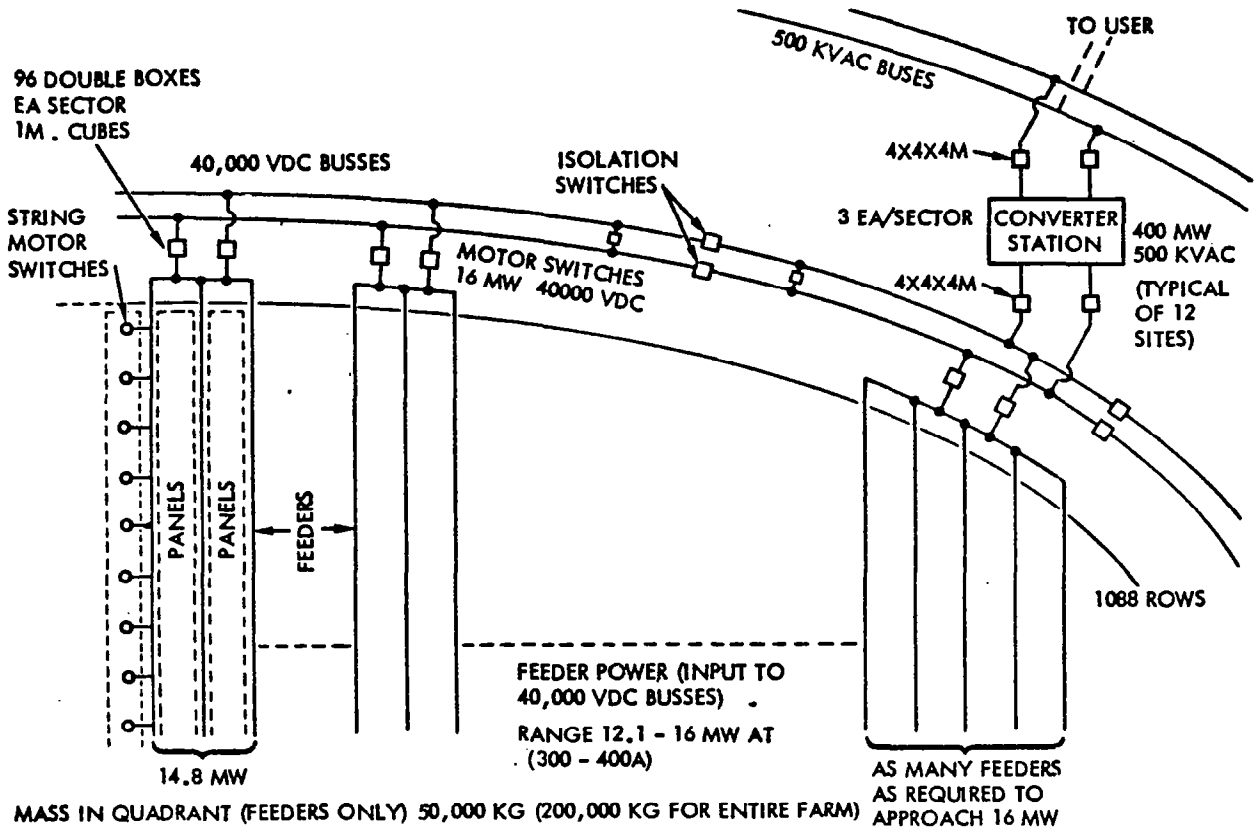

Figure 3.3-74. Ground Receiving Station Schematic
Block Diagram - Preliminary

Each feeder line is specified to handle a maximum of 5.0 MW. The feeder lines are then grouped (summed) to establish equivalent power sources of from 14-16 MW. The actual power level available from the feeder groups will vary depending upon incident energy levels and the number of voltage strings connected at any given time. The point design encompasses 1088 feeders grouped into 384 power "sources".

The individual "source" groups are switched onto a 40 kV secondary bus, which is routed entirely around the rectenna perimeter, as power demand requires. The secondary bus is a complete loop to permit even draw of power from the various rectenna sectors even in the case of system abnormalities. The power conversion stations then draw their power from the secondary bus.

Switching. Switch gears are used for:

• Isolation/selection of various power feeders as a result of changes in power demand or as the result of systematic element failures.

3-90

- Isolation/selection of power conversion stations as load demand varies or due to systematic failure.

- Isolation of loads as satellite power capability varies due to predicted (eclipse, maintenance, etc.) power reductions or due to unpredicted (systematic failures) power reductions.

The switch gears may be solid-state or electromechanical. The voltages and currents being handled by these switches will be monitored by the IMCS to determine their status and to establish a need for the automatic opening of these switches (circuit breaker function). Switch closure will be based upon fault status and power demand. During shutdown operations the system will be monitored and when certain conditions are reached a command signal will automatically open or close selected switches as required.

Transmission Towers

The periphery of the panel farm is ringed by 40 kV dc and 500 kV ac buses mounted on towers. The 40 kV dc bus is located approximately 50 meters outside the ellipse containing the panels; the 500 kV ac bus about 450 meters further out.

Based on Southern California Edison data, the 40 kV dc buses would be suspended on a series of hollow tapered steel poles. Four poles, connected by a crossbeam upon which the insulators are mounted, constitute one suspension unit. Each pole measures 0.46 meters diameter at the tip, 1.1 meters diameter at the base, and has a wall thickness of 0.013 meters. The poles are inserted into a 1.22 meter circular hole to a depth of 3 meters and surrounded by concrete. The spacing between pole units is about 91 meters; this requires 401 installations or a total of 1604 poles.

The 500 kV ac towers are similar to existing high tension towers, measuring 12.9 meters at the base with a height of about 70 meters above ground. The towers are spaced every 457 meters; since they do not completely rim the perimeter, only 54 towers are required, including 18 "deadend" towers.

The deadend towers are mounted on four concrete pilings 1.83 meters in diameter and extending 10.7 meters into the ground. The remainder of the towers require less footing and are secured to four concrete pilings measuring 1.1 meters in diameter and 6.1 meters deep.

Design and Performance Characteristics

The design and performance characteristics for the power distribution subsystem are listed in Table 3.3-24.

Converter Stations

The converter stations accept 40 kV dc power and output 500 kV ac or dc. The initial concept utilizes a solid-state inversion/step-up concept typified by an existing dc-ac conversion station located in Sylmar, California. The block diagram of the subsystem is shown in Figure 3.3-75.

Table 3.3-24. Design and Performance Characteristics

| Major Assembly	Requirements	Technology Issue

GENERAL
  Mass
  MTBF
  Life
  Efficiency
  Resupply and maintenance
	Configuration dependent
	Subsystem dependent
	30 years
	88-98% (config. dependent)
	As needed	

POWER DISTRIBUTION (PD)
  Mass
  Material
  Insulation
  Efficiency
  Subsystem cabling
  Resupply and maintenance
  Life
	Mostly round conductor
	Configuration dependent
	Aluminum 6001-T6
	TBD
	88-98% (config. dependent)
	Location and power dependent
	As required
	30 years or greater	

SWITCH GEAR
  Density
  Type
  Power rating
  Voltage
  Efficiency
  Life
  Resupply and maintenance
	Approx. 0.00086 kg/kW
	Solid state
	Configuration dependent
	Config. and location dependent
	99-99.9%
	30 years
	As required
		Study is required to specify design requirements.

SECONDARY STRUCTURE Mass	TBD% of PDS weight was considered to be required for mounting and installation.	

CONTROL
  Temperature sensors
  Current sensors
  Voltage sensors
  Switch gear control
    Overcurrent
    Overvoltage
    Undercurrent
    Undervoltage
	No. of sensors config. dependent
	No. of sensors config. dependent
	No. of sensors config. dependent
	Configuration dependent	
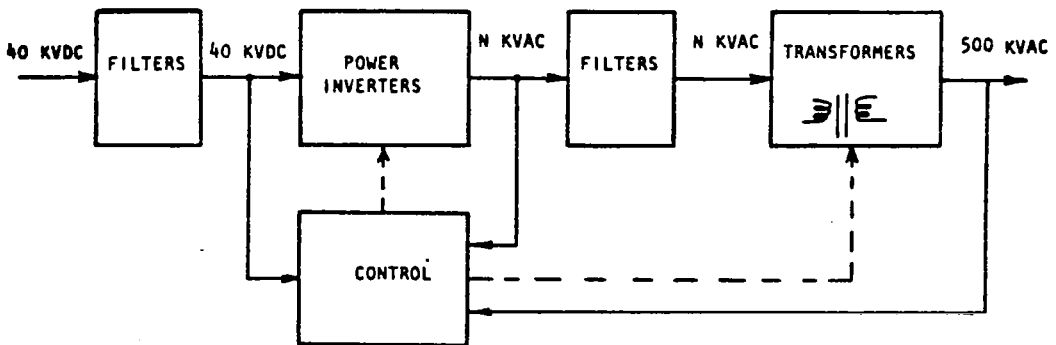
Figure 3.3-75. Simplified Block Diagram - Converter Station

Specific design details of this subsystem was not derived during the preceeding study and must await clarification in a future study effort.

3-92

Twelve stations are selected for the point design. Of these eleven are capable of handling the entire nominal power output (4.61 GW) of the GRS. The twelfth unit is a spare available in case of unexpected outage or during scheduled maintenance. Nominal power conversion capability of each station is specified as 400 MW.

Thermal

The rectenna configuration used to develop a thermal model to predict local temperature profiles is shown in Figure 3.3-76. Optical properties for the panel elements are based on those of mylar for the thicknesses shown on the module. Rectenna thermal model development included consideration of solar heating, local air convection, and waste heat arising from microwave conversion inefficiencies.
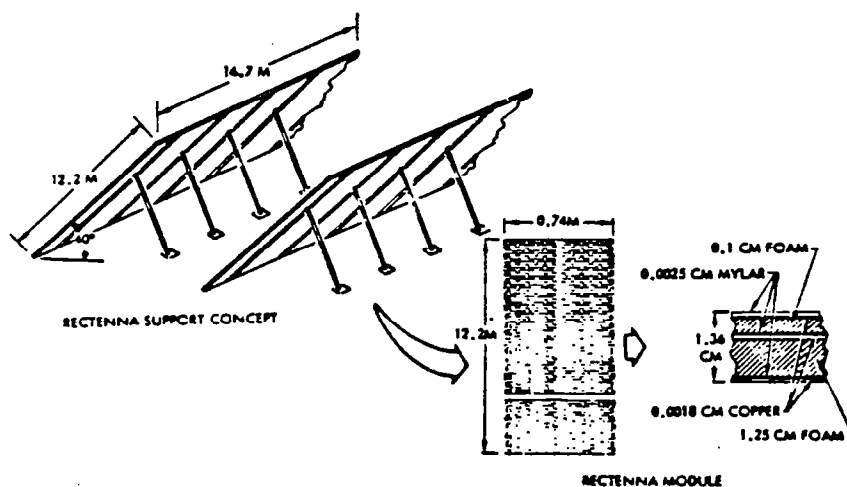

Figure 3.3-76. Rectenna Construction - Thermal Model

Temperature profiles are shown in Figure 3.3-77 for the rectenna panels in the high-density region. During the daylight hours, air convection tends to cool the panels and at night it acts as a heating source. The effect of air convection on the gradients is substantial, as evidenced by the large difference from the root to the end which arises due to transition from laminar to turbulent flow. Ground temperatures will typically be within 6°C of the module levels and will be somewhat warmer than the evening levels and cooler than the daytime values. For different climates (wind, overcast sky, air temperature) the temperatures will vary. In outer regions of the rectenna, the waste heat arising from conversion inefficiencies will be reduced--but this is a small fraction of the total heat load and will not greatly influence panel temperature levels. The thermal environments computed for the current rectenna configuration do not differ greatly from earlier analyses and it is expected that influences on the microclimate would be relatively unchanged from current predictions.

	DAY (PEAK SUN)	NIGHT
ROOT	56°C (132°F)	-17°C (2°F)
END	33°C (92°F)	18°C (64°F)

AIR TEMPERATURE = 27°C (80°F)

- CONDUCTION IN RECTENNA PANEL NEGLECTED

- ALL COMPUTATIONS BASED UPON STEADY STATE EQUILIBRIUM;
  GROUND HEAT SINK EFFECT NOT INCLUDED

*Figure 3.3-77. Rectenna Panel Temperatures,
High-Density Microwave Region*

Information Management and Control

It is assumed that the subarray control circuit includes an "intelligent terminal." A local microprocessor will first receive local data. Much of this data will not change by very much as long as the subarray is operating correctly. The microprocessor will periodically read this data on a short time scale. If it stays within a preset tolerance range and a preset rate-of-change tolerance, no data is put on the bus. If tolerances are exceeded, an immediate report is made to the central data processing station via the bus. In the case of data deviations which may indicate that equipment may be damaged the microprocessor may be programmed to take immediate action and then report. Indeed in the case of some critical events with short time constants, shutdown will be initiated by hard-wired paths and data reporting carried out after shutdown.

Data which stays within tolerance will be reported at much more infrequent intervals after averaging over this longer interval. Such data can be used to find secular changes in performance which indicate incipient failure. Such indications may be used to decide that unscheduled maintenance is needed. With proper array design, the subarray system will be accessible while the MPTS system is in operation. The maintenance is then carried out while the SPS is operating. This maintenance philosophy is the same as that used by the airlines.

Additional data will be collected from detectors located at specific intervals over the entire rectenna system to determine the relative shape and position of the microwave beam. This information as well as the health data collected from the array circuitry will be combined in a central processing complex where system status will be established and appropriate operational commands to the satellite and/or the ground complex will be generated.

The data management and control hierarchy for the ground complex is outlined in Figure 3.3-78. The primary approach, pyramidal, is similar to that selected for the satellite. Similar, but not necessarily space qualified, devices would be used to implement the ground data system. A description of the various IMCS devices is provided in Section 3.3.1.

Specific details on the number and type of measurements and controls for the GRS are TBD.

Figure 3.3-78. IMCS Hierarchy - Ground Receiving Station

1. Report No. NASA CR-3318	2. Government Accession No.	3. Recipient's Catalog No.
4. Title and Subtitle SATELLITE POWER SYSTEMS (SPS) CONCEPT DEFINITION STUDY VOLUME II, PART 1 - SYSTEM ENGINEERING		5. Report Date September 1980
		6. Performing Organization Code
7. Author(s) G. M. Hanley		8. Performing Organization Report No. SSD 79-0010-2-1
		10. Work Unit No.
9. Performing Organization Name and Address Rockwell International 12214 Lakewood Boulevard Downey, CA 90241		11. Contract or Grant No. NAS8-32475
		13. Type of Report and Period Covered Contractor Report
12. Sponsoring Agency Name and Address National Aeronautics and Space Administration Washington, D.C. 20546		14. Sponsoring Agency Code

15. Supplementary Notes

Marshall Technical Monitor: C. H. Guttman
Volume II, Part 1 of Final Report

16. Abstract

This volume presents the details of system engineering studies.
Top level trade studies are presented, including comparison of solid-
state and klystron concepts, higher concentration on the solar cells,
composite and aluminum structure, and several variations to the reference
concept. Detailed trade studies are presented in each of the subsystem
areas (solar array, power distribution, structures, thermal control,
attitude control and stationkeeping, microwave transmission, and ground
receiving station). A description of the selected point design is
also presented.

17. Key Words (Suggested by Author(s)) Satellite Power System System Engineering System Studies Trade Studies Subsystem Trades System Descriptions SPS	18. Distribution Statement Unclassified - Unlimited Subject Category 44

19. Security Classif. (of this report) Unclassified	20. Security Classif. (of this page) Unclassified	21. No. of Pages 268	22. Price A12